2024

The Assessment of Floating Offshore Wind Turbines in Extreme Conditions

White, Andre Onife Alwyn

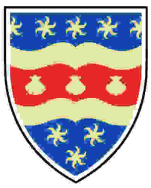

UNIVERSITY OF
PLYMOUTH

The Assessment of Floating Offshore Wind Turbines in Extreme Conditions

by

Andre White

A thesis submitted to the University of Plymouth
in partial fulfilment for the degree of

DOCTOR OF PHILOSOPHY

School of Engineering, Computing and Mathematics

January 2024

Acknowledgements

THIS PhD project would not have been possible without the support from a few individuals to whom I owe a tremendous debt of gratitude.

Firstly, I would like to say a heartfelt thank you to my supervisory team comprising of Professor Deborah Greaves, Dr. Martyn Hann, Dr. Jon Miles and Dr. Robert Rawlinson-Smith. Thank you for all the guidance and feedback that you provided in helping me to refine my research, for being consistent and helping me to stay motivated and encouraged when I felt like it would not have been possible to finish this research. It certainly would not have been possible with you.

I would also like to specially thank to these individuals who helped me to understand the concepts of extreme value theory, the environmental contour method, interpreting the results and utilizing software: Dr. Gilleland, of National Center for Atmospheric Research, US, Dr. Sofia Caires of Deltares, Netherlands, Dr. Steven Winterstein, formerly of MIT, Prof. Sverre Haver of the University of Stavanger and Professor Arne Huseby of the University of Oslo.

It would be remiss of me not to say a sincere thank you to Dr. Jason Jonkman and Dr. Garrett Barter of the National Renewable Energy Laboratory (NREL); and Dr. Spencer Hallowell of the University of Maine who assisted me with modelling in OpenFAST and TurbSim. Words cannot express how grateful I am for your support.

I would also like to say a big thank you to my colleagues and members of staff from the University of Plymouth who provided technical and (or) moral support and answered queries that I had about numerical modelling and hydrodynamics. They include Tom Tosdeven, Guixun Zhu, Dr. Ed. Ransley, Dr. Jessica Guichard, Dr. Ben Howey, Dr. Siming Zheng and Dr. Emma Edwards.

I must also say thanks to my parents, other members of my family and friends of Elijah Centre Global for providing good support during this process. I would also like to say a heartfelt thank you to my wonderful girlfriend Natalie Nunes for believing in me, encouraging me, listening to me and providing advice when I needed perspective about how to move forward.

Finally, I would like to say thanks to God for giving me the strength everyday to keep believing and pressing on.

This research was made possible by funding from the Commonwealth Scholarship Commission UK (CSC). The CSC is an executive nondepartmental public body, spon-

sored by the Foreign, Commonwealth & Development Office. The CSC operates within the framework of the Commonwealth Scholarship and Fellowship Plan (CSFP) and is a vivid demonstration of the UK's enduring commitment to the Commonwealth.

Abstract

The Assessment of Floating Offshore Wind Turbines in Extreme Conditions

Andre White

THE purpose of this research is to assess if a floating offshore wind turbine (FOWT) system that is suitable for the environmental conditions in the Scottish North Sea (SNS) is also suitable for the environmental conditions in the Jamaica Caribbean Sea (JCS). A FOWT within Jamaica is an important structure because it produces renewable energy which helps to reduce the dependence on fossil fuel as the primary source of energy. At the same time, it also contributes to reducing global warming caused by climate change effects. These structures, therefore, must be robust enough to withstand the most extreme environmental conditions in the JCS. The extreme sea and wind conditions are determined in the JCS and the SNS and used as inputs to an OpenFAST numerical model to determine the floater dynamic and structural response.

Hindcast environmental data at appropriate site locations is sourced from the European Centre for Medium Range Weather Forecasts (ECMWF) repository. The data is used to compute the normal sea and wind conditions and the extreme (50-year return period) sea and wind conditions. The extreme conditions are determined using extreme value analysis and the environmental contour method. The responses of the FOWT system are determined using OpenFAST software code for a baseline OpenFAST floating wind turbine model, available for download on Github. In the initial design of the research only the 50-year extreme sea state and wind conditions were computed and used to compare the response of the FOWT in the JCS and the SNS but the study is extended to include the hurricane wind and sea conditions in the JCS as this is the most extreme condition within the jurisdiction. The response of the FOWT system within the JCS are then compared using the 50-year extreme loads and the hurricane loads. The hurricane loads are found using data from a large eddy simulation (LES) model of a category 5 hurricane within the North Atlantic.

The research shows that the 3 parameter Weibull statistical distribution (Weib3P) which is suitable to fit hindcast data to determine the 50-year extreme sea state for the SNS is not appropriate for the JCS. To determine the 50-year extreme sea state for the JCS, the Weib3P distribution model is fitted to hurricane wave height data. For the extreme 50-year conditions the dynamic response of the floater and the structure are predominantly greater in the JCS than the SNS. For example, the surge motion in the

JCS of 28.6 m is 1.2 times the value in the SNS. The heave motion of 6.0 m in the JCS is 1.1 times the value in the SNS. The pitch motion of 9.1 deg in the JCS is 1.7 times the value in the SNS. For the 50-year response compared to the hurricane loads, all of the responses of the FOWT are greater for the hurricane loads. For example, the maximum tension in the mooring line is 2.38E+07 N for the hurricane is 4.43 times the tension for the 50-year extreme case. The blades, the mooring lines and the tower are at a greater risk of failure when hurricane conditions are considered. These findings show that a more robust FOWT system is required in the JCS when hurricane conditions are considered.

The extreme environmental conditions determined for the JCS in this research can be used as a basis for investigating the response of other FOWT models or even fixed-bottom models where that becomes necessary. The approach can also be used to investigate the responses of FOWT systems in other regions of the Caribbean.

Authors declaration

At no time during the registration for the degree of Doctor of Philosophy has the author been registered for any other University award. Work submitted for this research degree at University of Plymouth has not formed part of any other degree either at University of Plymouth or at another establishment. Relevant scientific seminars and conferences were regularly attended at which work was often presented. Two papers have been accepted for publication in refereed journals.

Word count for the main body of this thesis: **60551**

Signed: A. White

Date: 04/Jan/2024

Posters and conference presentations:

White, A.; Hann, M.; Miles, J.; Rawlinson-Smith, R. & Greaves, D. (2021), An Univariate Extreme Sea State and Extreme Wind Speed for An Offshore Wind Turbine off the South Coast of Jamaica, *in* '31st International Ocean and Polar Engineering Conference', pp. ISOPE-I-21-1217.

Contents

Acknowledgements i

Abstract iii

Author's declaration v

List of figures xii

List of tables xix

1 Introduction 1

1.1 General 1

1.2 Harnessing Wind Energy 4

1.3 Offshore Wind Turbines 5

1.4 Floating Offshore Wind Turbines 7

1.4.1 The Semi-submersible Floater 8

1.4.2 The Spar-buoy Floater 9

1.4.3 The Tension Leg Platform (TLP) Floater 10

1.5 Trends in FOWT Support Structures 10

1.6 Some of the Challenges in Analysing FOWT 12

1.7 Research Focus 16

1.8 Outline of the Thesis 17

2 Literature Review 19

2.1 General 19

2.2 Wind Resource Assessment 19

2.2.1 Quality of the wind resource in different regions worldwide 23

2.3 Extreme Value Theory 28

2.3.1 General . . . 28
2.3.2 Extreme value theory models . . . 30
2.3.3 Modelling threshold excesses . . . 33
2.3.4 Model checking . . . 34
2.4 Applications of Univariate EVA to Determine the Extreme Design Sea State . . . 35
2.4.1 Univariate extreme value analysis . . . 37
2.5 Multivariate Extreme Value Analysis . . . 42
2.5.1 The joint distribution of H_s and T_p by conditional modelling approach 42
2.5.2 Environmental contour method . . . 44
2.5.3 Applications of multivariate EVA to determine the extreme design sea state . . . 48
2.6 Floating Offshore Wind Turbines . . . 53
2.6.1 General . . . 53
2.6.2 Wind turbine components . . . 53
2.7 Wind Turbine Theory . . . 56
2.7.1 General . . . 56
2.7.2 Software codes used to carry out numerical modelling of FOWT systems . . . 56
2.7.3 Brief overview of FAST . . . 57
2.7.4 Aerodynamics – Blade element momentum theory . . . 59
2.7.5 Hydrodynamic theory . . . 69
2.7.6 Mooring line theory . . . 72
2.7.7 Governing equation of motion for a floating platform . . . 75
2.8 Floating Offshore Wind Turbine Design Manuals . . . 75
2.9 Numerical Modelling of Floating Offshore Wind Turbines . . . 77
2.10 Conclusion . . . 80

3 Development of a Univariate Extreme Sea State and Extreme Wind Speed off the South Coast of Jamaica 82

3.1 Introduction . . . 82
3.2 Selection of Software for Extreme Value Analysis . . . 82
3.3 Development of Extreme Sea State and Wind Speed at Location 17.5N, 77.0W . . . 85
3.3.1 Data preparation – checking the quality of the data . . . 86
3.3.2 Checking the accuracy of the results from extRemes . . . 86
3.3.3 Extreme Value Theory . . . 87
3.3.4 Analysis of block maxima . . . 87
3.3.5 GPD/POT Analysis . . . 93
3.4 Conclusion . . . 101

4 Comparing the environmental conditions in the Scottish North Sea with the conditions in the Jamaica Caribbean Sea 102

4.1 Introduction . . . 102
4.2 An Examination of the Environmental Data from the Scottish North Sea and the Jamaica Caribbean Sea . . . 102
4.2.1 Looking at some summary statistics . . . 102
4.2.2 Normal sea and wind conditions . . . 103
4.2.3 Extreme Sea State - Joint Probability Distribution of H_s and T_p and 50 and 100 Year Environmental Contours . . . 107
4.2.4 Selection of the normal and extreme sea state conditions for the SNS and JCS . . . 115
4.2.5 Comparing the 50-year univariate and 50-year multivariate EVA sea states . . . 122
4.2.6 Steady and turbulent wind conditions in OpenFAST . . . 122
4.2.7 Turbulent Wind Conditions . . . 123
4.2.8 Wave spectrum . . . 128
4.3 Conclusion . . . 132

5 Definition of a FOWT Numerical Model to Assess Its Performance in the SNS and the JCS 134

5.1 Introduction . . . 134
5.2 Description of the FOWT system . . . 134
5.2.1 IEA-15 MW Reference Wind Turbine and Controller . . . 135
5.2.2 UMaine VolturnUS-S Semi-Submersible Floater . . . 135
5.2.3 Mooring system . . . 135
5.2.4 The Tower . . . 135
5.3 Numerical Model Set Up and Description . . . 141
5.3.1 Numerical Model Verification . . . 141
5.4 Proposed Wind Turbine for the SNS and the JCS . . . 143
5.4.1 Modification to the mooring line . . . 143
5.4.2 Design load conditions . . . 146
5.5 Comparing the response of the FOWT in the SNS and the JCS . . . 148
5.5.1 FOWT respose for the normal sea state, SNS and the JCS - wave only condition . . . 148
5.5.2 FOWT response for the normal sea state, SNS and JCS - wind and wave condition . . . 154
5.5.3 FOWT response for the extreme sea state, SNS and the JCS - wind and wave condition . . . 161
5.6 Conclusion . . . 164

6 Investigation of the response of a FOWT in the JCS for Selected Characteristics of a Hurricane 168

6.1 Introduction . . . 168
6.2 DTU 10MW Wind Turbine Properties . . . 170
6.3 Characteristics of the Hurricane Wind Field . . . 172
6.4 Reproducing the Hurricane Wind Fields from Kapoor et al. (2020) using TurbSim . . . 178
6.5 Using the output from TurbSim to reproduce Kapoor et al (2020) wind turbine responses in OpenFAST . . . 180
6.5.1 Turbine responses 20 km from hurricane centre . . . 180

6.5.2 Turbine responses 15 km from hurricane centre 185
6.5.3 Turbine responses 12 km from hurricane centre 190
6.5.4 Concluding remarks on reproducing of TurbSim hurricane wind fields and OpenFAST wind turbine responses given by Kapoor et al. (2020) 193
6.6 Assessing the behaviour of a FOWT during hurricane conditions 195
6.6.1 Description of FOWT system 195
6.7 Numerical Model Set Up and Verification 196
6.7.1 Numerical Model Verificationon 198
6.8 Response of DeepCwind FOWT 12 km from the hurricane centre 199
6.8.1 Responses investigated for the FOWT system. 199
6.8.2 Modifications of the mooring line. 200
6.8.3 Hurricane Wind Field and Sea State. 201
6.8.4 DeepCwind FOWT in Idle conditions, hurricane loads compared to 50-year extreme loads. 204
6.8.5 DeepCwind FOWT in Idle vs Standstill conditions, hurricane loads. 209
6.9 Conclusion 214

7 Conclusion and Recommendations 216
7.1 Conclusion 216
7.2 Recommendations 220

A The History of Offshore Wind 222
A.1 Brief overview of the history of offshore wind 222

B List of major hurricanes in Jamaica by category from 1900 to 2018 229

C Return level and qq-plots of significant wave height and wind speed for the Scottish North Sea (SNS), location 57.5 N, 1.0 W 230
C.1 GPD Plots of H_s and Wind Speed, SNS 230
C.2 GEV Plots of H_s and Wind Speed, SNS 234

D Request to authors to include their figures in my work 238

List of references 277

List of Figures

1.1 Global cumulative installed wind capacity 1998 to 2018 (Source: GWEC, 2012; GWEC, 2018; GWEC, 2019; GWEC, 2023) 2

1.2 Main GHGs emitted globally by human activities (Source: Edenhofer et al. (2014)) 3

1.3 Renewable energy generation capacity by energy source (Source: IRENA (2019*b*) 5

1.4 Global cummulative offshore wind installed capacity 2008 to 2022 (Source: GWEC (2022)) 6

1.5 Types of floating offshore wind turbines (Source: IRENA (2016b)) 7

1.6 Catenary and Taut Mooring Configurations (Source: World Forum Offshore Wind) 9

1.7 Properties of VolturnUS Semi-sub (Source: CarbonTrust (2015)) 9

1.8 Properties of Windfloat Semi-sub (Source: CarbonTrust (2015)) 10

1.9 Properties of Pelastar (Source: CarbonTrust (2015)) 11

1.10 Properties of Blue H TLP (Source: CarbonTrust (2015)) 11

1.11 Illustration showing the six degrees of freedom of a FOWT (Source: `www.windpowerengineering.com` from an article written by Lloyd's Register) 13

2.1 The FOWT concept (Adapted from: Manolas et al., 2020) 20

2.2 Mean wind speed (m/s) at 10m, at proposed FOWT site, Jamaica (Source: Global Wind Atlas) 25

2.3 Mean wind speed (m/s) at 10m, approx. location of Vattenfall OWF, North Sea (53.04N, 2.61W) (Source: Global Wind Atlas) 25

2.4 Wind energy classification across the global ocean (Source: NREL (2005)) 26

2.5 Mean wind power density (W/m^2) at 10m, at proposed FOWT site, Jamaica (Source: Global Wind Atlas) 27

2.6 Mean wind power density (W/m^2) at 10m, approx. location of Vattenfall OWF, North Sea (53.04N, 2.61W) (Source: Global Wind Atlas) 27

2.7 Illustration of (true) failure surface and linearized failure surface (FORM failure boundary) by FORM in U space. (From: Haver & Winterstein, 2008; Chai & Leira, 2018) 45

2.8 Major components of a floating offshore wind turbine (Adapted from: Manwell et al. (2009)) 54

2.9 Wind turbine rotor configurations (Source: Manwell et al. (2009)) 55

2.10 Actuator disc model of a wind turbine. U is the mean air velocity and 1 to 4 indicate locations along the stream tube (Source: Manwell et al. (2009)) 60

2.11 Actuator disc model of a wind turbine when wake rotation is considered. U is the velocity of undisturbed air; a is the induction factor, r is the radius and 1 to 4 indicate locations along the stream tube (Source: Manwell et al. (2009)) 64

2.12 Illustration of blade elements. c is the aerofoil chord length; dr is the radial length of the element, r is the radius, R is the root radius and Ω is the angular velocity of the rotor (Source: Manwell et al. (2009)) 66

2.13 Blade geometry, forces and velocities for a horizontal axis wind turbine (Source: Manwell et al. (2009)) 67

2.14 Definition sketch of 2d-sea (Adapted from: Reeve et al. (2004)) 71

2.15 Definition sketch of a mooring line (Source: Zhao et al. (2019)) 73

2.16 Illustration of lumped-mass model used in MoorDyn (Source: Hall (2017)) 74

3.1 Map of Jamaica showing location of proposed FOWT site (17.5 N, 77.0 W) 83

3.2 GEV return levels of H_s for site at 17.5N, 77.0W 89

3.3 Q-Q plot of H_s for site at 17.5N, 77.0W(GEV analysis) 90

3.4 GEV return levels of u_{10} for site at 17.5N, 77.0W 91

3.5 Q-Q plot of u_{10} for site at 17.5N, 77.0W(GEV analysis) 92

3.6 Mean residual life plot of H_s for site at 17.5N, 77.0W 94

3.7 Threshold stability parameters of H_s for site at 17.5N, 77.0W(GPD analysis). Vertical lines are the width of the confidence interval band. 95

3.8 Q-Q plot of H_s for site at 17.5N, 77.0W(GPD analysis) 97
3.9 Return level plot of H_s for site at 17.5N, 77.0W(GPD analysis) 98
3.10 Q-Q plot of u_{10} for site at 17.5N, 77.0W(GPD analysis) 99
3.11 Return level plot of u_{10} for site at 17.5N, 77.0W(GPD analysis) 100

4.1 Scatter plot of 3hr-storms(H_s and T_p) for SNS and JCS from 1979 to 2018 104
4.2 Histogram of SNS H_s from 1979 to 2018 105
4.3 Histogram of JCS H_s from 1979 to 2018 106
4.4 Weibull-3P q-q plot of SNS H_s from 1979 to 2018 109
4.5 Weibull-3P q-q plot of JCS H_s from 1979 to 2018 110
4.6 Lognormal distribution parameters, μ and σ, bin-averaged, as function of H_s for (a) SNS and (b) JCS, 3hr-storms from 1979 to 2018 111
4.7 Weib3P-lognormal 50-year and 100-year environmental contour for (a) SNS and (b) JCS using 3hr-storms from 1979 to 2018 112
4.8 (a) GPD q-q plot of H_s for JCS, threshold =1.55 m (b) GPD 50-year and 100-year environmental contours, JCS, threshold = 1.55 114
4.9 (a) Weib3P q-q plot of H_s for JCS normal season data, (b) Weib3P 50-year and 100-year environmental contours, JCS, normal season data . 116
4.10 (a) Weib3P q-q plot of H_s for JCS hurricane season data, (b) Weib3P 50-year and 100-year environmental contours, JCS, hurricane season data 117
4.11 (a) GPD q-q plot of H_s for JCS hurricane season data, (b) GPD 50-year and 100-year environmental contours, JCS, hurricane season data . . . 118
4.12 (a) Weib3P q-q plot of H_s < 3.5 m for JCS hurricane season data, (b) Weib3P 50-year and 100-year environmental contours, JCS, hurricane season data for H_s < 3.5 m 119
4.13 (a) Weib3P q-q plot of hurricane H_s for JCS, (b) Weib3P 50-year and 100-year environmental contours, JCS, hurricane H_s data 120
4.14 Simultaneous wind velocities in the wind direction at different heights above the ground (Source: Dyrbye & Hansen (1997)) 123
4.15 Variation of turbulence intensity with wind speed (a) SNS, (b) JCS. . . . 126
4.16 Variation of turbulence intensity with wind speed SNS vs JCS 127

4.17 Variation of turbulence intensity with wind speed (Comparison with DNVGL offshore turbulence model) (a) SNS, (b) JCS. 129

4.18 Variation of turbulence intensity with wind speed (Comparison with IEC-61400-1:2019) (a) SNS, (b) JCS. 130

4.19 Variation of turbulence intensity with wind speed (Comparison with IEC-61400 modified) (a) SNS, (b) JCS. 131

5.1 Layout Plan and Section UMaine VolturnUS-S Semi-sub Floater (Source: Allen et al. (2020)) 138

5.2 Mooring System Arrargement UMaine VolturnUS-S Semi-sub Floater (Adapted from: Allen et al. (2020)) 139

5.3 Reference Coordinate System UMaine VolturnUS-S Semi-sub (Source: Allen et al. (2020)) 142

5.4 UMaine VolturnUS-S free decay time histories(a) Surge and Sway (b) Heave (c) Roll and Pitch (d)Yaw 144

5.5 Comparison of the magnitude of the motion of the VolturnUS-S platform in surge, heave and pitch during three different normal sea conditions, for wave only, SNS vs JCS. 151

5.6 Comparison of the magnitude of the tensions in the fairleads for the VolturnUS-S platform during three different normal sea conditions, for wave only, SNS vs JCS. 152

5.7 Comparison of the magnitude of the bending moment at the blade root and at the base of the tower for the VolturnUS-S platform during three different normal sea conditions, for wave only, SNS vs JCS. 153

5.8 Comparison of the magnitude of the motion of the VolturnUS-S platform in surge, heave and pitch during three different normal wind and sea conditions, SNS vs JCS. 157

5.9 Comparison of the magnitude of the motion of the VolturnUS-S platform fairlead tensions during three different normal wind and sea conditions, SNS vs JCS. 158

5.10 Comparison of the magnitude of the VolturnUS-S moments during three different normal wind and sea conditions, SNS vs JCS. 159

5.11 Comparison of the magnitude of the motion of the VolturnUS-S platform in surge, heave and pitch; fairlead tensions and moments for 50-year extreme wind and wave conditions, SNS vs JCS 162

5.12 Power spectral density of the 50-year wave, SNS vs JCS. 163

6.1 Process of assessing wind turbine for hurricane conditions using TurbSim and OpenFAST 170

6.2 Structure of a mature tropical cyclone (Source: NOAA, National Weather Service) 172

6.3 Shear profile a) 10 km, b) 12 km, c) 15km and d) 20 km from the hurricane centre (Source: Kapoor et al. (2020)) 175

6.4 Veer profile a) 10 km, b) 12 km, c) 15km and d) 20 km from the hurricane centre (Source: Kapoor et al. (2020)) 176

6.5 Illustration of (a) Base (b) Veer (c) Rated (d) Misal(Plan View) Load Cases. Base, Veer and Misal are the hurricane load cases for a respective distance from the hurricane centre; 12 km is shown here. . . . 177

6.6 Potential locations of the FOWT at distances of 10 km, 12 km, 15 km and 20 km from the hurricane centre. 178

6.7 Correlation coefficient of the wind velocity at each elevation to the velocity at hub height, Kapoor et al (2020) vs computed for 6 random seeds from TurbSim. (a) 12 km from hurricane centre (b) 15 km from hurricane centre and (c) 20 km from hurricane centre 181

6.8 (a) Blade out-of-plane tip deflection (b) Blade in-plane tip deflection (c) Resultant blade root moment (d) Fore-aft moment at tower base - 20 km from hurricane centre, Kapoor et al (2020) vs present results. 182

6.9 (a) Side-side moment at tower base (b) Tower base resultant moment - 20 km from hurricane centre, Kapoor et al (2020) vs present results. . . 183

6.10 (a) Blade out-of-plane tip deflection (b) Blade in-plane tip deflection (c) Resultant blade root moment (d) Fore-aft moment at tower base - 15 km from hurricane centre, Kapoor et al (2020) vs present results. 186

6.11 (a) Side-side moment at tower base (b) Tower base resultant moment - 15 km from hurricane centre, Kapoor et al (2020) vs present results. . . 187

6.12 (a) Blade out-of-plane tip deflection (b) Blade in-plane tip deflection (c) Resultant blade root moment (d) Fore-aft moment at tower base - 12 km from hurricane centre, Kapoor et al. (2020) vs present results. 190

6.13 (a) Side-side moment at tower base (b) Tower base resultant moment - 12 km from hurricane centre, Kapoor et al. (2020) vs present results. . . 191

6.14 DeepCWind Floating Wind Turbine System (Li et al. (2019)) 197

6.15 a) Surge Free Decay and b) Heave Free Decay, DeepCwind Motion Response 199

6.16 FOWT wind turbine response for Base Case compared with the 50-year extreme loads: (a) Platform motions and blade tip deflections (b) Tension in the fairleads (c) Moments. 204

6.17 FOWT wind turbine response for Veer Case compared with the 50-year extreme loads: (a) Platform motions and blade tip deflections (b) Tension in the fairleads (c) Moments. 205

6.18 FOWT wind turbine response for Misal Case compared with the 50-year extreme loads: (a) Platform motions and blade tip deflections (b) Tension in the fairleads (c) Moments. 206

6.19 FOWT wind turbine response for standstill vs idling conditions. Base Case: a) Platform motions and blade tip deflections (b) Tensions in fairleads (c)Bending moments. 210

6.20 FOWT wind turbine response for standstill vs idling conditions. Veer Case: a) Platform motions and blade tip deflections (b) Tensions in fairleads (c)Bending moments. 211

6.21 FOWT wind turbine response for standstill vs idling conditions. Misal Case: a) Platform motions and blade tip deflections (b) Tensions in fairleads (c)Bending moments. 212

C.1 Q-Q plot of H_s for SNS site, 57.5N, 1.0W (GPD analysis) 230

C.2 Return level plot of H_s for SNS site, 57.5N, 1.0W (GPD analysis) 231

C.3 Q-Q plot of wind speed for SNS site, 57.5N, 1.0W (GPD analysis) . . . 232

C.4 Return level plot of wind speed for SNS site, 57.5N, 1.0W (GPD analysis) 233

C.5 Q-Q plot of H_s for SNS site, 57.5N, 1.0W (GEV analysis) 234

C.6 Return level plot of H_s for SNS site, 57.5N, 1.0W (GEV analysis) 235

C.7 Q-Q plot of wind speed for SNS site, 57.5N, 1.0W (GEV analysis) 236
C.8 Return level plot of wind speed for SNS site, 57.5N, 1.0W (GEV analysis) 237

List of Tables

2.1 Classes of wind power density at 10m and 50m 21

3.1 Comparison of GEV and GPD results for H_s(Caires (2011) vs Plymouth) 87

3.2 Extreme value analysis results of H_s, T_p and u_{10} at Jamaican site(17.5N,77.0W) 88

3.3 Summary of GEV and GPD 50 and 100 year design sea states and wind speeds, Jamaica(17.5N, 77.0W) 96

4.1 Summary Statistics of H_s (m) from 1979 to 2018 for SNS and JCS 104

4.2 Weib3P and lognormal distribution parameters for SNS and JCS, 3h-storms from 1979 to 2018 109

4.3 Load cases for SNS and JCS 121

4.4 Summary of GEV and GPD 50 and 100 year design sea states and wind speeds, Scottish North Sea (57.5N, 1.0W) 121

4.5 Wind turbulence intensity for SNS and JCS 125

5.1 Properties of IEA-15MW Wind Turbine 136

5.2 Properties of UMaine VolturnUS-S Semi-Sub 137

5.3 Properties of UMaine VolturnUS-S Mooring Line 140

5.4 Tower Properties - UMaine VolturnUS-S Semi-Sub 140

5.5 System natural frequency UMaine VolturnUS-S FOWT 143

5.6 Properties of UoP Mooring Line for 100m Deep Water 145

5.7 System Natural Frequency of the 100 m Deep Water FOWT System alongside the solution for the 200 m water depth condition 146

5.8 Mean responses of VolturnUS-S FOWT - SNS and the JCS, normal wave conditions (SNS9, JCS9, etc., are the sea states in Table 4.3 and notes below) 150

5.9 Mean responses of VolturnUS-S FOWT - SNS and the JCS, normal wind and wave conditions (SNS9, JCS9, etc., are the sea and wind conditions in Table 4.3 and notes below) 156

5.10 Maximum responses of VolturnUS-S FOWT - SNS and the JCS, 50-year wind and wave conditions (the sea and wind conditions are in Table 4.3 and notes below) 163

6.1 Properties of DTU 10 MW Reference Wind Turbine (Bak et al., 2013) . . 171

6.2 Wind Field Characteristics of Simulation Cases (Source: Kapoor et al., 2020) 179

6.3 Responses of DTU 10 MW wind turbine for Rated, Base, Veer and Misal load cases, Kapoor et al. (2020) vs present results, 20 km from the hurricane centre 184

6.4 Responses of DTU 10 MW wind turbine for Rated, Base, Veer and Misal load cases, Kapoor et al. (2020) vs present results, 15 km from the hurricane centre 188

6.5 Responses of DTU 10 MW wind turbine for Rated, Base, Veer and Misal load cases, Kapoor et al. (2020) vs present results, 12 km from the hurricane centre 192

6.6 Properties of NREL's 5MW Baseline Wind Turbine (Jonkman & Matha (2011)) 196

6.7 Properties of DeepCwind Semi-submersible Floater (Robertson et al. (2014)) 197

6.8 Properties of DeepCwind Mooring System (Robertson et al. (2014)) . . 198

6.9 System natural frequency NREL's DeepCwind FOWT 199

6.10 Properties of mooring line for DeepCwind at 100 m water depth 200

6.11 Wind Field Characteristics and Sea State of Simulation Cases for DeepCwind 203

6.12 Response of the DeepCwind FOWT in the JCS, Extreme 50-year vs Category 5 Hurricane: a) Base b)Veer c) Misal Load Cases 207

6.13 Response of DeepCwind FOWT in the JCS to Category 5 Hurricane Winds: a) Base b)Veer c) Load Cases - Idle vs Standstill Conditions . . 213

B.1 List of major hurricanes and tropical storms in Jamaica, 1900 to 2018 . 229

Chapter 1

Introduction

1.1 General

A review of the history of wind energy shows that three important factors have driven the development of wind energy technology, namely (Kaldellis & Zafirakis, 2011; Shahan, 2014; Wind-Europe, 2019*a*):

1. The oil crisis of 1973 and 1986, which saw wind turbines evolve from domestic and agricultural applications to utility interconnected wind farm applications;
2. The climate change effect due to the emission of greenhouse gasses (GHGs) such as Carbon Dioxide (CO_2);
3. The nuclear power disasters: 1986 in Chernobyl, Ukraine and Fukushima, Japan, 2011.

These same factors continue to drive the development of wind energy today, with the most persistent being climate change. The factors provide an answer to the question, "Why wind energy development?"

Wind energy is considered a mature renewable energy technology today. Figure 1.1 shows the increase in global wind energy capacity from 1996 to 2018. The development of wind energy dates from AD1, where windmills were used to harness wind energy; to the first onshore wind farm connecting to the grid in the US in 1980; the first fixed-bottom offshore wind farm 1991, in Denmark; to the early stages of the development of floating offshore wind farm by Equinor in September 2009. This resulted in the commissioning of the first floating offshore wind farm, the Hywind Scotland in October 2017. See Shahan (2014), Wind-Europe (2019*a*) and Appendix A for more on the history of wind energy. Mature wind energy technology should be looked at as more than GW of wind power produced per period, since it would also include, inter alia:

1. The establishment of the policy framework to support the development of wind energy;

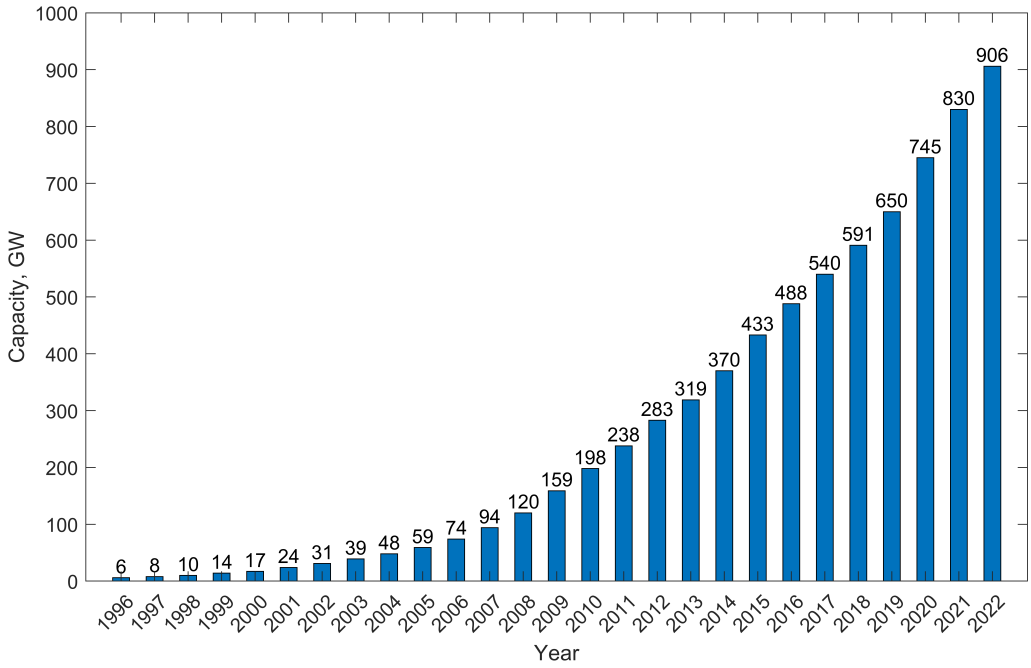

Figure 1.1: Global cumulative installed wind capacity 1998 to 2018 (Source: GWEC, 2012; GWEC, 2018; GWEC, 2019; GWEC, 2023)

2. The provision of jobs, which includes the development of new skills;
3. The development of wind turbine manufacturing companies and other technology within various regions, which has caused wind turbines to grow from kW capacity to MW capacity with larger rotor diameters and blade length;
4. The development of capacity (which includes the development of new equipment, for example cranes to assemble the wind turbines) within the construction sector;
5. The increase in contribution of the construction sector to the GDP within regions.

The increase in the GW of energy each period has these hidden factors at work, which should also be considered to give a holistic view of the growth of wind energy.

The climate change effect continues to drive the need for more renewable sources of energy globally. The United Nations has included this critical global issue as one of their sustainable development goals, under UN sustainable development goal number 13, Climate Action (Sengupta, 2020). Climate change due to global warming is one of the most significant threats to humankind (Papadimitriou, 2004). Anderson et al. (2016) also stated that climate change is a major risk facing humankind. IPCC (2023)

stated that global surface temperature in the first two decades of the 21st century (2001-2020) was 0.99 [0.84 to 1.10]℃ higher than 1850-1900. One of the primary reasons for the climate change effects is the high levels of Carbon Dioxide (CO_2) being emitted into the atmosphere by human caused activities. CO_2 account for 76% of the greenhouse gases being emitted into the atmosphere due to these factors (see Figure 1.2).

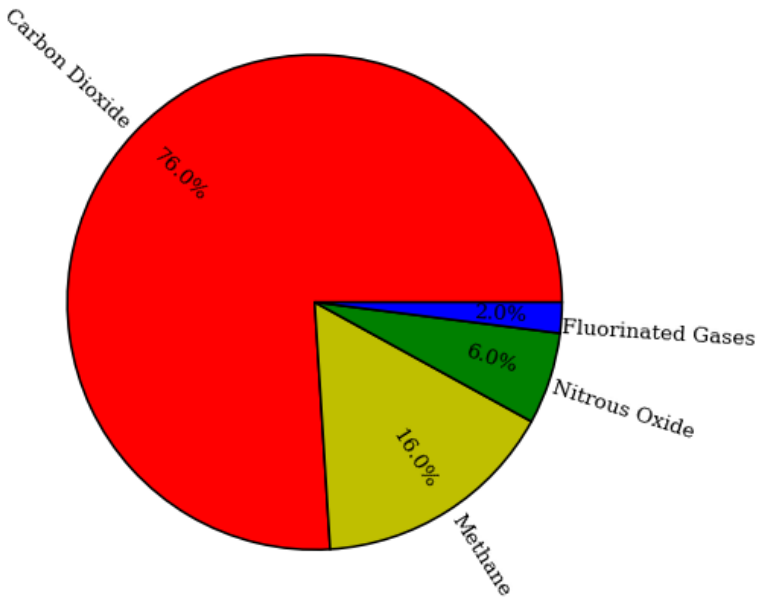

Figure 1.2: Main GHGs emitted globally by human activities (Source: Edenhofer et al. (2014))

In 1987, the United Nations World Commission on the Environment and Development published a report entitled “Our Common Future” (UN, 1987) which argued that pre-industrial CO_2 levels was about 280 parts of CO_2 per million parts of air by volume. This concentration of air reached 340 in 1980; and was expected to double to 560 between the middle to the end of the 21st century. It was also argued that if the concentration of CO_2 doubles from pre-industrial levels, average surface temperature rises could range from 1.5 ℃to 4.5 ℃. This kind of rise in temperatures could result in sea level rising between 25-140 centimetres and inundate low-lying coastal and agricultural areas. It could also disrupt social and political structures of nations. The global average level of CO_2 in the atmosphere as at 2022 was 417.1 ppm (Lindsey, 2023). The highest monthly value of 424 ppm occured in May 2023. Climate change therefore poses a major threat to a sustainable world for us all.

The issue of the effect of climate change on the world’s environment is complex (Anderson et al., 2016). The research that is produced by the authorities in the field of climate

science is still uncertain about the amount of heating that will take place on the earth's atmosphere because of CO_2 emission. However, researchers conclude that what is certain is that the earth's surface will continue to undergo warming due to the emission of GHGs into the atmosphere. The current and potential impacts of climate change on humankind due to the predominant use of fossil fuel based energy sources show that there is a need for alternate sources of energy. Edenhofer et al. (2011) argued that renewable energy is potentially the key source of energy to displace fossil fuels as the world's primary source of energy and hence mitigate against climate change impacts.

Renewable energy is any form of energy that is derived from solar, geophysical or biological sources, that is replenished by natural processes that is equal to or exceeds the rate of its use (Edenhofer et al., 2011). The main sources of renewable energy include wind energy, solar energy, geothermal heat, hydropower, tide and wave, ocean thermal energy and biomass. Wind is said to be the most mature form of renewable energy (Esteban et al., 2011). It is also one of the fastest growing renewable energy technologies globally and accounts for 24% of the world's installed renewable energy capacity (see Figure 1.3). The focus of this study is wind energy and specifically, assessing the behaviour of a floating offshore wind turbine at an appropriate site off the south coast of Jamaica. This includes carrying out analysis to determine its suitability for the proposed site.

In the following sections floating offshore wind concepts are described and the focus of the research project and thesis outline are described in sections 1.8 and 1.9.

1.2 Harnessing Wind Energy

The harnessing of the power from the wind to convert it to electrical energy is done using wind turbines. Wind turbines fall into two broad categories namely, onshore wind turbines and offshore wind turbines. Most of the wind turbines in use today are located onshore. At the end of 2022, offshore wind farms accounted for 7% of the globally installed wind power (GWEC, 2022). Despite onshore wind turbines being greater in abundance they have some disadvantages (Esteban et al., 2011; Kaldellis & Kapsali, 2013). Some of the disadvantages of onshore wind turbines include:

1. Scarcity of appropriate installation sites on-land
2. Public concerns such as noise level and visual impact
3. Land use conflicts (which prevent approvals)

These disadvantages (together with greater and steadier wind resource being available offshore) have created the impetus for the development of offshore wind farms. The

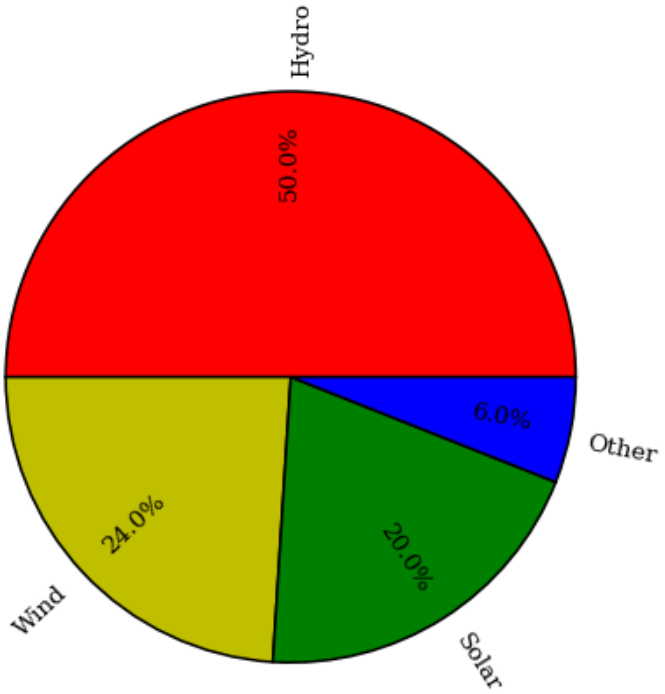

Figure 1.3: Renewable energy generation capacity by energy source (Source: IRENA (2019*b*)

installed capacity of offshore wind has grown yearly from 2008 to 2022 (see Figure 1.4).

1.3 Offshore Wind Turbines

Offshore wind turbines are categorized based on their foundation type. There are two broad categories of offshore wind turbines namely, fixed-bottom offshore wind turbines (OWT) and floating offshore wind turbines (FOWT). The different types of fixed-bottom OWT supports are (Zhang et al., 2016):

1. Monopile foundations
2. Gravity type foundations
3. Tripod foundations
4. Jacket foundations (and variations e.g., twisted jacket)
5. Suction bucket foundations

The most common type of fixed-bottom OWT is the monopile supported OWT (Esteban et al., 2014; Failla & Arena, 2015). According to IRENA (2016a) the typical offshore

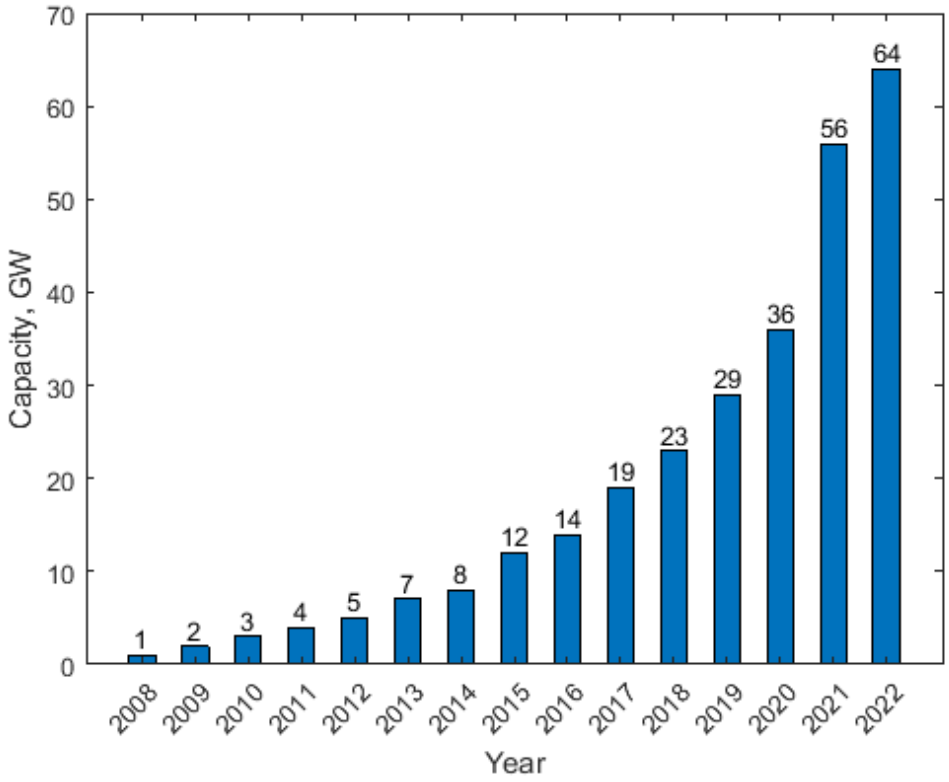

Figure 1.4: Global cummulative offshore wind installed capacity 2008 to 2022 (Source: GWEC (2022))

wind farm had a monopile based foundation between 2001 and 2015. Negro et al. (2017) reported that at the beginning of 2016 about 80% of cumulative globally installed OWT were on monopiles. This figure remains the same at the beginning of 2019 (Wind-Europe, 2019*a*). The monopile based OWT is suitable in areas where there are shallow water depths (DNV, 2014). That is between 0 to 25 m. According to Failla & Arena (2015) monopiles are not suitable in water depths greater than 30 m deep as in those depths they become economically unfeasible. Vázquez et al. (2022) argued that very large monopiles (termed XXL) could be installed to depths up to 70 m. The use of the word could, indicates that these monopiles are yet to be deployed and are in the testing and development stage. This is supported by Sparrevik (2019) who indicated that monopiles supporting large turbines to up to 70 m water depths will be feasible in the near future. The water depths in the North Sea, in which monopile based OWT are installed, range between 0 to 30 m at the beginning of 2016 (Negro et al., 2017). The average water depth of offshore wind farms under construction at the beginning of 2019 is 27.1 m (Wind-Europe, 2019*b*). Malhotra (2007) reported that the water depth for monopile based OWT range between 0 to 30 m, and jackets are suitable

in depths up to 50 m. CarbonTrust (2015) reported that fixed-bottom structures are good for water depths less than 50 m. However, where water depths are greater than 50 m floating supports are recommended (IRENA, 2016c). The next section gives a description of the different types of FOWT.

1.4 Floating Offshore Wind Turbines

There are three main types of floating foundations(floaters), see Figure 1.5, for floating offshore wind turbines (EWEA, 2013; IRENA, 2016b):

1. Semi-submersible(column stabilized)
2. Spar-buoy type
3. Tension-leg platform (TLP)

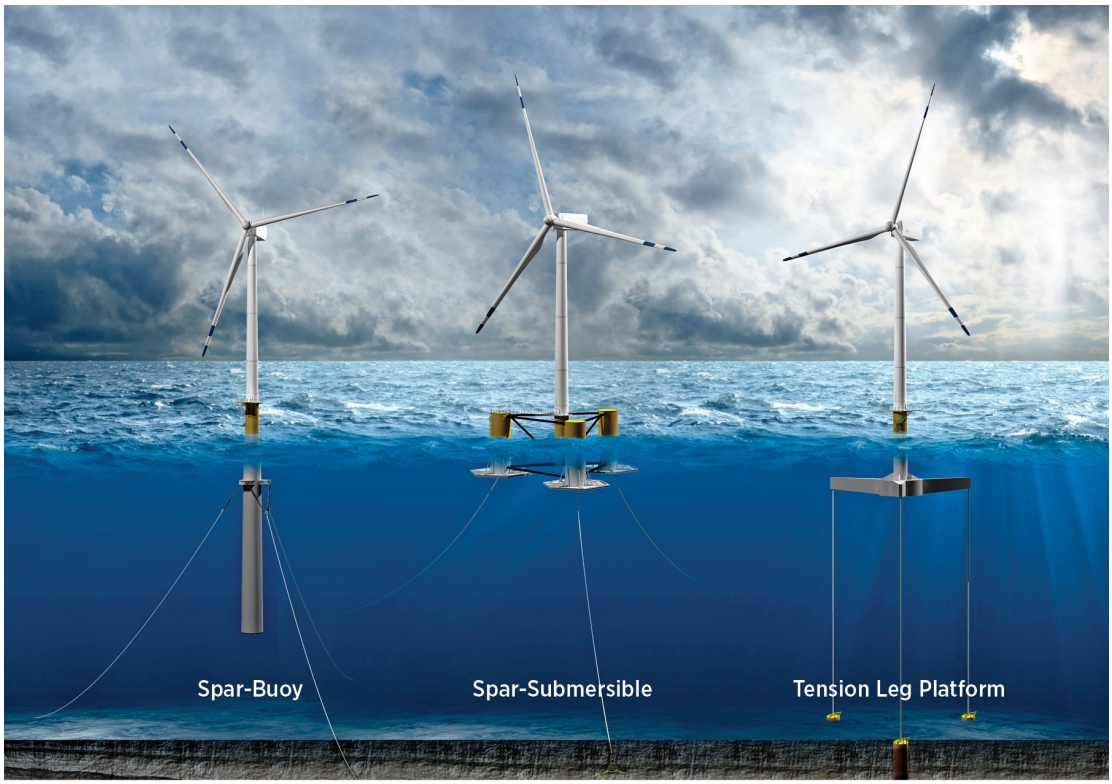

Source: NREL. Illustration by Joshua Bauer, NREL.

Figure 1.5: Types of floating offshore wind turbines (Source: IRENA (2016b))
(Permission has been granted by IRENA/Joshua Bauer of NREL to reproduce this figure)

The floaters are classified in accordance with how they achieve stability under the action of external forces. The semi-submersible (semi-sub) is buoyancy stabilized (Butterfield et al., 2005), the spar-buoy type is ballast stabilized and the TLP is mooring line

stabilized. Wang et al. (2010), Zhang et al. (2016), van Kuik et al. (2016) and Edwards et al. (2023) mentioned four types of floaters by describing the barge type floater as a separate type of floater. However, the barge type floater is also buoyancy stabilized. It will therefore be considered in the same category as a semi-sub for the purpose of this research. The semi-sub will thus be classified (where necessary) as semi-sub, for the column-stabilized type and semi-sub barge, for the barge type.

1.4.1 The Semi-submersible Floater

The semi-sub platform is a buoyancy-stabilized platform made of horizontally spaced columns, which are usually connected via a lattice of bracing or beams. The pontoons have positive buoyancy to counteract both the weight of the wind turbine and mooring system and to provide rotational stability due to motions within the tower and rotor nacelle assembly (RNA). The primary motions are typically dampened out by heave plates, connected to the bottom of the pontoons, which add drag resistance to up and down motions within the water column.

Floating systems like semi-subs require a mooring system to anchor it to the seabed and maintain station keeping within the floating platform. Station keeping in a floater is important because the risers, which carry the electrical transmission cables down to the ocean floor, can only handle a few metres of deflection before they are damaged.

There are typically two types of mooring systems for floating structures such as semi-subs, catenary and taut mooring systems (See Figure 1.6). The catenary mooring system is typically spread over large distances, of say, 100s of metres. The catenary system relies on the self-weight of either chains, or cables, or a combination of chains and cables to provide restraining tensile forces on the floater. The taut mooring system typically extends to the seabed with very little lateral spread and depends on pre-tensioned cables to provide lateral resistance to the floater. Whichever type of mooring system is used, the design of the anchor has to be designed for the specific soil conditions that exist in an area.

One of the advantages of the semi-sub is that is has lower draft requirements and this allows for more flexible and simpler installations. It can be manufactured and assembled at quayside and towed out to the location for installation, without the need for heavy-lift installation vessels (DOE, 2019). One of the main disadvantages is that it requires a large heavy structure, thus large material and manufacturing costs of the hulls and mooring systems (CarbonTrust, 2015). Some examples of semi-subs are VolturnUS by DeepCWind Consortium (Figure 1.7), WindFloat by Principle Power (Figure 1.8) and Floatgen by IDEOL, semi-sub barge (CarbonTrust, 2015). The prototype for the DeepCWind project was installed off the Gulf of Maine, US in 2013. The Wind-

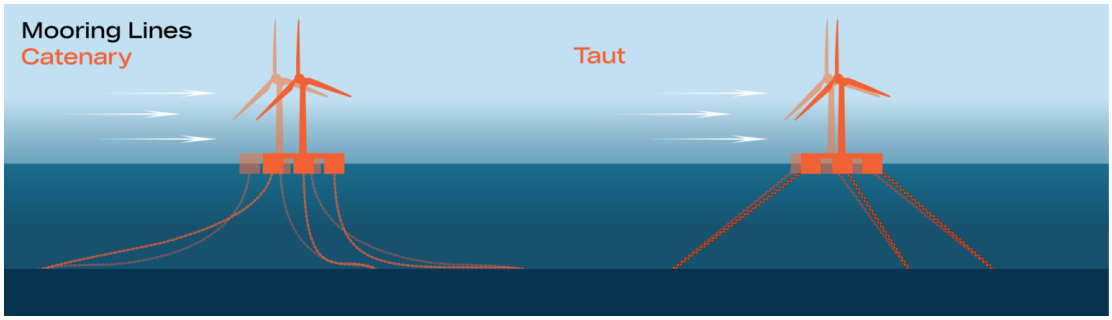

Figure 1.6: Catenary and Taut Mooring Configurations (Source: World Forum Offshore Wind)
(Permission has been granted by Andrew Lowery of Bekaert to reproduce this figure)

Float was installed in 2011 in Portugal and the Floatgen was installed in 2018 in France (CarbonTrust, 2015).

Classification:	Semi-sub	**Primary material:**	Concrete
Depth range:	Undisclosed	**Moorings:**	Undisclosed
Turbine axis:	Horizontal	**No. blades:**	3
Industrial partner(s):	-	**TRL:**	3
Full-scale prototype:	2018	**Pre-commercial array:**	TBC

Figure 1.7: Properties of VolturnUS Semi-sub (Source: CarbonTrust (2015))
(Permission has been granted by Taylor Ward of University of Maine, Advanced Structures and Composites Center to reproduce this figure)

1.4.2 The Spar-buoy Floater

The Spar mounted wind turbine relies on a heavy deep ballast to provide resistance to overturning moments. The Spar-buoy is the vertical portion of the platform. It is typically hollow with a large mass placed at the deepest portion of the buoy. The mass within the buoy can be adjusted so that the spar can float higher or shallower within the water as needed for stability requirements. The large mass provided at deep locations provides a strong righting moment to counter roll or pitch motions within the RNA. The buoy portion of the spar is typically connected to the tower through a transition piece located above the water line, where the highest expected wave that the wind turbine might see in storm conditions occur. Station keeping of the spar is provided via mooring

Classification:	Semi-sub	**Primary material:**	Steel
Depth range:	40m-1000m	**Moorings:**	3 catenary
Turbine axis:	Horizontal	**No. blades:**	3
Industrial partner(s):	EDPR; Repsol; Pilot Offshore; Atkins	**TRL:**	4
Full-scale prototype:	2011	**Pre-commercial array:**	2018

Figure 1.8: Properties of Windfloat Semi-sub (Source: CarbonTrust (2015))
(Permission has been granted by Fabio Espirito Santo of Principle Power to reproduce this figure)

lines. The Spar-buoy is usually installed in water depths of 100m and above because of the large draft requirements. The simple structure of the Spar buoy makes it easy to fabricate but because of the large depth requirements it is hard to transport and install (CarbonTrust, 2015). In addition, the cost to do geotechnical investigation at those great depths is also a challenge. An example of a Spar-buoy floater is the HyWind by Equinor (formerly Statoil). The HyWind (CarbonTrust, 2015) was installed off the coast of Norway in 2009.

1.4.3 The Tension Leg Platform (TLP) Floater

The TLP derives its stability from the tension in the mooring lines. It is a semi-submerged structure anchored to the seabed with tensioned mooring lines. In essence, the TLP could be thought of as a lighter version of a semi-sub where the tensioned legs instead of buoyancy provides stability. Although the TLP is a relatively lighter structure, because of the tendons it can be difficult to install. In addition, because it is tension line stabilized if one of the tension lines fail then the structure is at risk of failure. Examples of the TLP are PelaStar (Figure 1.9) by Glosten and Blue H TLP (Figure 1.10) by Blue H Group. The Blue H TLP was installed off the coast of Italy in 2008 (CarbonTrust, 2015).

1.5 Trends in FOWT Support Structures

In the development of a FOWT project, one of the most important considerations is the type of support structure that is used. The type that is selected depends on its suitability for the characteristics of the site where it is installed, the ease of fabrication and installation, as well as the cost of installation.

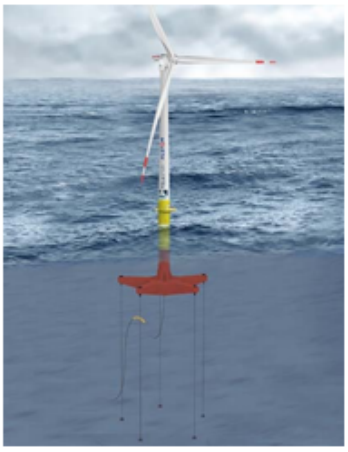

Classification:	TLP	**Primary material:**	Steel
Depth range:	70-200m	**Moorings:**	5 taut-leg
Turbine axis:	Horizontal	**No. blades:**	3
Industrial partner(s):	Alstom	**TRL:**	3
Full-scale prototype:	TBC	**Pre-commercial array:**	TBC

Figure 1.9: Properties of Pelastar (Source: CarbonTrust (2015))
(Permission has been granted by Benjamin B. Ackers of PelaStar, LLC to reproduce this figure)

Classification:	TLP	**Primary material:**	Steel
Depth range:	50-250m	**Moorings:**	3 taut-leg
Turbine axis:	Horizontal	**No. blades:**	3
Industrial partner(s):	-	**TRL:**	3
Full-scale prototype:	2018	**Pre-commercial array:**	2020

Figure 1.10: Properties of Blue H TLP (Source: CarbonTrust (2015))
(Permission has been granted by Nico C.F. Bolleman of Blue H Engineering to reproduce this figure)

EWEA (2013) outlined 35 different floating offshore wind projects globally and the semi-sub accounted for 37%, the spar for 20% and the TLP for 9%, while hybrids accounted for 34%. It should be noted that some of these hybrids were listed as floaters and might be considered semi-submersibles. DOE (2019) stated that of all the demonstration projects in the pipeline in 2018, 95.2% were semi-subs (this includes 0.8% for the barge type), 4.0% were Spar-buoy and the balance of 0.8% were TLP. DOE (2017) reported that of the FOWT as of June 2017, 70.4% were semi-subs (this includes 15.8% for the barge type), 14.8% were Spar-buoy, 7.4% were TLP and 7.4% were semi-spar hybrid. According to CarbonTrust (2015), 33 different floater concepts were discovered globally. The semi-sub accounted for $\sim$ 43%, TLP accounted for 21%, spar accounted for 18% and hybrids accounted for 18%.

Hannon et al. (2019) argued that the Spar-buoy is the most common foundation type by installed capacity. However, the trend shows that most of the FOWT projects in the pipeline will use a semi-submersible floater. The semi-submersible will become the most dominant floater by 2020, accounting for 65% of installed capacity. This is because it can be fabricated and assembled quayside and wet towed from the port to the respective site. This eliminates the need for heavy-lift installation vessels. They are also flexible, in that they can be deployed in either shallow or deep water (CarbonTrust, 2015; DOE, 2019; Hannon et al., 2019). DOE (2022) shows that of the projects in the pipeline, the semi-submersible type floater is the most favoured, accounting for 79.6 % of future FOWT projects.

The next section will focus on some of the challenges that have to be taken into consideration when analyzing FOWT.

1.6 Some of the Challenges in Analysing FOWT

At present, there are a large number of floater concepts under development and a large number of projects in the pipeline. The existing conditions determine the floater that is selected for development. These conditions include water depth, sediment conditions at the seabed, local infrastructure and local supply chain capabilities. However, regardless of the floater that is selected, the analysis of a floating wind turbine is more complex than onshore and fixed-bottom offshore wind turbines. The complexities in the analysis of onshore wind turbines are due primarily to the aerodynamic loads from the air passing over the blades. In the case of offshore wind turbines, not only are aerodynamic loads accounted for but the hydrodynamic loads also have to be taken into consideration. This makes for a more complex analysis when compared to an onshore wind turbine. For fixed-bottom offshore wind turbines such as those that are on monopiles analysis is carried out on the structure as a whole, taking wind and wave

loads into consideration. The critical hydrodynamic loads would be those that occur due to the impact of a wave against the monopile support. In addition, the periodic behaviour of waves would require fatigue analysis to be done to determine the effect of the wave loads on the monopile over its useful life. The analysis of a floating wind turbine is more complex. It is a floating structure and therefore has to be analyzed for movements in six degrees of freedom. The surge, sway and heave motions are the three translational degrees of freedom and roll, pitch and yaw motions are the rotational degrees of freedom (See Figure 1.11).

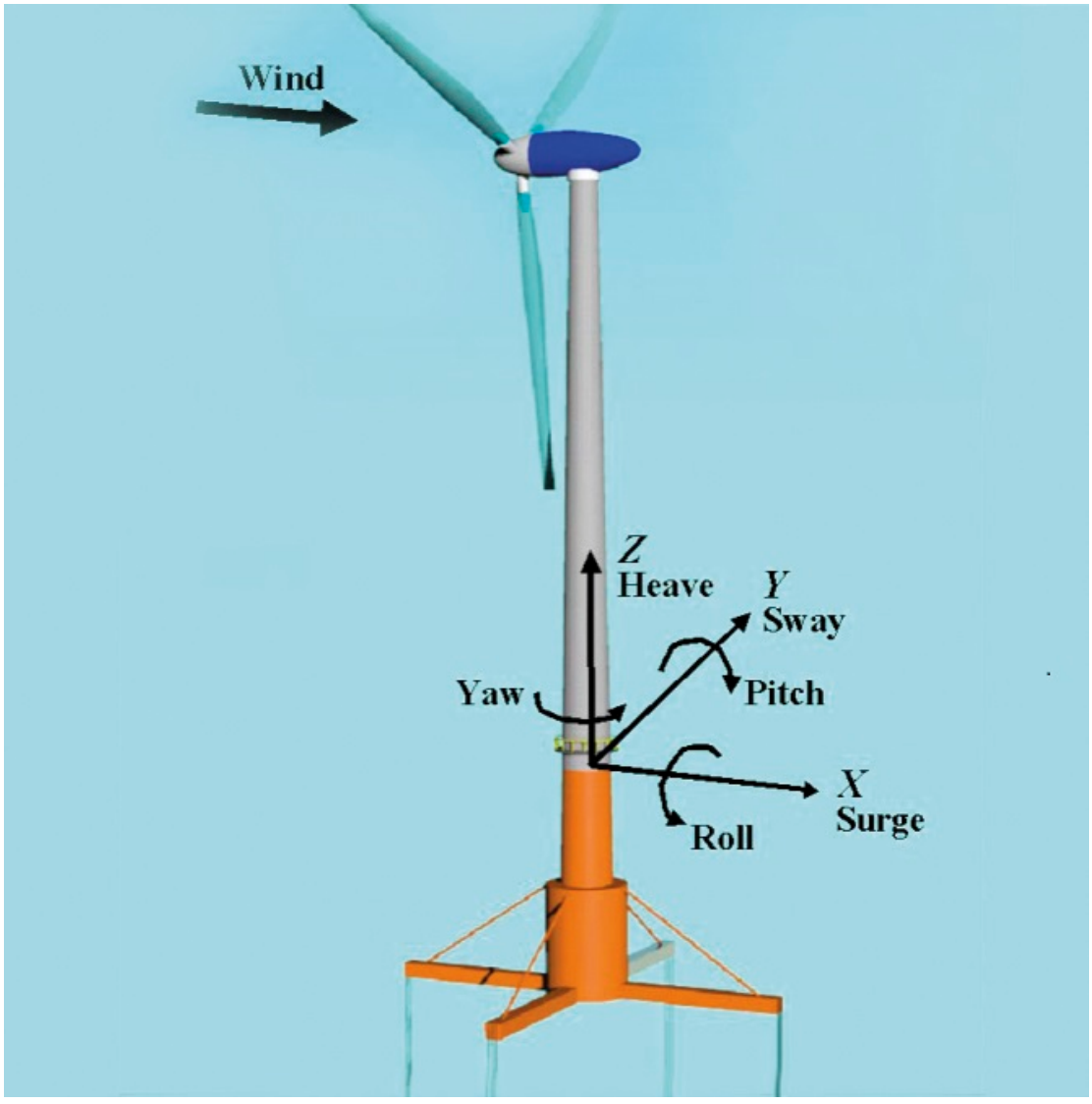

Figure 1.11: Illustration showing the six degrees of freedom of a FOWT (Source: `www.windpowerengineering.com` from an article written by Lloyd's Register)

(Permission has been granted by Wind Power Engineering & Development to reproduce this figure)

A floating structure must provide enough buoyancy to support the weight of the turbine and to restrain pitch, roll and heave motions within acceptable limits. The turbine design philosophy may be impacted if the platform dynamics require a more dynamically complaint machine (Butterfield et al., 2005). It should be noted that in addition to meeting these technical requirements, the floater must also be economical. Balancing the technical and economic requirements is the primary reason why the design of a FOWT is so challenging. Jonkman & Matha (2011) carried out dynamic analysis on three wind-turbine floater concepts. They indicated that the knowledge gained from analyzing floating platforms in the oil and gas industry can be transferred to the floating offshore wind industry, but there are some challenges. The core challenge being to design a floater that is cost effective. Some of the main challenges outlined when carrying out design of a FOWT were as follows (Wang et al., 2010; Bae et al., 2011; Jonkman & Matha, 2011; Lefebvre & Collu, 2012; Arshad & O'Kelly, 2013; Kim & Kim, 2016; Tran & Kim, 2016; van Kuik et al., 2016; Zhang et al., 2016; Liu et al., 2017b; Kim et al., 2019; Le et al., 2019):

1. Introduction of low frequency modes that can affect the aerodynamic damping and stability of the system.
2. The possibility of significant translational and rotational motions of the support structure that can couple with the motions of the rotor nacelle assembly (RNA) which can introduce complex transient aerodynamic flow field conditions.
3. The use of support structures that need not be slender and cylindrical, such that hydrodynamic radiation, diffraction and other wave effects can become important.
4. The potential for complicated construction, installation, operations & maintenance and decommissioning procedures.
5. The presence of a mooring system, which adds to the complexity of the analysis.
6. Provision of a structure that has a good wave response to prevent the structure from experiencing large dynamic load or compromise wind-turbine performance.
7. The coupled dynamic analysis of the floater, the mooring system and the wind turbine (including the control system).
8. Achieving survivability in extreme environmental conditions.
9. The ability to predict, accurately, critical loads due to various turbulent-wind and stochastic-wave conditions.

The main challenges that are involved in the design of a FOWT system have been identified. To identify and deal with these challenges, various aspects of the FOWT have been studied by the authors above. This includes studies on control system dynamics, motion of the floater in different sea environments and comparative analysis of different floaters to determine the most appropriate. However, of the various challenges, the one about the determination of the loads on a FOWT structure (Butterfield et al., (2005); Tran & Kim,2016) is significant. Butterfield et al. (2005) mentioned that one of the immediate challenges common to all support structure designs is the ability to predict loads and resulting dynamic responses of the coupled wind turbine and platform system to combined stochastic wave and wind loading. Further, it was stated that because of the nonlinearities associated with the aerodynamics and hydrodynamics, the simulation of FOWT systems is typically run in the time domain. This requires that the wind and wave data that is available for a certain period (say 20 years) be simulated to capture the range of possibilities of the loads on the system. It was concluded that extrapolating to the extreme load possible in the presence of two different stochastic load environments is not a well-developed technical capability. Huebler et al. (2018) argued that as turbines are built in increasingly harsher environmental conditions and as weather conditions tend to become more extreme the consideration of ULS loads is a topic of relevance. The question was also posed as to whether the current design load cases (DLCs) in the OWT standards are adequate. DLCs for ULS design given in the IEC:61400 wind turbine standard are broken down into three categories: a) extrapolated 50-year return period values for normal operation conditions (DLC1.1) b) ULS loads from extreme environmental conditions with a return period of 50 years (DLC6.1) and c) fault and controller actions (DLC2.1). A comparison was made between a probabilistic version of DLC1.1 (for ULS) and various deterministic DLCs for extreme events. This comparison was done using the National Renewable Laboratory (NREL) 5MW monopile based OWT and the FAST code. (FAST is a time domain wind-turbine simulation tool that is used in analyzing wind turbines. It couples structural dynamics, aerodynamics, wind-turbine control, and hydrodynamics for two and three bladed horizontal axis wind turbines. More is said about FAST in chapter 2, literature review). The results from the analysis showed that probabilistic extrapolated ULS values were high, mainly because of wave resonance effects. These loads were greater than the deterministic 50-year ULS DLCs loads from the OWT standards. It was therefore concluded that the current DLC approach used by OWT standards might not be always conservative. Therefore, consideration should be given to the DLC cases used in the OWT standards as they might not give be the most extreme loads on the wind turbine. The argument put forward by Butterfield et al. (2005) is still relevant today. There is still need for research in the determination of the extreme load cases and the

extrapolation of the load cases over the life cycle of the turbine.

The determination of the loads on an offshore structure is a foundational part of the design process. Accurate loads will guarantee that the output results are credible. The determination of the design sea state and wind speed is one of the critical steps in computing the loads. The extreme design sea state is determined by finding the n-year significant wave height (H_s) and wave period (T_p) by statistical analysis. This is done using historical data. Chakrabarti (1987) indicated that a long-term probability defines events and extreme value statistics for a period of the order of 20 to 100 years and that the maximum value of n used for the n-year return level when designing coastal structures is usually 50. The design load cases (DLC) given in the DNV GL guideline, DNV-GL (2016), are based on the 50-year event. A higher year event, say the 100-year event, can also be used where necessary.

1.7 Research Focus

The GWEC (2022) reported the UK accounted for 13.4 % of global offshore wind installations in 2022 and are the market leaders in Europe. The location of the wind turbines in the UK is the North Sea. The wind turbine systems that have been deployed in the UK are therefore designed to suit the North Sea conditions but the environmental conditions in other jurisdictions around the world vary. There is no offshore wind turbine in the Caribbean and the specific response of a wind turbine in Caribbean waters is unknown. In addition, no studies have been conducted to determine which type of floating support structure would be most appropriate for the environmental conditions of the Caribbean. Furthermore, when determining the extreme sea state one of the methods used is the environmental contour method. This would yield a set of n-year contours of H_s and T_p. One of the critical steps in this process is the determination of the statistical distribution that best fits the marginal distribution of H_s data. Presently there have been no studies discovered in the literature that identify a statistical distribution that is suitable for the environmental conditions in the Caribbean and that would therefore be appropriate for determining the sea state. The focus of this research is to investigate design approaches for a FOWT deployed in the Caribbean Sea environment. This is done by first selecting an appropriate site location off the south coast of Jamaica. The approach to determine the sea state and in particular, the kinds of distributions required to predict the extreme sea state are investigated. In addition, an appropriate floating support structure is selected and the structural and hydrodynamic performance of the system are investigated. The sea state is determined using historical data at the respective site. The sea state is inputted into a numerical model that is developed using the OpenFAST (formerly FAST) software code.

As was mentioned previously, the specific response of FOWT systems in the Caribbean is unknown and therefore another aspect of the research is to compare the response of the system within an area in which the response is well known. That location is the North Sea. An appropriate location is selected in the North Sea and the sea state and response of the FOWT system is determined in the same manner as was done for the Jamaica site. The primary aim of the research, therefore, is to find out if a FOWT system that has developed for the North Sea could be used off-the-shelf in the Jamaica Caribbean Sea. This study on offshore wind energy aligns with the renewable energy development objectives of the government of Jamaica (GOJ) as they intend to develop the renewable energy capacity of Jamaica utilizing, inter alia, wind energy (GOJ, 2010).

The objectives of the research are:

1. To investigate the distribution models used to develop a design sea state and to determine the most appropriate models for the given site conditions in the Caribbean Sea and the North Sea.
2. To develop a univariate extreme-value analysis sea-state and determine the extreme wind speed. That is, to determine the 50 and 100-year return levels for significant wave height (H_s), significant wave period (T_p) and mean wind speed (u_{10}) for the environmental conditions at both site locations.
3. To develop a multivariate extreme value analysis sea state using the environmental contour method. Specifically, to determine the 50-year return levels at both locations.
4. To assess the performance of the FOWT system in both sea environments (determined in item 2 and 3 above) utilizing a state-of-the-art FOWT numerical model together with NREL's FAST code and the appropriate design load cases from the DNV GL guideline and other approved wind turbine design standards.
5. To assesss the performance of the FOWT system in hurricane conditions of the Caribbean to see how it compares with the 50-year extreme loads in 2) and 3) above.

1.8 Outline of the Thesis

The rest of the Chapters contain the work that is done to determine if a FOWT system in the SNS can be used off-the-shelf in the JCS.

- *Chapter 2* presents a review of the literature on the analysis and design of FOWT systems. It covers areas such as wind resource assessment, sea conditions of

the Caribbean compared to other geographical areas such as the UK, development of extreme design sea states, design manuals and standards for FOWT design and numerical modelling of floating offshore wind turbines.

- *Chapter 3* demonstrates how wind and wave data for the Jamaica Caribbean Sea are used to determine the univariate extreme sea (H_s, T_p) and extreme wind speed. This is done by using extreme value analysis to determine the n- year return levels for significant wave height and wave period (H_s, T_p) and wind speed (u_{10}).

- *Chapter 4* is an extension of *Chapter 3* and uses multivariate extreme value analysis to determine the extreme sea state in the Jamaica Caribbean Sea and the Scottish North Sea. In particular, the environmental conditions in the Jamaica Caribbean Sea (JCS) are compared with the environmental conditions in the Scottish North Sea (SNS). The normal sea state and wind speeds, the extreme wind speed and the wind turbulence intensity at both locations are determined as appropriate and compared.

- In *Chapter 5*, the extreme sea state and wind speed for the SNS and the JCS are used as input to an OpenFAST numerical model of the 15MW VolturnUS-S FOWT system. It assesses the floater dynamics and structural dynamics of this large FOWT system in normal sea conditions and extreme environmental conditions (50-year) at the SNS and JCS sites.

- *Chapter 6* extends the work in *Chapter 5* to examine the behaviour of a FOWT system in hurricane conditions. Category 5 hurricane conditions from the North Atlantic are simulated in the wind field simulator, TurbSim and the hurricane wind conditions are inputted in the OpenFAST software code to determine the floater dynamics and structural dynamics of a selected FOWT system. The specifc aspects of a FOWT that are at risk in the event of a hurricane are highlighted.

- Chapter 7 outlines the conclusions and recommendations of the research.

Chapter 2

Literature Review

2.1 General

Following from the aim and objectives given in chapter 1, this chapter presents a review of the literature on the analysis and design of FOWT systems. It covers areas such as wind resource assessment, sea conditions of the Caribbean compared to other geographical areas as appropriate, development of extreme design sea states, design manuals and standards for FOWT design and numerical modelling of floating offshore wind turbines. The purpose of the literature review is to assess some of the past work that has been done on the analysis and design of a FOWT to get an idea of the approaches that have been taken, problems that have been encountered and best practices that have been used in carrying out work of this nature. It informs the approach that is taken in carrying out this study and provides a foundation for the findings that are determined.

A FOWT system can be captured in one illustration (see Figure 2.1). It shows the primary components of the system and the loads acting on the system. The system includes the rotor nacelle assembly (RNA), the tower, the floater, and the mooring lines and anchors. The loads generated from the wind, acts on the rotor blades and the tower, the hydrodynamic loads, from the wave, acts on the floater and the mooring line and reactions are generated at the anchors. Although the analysis of a FOWT is a complex process, the breaking down of the system in its componential parts makes something that is complex appear somewhat simple. It is believed that this simple illustration brings into clearer focus the system that is being worked on for this research and on which the problems are being solved. We can always return to this model to understand and remind ourselves of the problem that is being investigated. It is presented first to give the reader an idea of where we are going before we get there, as all of the ensuing discussions is about this model.

2.2 Wind Resource Assessment

Among the first activity that is usually carried out when planning to undergo wind turbine development, is the determination of the availability of the wind resource. One of the primary factors used to determine if a site is suitable for placing a wind farm is

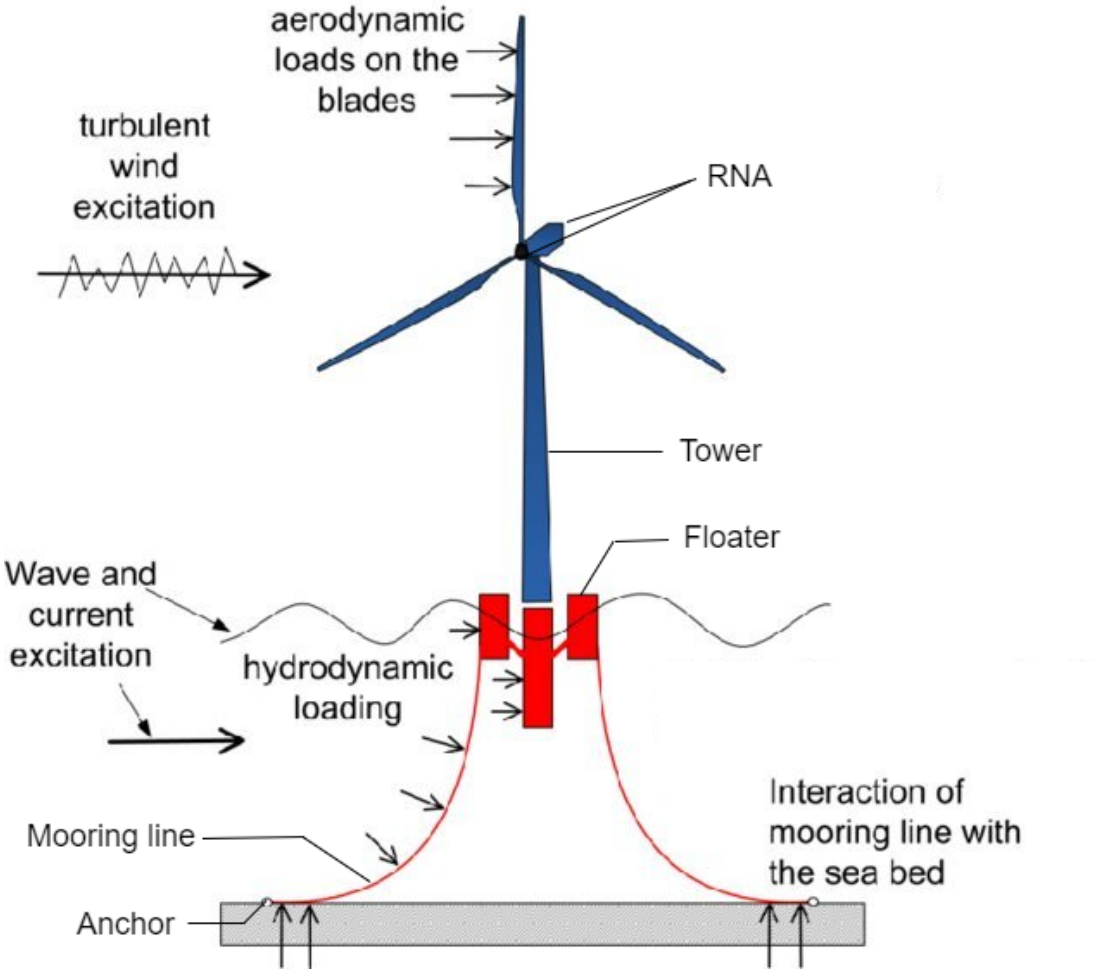

Figure 2.1: The FOWT concept (Adapted from: Manolas et al., 2020)
(Permission has been granted by Dimitris Manolas to reproduce this figure)

access to good quality wind resource (ETI, 2015). Wind resource estimates are classified based on wind power classes ranging from 1 to 7 (NREL, 1997). The original wind-power class scale was developed by Elliott & Barchet (1980) of National Renewable Energy Laboratory (NREL). Table 2.1 shows the wind-power class scale at 10m and 50m above ground level.

Wind power density. The wind power, P, available from the wind is given by Chadee & Clarke (2014):

$$P = \frac{1}{2}\rho A U^3 \tag{2.1}$$

where ρ is the density of air, A is the area swept out by the wind turbine blades in a vertical plane perpendicular to the wind flow, and U is the wind speed. The wind power

Table 2.1: Classes of wind power density at 10m and 50m

Wind Power Class	10m		50m		General Description
	*Wind Power Density(W/m^2)	Wind Speed(m/s)/(mph)	*Wind Power Density(W/m^2)	Wind Speed(m/s)/(mph	
1	<100	<4.4(9.8)	<200	<5.6(12.5)	Poor
2	100-150	4.4(9.8)/5.1(11.5)	200-300	5.6(12.5)/6.4(14.3)	Marginal
3	150-200	5.1(11.5)/5.6(12.5)	300-400	6.4(14.3)/7.0(15.7)	Useful
4	200-250	5.6(12.5)/6.0(13.4)	400-500	7.0(15.7)/7.5(16.8)	Good
5	250-300	6.0(13.4)/6.4(14.3)	500-600	7.5(16.8)/8.0(17.9)	Very Good
6	300-400	6.4(14.3)/7.0(15.7)	600-800	8.0(17.9)/8.8(19.7)	Excellent
7	>400	>7.0(15.7)	>800	>8.8(19.7)	Superb
*The wind power densities are the mean wind power densities at 10m and 50m above ground.					

Source: Elliott & Barchet (1980); www.daviddarling.info/encyclopedia/W/AE_power_density.html

per unit area is referred to as the wind power density. It is also referred to as the mean wind energy flux and is a measure of the amount of energy in the wind (Elliott et al., 1987). Wind power density, *WPD*, is computed as follows:

$$WPD = \frac{1}{2}\rho U^3 \tag{2.2}$$

WPD can be determined as follows for hourly wind data (Elliott et al., 1987):

$$WPD = \frac{1}{2n}\sum_{i=1}^{n}\rho_i U_i^3 \tag{2.3}$$

where *WPD* is the mean wind power density (W/m^2) in a vertical plane perpendicular to the wind direction, n is the number of observations in the averaging period, ρ_i is the air density (kg/m^3) at the ith observation time and U_i is the wind speed (m/s) at the ith observation time.

The WPD can also be computed using wind-speed distribution summaries of wind speed data. The summaries are usually expressed as frequency of wind speeds within several ranges or intervals of wind speed. If a frequency distribution of observed wind speed is available, WPD is computed as follows:

$$WPD = \frac{1}{2}\rho\sum_{j=1}^{c} f_j U_j^3 \tag{2.4}$$

where WPD is the mean wind power density (W/m^2) in a vertical plane perpendicular

to the wind direction, ρ is the mean air density (kg/m^3), c is the number of wind speed intervals, f_j is the frequency of occurrence of winds in the jth interval and U_j is the median wind speed of the jth interval.

Elliott et al. (1987) stated that the mean wind speed alone is not sufficient to describe the wind energy resources at a particular site. This also applies to the wind power density. The wind power density alone is also not adequate to describe the wind energy characteristics at a site. The stability or sustainability of the wind at the site location is also essential. A site may have an acceptable wind speed at a particular period but it is not sustainable for long durations. In order to account for the sustainability of the wind, and therefore more accurately characterize the quality of the wind resource at a site, the parameters of the distribution are also required. The two-parameter Weibull distribution has been found to agree well with the frequency distributions of observed wind data, including those taken over water surfaces (Chadee & Clarke, 2014). The two-parameter Weibull distribution has a distribution function of the form (Elliott et al., 1987):

$$F(U) = \left(\frac{k}{c}\right)\left(\frac{U}{c}\right)^{k-1} exp\left[-\left(\frac{U}{c}\right)^{k}\right] \tag{2.5}$$

where c is the scale parameter with units of wind speed, k is the dimensionless shape parameter, which is an indication of the width of the distribution and U is the mean wind speed. In real terms, k is an indication of whether the wind is steady/stable or variable. The greater the value of k, the steadier the wind. It is a measure of the degree of sustainability of the wind power for a given WPD. Once the parameters of the Weibull distribution have been determined, the mean wind power density can be computed as follows (Chadee & Clarke, 2014):

$$WPD = \frac{1}{2}\rho c^3 \Gamma\left(1+\frac{3}{k}\right) \tag{2.6}$$

where Γ is the Gamma function. Now the mean, U, is given by:

$$U = c\Gamma\left(1+\frac{1}{k}\right) \tag{2.7}$$

rearranging this equation in terms of c, and substituting into equation 2.6, WPD is given by (Elliott et al., 1987):

$$WPD = \frac{1}{2}\rho U^3 \left[\frac{\Gamma(1+3/k)}{\Gamma^3(1+1/k)}\right] \tag{2.8}$$

The stability of the wind can also be measured using two indices, the coefficient of variation index (C_v) and the monthly variability index (M_v) (Costoya et al., 2019; Zheng & Pan, 2014; Zheng et al., 2018). The C_v is given by:

$C_v = S/\bar{X}$

where S is the standard deviation of the respective variable, wind speed in this case, and $\bar{X}$ is the mean value of the wind speed.

The M_v is given by (Costoya et al., 2019):

$M_v = (PM_1\text{-}PM_2)/P_{year}$

where PM_1 and PM_2 are the average WPD calculated at the months with the highest and the lowest mean WPD, respectively. P_{year} is the annual average WPD. The smaller the values of C_v and M_v the more stable the wind resource.

The important thing to note is that regardless of whether k or C_v and M_v are used to determine the degree of stability, the WPD should always be considered in combination with the stability parameter as this gives the full characterization of the quality of the wind resource. Elliott et al. (1987) underscored this by stating that the mean wind speed alone is not a reliable indicator for comparing the wind energy resource for different areas or different seasons that may have different Weibull k values (or C_v and M_v if that is the parameter being used to assess the stability of the wind). Therefore, the wind power class (given in Table 2.1) should not be the only factor used to classify the quality of the wind resource within a particular location. It should always be used in conjunction with the wind power stability.

Now that the principles of characterizing the quality of the wind resource have been presented, we will look at the quality of the wind resource in different regions across the world. Particular attention is paid to the Caribbean region and the North Sea because they are the geographical locations of the wind turbine, which is currently under study.

2.2.1 Quality of the wind resource in different regions worldwide

Wind speed. Zheng & Pan (2014) in using 6-hourly wind speed data from 1988 to 2011 (24 years) to assess the global ocean wind resource, defined the effective wind speed as the wind speed that is suitable for the development of wind energy resources and it ranges from 5.0 to 25 m/s. In considering annual effective wind speeds, Zheng & Pan (2014) showed that the large areas of consistently high effective wind speeds were mainly distributed around the Southern Hemisphere westerlies (> 80%), the Northern Hemisphere westerlies (> 70%), the Northern Hemisphere near 10 deg. N ($\approx$ 80%)and about 20 deg. S in the Southern Hemisphere ($\approx$ 80 to 90%). The North Sea is located in the Northern Hemisphere westerlies region and the Caribbean is located in

the Northern Hemisphere near 10 deg. According to Zheng & Pan (2014), the occurrence of the effective wind speed across the global ocean is high, that is above 60%. It also shows that the effective wind speed within the Caribbean Sea and the North Sea would be considered high. Costoya et al. (2019) in studying the future projections of the mean wind speed for the Caribbean over the 2019 to 2099 period showed that the mean wind speeds off the south coast of Jamaica ranged between 4 to 6 m/s. Chadee & Clarke (2014) carried out an assessment of the wind energy potential of the Caribbean using near surface reanalysis data. It was shown that the wind speeds off the south coast of Jamaica ranged between 6.0 and 7 m/s and the prevailing wind was from the east. Elliott et al. (1987) showed that the average annual wind speed off the south coast of Jamaica was 5.5 m/s and the prevailing wind was from the east. These all indicate that the effective wind speed necessary to develop wind energy resources in the respective location is satisfactory. Although this study gave no information about the resources in the North Sea, it was observed, based on the work by Zheng & Pan (2014) that the effective wind speeds in the North Sea are greater than the effective wind speeds in the Caribbean. To confirm this, the global wind atlas is used to compare the mean wind speed at the site location in Jamaica (17.5N, 77.0W) with the wind speed of the Vattenfall OWT, UK (53.038N, 2.61W). The mean wind speed at the site is found to be 5.96 m/s at 10 m and the mean wind speed at the named location in the North Sea is found to be 7.61 m/s (see Figures 2.2 and 2.3). At 50 m, the mean wind speeds were 7.08 m/s for the Jamaica site and 8.95 m/s for the respective location in the North Sea. These are satisfactory resources based on the classification in Table 2.1 and confirms that the effective wind speeds in the North Sea are greater than those in the Caribbean Sea. If we were to consider the wind speeds at 100m (approx. hub height), the mean wind speeds would be 7.73 m/s for the Jamaica site and 9.68 m/s for the North Sea. It was indicated in OREAC (2020) that at 100m a wind speed of 7.0 m/s is the minimum wind speed required for a wind turbine site to be considered economically viable.

Wind power density. Zheng & Pan (2014) showed that the using annual average values, the areas of highest wind power density are distributed mainly around the Southern Hemisphere westerlies (800-1600 W/m^2) and the Northern Hemisphere westerlies (600-1000 W/m^2). Wind power density in the middle and low latitude waters (Caribbean region) ranged from 200 to 400 W/m^2. Zheng and Pan (2004) further stated that areas with wind power densities above 200 W/m^2 were classified as energy rich regions. From Table 2.1, the wind energy resources in the Caribbean would range from good to excellent and the resources in the North Sea would be classified as superb. They are both located in energy rich regions. Zheng et al. (2018) in carrying out studies on the global offshore wind energy resource showed that the potentially rich areas for offshore

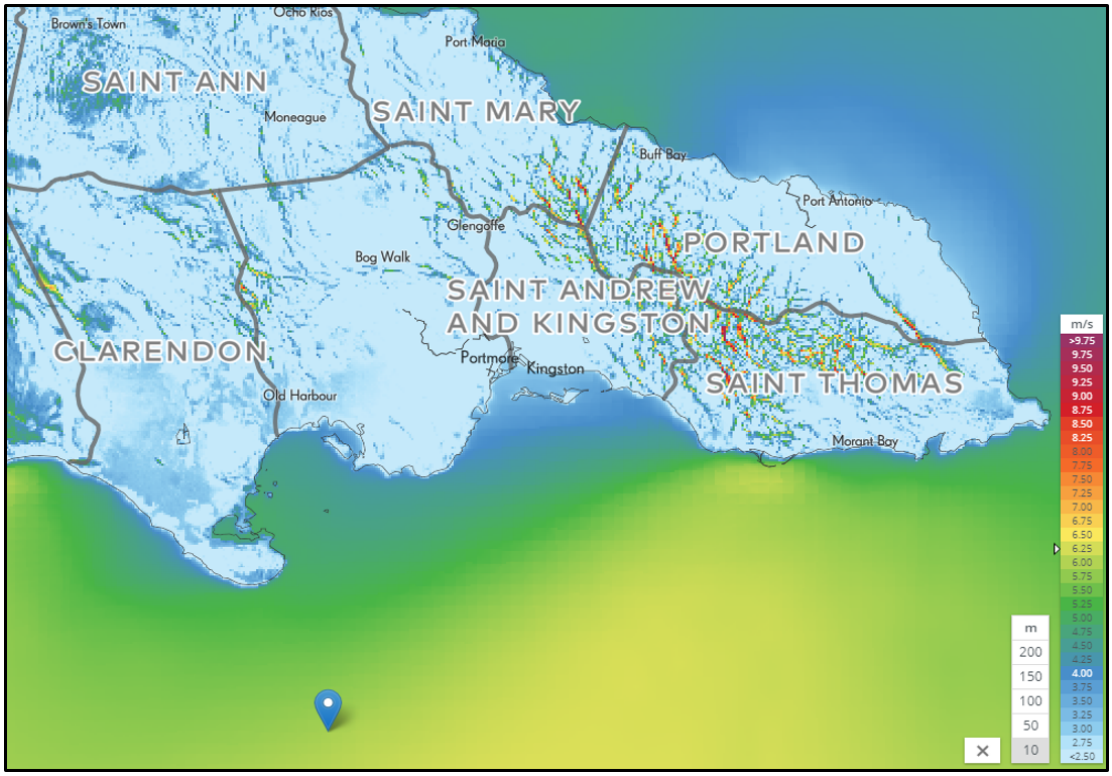

Figure 2.2: Mean wind speed (m/s) at 10m, at proposed FOWT site, Jamaica (Source: Global Wind Atlas)

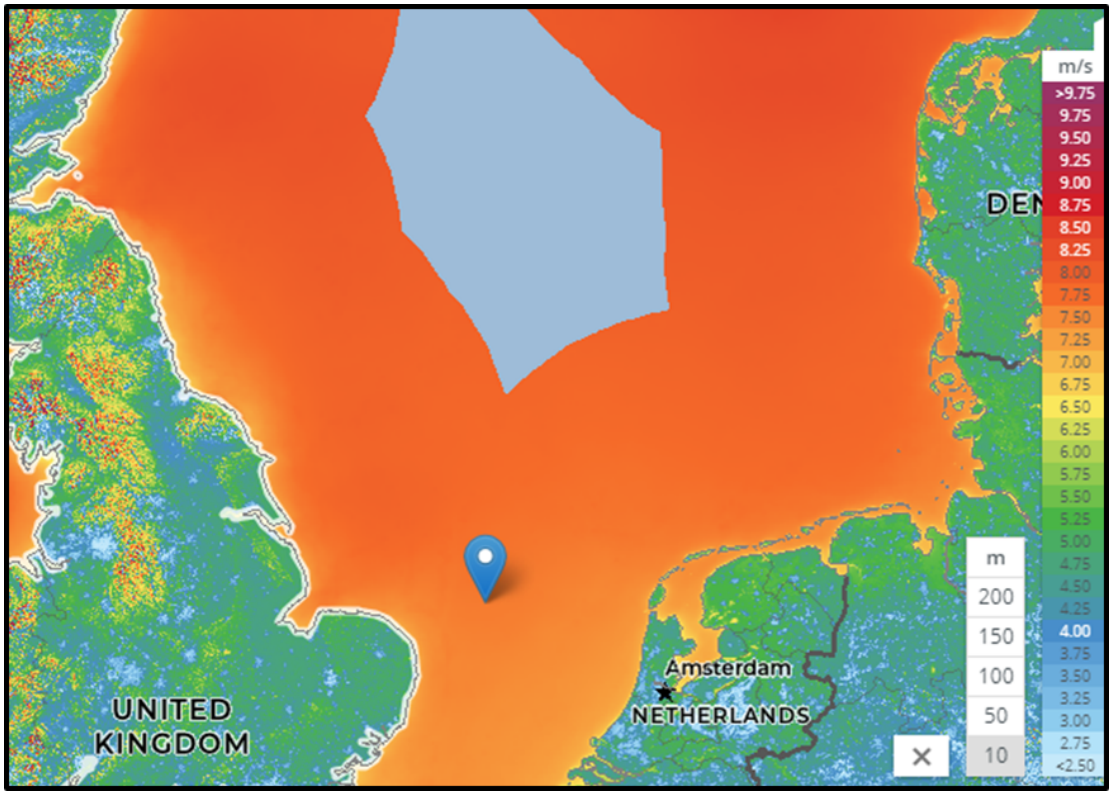

Figure 2.3: Mean wind speed (m/s) at 10m, approx. location of Vattenfall OWF, North Sea (53.04N, 2.61W) (Source: Global Wind Atlas)

wind energy are primarily located inter alia in the Southern Hemisphere westerlies, the North Atlantic westerlies and some low latitude areas such as the Caribbean. This is in keeping with the studies done by Zheng & Pan (2014) and the global offshore wind resources map developed by NREL using the Quick Scatterometer (QuickSCAT) dataset to show annual wind power densities at 10m (see Figure 2.4).

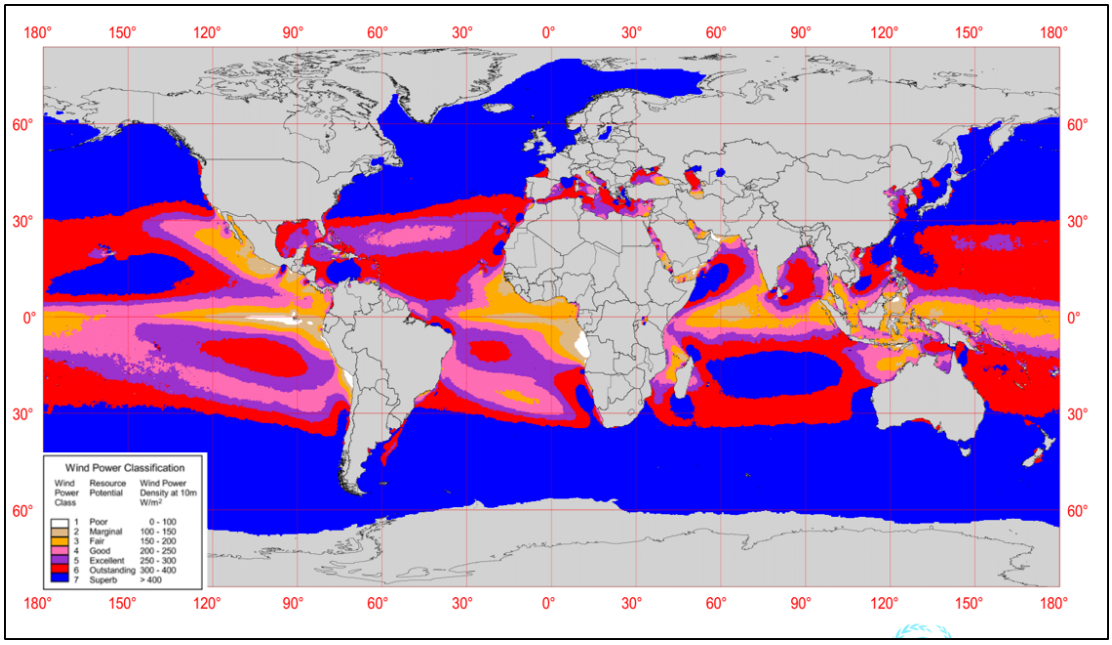

Figure 2.4: Wind energy classification across the global ocean (Source: NREL (2005))

The global wind atlas is also used to compare the mean wind power densities of the Jamaica site against that at the respective location in the North Sea. The WPD at 10m at the Jamaica site is 206 W/m^2 and the WPD at the named location in the North Sea is 559 W/m^2. At 50m, the WPD at the Jamaica site is 325 W/m^2 and 848 W/m^2 at the North Sea location. At 100m (approx. hub height), the wind power density is 396 W/m^2 at the Jamaica site and 1002 W/m^2 at the location in the North Sea. See Figures 2.5 and 2.6.

Wind power stability. A stable wind power density is essential for the development of wind energy resources (Zheng & Pan, 2014). Unstable wind could result in lower energy conversion efficiency and might cause damage to the generating equipment. In addition, as mentioned previously, the full character of the wind resource can only be realized if the stability of the wind power density is determined. Zheng & Pan (2014) used the coefficient of variation (C_v) and the monthly variability index (M_v) to determine if the wind power was stable. It was shown that the C_v in the Southern Ocean were lower (more stable) than in the Northern Ocean and that the stability is better offshore

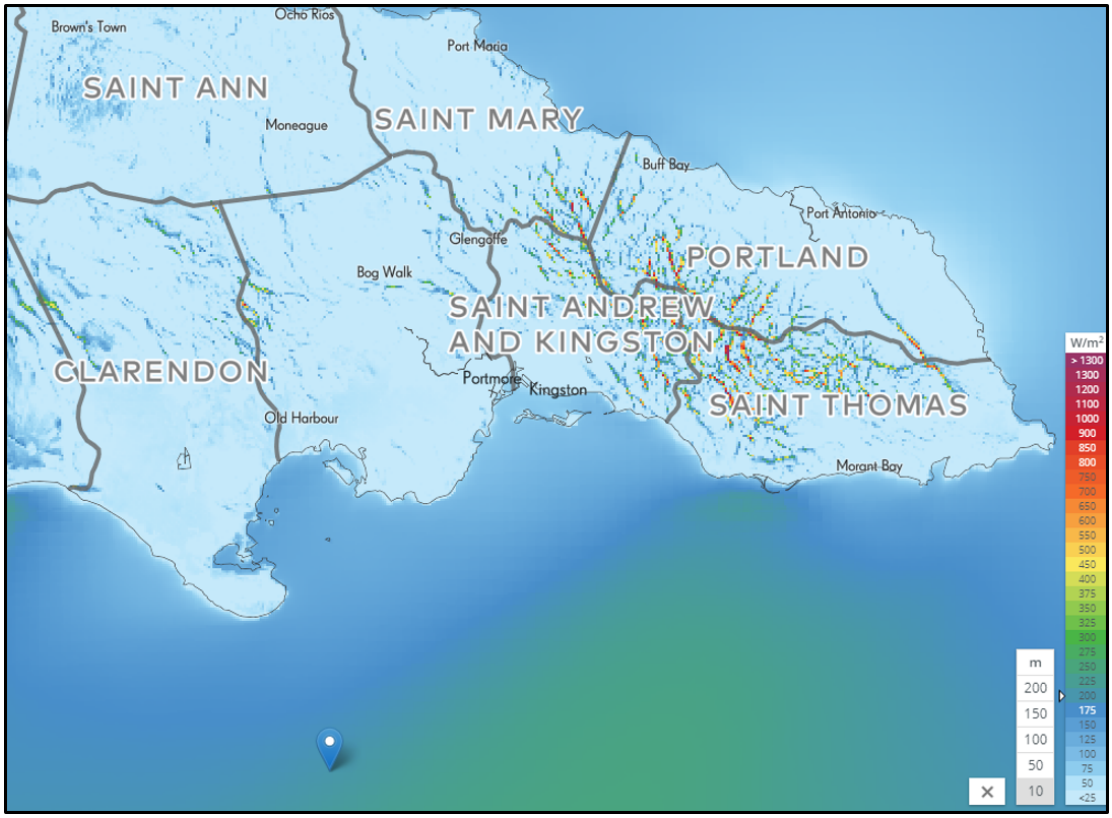

Figure 2.5: Mean wind power density (W/m^2) at 10m, at proposed FOWT site, Jamaica (Source: Global Wind Atlas)

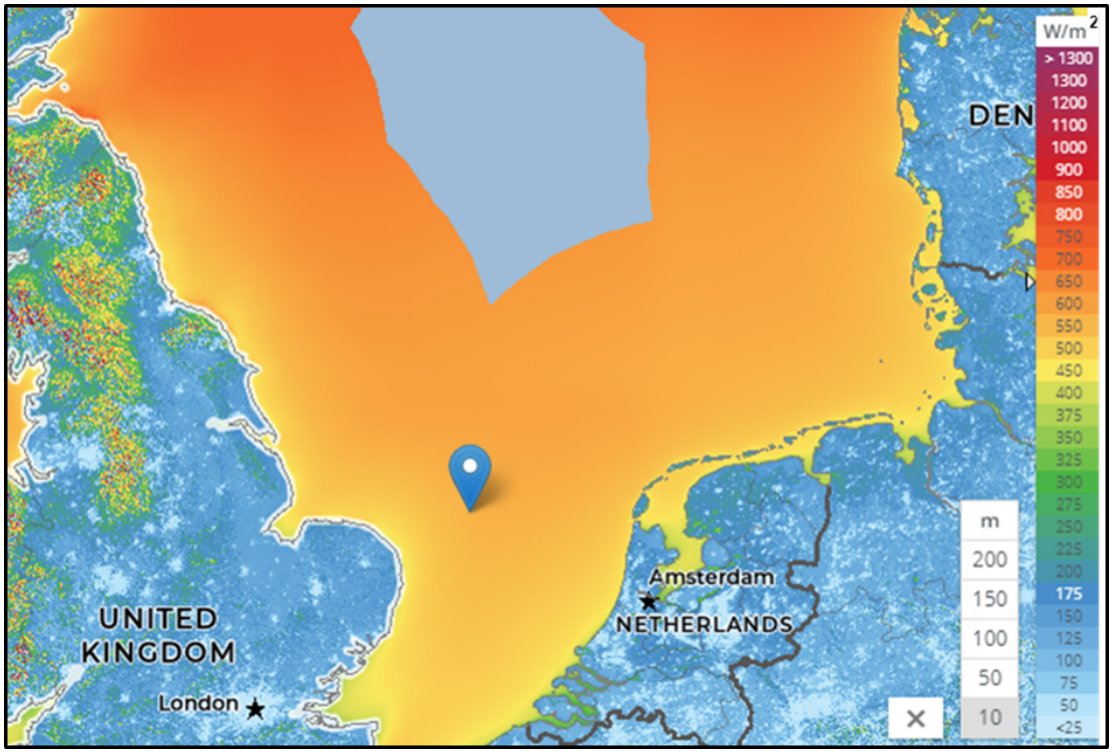

Figure 2.6: Mean wind power density (W/m^2) at 10m, approx. location of Vattenfall OWF, North Sea (53.04N, 2.61W) (Source: Global Wind Atlas)

than nearshore in the middle-to-low latitude regions. On a scale of 0 to 2.8, 0 being stable and 2.8 being unstable, the C_v of the North Sea region was shown to range from 1.2 to 1.6. The C_v of the Caribbean region ranged between 0.4 to 1.2. It was shown that the areas with the best C_v had values of 0.8 all year round. The Mv index indicated that the wind power density was more stable in the Southern region than in the Northern region. On a scale of 0.0 to 6.0, 0.0 being stable and 6.0 being unstable, the Mv of the North Sea region was shown to range from 2.0 to 4.0. The Mv of the Caribbean region ranged from 1.0 to 3.0. From the data presented, both the North Sea and the Caribbean Sea have wind power densities that are sufficiently stable, justifying the classification of the wind resource as rich in both regions. The Weibull k was used to classify the wind resource in the Caribbean by Elliott et al. (1987) and Costoya et al. (2019). Elliott et al. (1987) showed that the average Weibull k off the south coast of Jamaica was 2.0. The values of k ranged from 1.0 to 4.0, with higher values indicating steadier wind. Costoya et al. (2019) showed that the Weibull k off the south coast of Jamaica ranged between 3.0 and 3.5. The studies indicate that the stability of the wind power is adequate and provides the basis for Jamaican site being classified as having good wind resource.

2.3 Extreme Value Theory

2.3.1 General

Now that an overview of the wind resource globally, and more specifically the wind resource in the Caribbean Sea and the North Sea, has been given, we will discuss how the environmental data at a particular site is used to determine an extreme sea state. The same principles are used to determine the extreme wind speed.

A n-year design sea state is defined in DNV (2010*a*) guideline as a sea state of duration 3 to 6 hrs, with significant wave height H_{s-n} combined with an adequately chosen characteristic, value for the other sea state parameter, for example T_p or T_z (zero up-crossing period). The design sea state can be determined by calculating the extreme values of the significant wave height (H_s) and the peak wave period (T_p), that is, the n-year return levels of H_s and T_p. This is done by univariate or multivariate extreme value analysis. Univariate extreme value analysis (EVA) is done by finding the extreme value of each variable in turn. Multivariate EVA is done by finding extreme value of more than one variable at the same time. For example, for H_s, the extreme value of H_s dependent on T_p would be determined. One of the ways to do this is by creating environmental contours. More is said on environmental contours later.

The development of an extreme sea state is done by extreme value analysis. The principles are outlined in Coles (2001). According to Coles (2001) extreme value anal-

ysis is utilized in many disciplines. This includes the financial markets, the insurance industries and telecommunications. It is also utilized inter alia in wind engineering, assessment of meteorological change, non-linear beam vibrations and ocean wave modelling.

The distinctive feature of extreme value theory is that it is used to quantity the stochastic behaviour of a process at extremely large or small levels. Specifically, it is used to estimate the probability of an event that is "more extreme" than has been previously recorded. It is therefore a useful technique to determine extreme sea states using historical significant wave height and periods of a particular location or region. Provided a long enough wave record exists, say a minimum of 10 years, extreme-value-analysis can be used to determine the significant wave height over the next 100 years, for example. In essence, the theory of extreme value analysis allows data for a known period to be extrapolated to periods in the future to determine characteristics that would otherwise have been unknown in the present.

Notwithstanding that extreme value analysis models can be used for extrapolations there are limitations (Coles, 2001). The first limitation is that the models are developed from asymptotic arguments, and therefore should be treated with caution when considered as exact results of finite samples. Secondly, the models are derived under idealized circumstances, which may not be exact (reasonable) for the process that is being studied. For example, in carrying out studies using the annual maxima, maximum values of the variable being studied might be eliminated to satisfy the assumptions made for the model. To be more specific, in satisfying the assumption that storms are from independent events, a large significant wave height for the following year could be omitted, because it occurs too close the maximum value for the previous year. To account for these limitations, statistical implementations are used to complement the development of extreme value analysis models. In other words, statistical implementations help to augment the shortfall, in models, that would have resulted from the assumptions.

For statistical implementation, four characteristics need to be considered, namely, method of estimation, quantification of uncertainty, model diagnostics and maximal use of information. These are explained by Coles (2001) as follows:

Method of estimation. This is how unknown parameters of a model are inferred based on the historical data. There are many methods used to determine the parameters for extreme value analysis models. These techniques have their advantages and disadvantages. However, the likelihood-based techniques are unique in that they can be adapted to model change. That is, if the equations of a model changes due to a change in the model, the underlying methodology remain the same. The method that is

mostly adopted is the maximum likelihood method, which is convenient to use because of it has “off the shelf” large sample inference properties.

Quantification of uncertainty. In any statistical analysis, estimates are best guesses of the truth based on the available historical information. Therefore, it is necessary to complement the estimate of a model with measures of uncertainty, due to variability in the sample. That is sample studied in one location, to investigate a process, may be different from a sample studied at a separate location, to investigate the same process. This uncertainty in a model is even more necessary for extreme value modelling, as small changes in the model can result in great amplifications when the model is extrapolated. The estimate of the uncertainty in a model can be determined by basing inference on the likelihood function.

Model diagnostics. This is concerned with the goodness-of-fit. That is, how well does the model fit or describe the data being investigated. If a model is found to be a bad representation of the extreme values of the data under study, it will also be a bad representation when it is extrapolated.

Maximal use of information. This is concerned with minimizing uncertainties in the data by using as much of the data as possible to carry out an analysis. For example, the analysis of extreme values, the method of block maxima can be utilized. However, the peaks over threshold method, which considers the peaks of the data over a certain threshold value, allows for more of the data to be utilized. This helps to minimize uncertainty. The analysis of the data that is used in this study is carried out using both the block maxima method as well as the peaks over threshold method to illustrate this characteristic. In essence, if there are more uncertainties in the design characteristics, it results in a more conservative design approach. The application of the peaks over threshold method allows for a design that is less conservative. This invariably leads to minimization in design costs, which is at the heart of the consideration to determine if a project is feasible. In addition to comparisons, between block maxima and peaks over threshold, in an extreme value context, the use of covariate information, the construction of multivariate models, or the incorporation of additional sources of information into a model, all help to reduce uncertainties. In other words, the more information that is used in the development of the model minimizes the uncertainties. This results in a model that is more credible and a less conservative design approach.

2.3.2 Extreme value theory models

It was previously mentioned that the standard models for extreme value theory are developed based on asymptotic arguments. In statistics, asymptotic theory or large sample theory is framework for assessing properties of estimators and statistical tests.

(https://en.wikipedia.org/wiki/Asymptotic$_$theory$_$(statistics)). Within this framework, it is assumed that the sample size, *n*, grows indefinitely. The estimators and tests are then estimated in the limit n $\rightarrow \infty$. In practice, a limit evaluation is treated as being approximately valid for large finite sample sizes. In mathematics, an asymptote is defined as a line that a curve approaches but never touches it. That is, the curve heads to infinity. In essence, the asymptotic model aims to develop statistical parameters by looking at a finite sample and making extrapolations for very large sample sizes. Pellizzari (of Bocconi, University of Milan at the time when the notes were prepared) stated that asymptotic theory is the study of the characteristics of statistics produced with samples of finite size as the size of such samples converge to infinity. The asymptotic properties of estimators are such that they are independent of sample size. A consistent estimator is consistent, whether it was produced from a large or small sample. In essence, the parameters for a small sample size can be used to make extrapolations to estimate the variables of a larger sample. This is the reason why the theory is useful to determine the significant wave height, for the 100-year event (large sample), say, using data of significant wave height for a known historical period (small sample).

Two of the foundational models used in EVA are the annual maxima /generalized extreme value (GEV) model and the peaks over threshold (POT)/ Generalized Pareto Distribution (GPD) model.

Annual maxima model

The GEV distribution has a distribution function of the form:

$$G(z) = exp\left\{-\left[1+\xi\left(\frac{z-\mu}{\sigma}\right)^{-1/\xi}\right]\right\} \tag{2.9}$$

Defined on the set {z:1+ξ(z-μ)/$\sigma > 0$}, where the parameters satisfy -$\infty < \mu < \infty$, $\sigma >$ 0 and -$\infty < \xi < \infty$. The GEV model has three parameters, a location parameter, μ; a scale parameter, σ; and a shape parameter, ξ.

For large values of n the GEV family can be used to model the distribution of maxima of long sequences.

Coles (2001) give the approach to modelling extremes of a series of independent observations, say, X_1, X_2,...,X_n. It involves dividing the data into blocks of sequences of observations of length n, for some large value of n. This generates a series of block maxima, $M_{n,1}$,...,$M_{n,m}$, say, to which the GEV distribution is fitted. The blocks often relate to a time-period of one year in length, where n is the number of observations in a

year and the block maxima are the annual maxima. Estimates of extreme quantiles of the annual maximum distribution are obtained by inverting the GEV family distribution equation 2.9. This yields the following:

$$z_p = \begin{cases} \mu - \frac{\sigma}{\xi}[1 - [-log(1-p)]^{-\xi}], & \text{for } \xi \neq 0, \\ \mu - \sigma log[-log(1-p)], & \text{for } \xi = 0, \end{cases} \tag{2.10}$$

where G(z_p) = 1 - p. The variable z_p is the return level associated with the return period 1/p. Exceedance of the level z_p is expected to occur on average once in every 1/p years. Specifically, z_p is the exceedance of the annual maxima in any of the given years and has a probability of p.

In developing GEV models to fit block maxima the thing that is of interest to engineers and others who design offshore structures is the n-year return levels of a respective variable. This research is concerned with the 50-year return levels of H_s, T_p and u_{10}. To determine this, Eq. 2.10 is expressed in terms of the quantile of expressions by defining y_p=-log(1-p) such that

$$z_p = \begin{cases} \mu - \frac{\sigma}{\xi}[1 - y_p^{-\xi}], & \text{for } \xi \neq 0, \\ \mu - \sigma log[y_p], & \text{for } \xi = 0, \end{cases} \tag{2.11}$$

Then z_p is plotted against logy_p. The plot is linear in the case ξ = 0. If $\xi < 0$ the plot is convex with asymptotic limit as p $\rightarrow$ 0 at μ - σ/ξ; if $\xi > 0$ the plot is concave and has no finite bound. This graph is the return level plot and it gives the return level (of the block maxima variable under consideration) against return period in years.

Generalized Pareto distribution (GPD) model

The greater the number of observation points used to fit a model the greater the improvement in the accuracy of the model. Coles (2001) indicated that modelling only block maxima is a wasteful approach to extreme value analysis if other data on extremes is available. This is so because within a block, of a year, there could be values that are not the maximum value within that year but are greater than the maximum value in a succeeding year. In accordance with block maxima, values of this nature are omitted from the data that is used to fit an extreme value model. Therefore, another type of model, that accounts for more of these other large values is utilized to deal with this shortfall. This type of model is called a threshold model, otherwise called a POT model. In this type of model, the data is fitted to the Generalized Pareto Distribution (GPD).

Referring to Caires (2011), in the POT model the peak excesses over a high threshold,

u, of a time series are assumed to occur in time, according to a Poisson process (with rate λ_u) and be independently distributed as a GPD, with the following distribution function:

$$F_u(y) = \begin{cases} 1 - 1 + \xi(\frac{y}{\sigma_u})^{-1/\xi}], & \text{for } \xi \neq 0, \\ 1 - exp(-\frac{y}{\sigma_u}), & \text{for } \xi = 0, \end{cases} \tag{2.12}$$

where 0 $< y <$ ∞, $\sigma_u > 0$ and -∞ $< \xi <$ ∞ . The GPD has two parameters. The scale parameter, σ_u, and the shape parameter, ξ. The GPD has the following important characteristics based on the value of the shape parameter, ξ:

1. When ξ = 0, the GPD is said to have a type I tail and equates to the exponential distribution with mean σ_u.
2. When $\xi > 0$, the GPD has a type II tail and is the Pareto distribution.
3. When $\xi < 0$, the GPD has a type III tail and is a special case of the beta distribution.

The return level, z_m, for a GPD model is given by

$$z_m = \begin{cases} u + \frac{\sigma_u}{\xi}[(\lambda_u m)^{\xi} - 1], & \text{for } \xi \neq 0, \\ u + \sigma_u log(\lambda_u m), & \text{for } \xi = 0, \end{cases} \tag{2.13}$$

It should be noted that this equation is obtained from Equation (2.12) by solving 1-$F_u(y)$=1/$\lambda_u m$ for y and adding the threshold u.

In the same way that block maxima has the GEV as its approximate distribution, the threshold excesses have a corresponding approximate distribution within the GPD family. In addition, the GPD model parameters of the threshold excesses have a unique relationship with the GEV parameters of block maxima. Specifically, the shape parameter of both models is the same and the scale parameters have the following relationship.

$$\sigma_u = \sigma + \xi(u - \mu) \tag{2.14}$$

2.3.3 Modelling threshold excesses

Modelling threshold excesses is essentially done by a three-stage process, as follows:

1. Determine(select) a threshold
2. Determine the parameters of the GPD using the threshold excesses.
3. Determine the return level vs return period plot

However, there are two caveats when modelling threshold excesses, the data must be independent and homogenous. The data is usually checked for homogeneity during the data preparation process. Independence is achieved by a process called de-clustering. It can be achieved by physical considerations or statistical considerations (Jonathan & Ewans, 2013). It is done to prevent the n-observation, from influencing the (n+1)-observation. De-clustering is done by dividing the total n-observations into blocks and the largest values within the blocks are chosen. The other values, which remain in each block, are pushed to the threshold, so that they are not used to fit the GPD model. If de-clustering is done by a physical separation, a block period of 48hrs is usually used to achieve independence (Caires, 2011; Palutikof et al., 1999). If de-clustering is done statistically, a factor called the extremal index is used to check the degree of dependence in the POT sample. The extremal index ranges between 0 and 1. If it is closer to zero, it suggests strong dependence and if it is closer to 1.0 it suggests strong independence. This is the methodology that was used to check for independence in chapter 3 and not the physical separation of 48 hrs.

The maximum likelihood estimation (MLE) method is used extensively to estimate model parameters, where a likelihood-based technique, the MLE method, is used for estimating the model parameters (Coles, 2001). However, the method used to estimate the parameters estimates has a direct bearing on the parameters and related return levels. In particular, the probability weighted moments (PWM) method yields slightly higher values for the return levels than the maximum likelihood estimation (MLE)(Caires, 2011). To address this matter, a more conservative design approach could be considered when using the MLE method. This could be done by selecting a return level closer to the upper bound value of the confidence interval to bring it closer to the likely value that would be obtained by the PWM.

The process of modelling threshold excesses is similar to other design or modelling activity, in that it is an iterative process. If the parameters in step 2, based on the selected threshold, do not result in a GDP model that is a good fit to the data, further thresholds are investigated until the threshold that yields the best results is discovered. That threshold is used to determine a new set of threshold excesses to which the GPD model is fitted and finally the return level plot is obtained.

2.3.4 Model checking

The graphical method is one of the methods used to check how well the model fits the data. This is the method that was used for model checking in this study. In particular, q-q plots were used. A q-q plot is a graphical tool that is used to assess if a set of data came from a particular distribution (in this case the GEV and GPD). It is done

by taking the sample data, sorting it in ascending order, and plotting them against quantiles calculated from the theoretical distribution. If the respective model is a good fit for the data, the q-q plot should show the data points close to the best fit theoretical line. Notwithstanding that the q-q plot was used, the final check for the suitability of the model was how well the model fitted the data on the return period plot. A good fit will show most the data points close to the line. However, if a small number of data points veer away from this line, they should fall within the 95% confidence interval band.

2.4 Applications of Univariate EVA to Determine the Extreme Design Sea State

One of the most important aspects of the analysis and design of offshore structure is the determination of the critical design loads. Integral to the determination of the design loads is the determination of the design sea state.

As mentioned previously, length of the dataset used for EVA is essential. The length of the datasets used for EVA are usually stipulated in the offshore structures design code or might have been determined based on the tradition in the offshore industry. The ISO standard recommends that for the peaks over threshold (POT) EVA, the length of the data should be at least a quarter of the desired return period (Neary et al., 2020). Hence, for 10 years of data, the maximum return period that should be computed is 40-year. Panchang et al. (2013) stated that for the generation of estimates corresponding to the n-year event, a rule of thumb states that the dataset should preferably be at least n/3 years long. That is for a 30-year return level; at least 10 years of data should be available. On balance, the data used to carry out EVA should be sufficiently long to get the best results. The greater length of data reduces the statistical uncertainties. The length of the data that is used for this study is 40 years and is satisfactory for the 50-year design event.

In addition to the length of the dataset, the codes and industry practice also stipulate the maximum return period for which offshore structures are to be designed. The offshore codes base their critical design load case (DCL) on the 50-year event (DNV-GL, 2016; IEC-61400-1, 2019). For example, in the LIFE 50+ project (LIFE50+, 2015*a*), the 50-year event constituted the DLC for the OWT structures that were under investigation. In the Upwind project (UpWind, 2010) the 50-year event was also used. This a consistent feature throughout the literature. It should be noted that in the design of the, WindFloat FOWT, Roddier et al. (2010) argued that the extreme wave event assumed a 100 year return period. This was based on the practice in the offshore (oil and gas) industry, since the GL offshore wind turbine code, GL (2010); only require a 50-year return period for design. In keeping with the OWT design codes the 50-year design event is considered in this study.

There are many uncertainties with EVA (Coles, 2001). It is important that those involved in the analysis and design of offshore structures are aware this. Designers should try to employ a balanced approach and proper judgement when interpreting and utilizing the results from EVA models. Vanem & Bitner-Gregersen (2015) argued that there are large uncertainties associated with EVA and that these uncertainties increase at higher return periods. In the ideal situation, the time series would be longer than the return period to which one would like to extrapolate. However, a finite set of data is used to extrapolate return periods that are longer than the data. This results in uncertainties as there are more uncertainties the further away from the data one has to extrapolate. The uncertainties in EVA come from different factors (Orimolade et al., 2016; Vanem & Bitner-Gregersen, 2015; Neary et al., 2020; Roscoe et al., 2010). This include:

1. The source of the model data for example, SWAN vs NOAA.
2. Whether the data is from buoy data or model data.
3. The length of the data used and the size of the sample that is used to fit the data. For example, for block maxima/GEV analysis, the maximum data within each block period, usually one year, is used. However, for POT the peaks over a particular threshold is used giving rise to more data to fit the model than a GEV model. Hence, there is usually more uncertainty associated with the GEV than a POT model.
4. The choice of distribution model, for example, GEV vs GPD.
5. The method used to estimate the model parameters, for example, probability weighted method (PWM) vs maximum likelihood estimate (MLE).
6. The value used for the threshold in the case of POT/GPD analysis.
7. Whether univariate or multivariate EVA method is used.
8. Whether localized or regional frequency analysis is carried out. This has an effect on the values of the shape parameters. A lower shape parameter results in a higher return level (Roscoe et al., 2010).
9. Changes in the wave climate because of climate change.

These are some of the important areas of uncertainty when carrying out EVA analysis. It therefore means that engineering judgement is required when making a determination about the finals values to be used in numerical models. Furthermore, because

there are so many uncertainties, the final arbiter about an offshore structure should be how it behaves in reality. This is why demonstrations in real environmental conditions are important. This is one-step higher, than lab experiments, which are also essential. The observance of the behaviour of a structure over a long time can inform designers about how model inputs can be tweaked to allow for optimum performance of offshore structures.

2.4.1 Univariate extreme value analysis

There are number of methods given in the literature for carrying out univariate extreme analysis. These include:

1. The r-largest method. This method is not used in practice (Caires, 2011) therefore nothing else is said about it.

2. The initial distribution method. This method uses all of the data to fit a probability distribution function and the extremes are estimated from the fitted distribution by extrapolation to higher return periods (Vanem & Bitner-Gregersen, 2015). It has an advantage is that it uses all of the data to fit a model. However, Caires 2011 argued that the initial distribution approach should not be used for EVA because, it invalidates the application of common statistical methods used (confidence intervals and tests) and the definition of the return value. This invalidation is caused because it does not satisfy the fundamental requirements of EVA for the data to be independent and identical, since all of the data is used and declustering is not carried out. Based on this, nothing more is said about this approach. See Caires (2011) for further information.

3. The average conditional exceedance rate (ACER) method. This method does not consider the independence of the data in the analysis. Instead, it considers the dependence of the data. It accounts for dependence by conditioning on previous data points in the time series, by using the k parameter (Vanem & Bitner-Gregersen, 2015). This parameter represents the (k-1)-step memory of the data. When k = 1, this represents independent data, k=2 corresponds to conditioning on the previous value only. That is the 1-step memory and k=3, correspond to conditioning on the two preceding values that is 2-step memory, the same applies to higher values up to k = n, say. In a typical analysis a value of k >= 2 is assumed. This method does not follow the classical extreme value theory therefore nothing more is said about it. However, further information on how it used can be found in Vanem & Bitner-Gregersen (2015).

4. The block maxima/GEV method.

5. The POT/GPD method.

The most prominent methods used in the literature to carry out extreme value analysis are, the block maxima/GEV method and the POT/GPD method. More will therefore be said about their application.

Block maxima/GEV method. It was previously mentioned that in this approach, the GEV model is used to fit a series of independent observations. The data is seperated into blocks of observations of length n, for some large value of n, creating a series called block maxima, to which a GEV distribution is fitted. The blocks are chosen to correspond to a period of one year in length, where n is the number of observations in a year and the maximum value in the blocks are the annual maxima (Coles, 2001). For example, for 40 years of data, there are 40 data points to fit the GEV, where each point is the maximum value of the respective variable (H_s, say) within each year. This method satisfies two of the foundational principles of EVA, that is, the data used to fit EVA models should be independent and homogenous (or identical as referred in other papers) (Vanem & Bitner-Gregersen, 2015). Independence is achieved by ensuring that the data used to fit the distribution is from independent storms. That is done by choosing storms that are separated by a certain distance from each other in time. The selection of the maximum value for each year results in independence. To determine that the data is homogenous, one has to examine the data and ensure that the storms being used are not biased based on the time of the year. Therefore, in colder climates, where winter is distinct from summer, the data may be separated such that a year starts in November, say, and finishes in May. This kind of approach ensures that homogeneity is achieved. In tropical climates, like the Caribbean, there are no extremes in the weather conditions and therefore homogeneity can be assumed unless that data shows otherwise. The block maxima method is simple and easy to apply because it free from the bias of designers as it does not require a selection of a threshold, like the POT/GPD method, for example (Palutikof et al., 1999; Neary et al., 2020; Vanem & Bitner-Gregersen, 2015; Orimolade et al., 2016). However, it requires a dataset with a minimum period of record of 20 years (Neary et al., 2020; Orimolade et al., 2016). This requirement is difficult to achieve when using buoy data because either some locations have no buoy or the data available is inadequate. However, it is readily achieved with model data.

There have been studies carried out by other researchers to investigate how fitting other types of models to block maxima affect the results. Therefore, the Gumbel, 2-parameter and 3-parameter Weibull models have all been used to fit block maxima (Vanem & Bitner-Gregersen, 2015; Orimolade et al., 2016). However, it has been

discovered that the GEV model is most suited for block maxima and therefore it is usually the preferred model. There have also been attempts made to fit the GEV to blocks that are less than one year, for examples 6 months or blocks that are more than a year, for example 24 months. Six-months blocks would give more data points to fit the GEV, which is a good thing, as this would reduce the uncertainties. On the contrary, 24-months blocks would give fewer data points; this not only increases the uncertainties within the model but also needs more data to satisfy the requirement of using a minimum of 20 data points to fit the GEV. Vanem & Bitner-Gregersen (2015) fitted block maxima to models of various block sizes and it showed that the GEV with blocks of one year gave the most accurate results.

GPD/POT analysis. The greater the number of observation points used to fit a model the greater the improvement in the accuracy of the model. Coles (2001) indicated that modelling only block maxima is a wasteful approach to extreme value analysis if other data on extremes is available. This is so because within a block, of a year, there could be values that are not the maximum value within that year but are greater than the maximum value in a succeeding year. In accordance with block maxima, values of this nature are omitted from the data that is used to fit an extreme value model. Therefore, another type of model that accounts for more of these other large values is utilized to deal with this shortfall. This type of model is called a threshold model, otherwise called a POT model. In this type of model, the peaks over a particular threshold are fitted to the Generalized Pareto Distribution (GPD).

One of the advantages of the POT method is that unlike block maxima, there is more than one data point per block to fit the model. This effectively means more data points are available to fit the model. The POT method is also more accurate in computing the return levels for lower return levels. For low return levels, that is, 5 years and below, the POT method is recommended (Neary et al., 2020). This may not be immediately applicable to the return levels on offshore structures since the design standards specify the 50-year event for determining extreme design loads. Although the POT method has its advantages, the matter of determining the threshold value causes uncertainty. The POT/GPD model parameters and subsequent return levels are sensitive to the value of the threshold. Determining it is not an exact science and is based on the judgement of the designer. Neary et al. (2020) argued that the most notable disadvantage of the POT method is its sensitivity to the threshold value selected and that despite the best efforts to objectively select threshold values it is difficult not to introduce user bias. The threshold has to be selected that maintains the balance between bias and variance. Too low a threshold is likely to violate the asymptotic basis of the model, leading to bias and too high threshold will result in fewer data points to fit the model, leading to a

high variance (Roscoe et al., 2010; Caires, 2011).

Similar to GEV analysis, studies have been conducted which fit the data for POT analysis to other distributions besides the GPD. Some of the other distributions used to fit POT data are the exponential distribution, the 2-paramter Weibull distribution, and the 3-parameter Weibull distribution (referred to as the conditional Weibull distribution, CWD) (Roscoe et al., 2010; Caires, 2011; Vanem & Bitner-Gregersen, 2015; Orimolade et al., 2016). There is no definite position on whether these distributions are more appropriate to carry out POT analysis. However, some of these distributions yield higher return levels that the classical approach of using the GPD distribution. They might therefore be selected in place of the GPD because they yield estimates, which are more conservative. This is sometimes more favoured for management decisions. Roscoe et al. (2010) in carrying out POT analysis in the Dutch North Sea compared the results from the GPD with those from the CWD. It was shown that the CWD returns consistently higher return values than the GPD. Of the nine different locations studied, the CWD values were more than the GPD values by a range of 5% to 16%. This is because the GPD can be characterized by more than one type of tail, based on the value of the shape parameter. The GPD can be represented by a Type1, Type II or a Type III tail. When $\xi = 0$, the GPD is said to have a Type 1 tail and amounts to the exponential distribution with mean σ. When $\xi < 0$ the GPD is said to have a Type II tail and it is the Pareto distribution; when $\xi > 0$ it has a Type III tail, a special case of the beta distribution. This has an upper bound, σ/ξ, which is also referred to as the upper end-point of the GPD. Which is considered the upper limit of the excesses; so that the upper limit of the variable of interest, say H_s, is $u + \sigma/\xi$. The limit is suitable for wave data since the wave height has a physical limit. The GPD is flexible in that it allows the data to determine the type of tail to use to fit the data. For example, if $\xi = 0$; the GPD will morph to a Type I tail fit and if $\xi > 0$, based on the data, it will morph to a Type III tail fit. The CWD on the other hand is only represented by a fixed Type I tail regardless of the data and has no upper limit. The return levels of the CWD are therefore not as sensitive to the change in threshold value like the GPD. This results in return levels that are higher than the GPD and might be more favoured from a managerial perspective, even though the statistical principles are better espoused by the GPD (Roscoe et al., 2010). The exponential distribution also yields higher return levels than the GPD (Caires, 2011). However, this only occurs if the tail of the data is closer to the exponential distribution. If, the tail of the data is represented by a type III and the exponential distribution is used instead of the GPD it would produce return levels, which are overestimated, and the statistics would not be correct. It is clearly illustrated in the literature that there are other models that could yield give higher return levels than the GPD model. However, for this research the GPD model is used for POT anal-

ysis because although it may not be as robust, it has a stronger theoretical framework and thus produces statistics that are more accurate. In addition, the open source tools that are available for POT analysis seem to utilize GPD models.

Block maxima/GEV vs POT/GPD models. The question about whether the GEV model is better than the GPD model for determining the extreme environmental conditions of offshore structures might be posited. There is no clearly agreed position about this among researchers and within the wider offshore wind industry. Neary et al. (2020) argued that international standards allow designers to choose from a variety of statistical methods to meet minimum design requirements. These methods include simple univariate methods like the POT method or more complex bivariate methods that calculate environmental contours, that is, the joint distribution of the statistics for the environmental conditions being investigated. For example, a joint distribution function of H_s and T_p to determine the n-year design sea sate using the inverse first order reliability method (IFORM) to compute the contours. In carrying out analysis to compare extreme values of H_s using POT and GEV methods, Neary et al. (2020) reported that for higher return levels, the $H_{s(5)}$ and $H_{s(50)}$ return levels for both methods were in good agreement. However, for lower return levels, $H_{s(1)}$ the block maxima/GEV model underestimated the return periods and therefore the POT method is recommended for low return periods i.e. periods below 5 years. The simplicity of the block maxima/GEV method, while being in good agreement with the POT method, is the reason why designers would tend to gravitate to it. Palutikof et al. (1999) argued that because more decisions are required by designers when using the POT method, designers should proceed with care and pay attention to detail if they chose to use this method to carry out EVA. Unlike Neary et al. (2020), Caires (2011) and Orimolade et al. (2016) showed that the POT return levels could be higher than the block maxima/GEV return levels. The POT $H_{s(100)}$ value was 8.5% greater than the block maxima/GEV $H_{s(100)}$ for Caires (2011). Of the four locations studied by Orimolade et al. (2016), two locations showed the POT return levels for $H_{s(100)}$ being higher than the $H_{s(100)}$ return levels of the GEV; being 3.4% and 6.6% higher than the block maxima/GEV respectively. The other two locations showed good agreement between the $H_{s(100)}$ return levels for POT and GEV. Vanem & Bitner-Gregersen (2015) showed good agreement between the POT $H_{s(100)}$ return levels and the GEV $H_{s(100)}$ return levels. On balance, coming to a conclusion about whether the POT method is better than the GEV method is not straightforward. However, what can be said with certainty is that the GEV method is simpler to use than the POT method and in some cases gives comparable results to the GPD. It might thus be favoured by designers than the POT method. Further, the POT method should be preferred to the GEV when determining low return levels, that is, return levels less than 5 years. In the case offshore structures, this issue of low return levels would not be a

problem as what is of interest are return levels 50-year and above.

2.5 Multivariate Extreme Value Analysis

As was said previously, multivariate EVA is carried out by finding the extreme value of more than one variable at the same time. This has particular application for the sea state variables i.e. H_s and T_p. Multivariate EVA could be considered a step up from the POT method. That is, there are more data points to fit a model. We now have H_s and T_p in the same space instead of only one variable. In principle, this is supposed to reduce the uncertainties and make the results more credible. Another feature of the multivariate EVA is that there are many combinations of H_s and T_p on the n-year contour line and therefore more than one pair of H_s and T_p has to be investigated to find the critical load. This is necessary because the H_s, T_p combination that causes the critical load on an offshore structure may not necessarily be the one with the maximum H_s. One of the methods used to find the extreme values of multiple variables is the environmental contour method. In the case of the sea state, the environmental contour method is used to determine the extreme sea state using the joint probability distribution of H_s and T_p.

2.5.1 The joint distribution of H_s and T_p by conditional modelling approach

The joint distribution of H_s and T_p can be found using the total probability theorem (Lucas & Guedes Soares, 2016). In this process the conditional modelling approach (CMA) is used to determine the joint distribution of two random variables, say X and Y. In general, for the CMA a marginal distribution is fitted to the data for variable X (similar to what is done for the univariate case) and the conditional distribution (of Y given X) is fitted to Y. The joint probability density function is found from the product of these two distributions and is given by:

$$f(X,Y) = f(X)f(Y|X) \tag{2.15}$$

where f(X,Y) is the joint probability density function of X and Y, f(X) is the marginal distribution of X and f(Y|X) is the conditional distribution of Y given X.

In the case where the random variables are H_s and T_p, such that X = H_s and Y = T_p, say, respectively; the joint probability density function of H_s and T_p is given by (Lucas & Guedes Soares, 2016):

$$f(H_s,T_p) = f(H_s)f(T_p|H_s)$$

where $f(H_s,T_p)$ is the joint probability density function of H_s and T_p, $f(H_s)$ is the marginal distribution of H_s and $f(T_p|H_s)$ is the conditional distribution of T_p given H_s.

The primary challenge when utilizing the conditional modelling approach is to find a suitable marginal distribution to fit H_s. On the contrary, finding a suitable distribution for the conditional distribution of T_p given H_s is usually non-problematic, since the log-normal distribution is usually appropriate and is most frequently used. Pasilliao (1995) gave what could be considered a comprehensive list of the marginal distributions that have been used to fit H_s. They include:

1. The lognormal distribution.
2. The modified lognormal distribution.
3. The three-parameter Weibull distribution (otherwise called the conditional Weibull distribution).
4. The combined exponential and power of significant wave height distribution and
5. The modified distribution.

Pasilliao (1995) used the generalized Gamma distribution to fit the marginal distribution of H_s for study areas off the Norwegian Coast (Tromsoflaket dataset) and National Data Buoy Centre buoy 46001 in the Gulf of Alaska, US. This was based on the work done by Ochi (1993) who used the generalized Gamma distribution to fit the marginal distribution of H_s at different geographical locations. The locations include the Norwegian Coast, North Sea, Japan North Pacific, Canada North Pacific, Georgia, US, Atlantic Ocean, Florida East Coast and the Gulf of Mexico. It was argued by both Pasilliao (1995) and Ochi (1993) that the generalized Gamma distribution was able to represent significant wave height data from anywhere in the world. Other distributions that have been used to fit the marginal distribution of H_s include the empirical probability distribution up to a particular (threshold) value and the Pareto distribution to fit the tail of the data (Hiles et al., 2019). It was argued that the 3-parameter Weibull did not give a good fit to the tail of the data. Velarde et al. (2019) used the environmental contour method to determine the extreme sea states at four sites in the North Sea (bet lat 50 and 55) and it was discovered that the 3-parameter Weibull gives a good fit to the marginal distribution of H_s but at lower values of T_p, H_s was overestimated. The 3-paramater Weibull was also found to be a good fit to the marginal distribution of H_s for Orimolade et al. (2016), who used the ECM to determine the extreme sea states for four locations off the coast of Norway (bet 71N to 74N, 16E to 23E). This approach was also used by Vanem & Bitner-Gregersen (2015), who determined extreme sea states in West Shetland, Scotland, West Africa, Nigeria and Northwest Australia. From these studies, it was shown that a single distribution that represents the environmental conditions in varied geographical locations has not been found yet. This does not

agree with what Pasilliao (1995) and Ochi (1993) have posited. This is something that is of interest in the Jamaica Caribbean Sea. The extremes in the region is characterized by the occurrence of hurricanes and this might make it more challenging to find a marginal distribution of H_s that is appropriate. Haver & Winterstein (2008) sated that in areas where the extremes are governed by somewhat frequent hurricanes that the joint density function of H_s and T_p should be valid for $H_s > h_o$. This value, h_o, is similar to the threshold, u, for the POT analysis. Where the joint distribution model for H_s and T_p are characterized by a 3-parameter Weibull-lognormal model, the 3-parameter Weibull distribution is given as follows (Eskeland, 2017):

$$f(h) = \frac{\beta}{\alpha}\left(\frac{h-\gamma}{\alpha}\right)^{\beta-1} exp - [(h-\gamma)/\alpha]^{\beta}, \quad h \geq \gamma \tag{2.16}$$

where γ is a location parameter, α is the scale parameter and β is the shape parameter. The lognormal distribution, which has two parameters, is given by (Ekeland 2017):

$$f(t|h) = \frac{1}{t\sqrt{2\pi}} exp - \left[(\ln(t)-\mu)^2/(2\sigma^2)\right], \quad t \geq 0 \tag{2.17}$$

where μ is the log-mean and σ is the log-standard deviation. The dependence between H_s and T_p is modelled by expressing the parameters μ and σ in terms of H_s as follows (Eskeland, 2017; Haver & Winterstein, 2008):

$$\mu(h) = E[\ln(T)|H = h] = a_1 + a_2 h^{a^3} \tag{2.18}$$

$$\sigma(h) = SD[ln(T)|H = h] = b_1 + b_2 exp - (b_3 h) \tag{2.19}$$

2.5.2 Environmental contour method

Having established the joint distribution of H_s and T_p the environmental contours representing the extreme sea state can be determined. In order to construct the n-year contour which represents the extreme wave event, the fitted probability distributions for the variables of interest (in this case the joint distribution of H_s and T_p as described above) are used in an Inverse First-Order Reliability Method (IFORM) (Eckert-Gallup et al., 2014).

In order to understand the IFORM we first have to understand the FORM. The illustration shown in Figure 2.7 is used to explain the concept.

If we would like to estimate the exceedance probability of a given high threshold, y_c

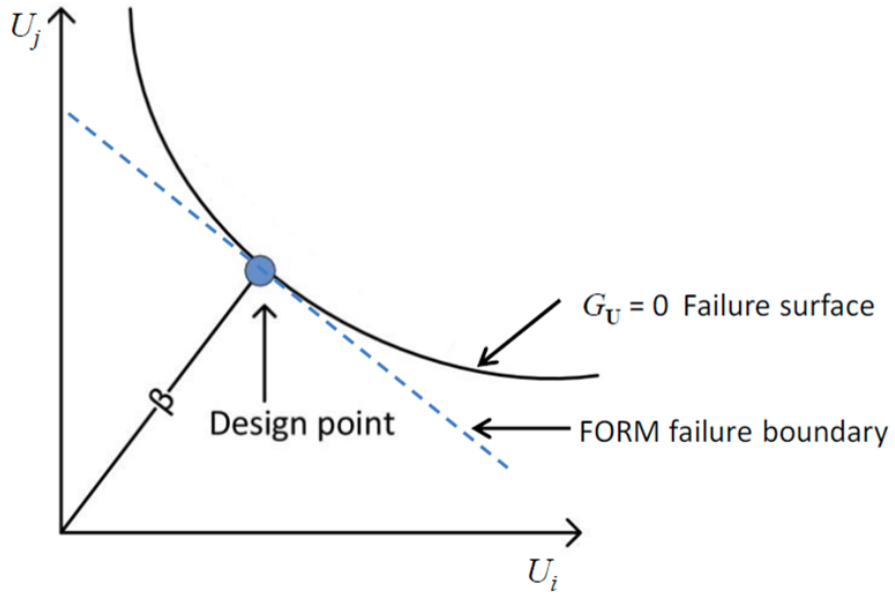

Figure 2.7: Illustration of (true) failure surface and linearized failure surface (FORM failure boundary) by FORM in U space. (From: Haver & Winterstein, 2008; Chai & Leira, 2018)
(Permission has been granted by Steve Winterstein to reproduce this figure)

and the failure function, (i.e., the limit state function) is given as (Chai & Leira, 2018):

$$G(y_c, S) = y_c - Y \tag{2.20}$$

and

$$G(y_c, S) = \int_{G(y_c,S)\leq 0} F_{\hat{Y}|S}(y|s) f_s(s)\,\mathrm{d}s \tag{2.21}$$

where the exceedance probability (the probability distribution), $Q_y(y)$, is given as $Q_y(y)$=1-$F_y(y)$.

The integral given in equation 2.21 can be solved numerically. This is done by transforming the integral to a space, called U space, consisting of independent, standard Gaussian (normal) variables, say, U_1, U_2,...$U_(n+1)$ (Haver & Winterstein, 2008; Chai & Leira, 2018). The transformation is usually carried out using the Rosenblatt transfor-

mation given as:

$$\begin{aligned} U_1 &= \Phi^{-1}(F_{s_1}(s_1)) \\ U_2 &= \Phi^{-1}(F_{s_2}(s_2)) \\ &\vdots \\ U_{n+1} &= \Phi^{-1}(F_{\hat{Y}|s_1,s_2,\ldots},{}_{s_n}(y|s_1,s_2,\ldots,s_n)) = \Phi^{-1}(F_{\hat{Y}|S}(y|s)) \end{aligned} \tag{2.22}$$

where Φ is the cumulative distribution function (CDF) of the standard normal distribution and F is the CDF of the original random variables, in this case H_s and T_p. In U space the exceedance probability is given as (Chai & Leira, Chai & Leira):

$$Q_Y(y_c) = \int_{G_U(u)\leq 0} \phi_u(u)\,\mathrm{d}u \tag{2.23}$$

where the vector **U**= $(U_1,U_2,\ldots,U_{n+1})^T$ is the failure function, G_U, transformed into U space and ϕ_u is the standard multivariate normal probability density function. This transformation allows for relationship between the variables in U space and the variables in the physical parameter space. The transformation is a unique two-way transformation between a point in U space and the corresponding point in the physical parameter space where H_s and T_p lies (Haver & Winterstein, 2008).

In U space, lines of constant probability, called isolines of probability, form a circle. The larger the circle the lower the probability and vice versa. The basic principle of FORM is that to approximate the failure probability, the failure surface is replaced by an n-dimensional hyperplane at the design point. The design point defined as the point on the failure surface (in U space) closest to the origin (Wintersten and Haver, 2008). This is explained in figure 2.9 above. The closet distance to the origin, (design point) is given as (Chai & Leira, 2018):

$$\beta = \sqrt{\sum_{i=1}^{n+1} \hat{u}_i{}^2} \tag{2.24}$$

where $(\hat{u}_1,\hat{u}_2,\ldots,\hat{u}_{n+1})$ is the design point, and the failure probability given in equation 2.21 is estimated as:

$$Q_Y(y_c) \approx 1 - \Phi(\beta) \tag{2.25}$$

In essence, FORM is used to calculate the exceedance probability (or probability of failure) for a given extreme response, y_c. However, in determining the extreme sea state, we are interested in the opposite. That is we would like to find the extreme

response for a given probability. This done by using the IFORM approach. The main idea behind the IFORM is that we have to first specify the exceedance probability and seek the corresponding extreme level response (Chai & Leira, 2018). The principles of the IFORM approach are as follows (Chai & Leira, 2018):

1. For a given exceedance probability, P_f, the reliability index is Φ^{-1} (1-P_f).
2. A sphere of radius Φ^{-1} (1-P_f) is created in U space and a target extreme level is sought, which must be somewhere on the sphere.
3. The sphere is transformed from U space to the physical parameter space, and the target response level, Y_N, say, is found as the highest value on the surface of the physical parameter space. The output of the transformation of the sphere from U space to the physical parameter space yields the environmental contour.

The development of the environmental contour by IFORM is done by (Chai & Leira, 2018): First creating an (n+1)-dimensional sphere of radius Φ^{-1} (1-P_f) in U space, given by:

$$\sum_{i=1}^{n+1} u_i^2 = [\Phi^{-1}(1-P_f)]^2 \tag{2.26}$$

where u_i are the values of the standard normal variables on the sphere. Transforming the variables in U space into the physical parameter space using the Rosenblatt transformation in equation 2.22 to obtain:

$$\Phi(u_{n+1}) = F_{\hat{Y}|S}(y|s) \tag{2.27}$$

and hence

$$y = F^{-1}_{\hat{Y}|S}(\Phi(u_{n+1})|s) \tag{2.28}$$

The values of y (the respective varibales, say H_s, T_p) represent the environmental contour that corresponds to the n-year return level. See illustration in Eckert-Gallup et al. (2016) which shows the process of transformation of points from U space to the physical parameter space using the Rosenblatt transformation. The maximum n-year return level of H_s and related T_p is usually considered design return level. However, in the case of a floating offshore wind turbine, the maximum H_s and related T_p may not produce the critical design load on the structure (Valamanesh et al., 2015). The extreme design variables might be the one that causes the resonant response of the structure. In this case, it could be an H_s lower than the maximum H_s and the corresponding T_p. The tra-

ditional method that is used to establish environmental contours is the IFORM (Vanem & Bitner-Gregersen, 2015). Eckert-Gallup et al. (2016) indicated that the inverse first order reliability method (I-FORM) was the standard design method for generating environmental contours. These contours are used for estimating extreme sea states of a given recurrence interval or return period. The environmental load determined from the environmental contours are used in the design of offshore structures. These structures include ships, dynamic risers, position moorings, offshore floating platforms, and wave energy converters (WEC). The IFORM method will therefore be used to create the environmental contours in this research. However, the reader ought to be aware that there are other methods of creating environmental contours that correspond to a given return period, this includes the Inverse Second-Order Reliability Method (ISORM), the highest density function method, direct Monte Carlo simulations and the principal component analysis (PCA) method (Chai & Leira, Chai & Leira).

2.5.3 Applications of multivariate EVA to determine the extreme design sea state

The process to carry out the design of an extreme wave is given by Eckert-Gallup et al. (2016) as follows:

1. Consideration of hindcast simulations or buoy observations of sufficient duration and appropriate location.
2. Application of extreme value theory and models used for extrapolation to more extreme events than those observed in a shorter period of record.
3. Generation of environmental contours consisting of pairs of significant wave height H_s and either peak period T_p or energy period T_e that elicit extreme structural responses for a given return period.
4. Identification of one or more extreme sea states, which can be used with a wave spectrum (often Pierson–Moscowitz or JONSWAP) to reconstruct time series data generated with a random phase/amplitude model as input for numerical or physical model simulation.

There are various questions that designers could consider when deciding to use a multivariate (environmental contour) approach to design offshore structures. Some of those considerations are:

1. Is it better to use multivariate EVA results instead of univariate EVA results in numerical models?

2. How do the results vary across region i.e. can the same distribution model be used across different geographical locations?

3. Do these distributions apply across hurricane prone regions like the Caribbean? What are the customarily used or preferred distributions? How does the period of record affect the output results?

These questions were raised to highlight the complexity of the multivariate EVA process. These complexities are the reasons why a designer might determine to go with the simpler univariate EVA process to design offshore structures.

As stated previously, the multivariate EVA analysis could be considered a step up from the POT method. That is, there are more data points to fit a model. We now have H_s and T_p in the same space instead of only one variable. However, the H_s, T_p combination that causes the critical load on an offshore structure may not necessarily be the one with the maximum H_s. Caires & van Gent (2008) argued that extreme wave periods do not necessarily occur during storm periods. Haver & Winterstein (2008), in demonstrating this same phenomenon argued that extreme heave motions of a TLP may be governed by sea states along the contours for which T_p is twice the structural period, due to resonance with second-order load effects. In other words, the maximum H_s may not necessarily result in the critical response of the structure. This is one of the defining features of multivariate EVA when compared to univariate EVA. It also becomes very useful when investigating the hydrodynamic performance of low natural frequency structures, for example FOWT (Butterfield et al., 2005; Hiles et al., 2019). These systems may be prone to resonance and compromise the performance of the wind turbine system. The result is that the energy output could be affected.

Regarding how the multivariate EVA results compare with the univariate EVA results, Caires & van Gent (2008) in assessing the extreme wave loads in the Dutch North Sea compared the univariate EVA approach with multivariate approach. The results suggested that the estimates were agreeable and the H_s values from the univariate POT case were the same as the bivariate case. However, the wave period was greater for the bivariate case. It was concluded that coastal structures are subjected to different types of loads, and knowing the joint extreme wave conditions provide a more flexible and expedient way of estimating extreme loads than performing a univariate analysis separately for each choice of load. In carrying out investigations on extreme wave conditions in the US West (Pacific Ocean) and East (North Atlantic) Coasts Neary et al. (2020) reported that the maximum $H_{s(5)}$ and $H_{s(50)}$ levels on the environmental contours agreed well with the corresponding Hs levels estimated using the univariate POT method. The univariate GEV results agreed less well. It was said that this might be

because the univariate POT methods are more consistent with those used in the environmental contour method. Similar to Caires & van Gent (2008), Neary et al. (2020) demonstrated that univariate EVA methods produce similar results to the environmental contour method for H_s. This might be a reason to select the univariate approach for preliminary design of offshore structures as opposed to the more complex environmental contour method. In addition, since the univariate POT method gave results that better agreed with the environmental contour results it might be one of the criteria used to choose the POT method over the block maxima/GEV method. However, because environmental contours give many combinations of H_s and T_p in arriving at the critical design load the univariate approach might not be the best approach to use when the most critical load is not produced by the maximum return levels of H_s and T_p. The same phenomenon between the univariate and multivariate case was also reported by Hiles et al. (2019). In investigating extreme wave statistical methods in the Canadian Pacific Coast (British Columbia, Washington and Oregon) it was reported that the maximum $H_{s(50)}$ and $H_{s(100)}$ contours agreed reasonably well with the corresponding return levels derived from univariate EVA.

Although the multivariate EVA approach gives more H_s and T_p values from which to determine the critical design load, it also introduces some complexity. This is because the critical design load has to be determined from these H_s and T_p combinations. This determination is made by inputting the combinations in the numerical model to check which one produces the critical response of the structure. This process is simplified if we know the likely range of values of H_s that produces the critical response. Vanem & Bitner-Gregersen (2015) in studying environmental contours for marine structure design in West Shetland, Scotland; Nigeria, Western Africa and Northwest Australia, argued that in many cases high values of the significant wave height would give the critical design point, even though not necessarily the highest value. This characteristic was also shown by Valamanesh et al. (2015) who investigated by multivariate analysis the extreme conditions for a fixed-bottom offshore wind turbine in three locations off the US Atlantic Coast (off the coast of Maine, Delaware and Georgia). For one option, a 3D environmental contour was done to create what is called an environmental surface. The variables under consideration were H_s, T_p and V (10 m mean wind speed). It was reported that in all cases critical load was given by a higher, H_s and V and a lower bound T_p value. This was also true for the univariate EVA case where a lower bound T_p in combination with higher values of H_s and V gave the critical load. This provides a basis on which to determine the critical load. That is, it should be a combination of higher values of H_s and V and a lower bound value of T_p. This allows for eliminating some of the combinations on the contour line thus making the process of determining the critical load less tedious and less expensive computationally. There is

also an important aspect of determining the critical design load, which was not considered by Valamanesh et al. (2015) but was done by Winterstein et al. (1993) and is also given in the DNV GL code for determining extreme environmental conditions (DNV, 2010*a*). The critical design response level from the environmental contour tends to be underestimated because response variability is neglected. When carrying out numerical analysis using the design environmental variables (H_s and T_p, say) the design code recommends that more than one simulation be done and the average of the maximum value (most probable maximum) used for the design response. In the case of IEC-61400 DLC 6.1(turbine in parked condition) six-one hour simulations are done and the average maximum value used for the critical response. However, Winterstein et al. (1993) argued that for a stochastic response, the most probable maximum estimated from an environmental contour tends to be underestimated because the contours neglect response variability and so the final responses are underestimated. In order to account for this, the environmental contour should be inflated by a factor, α_o^2 (relative variance). This is like a factor of safety in design. It is termed an uncertainty and accounts for the uncertainties in the response from the environmental parameters. This factor for offshore structural problems typically lies between 0.05 and 0.25 and mostly from 0.1 to 0.2. To make it applicable, it is used to inflate the return period and therefore the environmental contour used to determine the critical response. The desired result is found by defining contours with α_o^2 between 0.1 and 0.2. In order to estimate the 100-year return level from the median response we use contour with a return period of range 140 to 215 years (annual extreme sea states) and about 320 to 1400 years if all sea states are used to generate the contours. This concept was adopted by DNV (2010*a*). DNV (2010*a*) also stated further that instead of inflating the contours, a factor of safety on the response could be used. This factor of safety ranges between 1.1 and 1.3 and is used to multiply the 75% - 90% percentile of the 100-year response, which was determined from the environmental contours. The concept of inflating the probable response was also proposed by Ochi (1993). A design risk parameter, alpha, was applied to the probable extreme state to derive the extreme design sea state. The extreme sea state derived was about 40% greater than the probable sea state.

When carrying out multivariate EVA, the geographical location, from which the environmental variables are obtained, has the potential to create uncertainties. This could determine the distribution models that are used to generate the environmental contours. Ochi (1993) argued that sea severity as evaluated from wave height measurements depends to a large extent on the geographical location where the data is obtained, since the critical factors for sea severity are the frequency of occurrence of storms, water depth and fetch length. In addition, sea severity depends on the growth and decay stage of a storm even though wind speed is the same. Ochi (1993) further stated

that there was no scientific basis for selecting a specific probability distribution function to represent the statistical distribution of sea state (significant wave height). The generalized gamma distribution was thus posited as a distribution that fits sea state characteristics in all geographical locations. Eckert-Gallup et al. (2016) carried out multivariate extreme value analysis in four locations off the US Pacific Coast (2 locations in Northern California, Oregon and Oahu, Hawaii). The study involved comparing the principal component analysis approach to the standard I-FORM approach. In the PCA approach, the variables are transformed into a principal component space and those transformed variables are used to generate the contours using the I-FORM. The models used to fit the transformed variables (C1 and C2) were an inverse Gaussian distribution for C1 and a normal distribution to fit C2 given C1. It was discovered that the inverse Gaussian was a good fit for all of the areas except Oahu. The model did not fit the extreme values well and this resulted in an underestimation of extreme events by environmental contour. It was argued that this phenomenon was due to the inverse Gaussian distribution not being appropriate for the study site. That a more generic distribution or a mixed distribution that fits the variation in behaviour of the extremes at the study site would be required. In the standard I-FORM approach, a Weibull distribution (2 parameter or 3 parameter) is used to fit the marginal distribution of H_s and a lognormal distribution to fit T_p given H_s. However, this approach did not work for Hiles et al. (2019) as the Weibull fit did not represent the upper tail (extremes) of H_s very well. An alternative model was used to fit the marginal distribution of H_s, that is an empirical distribution up to a specified threshold and the GPD was used to fit the upper tail. This in an indication that the distribution model can vary based on location and so part of the complexity of multivariate EVA is to find a distribution that fits the environmental conditions within a given region. This has implications for regions that are hurricane prone, where the majority of the data is of a certain characteristic and there are a few extremes, which are created because of hurricanes within the region. This might create a mix distribution problem as reported by Eckert-Gallup et al. (2016) and might be the case for the study site. It will therefore be investigated further when multivariate EVA is carried out using data for the site in the Caribbean Sea.

Lastly, on the matter of the period record that is used for carrying out multivariate EVA, Valamanesh et al. (2015) did not use the full dataset to fit the model. Instead, they fitted the related distributions (GEV or GPD) to the extreme value data. This is because these distributions better represented the tail behaviour as opposed to one of the standard distributions (Weibull, say) that fits to the whole dataset. On the contrary, Hiles et al. (2019) used the full dataset and used an empirical distribution together with a GPD to fit H_s. Similar to Hiles et al. (2019), Eckert-Gallup et al. (2016) also used the full dataset to generate the environmental contours. It was argued that given a

period of record of the order of ten years, the extreme contour of a return period of the order of hundreds of years should include all of the observed dataset. In principle, this is correct since a greater period of record minimizes the uncertainties. However, this would need further investigation as the model used to fit the data for the Oahu area did not fit the data well and a mixed distribution was proposed. This shows that the period of record is one of the areas of uncertainty in multivariate EVA and this factor is therefore considered for this research. The site is situated in a hurricane prone region, which may bias the distributions that can be used to fit the data and consequently, may determine if the full dataset is used.

Referring to the FOWT stick model in Figure 1.0, the environmental variables (H_s, T_p, u_{10}) obtained from the EVA process are input into a numerical model to assess the performance of the FOWT system. The FOWT system is the focus of the next section.

2.6 Floating Offshore Wind Turbines

2.6.1 General

We will now look at the wind turbine system and in particular, the FOWT system, the core focus of this study. A wind turbine is a machine, which converts the power in the wind to electrical energy. This is in contrast to a windmill, which converts wind power to mechanical power (Manwell et al., 2009). A wind turbine system can be broken down into three components, namely, the rotor nacelle assembly (RNA), tower and the foundation (see Figure 2.8). The foundation for a FOWT consists of a floater (as mentioned in Chapter 1) and a mooring system anchored to the seafloor.

Given that wind turbines generate electricity, they are usually connected to the electrical network by the use of electrical cables. The electrical network may include battery-charging circuits, residential scale power systems, isolated or island networks and large utility grids (Manwell et al., 2009). The make of a wind turbine is of two types, the horizontal axis wind turbine (HAWT) and the vertical axis wind turbine (VAWT). The HAWT is so referred because the axis of rotation is parallel to the ground The wind turbines that are in use today are HAWT and therefore all reference to wind turbines that follow will mean HAWT. In general, a wind turbine is usually classified as upwind or downwind based on the orientation of the rotor to the incoming wind. This is illustrated in Figure 2.9.

2.6.2 Wind turbine components

A brief description of the various parts of the wind turbine system will now be given beginning with the RNA. The RNA could be considered as the core of the wind turbine system and is described by Karimirad (2014) as the most important part of a

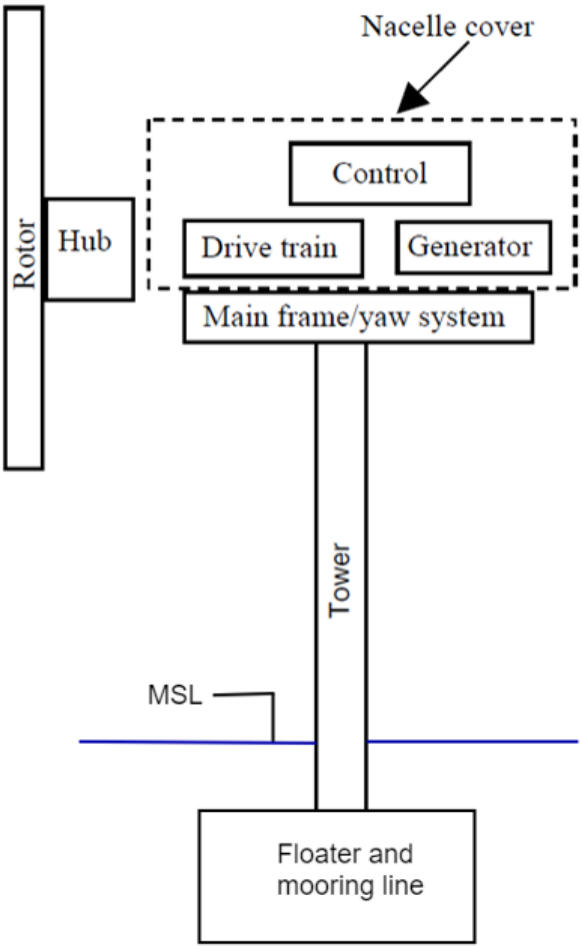

Figure 2.8: Major components of a floating offshore wind turbine (Adapted from: Manwell et al. (2009))
(Permission has been granted by John Wiley and Sons to reproduce this figure)

wind turbine. It is made up of three essential structural components that are used to transform wind energy into electrical energy (Ali et al., 2021). These components comprise the nacelle, gearbox and rotor (hub and blade combined). The nacelle houses the drivetrain, the generator and the controller and supports the anemometer. It is located on top of the tower and is very massive. Nacelles can be as much as 50 ft (15.24 m) long and weigh up to 300 tons (600, 000 lbs). To put things in perspective, a helicopter can weigh as much as 33,000 lbs. Some nacelles are large enough for a helicopter to land on (www.energy.gov/eere/wind/inside-wind-turbine & www.windpowerengineering.com/how-is-a-nacelle-manufactured).

The rotor. The rotor comprises the hub and the blades. Most wind turbines today have upwind rotors and three blades (Manwell et al., 2009). Blades can be as much as 69m long. The Vestas V90 2MW turbine consists of 148 ft (45 m) long blades and the

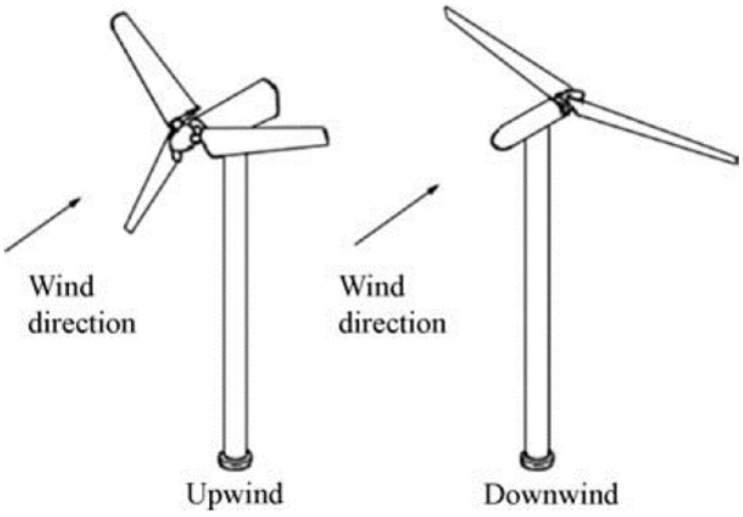

Figure 2.9: Wind turbine rotor configurations (Source: Manwell et al. (2009))
(Permission has been granted by John Wiley and Sons to reproduce this figure)

GE 3.6MW wind turbine consists of 182 ft (55.5 m) long blades (Schubel & Crossley, 2012). Wind turbine blades are usually made of composite material, primarily fibreglass or carbon fibre reinforced composites (Manwell et al., 2009; Mishnaevsky et al., 2017).

Drivetrain. The drivetrain usually consists of a low-speed shaft (on the rotor side), a gearbox and a high-speed shaft (on the generator side). It also includes the support bearings, one or more couplings, a brake, and the other rotating parts of the generator. The gearbox is used to drive the generator. It is used to speed up the rate of rotation of the rotor from a low value (tens of rpm) to a rate suitable for driving a standard generator (hundreds or thousands of rpm) (Manwell et al., 2009).

Generator. The generator is the main electrical part of the turbine that produces 60-Hz (cycle) alternating current (AC) electricity. It usually an induction generator that is obtained off the shelf (Karimirad, 2014).

Controls. The wind turbine control-system is used to optimize performance. It is important for both machine operation and power production. Wind turbine controls include achieving the balance between maximum-power-production, setting upper bounds to limit the torque and power experienced by the drive train and maximizing the useful life (fatigue and structural components) of the wind turbine system (Manwell et al., 2009). A wind-turbine control system consists of a number of computers, which continuously monitor the condition of the wind turbine and collect statistics of the operations from the sensors (Karimirad, 2014)). It consists of the following components (Manwell et al., 2009):

1. Sensors – for inter alia speed, position, flow, temperature, current and voltage.
2. Controllers – mechanical mechanisms and electrical circuits.
3. Power amplifiers – switches, electrical amplifiers, hydraulic pumps and valves.
4. Actuators – motors, pistons, magnets, and solenoids.
5. Intelligence – computers and microprocessors.

Further information on the different parts of the RNA such inter alia the rotor, the drivetrain, the generator and the controller can be found in Karimirad (2014) and Manwell et al. (2009).

Tower and foundation. The main types of towers are free standing (cantilever) type. They are primarily made of steel tubes, lattice (or truss), and concrete. Tower height is typically 1 to 1.5 times the rotor diameter. However, as the size of wind turbine blades increase, the rotor diameter is becoming larger such that the rotor diameter is 1 to 1.5 times hub height (DOE, 2023). The tower selection is usually based on the characteristics at the site (Manwell et al., 2009). The foundations have already been discussed. The fixed-bottom OWT system mainly uses a monopile to support the tower and RNA, and the FOWT uses a floater, connected to moorings anchored to the seafloor, to support the tower and RNA.

2.7 Wind Turbine Theory

2.7.1 General

Now that we have learnt about the components of the wind turbine system, we will look at the theory behind wind turbines and in particular, the FOWT system. The theory is presented within the context of the numerical modelling tool that is used to carry out numerical modelling, the software code FAST.

2.7.2 Software codes used to carry out numerical modelling of FOWT systems

The customary approach to carry out analysis of a FOWT structure is to develop a numerical model to assess its behaviour in different environmental conditions. It was stated previously that to carry out analysis on a complex system such as a FOWT a fully coupled analysis is required (CarbonTrust, 2015); **?**, **?**). This analysis integrates the hydrodynamics, aerodynamics, structural dynamics, mooring line dynamics and control system dynamics to create one model. There are a number of tools available to carry out such an analysis. The work by LIFE50+ (2015*b*) and Cordle & Jonkman (2011) give a comprehensive overview of the state of the art numerical

modelling tools that are used to carry out integrated analysis of FOWT systems. The tools used include WAMIT, AQUA, FAST, BLADED, OrcaFlex, 3DFloat, Flex5, HAWC2, SIMA (SMIO/REFLEX), Sesam/Wadam, SIMPACK Wind, SLOW, TimeFloat, Charm3D and ADAMS. All of the numerical tools listed are either commercially available or propriety owned, except FAST, which is open source. Some of the work mentioned in Chapter 1, used FAST to carry out numerical analysis. In addition, the LIFE50+ 10MW wind-turbine qualification project used FAST to model two different FOWT concepts supporting the Technical University of Denmark(DTU) 10MW reference wind turbines (LIFE50+, 2015*c*). FAST was characterized as a state of the art numerical code, against which simplified numerical tools such as SLOW and QuLAF (frequency domain tool by DTU not given in list above) were compared. The fact that FAST is open source and well supported, coupled with its reputation in the industry it was selected to carry out this research.

2.7.3 Brief overview of FAST

FAST is short for Fatigue, Aerodynamics, Structures and Turbulence (Jonkman & Buhl, 2005). It was developed by the National Renewable Energy Laboratory (NREL) with funding from the US Department of Energy (DOE). The first version of FAST, FAST v4, was published in July 2002. FAST is a time-domain wind-turbine simulation tool that joins aerodynamic models, hydrodynamic models for offshore structures, control & electrical-system (servo) dynamic models and structural (elastic) dynamic models to enable a coupled non-linear aero-hydro-servo-elastic simulation in the time domain (OpenFAST, 2021). It can be used for carrying out analysis of different configurations of two and three bladed horizontal axis wind turbines. This includes, pitch or stall regulation, rigid or tethering hub, upwind or downwind rotor, and lattice or tubular tower. The wind turbine systems that can be modelled with FAST include on land or offshore fixed-bottom or floating substructures. It consists of eight submodules, an overview of each is given below (UMass, Amherst, US, 2020 course notes on modelling wind turbines with FAST and OpenFAST, 2021).

AeroDyn. AeroDyn handles aerodynamics, lift and drag forces on the blades. This model uses wind-inflow data to solve for rotor-wake effects and blade-element aerodynamic loads. The wind inflow data is read in using InflowWind.

InflowWind. InflowWind is a script that reads incoming wind and turbulence information and repackages it in a format that AeroDyn can read.

HydroDyn. HydroDyn is the hydrodynamics module for computing, hydrodynamic wave and current forces on offshore structures. It simulates the regular or irregular incident waves and currents and solves for the hydrostatic, radiation, diffraction and

viscous loads on the offshore substructure.

ServoDyn. ServoDyn is a sub-module dedicated to the control dynamics of the wind turbine. It simulates the controller logic, sensors, and actuators of the blade-pitch, generator-torque, nacelle-yaw, other control devices and the generator and power-converter components of the electrical drive.

ElastoDyn. ElastoDyn handles the structural dynamics. The change from the rigid to elastic model is made by setting the degrees of freedom of the blades and the tower to TRUE (OpenFAST, 2021).

BeamDyn. BeamDyn models the blade dynamics and structural responses. The structural dynamics models apply to forces and reactions from the various components of the wind turbine system. This includes control and electrical system reactions, aerodynamic and hydrodynamic loads, adds gravity loads, and simulate the elasticity of the rotor, drivetrain and support structure.

SubDyn. SubDyn is a module used for modelling complex substructures, like lattices or other floating or fixed-bottom structures.

MoorDyn /MAP++/FEA Mooring. These modules are all dedicated to modelling the mooring system for floating offshore wind turbines.

FAST is the glue code that holds all of the submodules. It allows for coupling between all models using a modular interface and coupler.

In 2017, FAST v8 was transitioned to OpenFAST. It was established by researchers at NREL with funding from the US Department of Energy Wind Energy Technology Office (DOE-WETO). The transition from FAST v8 to OpenFAST was done to better support the open source developer community who utilize FAST-based aero-hydro-servo-elastic engineering models (OpenFAST, 2021). This community comprise research laboratories, industry and academia. The transition included many organizational changes, which are outlined in OpenFAST (2021). The changes included inter alia:

1. The establishment of a new GitHub organization at `https://github.com/openfast`.
2. The OpenFAST glue codes, modules, module drivers, and compiling tools are contained within a single repository:

   `https://github.com/openfast/openfast`.

3. The FAST program was renamed OpenFAST (starting from OpenFAST v1.0.0). (OpenFAST v3.5.0 was released in 2023).

4. An online documentation system has been established to replace existing documentation of FAST v8: http://openfast.readthedocs.io/; during the transition to OpenFAST, most user-related documentation is still provided through the NWTC Information Portal, https://nwtc.nrel.gov.

5. GitHub Issues was made the primary platform for developers to report and track bugs, request feature enhancements, and to ask questions related to the source code, compiling, and regression/unit testing; general user-related questions on OpenFAST theory and usage should still be handled through the forum at https://wind.nrel.gov/forum/wind.

6. A new application programming interface (API) was added that provides a high-level interface to run OpenFAST through a C++ driver code helping to interface OpenFAST with external programs like CFD solvers written in C++ (starting in OpenFAST v1.0.0).

Given the transition from FAST v8 to OpenFAST. A transition was also made for this research and all modelling is done using OpenFAST. This allows for ongoing support from NREL National Wind Technology Centre (NWTC) online portal.

There are a number of different theories involved in creating an integrated wind turbine model. The theories that are dealt with in this research are the aerodynamics, hydrodynamics and mooring line dynamics. The other aspects of the theory are also important but are not considered in this research. The reader can refer to OpenFAST (2021) and Manwell et al. (2009) for information on the theory for those areas.

2.7.4 Aerodynamics – Blade element momentum theory

The blade element momentum (BEM) theory is used to determine the aerodynamic forces and the performance of the wind turbine. The momentum theory can be explained using a model that was originally developed by Betz. This model, which was originally used to determine the performance of ship propellers (Manwell et al., 2009), is used to explain how the power from a wind turbine is generated. The BEM theory could be considered the most important theory in the analysis and design of wind turbine systems because it is applicable to both onshore and offshore wind turbines. It is the theory that gives the primary forces acting on a wind turbine system and the theory that is used to determine the power output of the system. It couples with hydrodynamic and catenary theory to give the overall behaviour of the FOWT. However, the other two theories on their own cannot be used to determine the power output of the system.

The principles of the momentum and blade element theory, which follow, were obtained from Manwell et al. (2009) and Burton et al. (2001).

Momentum theory

The wind turbine system can be idealized as a disk in a tube with air passing through it. See Figure 2.10. The airflow is essentially idealized a stream tube and the turbine as a uniform actuator disc. The disc acts to block the air flowing through the tube but allows some air to pass through.

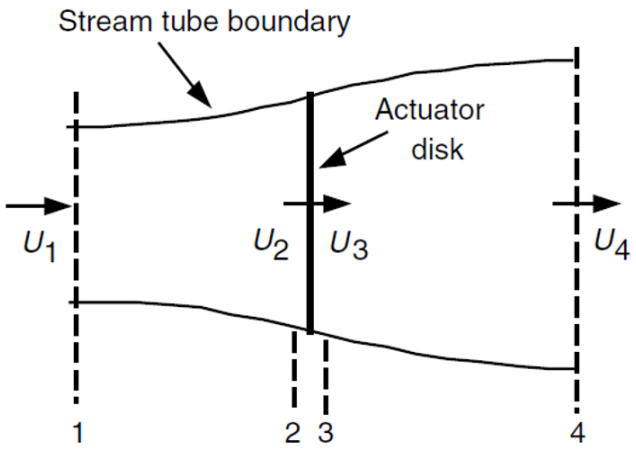

Figure 2.10: Actuator disc model of a wind turbine. U is the mean air velocity and 1 to 4 indicate locations along the stream tube (Source: Manwell et al. (2009))
(Permission has been granted by John Wiley and Sons to reproduce this figure)

This concept has the following assumptions for an ideal rotor (Manwell et al., 2009):

1. The fluid is homogenous, incompressible, has steady state flow
2. There is no frictional drag
3. The number of blades are infinite
4. The thrust over the disc or rotor swept area is uniform
5. There is a non-rotating wake
6. The static pressure far upstream and far downstream is equal to the undisturbed static pressure

Applying the principle of conservation of momentum, the thrust force, T, of the wind on the turbine is equal and opposite to the rate of change of momentum of the air stream

and is given as:

$$T = U_1(\rho AU)_1 - U_4(\rho AU)_4 \tag{2.29}$$

where ρ is the air density, A is the cross-sectional area, U is the air velocity and the subscripts indicate the value of a variable at respective cross-sections in figure **??**. For steady state flow, mass flow rate in is equal to mass flow rate out, such that $\dot{m}$=(ρAU)$_1$ = (ρAU)$_4$, where $\dot{m}$ is the mass flow rate. Hence:

$$T = \dot{m}(U_1 - U_4) \tag{2.30}$$

Assuming no work is done on either side of the rotor (ideal rotor); we apply the Bernoulli principle at each of the control volumes. In control volume 1(stream tube upstream of the disc) we obtain:

$$p_1 + \frac{1}{2}\rho U_1^2 = p_2 + \frac{1}{2}\rho U_2^2 \tag{2.31}$$

In the control volume 2 (stream tube downstream of the disc) we obtain:

$$p_3 + \frac{1}{2}\rho U_3^2 = p_4 + \frac{1}{2}\rho U_4^2 \tag{2.32}$$

where it is assumed that the far upstream and far downstream pressures are equal (p_1=p_4) and the velocity across the disc remains the same (U_2=U_3).

If the pressure difference across the actuator disc is known, the thrust, T, can be expressed as follows:

$$T = A(p_2 - p_3) \tag{2.33}$$

Solving for p_2-p_3 using equations 2.31 and 2.32 and substituting into equation for 2.33, we obtain:

$$T = \frac{1}{2}\rho A_2(U_1^2 - U_4^2) \tag{2.34}$$

Equating the thrust equations from equation 2.30 and 2.34 and noting that mass flow

rate is also equal to $\rho A_2 U_2$, we obtain:

$$U_2 = \frac{U_1 + U_4}{2} \tag{2.35}$$

This shows that the wind speed at the rotor plane, U_2, is the average of upstream and downstream wind speeds. For the wind turbine, we are interested in the maximum power that can be extracted. We therefore define the axial interference factor, also called the induction factor, a, as the fractional decrease in the wind velocity between the free stream and the rotor plane, given by:

$$a = \frac{U_1 - U_2}{U_1}, \tag{2.36}$$

$$U_2 = U_1(1-a), \tag{2.37}$$

and

$$U_4 = U_1(1-2a) \tag{2.38}$$

As the axial induction factor increases from 0, the wind speed behind the rotor decreases. If a =1/2, the wind speed behind the rotor is equal to zero and the simple theory is no longer applicable.

Now the power output, P, is equal to the thrust, T, times the velocity at the disc and is given as:

$$P = \frac{1}{2}\rho A_2(U_1^2 - U_4^2)U_2 = \frac{1}{2}\rho A_2 U_2(U_1 + U_4)(U_1 - U_4) \tag{2.39}$$

Substituting for U_2 and U_4 from equations 2.37 and 2.38 into equation 2.39, gives:

$$P = \frac{1}{2}\rho A U^3 4a(1-a)^2 \tag{2.40}$$

where the control volume area at the rotor, A_2, is replaced by A, the rotor area and the free stream velocity U_1 is replaced by U, to make the equation general. As mentioned previously, we are interested in the maximum power that the turbine can extract from the wind. The wind rotor performance is usually characterized by its power coefficient, C_p, which is given as

$$C_p = \frac{\text{Rotor Power}}{\text{Power in Wind}} = \frac{P}{\frac{1}{2}\rho U^3 A} \tag{2.41}$$

Hence substituting 2.40,

$$C_p = 4a(1-a)^2 \tag{2.42}$$

C_p, the non-dimensional power coefficient, indicates the amount of power in the wind that the rotor can extract. In order to find the maximum power that can be extracted, we first find the maximum value of C_p, by differentiating 2.42 with respect to a, and setting it equal to zero. This gives, a =1/3. Hence: $C_{p,max}$ = 16/27 = 0.5296 and occurs when a =1/3, and

$$P_{max} = \frac{1}{2}\rho A U^3 \left(\frac{16}{27}\right) \tag{2.43}$$

The value $C_{p,max}$=16/27 is known as the Betz limit. It is the maximum rotor power coefficient that is theoretically possible. There are three factors that lead to a decrease in the power extracted and they are:

1. Rotation of the wake behind the rotor
2. Finite number of blades and associated tip losses
3. Non-zero hydrodynamic drag.

If rotation of the wake is accounted for, the rotation of the rotor generates angular momentum. This rotation is imparted to the flow. The same principle of conservation of linear momentum can be applied to the control volumes. Let us make the angular velocity of the flow stream, ω, and the angular velocity of the wind turbine rotor, Ω. We will make the thickness of the annular disc (dr) and the stream tube radius, r such that the cross-sectional area is 2πrdr. See Figure 2.11. It is also assumed that the angular velocity of the flow stream is small compared to the wind turbine rotor, and therefore the pressure in the far wake is equal to the pressure in the free stream. The pressure, wake rotation and induction factors are all assumed, functions of the radius.

The pressure difference before and after the disc is shown to be:

$$p_2 - p_3 = \rho\left(\Omega + \frac{1}{2}\omega\right)\omega r^2 \tag{2.44}$$

The resulting thrust on the annular element, dT, is:

$$dT = (p_2 - p_3)dA = \left[\rho\left(\Omega + \frac{1}{2}\omega\right)\omega r^2\right] 2\pi r dr \tag{2.45}$$

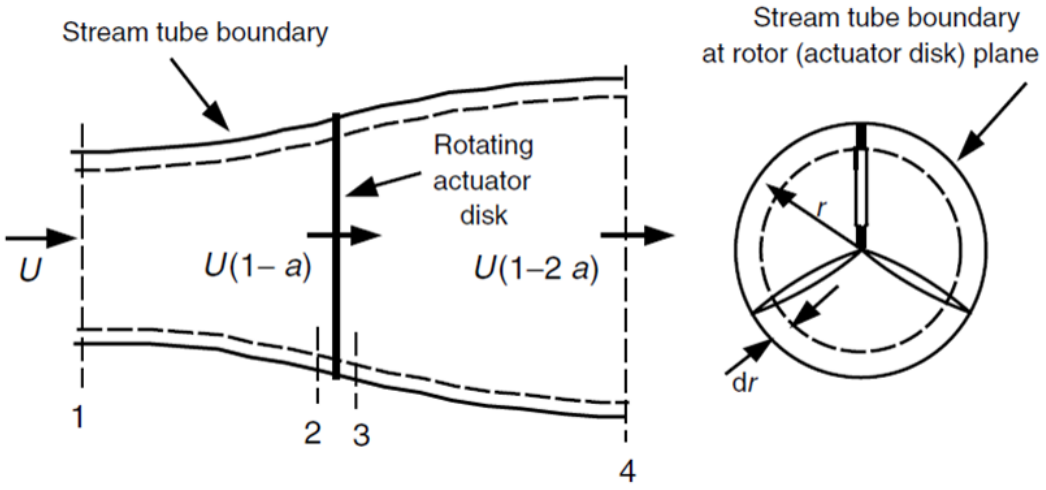

Figure 2.11: Actuator disc model of a wind turbine when wake rotation is considered. U is the velocity of undisturbed air; a is the induction factor, r is the radius and 1 to 4 indicate locations along the stream tube (Source: Manwell et al. (2009))

(Permission has been granted by John Wiley and Sons to reproduce this figure)

An angular induction factor, a', is then defined as:

$$a' = \frac{\omega}{2\pi} \tag{2.46}$$

The thrust therefore becomes:

$$dT = 4a'(1+a')\frac{1}{2}\rho\Omega^2 r^2 2\pi r dr \tag{2.47}$$

The linear momentum analysis that was used to determine the thrust on the disc, with no wake rotation, can also be used to derive the thrust on the disc. Using the axial induction factor, a, and U (instead of U_1) to represent the free stream velocity, the thrust is given as:

$$dT = 4a(1+a)\frac{1}{2}\rho U^2 2\pi r dr \tag{2.48}$$

The torque on each rotor can be determined by applying the principle of conservation of angular momentum. The torque exerted on the rotor, Q, must equal the change in angular moment of the wake. The torque applied to small area of the annular element

is given by:

$$dQ = d\dot{m}(\omega r)(r) = (\rho U_2 2\pi r dr)(\omega r)(r) \tag{2.49}$$

Given that U_2=$U_1(1-a)$ and $a' = \omega/2\Omega$, this equation becomes:

$$dQ = 4a'(1-a')\frac{1}{2}\rho U \Omega r^2 2\pi r dr \tag{2.50}$$

The power generated at each element, dP, is given by:

$$dP = \Omega dQ \tag{2.51}$$

Substituing into equation 2.50 gives:

$$dP = \frac{1}{2}\rho A U^3 \left[\frac{8}{\lambda^2}a'(1-a)\lambda_r^3 d\lambda_r\right] \tag{2.52}$$

where λ is the tip speed ratio, defined as as the blade tip speed to the free stream wind speed and is given by, λ = $\Omega R/U$; and λ_r, the local speed ratio, is the ratio of the rotor speed at some intermediate radius to the wind speed and is given by, λ_r = $\Omega r/U$ = $\lambda r/R$.

Blade Element Theory

The blade element theory uses a 2-dimensional aerofoil and an angle of attack to calculate the lift and drag forces on a blade element. The angle of attack is determined from the incident resultant velocity in the cross-sectional plane of the blade element. There are tables that have been developed that give the aerofoil coefficients (C_d) and (C_l) based on the angle of attack.

If we consider a turbine with B blades, tip radius R and each with cord length c. Let the pitch angle measured between the aerofoil zero lift line and the plane of the disc be θ_p. In addition, let the blades rotate at an angular velocity Ω and the wind speed be U_{rel}. The tangential velocity of the blade is Ωr and the tangential velocity of the wake is $a'\Omega$, therefore the net tangential velocity of the blade element is $(1+a')\Omega$. See figure 2.12 for blade elements and figure 2.13 for the forces and velocities relative to the blade chord line at radius r.

The variables shown in figure 2.13 are defined as follows:

θ_p is the section pitch angle, the angle between the cord line and the plane of rotation of the disc.

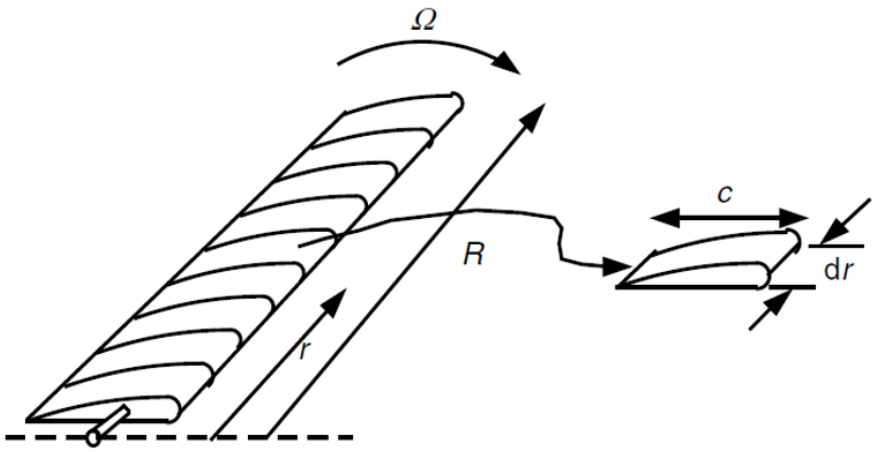

Figure 2.12: Illustration of blade elements. c is the aerofoil chord length; dr is the radial length of the element, r is the radius, R is the root radius and Ω is the angular velocity of the rotor (Source: Manwell et al. (2009))
(Permission has been granted by John Wiley and Sons to reproduce this figure)

$\theta_{p,0}$ is the blade pitch angle at the tip.

α is the angle of attack (the angle between the cord line and the relative wind).

ϕ is the angle of the relative wind.

dF_L is the incremental lift force.

dF_D is the incremental drag force.

dF_N is the incremental force normal to the plane of rotation (contributes to thrust).

dF_T is the incremental force tangential to the circle swept by the rotor (creates useful torque).

$U(1-a)$ is the wind velocity at the blades

U_{rel} is the relative wind velocity.

From figure **??**, the resultant velocity on the blade is given by:

$$U_{rel} = \sqrt{U_{rel}^2(1-a)^2 + \Omega^2 r^2 (1+a')^2} \tag{2.53}$$

or

$$U_{rel} = \frac{U(1-a)}{\sin\phi} \tag{2.54}$$

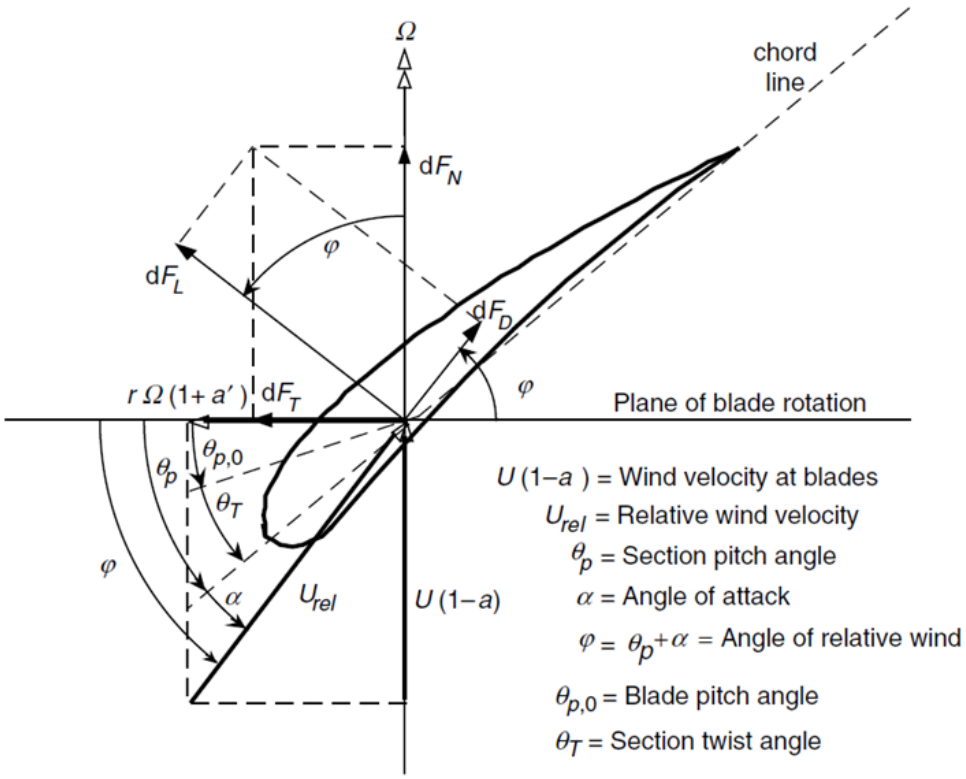

Figure 2.13: Blade geometry, forces and velocities for a horizontal axis wind turbine (Source: Manwell et al. (2009))
(Permission has been granted by John Wiley and Sons to reproduce this figure)

The resultant velocity acts at an angle to the plane of rotation,ϕ, such that:

$$\sin\phi = \frac{U(1-a)}{U_{rel}},\ \cos\phi = \frac{\Omega r(1+a')}{U_{rel}} \text{ and } \tan\phi = \frac{\sin\phi}{\cos\phi} = \frac{1-a}{(1+a')\lambda_r} \tag{2.55}$$

The angle of attack α is given by:

$$\alpha = \phi - \theta_p \tag{2.56}$$

If we consider a small element along the length of each blade, dr, the lift force on this length, normal to the direction of U_{rel}, is given by:

$$dF_L = \frac{1}{2}\rho U_{rel}^2 c dr C_l \tag{2.57}$$

and the drag force parallel to U_{rel} is given by:

$$dF_D = \frac{1}{2}\rho U_{rel}^2 c dr C_d \tag{2.58}$$

The incremental normal force is given by:

$$dF_N = dF_L cos\phi + dF_D sin\phi \tag{2.59}$$

and dF_T is given by:

$$dF_T = dF_L sin\phi - dF_D cos\phi \tag{2.60}$$

Since the rotor has B blades, the total normal force on a section of distance, r, from the centre is:

$$dF_N = \frac{1}{2}\rho U_{rel}^2 (C_l cos\phi + C_d sin\phi) c dr B \tag{2.61}$$

The differential torque due to a tangential force operating a distance at a distance, r, from the centre is given by:

$$dQ = Br(dF_T) \tag{2.62}$$

therefore

$$dQ = \frac{1}{2}\rho U_{rel}^2 (C_l sin\phi - C_d cos\phi) c r dr B \tag{2.63}$$

The power, dP, is given by:

$$dP = \frac{1}{2}\rho U_{rel}^2 (C_l sin\phi - C_d cos\phi) c \Omega r dr B \tag{2.64}$$

The blade element theory and the momentum theory essentially do the same thing. They are used to determine the thrust and torque on an annular section of the rotor. However, the momentum theory defines the thrust and torque in terms of the axial and angular induction factors (based on the flow conditions). While the blade element theory defines the thrust and torque in terms of the flow angles at the blade and the aerofoil characteristics.

These equations from the blade element theory and the momentum theory are used to formulate the strip theory or BEM theory. This theory is then used to determine the

wind turbine blade characteristics and the wind turbine performance.

OpenFAST uses the BEM theory to determine the loads on the wind turbine blades. This is done using the AeroDyn module in combination with InflowWind. InflowWind is used to generate the wind loads. This wind load can be inter alia steady wind or turbulent wind.

2.7.5 Hydrodynamic theory

The hydrodynamic loads in OpenFAST are computed by using the Morison equation or the potential flow theory or a combination of both. This is done using the HydroDyn module. The Morison equation is used to calculate wave loads on slender cylindrical structures when the effects of diffraction and radiation are negligible (Liu et al., 2019b). A structure such as a floating offshore platform is a large volume structure. For large volume structures, the Morison equation is not used to calculate the forces, as it does not take into consideration wave diffraction and wave radiation. Wave diffraction and radiation occur in large volume structures and hence a theory that considers these forces is used to compute the forces on these kinds of structures.

The potential flow theory is one such theory. The basic assumption of the potential flow theory is that the sea water is incompressible and inviscid and the fluid motion is irrotational (Faltinsen, 1990). A velocity potential can therefore be used to describe the velocity vector V$(x,y,z,t) = (u,v,w)$ at time t, at point x = (x,y,z) in a Cartesian coordinate system in fixed space. Since the water is incompressible, the velocity potential has to satisfy the Laplace equation. The solution of the Laplace equation with the appropriate boundary conditions on the fluid yields the velocity potential for irrotational and incompressible fluid motion.

For the potential flow theory, a potential function ϕ (x, y) is defined; the equation used to calculate ϕ is given by (Liu et al., 2019b):

$$\nabla^2\phi = 0 \tag{2.65}$$

where $\partial\phi/\partial$x = u , $\partial\phi/\partial$y = v and $\partial\phi/\partial$z = w; u,v and w are the velocity components of the flow field in Cartesian coordinates. The boundary condition at the free surface, the surface of the structures and at the sea bed are determined. These boundary conditions are used to determine the potential function, from which the velocity component of the flow is determined. These components are then used to determine the acceleration and pressure components and subsequently the hydrodynamic loads acting on the floater.

The HydroDyn User's Manual outlines how HydroDyn computes the forces. It states,

inter alia, that waves in HydroDyn are modelled as either first order (Airy) or first-plus second order- wave theory with the option to include directional spreading. However, no wave stretching or higher order wave theories are included. The following principles apply when modelling fixed-bottom structures and floating platforms:

1. Fixed-bottom structures - When modelling a fixed-bottom system, the use of a strip-theory (Morison) only model is recommended. When HydroDyn is coupled to OpenFAST, SubDyn is used for the substructure structural dynamics.

2. Floating Platforms - When modelling a floating system, you may use potential-flow theory (via a WAMIT pre-process) only, strip-theory (Morison) only, or a hybrid model containing both. WAMIT is to a tool that is used to analyze wave interactions on offshore structures and it is often used to find the hydrodynamic added mass and damping coefficients in the frequency domain. These values are pre-determined based on the geometry of the floater and inputted into OpenFAST.

Linear wave theory

Linear wave theory also referred to as first-order wave theory, small-amplitude wave theory, sinusoidal wave theory or Airy wave theory is applicable to sea conditions in which the wave height is assumed small in comparison to the wavelength and water depth (DNV, 2010*a*; Reeve et al. (2004). This assumption allows the free surface boundary conditions to be linearized by dropping the wave height terms beyond the first order. In addition, it allows the free surface conditions to be satisfied at the mean water level, rather than at the oscillating free surface (Chakrabarti, 1987). This makes the linear wave theory applicable for computing hydrodynamic loads on floating offshore structures, which are typically deployed in deep water. Hence, its suitability for analyzing FOWT structures in OpenFAST. However, where the sea conditions are non-linear such as for very large waves or in shallow water where waves are breaking, OpenFAST may not be appropriate and high fidelity modelling codes such as computational fluid dynamics (CFD), that consider higher order wave theories, would be better suited.

The Airy wave equations. Consider a two dimensional sea where the x-axis is the horizontal direction and the z-axis is the vertical direction, with positive z-direction pointing upwards (see figure 2.14). If a wave propagates along the positive x-direction, the variation of the free surface elevation with time (relative to mean sea level) regardless of water depth is given by (USFOS, 2010; Faltinsen, 1990):

$$\eta = \zeta_a \cos(\omega t - kx) \tag{2.66}$$

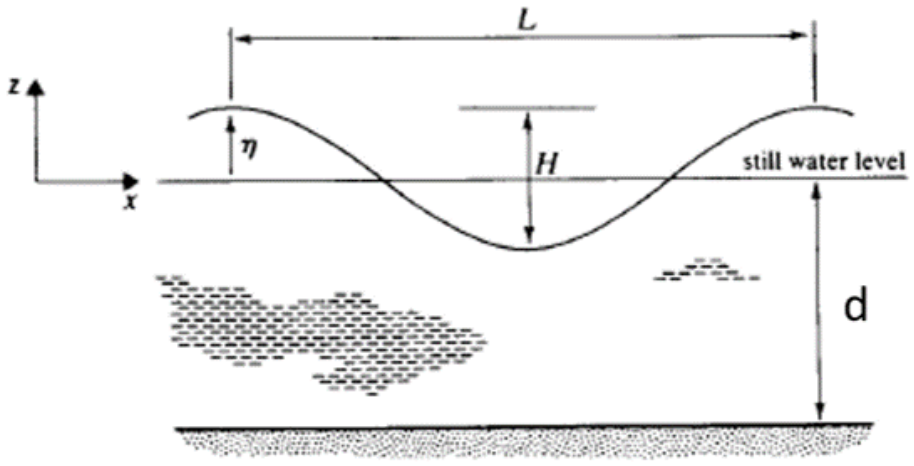

Figure 2.14: Definition sketch of 2d-sea (Adapted from: Reeve et al. (2004))
(Permission has been granted by Dominic Reeve to reproduce this figure)

where x, is the coordinate axis in the direction of wave propagation, t is time, ζ_a is the wave amplitude = $H/2$, $k = 2\pi/L$ is the wave number for wave length L and $\omega = 2\pi/T$ is the wave radian or angular frequency at wave period T.

In deep water (also referred to as infinite water depth), $d/L > 0.5$, the wave potential is given by:

$$\phi = \frac{g\zeta_a}{\omega} e^{kz} cos(\omega t - kx) \tag{2.67}$$

where g is the acceleration due to gravity, ζ_a is the wave amplitude, d is the water depth, ω is the wave angular frequency and k is the wave number defined by $\omega^2 = gk$.

For a wave propagating in the positive x-direction the horizontal particle velocity is given by:

$$u = \frac{\partial \phi}{\partial x} = \omega \zeta_a e^{kz} \sin(\omega t - kx) \tag{2.68}$$

and the vertical particle velocity is given by:

$$w = \frac{\partial \phi}{\partial z} = \omega \zeta_a e^{kz} \cos(\omega t - kx) \tag{2.69}$$

The horizontal particle acceleration is given by:

$$a_x = \frac{\partial u}{\partial t} = \omega^2 \zeta_a e^{kz} \cos(\omega t - kx) \tag{2.70}$$

and the vertical particle acceleration is given by:

$$a_z = \frac{\partial w}{\partial t} = -\omega^2 \zeta_a e^{kz} \sin(\omega t - kx) \tag{2.71}$$

The hydrodynamic pressure is given by:

$$p = \rho g \zeta_a e^{kz} \sin(\omega t - kx) \tag{2.72}$$

where the first term is the static part and the second term is the dynamic part.

The reader should note that there are also equations for a finite water depth ($0.05 < L < 0.5$) and a shallow water ($d/L < 0.05$). However, because the FOWT system is installed in deep water those equations are not included.

The frequency dependent hydrodynamic coefficients (added mass and damping) are needed before running the potential-flow solution in HydroDyn. Therefore, as stated previously, an external pre-processor, such as WAMIT or otherwise, has to be used to generate the frequency dependent hydrodynamic coefficients.

2.7.6 Mooring line theory

The purpose of the mooring system is to keep the offshore floating structure in place within the sea environment. A mooring system, as described by Faltinsen (1990), is made up of a number of cables which are attached to the floating structure at different points with the lower ends of the cables anchored to the seabed (see figure 2.15). In Chapter 1, it was stated that mooring systems used to anchor floating structures such as semi-subs and spar-buoy can be catenary or taut mooring systems. The system that is used for the floaters in this research is a catenary type mooring system.

The forces in the mooring line can be calculated using a quasi-static method or a dynamic analysis method. According to Zhao et al. (2019), the multi-segmented quasi-static method is based on classic catenary theory. This uses the average mooring line loads, the seabed friction of each mooring line and the non-linear geometric restoring force to analyze the mooring system. However, the quasi-static method does not consider the bending stiffness, the inertia and the hydrodynamic damping force in each mooring line. The dynamic analysis approach includes these properties, which are not considered by the quasi-static approach. The equations for finding the forces in the mooring line using the quasi-static approach are given by (Liu et al., 2019a; Liu et al.,

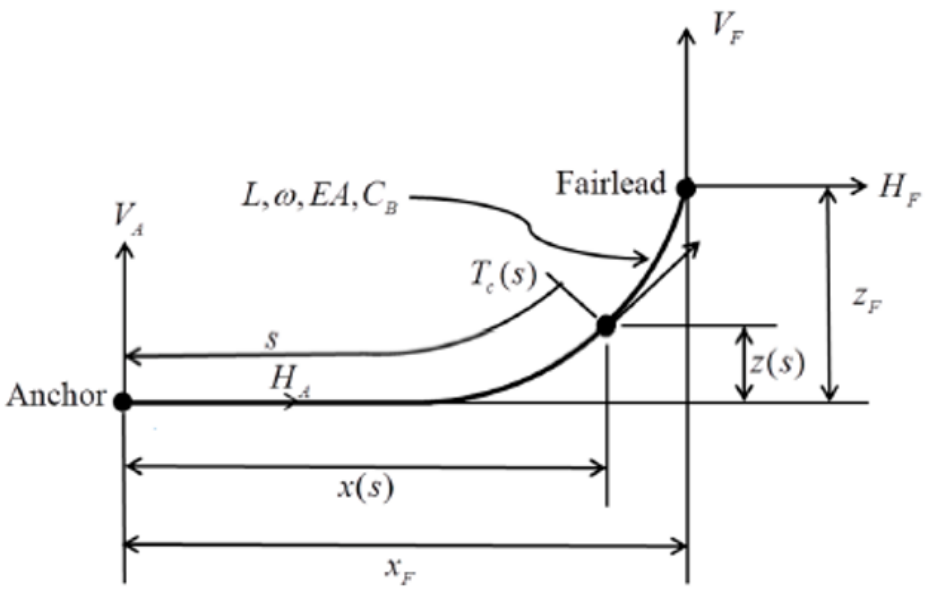

Figure 2.15: Definition sketch of a mooring line (Source: Zhao et al. (2019))
(Permission has been granted by Xin Li to reproduce this figure)

2019b; Zhao et al., 2019):

$$X_F(H_F,V_F) = L - \frac{V_F}{w_M} + \frac{H_F}{W_M} ln\left[\frac{V_F}{H_F} + \left\{\sqrt{1+\left(\frac{V_F}{H_F}\right)^2}\right\}\right] + \frac{H_F L}{EA} + \frac{C_B w_M}{2EA}\left[-\left(L - \frac{V_F}{w_M}\right)^2 + \left(L - \frac{V_F}{w_M} - \frac{H_F}{C_B w_M}\right) MAX\left(L - \frac{V_F}{w_M} - \frac{H_F}{C_B w_M}, 0\right)\right] \tag{2.73}$$

$$Z_F(H_F,V_F) = \frac{H_F}{W_M} ln\left[\frac{V_F}{H_F} + \left\{\sqrt{1+\left(\frac{V_F}{H_F}\right)^2}\right\}\right] + \frac{H_F}{W_M} ln\left[\frac{V_F}{H_F} + \left\{\sqrt{1+\left(\frac{V_F}{H_F}\right)^2}\right\}\right] + \frac{1}{EA}\left(V_F L - \frac{w_M L^2}{2}\right) \tag{2.74}$$

where H_F and V_F are the horizontal and vertical components of the effective tension in the mooring line at the fairlead, X_F and Z_F are the horizontal and vertical coordinates of the reference points, at distance s, along the mooring line, w_M is the apparent weight per unit length of line in fluid, L is the unstretched length of a mooring line, A is the cross-sectional area of a mooring line, C_B is the coefficient of the static-friction drag between the sea bed and a mooring line and EA is the extensional stiffness of a mooring line.

The equations can be solved iteratively using the Newton-Raphson method. The

MAPP++ mooring module, mentioned previously, uses the quasi-static approach to find the forces in the mooring line.

The dynamic analysis method can be carried out by coupling OpenFAST to the MoorDyn module. This method uses a lumped-mass model to compute the forces on the mooring line. Essentially, the mooring line is discretized into a number of segments such that the forces in each segment acts at the nodes. The total force in the mooring line is determined by summing the forces at each node. The lumped-mass model is illustrated in figure 2.16.

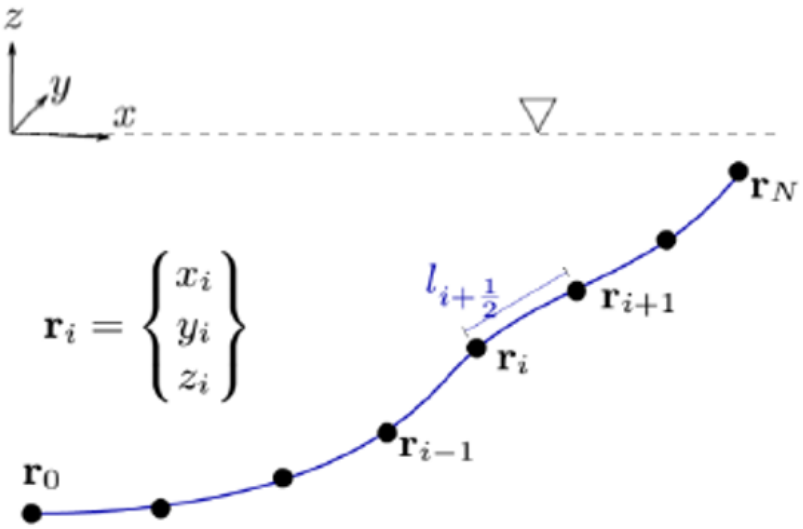

Figure 2.16: Illustration of lumped-mass model used in MoorDyn (Source: Hall (2017))
(Permission has been granted by Matthew Hall to reproduce this figure)

According to Hall (2017) with the lumped-mass approach the cable dynamics is discretized over the entire length of the mooring line. The cable is broken up into N evenly sized line segments connecting N+1 node points. The indexing starts at the anchor (or lower end), with the anchor node given a value of zero. The cable segment between node 0 (lower node) and 1(upper node) an index of ½. The model uses a right-handed inertial reference frame with the z-axis being positive upwards taken from SWL. This aligns the coordinate system with the one used in OpenFAST. Each node is defined by a position vector r. Each segment of the cable has identical properties of unstretched length, diameter, density and Young's modulus. However, different cables can have a different set of properties and other cables can be connected at the ends (nodes), to allow for a mooring system with interconnected lines.

The dynamic analysis approach is utilized to compute the forces on the mooring line

in this study. Therefore, the MoorDyn module is used in OpenFAST to compute the mooring loads.

2.7.7 Governing equation of motion for a floating platform

The platform governing equations is determined using Newton's second law of motion, F=ma. The platform is a considered as a rigid body with 6-DOF, three translationally and three rotationally. The dynamics of a FOWT in the time domain is given by the following equation (Liu et al., 2019b):

$$(M+A)\ddot{X(t)} + C\dot{X(t)} + KX(t) = F^{waves(t)} + F^{wind(t)} + F^{mooring(t)} + F^{vis(t)} \tag{2.75}$$

where the variables on the LHS are defined as follows:

$X(t)$ is the generalized displacement of the platform in the time domain, $\dot{X(t)}$ is the generalized velocity, $\ddot{X(t)}$ is the genaralized acceleration, M is the mass matrix, A and C are the hydrodynamic added mass and damping coefficient matrices (caused by the wave radiation), respectively and K is the hydrostatic restoring force matrix.

the external forces on the RHS are defined as follows:

$F^{waves}(t)$ is the incident wave induced force, $F^{wind}(t)$ is the wind loading on the blades of the tower, $F^{mooring}(t)$ is the mooring line tension and $F^{vis}(t)$ is the drag force caused by fluid viscosity.

2.8 Floating Offshore Wind Turbine Design Manuals

Wind turbine design manuals are normally used in the analysis and design of FOWT systems. This is in keeping with standard design practice and ensures that designs, which are carried out, satisfies particular requirements. This helps to minimize the risk of life and (or) property being destroyed. LIFE50+ (2015*c*) gave a comprehensive review of FOWT design standards. However, this review did not arrive at the conclusion that a single wind turbine standard could be considered the most appropriate for FOWT designs. In fact, it was argued that the complete design of a FOWT system requires the use of several codes. The codes can be selected from one produced by the different certification bodies. This includes those produced by DNV, IEC, ISO, API and similar bodies.

LIFE50+ (2015*c*) mentioned some of the major FOWT design standards that are used in the industry. They include inter alia:

- DNV-OS-J103:2013 Design of Floating Wind Turbine Structures. DNV-OS-J103 needs to be applied in combination with DNV-OS-J101 and DNV-RP-C205.

- DNV-OS-J101:2014 Design of Offshore Wind Turbine Structures
- DNV-RP-C205:2010 Recommended Practice Environmental Conditions and Environmental Loads
- DNV-RP-F205:2010 Global Performance Analysis of Deep Water Floating Structures
- GL-IV-2:2012 Guideline for the Certification of Offshore Wind Turbines
- IEC-6400-1:2019 Wind energy generation systems – Part 1: Design requirements
- IEC-6400-3-2:2019 Wind energy generation systems – Part 3-2: Design requirements for floating offshore wind turbine
- ABS-195:2013 Guidelines for Building and Classing Floating Offshore Wind Turbine Installations
- Class NK: 2012 Guidelines for the Design of Floating Offshore Wind Turbines

Although there are several standards available to analyse and design of FOWT systems, there is uncertainty about the application of these standards in different jurisdictions. In particular, the turbulent wind models used for the IEC standard were developed using mostly onshore wind measurements where the surface roughness differ from onshore (ABS, 2011). Ishihara et al. (2012) and Leu et al. (2014) have reported that the IEC wind turbulence models were developed using data from the North Sea and the US. Therefore, although the wind turbine standards are beneficial, a cautious approach has to be taken when using them. This is necessary because of the assumptions on which they were developed as well as the environmental conditions that exist in the regions that provide the basis for their development.

LIFE50+ (2015*c*) having carried out a review of the different FOWT standards used the DNV-OS-J103, as the main reference standard for the design of their floating wind concepts. The DNV suite of standards was also used as the main reference standard to carry out this research. This was selected on the basis that it was recommended by LIFE50+ (2015*c*) and that it as an open source document that can be downloaded online. The IEC, API, ISO suite of standards, and others like them, are not readily available as they are produced for commercial use. It should be noted that LIFE50+ (2015*c*) said that the DNV-OS-J103 should be used in combination with DNV-OS-J101 and DNV-RP-C205. Two other DNV standards, which were published subsequent to publication of LIFE50+ (2015*c*) include:

- DNVGL-ST-0119: 2018 Floating wind turbine structures
- DNVGL-RP-0286: 2019 Coupled analysis of floating wind systems

These other two DNV manuals were also used in combination with DNV-OS-J103.

2.9 Numerical Modelling of Floating Offshore Wind Turbines

The determination of the design loads is a foundational step in the numerical modelling and design of offshore structures. There is an inextricable link between the determination of the design environmental conditions and the development of the numerical model. This is because the design variables determined by EVA are the variables inputted into the numerical model to generate the loads and determine the design response. In chapter 1, it was mentioned that among the key challenges in the design of FOWT was the provision of a structure that has a good wave response to prevent the structure from experiencing large dynamic loads or compromise wind-turbine performance. It was also argued that the trend shows that the spar-buoy and the semi-sub are the most dominant floaters in use to date. However, the floater with the most projects in the pipeline was the semi-sub. This is the floater type that is investigated in this research. The performance of a FOWT system when exposed to various environmental loads is an important offshoot of the overall system design. Numerical modelling is one of the methods used to carry out the analysis and design of the FOWT and thereby assess the performance of the system. Jonkman & Matha (2011) gave a comprehensive overview of the process involved in the analysis of three wind turbine concepts. The MIT/NREL TLP, the OC3-Hydwind Spar buoy and the ITI energy barge. These represented three of the primary floating platforms that support the NREL baseline 5MW wind turbine. The overall design and analysis steps for the project were outlined. Although these steps were project specific, they gave a general outline of the process involved in comparative analysis and design of FOWT systems. The primary features of the steps were as follows:

1. Use the same wind turbine specifications (to ensure equal comparison) —including specifications for the rotor, nacelle, tower and controller—for each system. This applies if the same wind turbine system is being investigated in two different locations. Likewise, use the same environmental conditions for each analysis—including meteorological (wind) and oceanographic (wave), or metocean parameters. This applies if the performance of different floater types is being investigated.

2. Determine the properties of each floater, including the platform and mooring system designs. To be suitable, each floating platform must be developed specifi-

cally to support the rotor, nacelle, and tower of the wind turbine. Some platforms may require adaptation of the wind-turbine control system in this step to avoid controller-induced instabilities of the overall system.

3. Develop a model of each complete system within a comprehensive simulation tool capable of modelling the coupled dynamic response of the system from combined wind and wave loading. Modelling the dynamic response of land- and sea-based wind turbines requires the application of comprehensive aero-hydro-servo-elastic simulation tools that incorporate integrated models of the wind inflow, aerodynamics, hydrodynamics (for sea-based systems), controller (servo) dynamics and structural (elastic) dynamics in the time domain in a coupled nonlinear simulation environment.

4. Verify elements of each full system dynamics model from step 3 by checking its response predictions with responses predicted by a simpler model. This step is important for catching errors that could be difficult to identify in the much more exhaustive analysis of step 5.

5. Using each full system dynamics model from step 3, perform a comprehensive loads analysis to identify the ultimate loads and fatigue loads expected over the lifetime of the system. Loads analysis involves running a series of design load cases (DLCs) covering essential design-driving situations, with variations in external conditions and the operational status of the turbine. The loads are examined within the primary components of the wind turbine, including the blades, drive train, nacelle, and tower—and for the floating system, the mooring lines. Potential unexpected instabilities also can be found in this process.

6. Using the results of step 5, characterize the dynamic responses of the land- and sea-based systems. Comparing the responses of the three sea-based systems with each other enables quantification of the impact of the platform configuration on the turbine.

7. Improve each floating system design through design iteration (i.e., iterating on step 1 through step 6), ensuring that each of the system components is suitably sized through limit-state analyses. The results of step 6 can help identify where design modifications must be made to arrive at a suitable design for the floating system.

8. Evaluate each system's economics using cost models, including the influences of the turbine design, construction, installation, O& M and decommissioning. It is likely that the 'best' floating wind turbine concept for a given installation site is the concept with the least-expensive lifecycle cost of energy. Economic analysis

shows how the design choices affect the resulting cost of energy. It can also quantify to what extent the cost savings because of the simple design, construction and installation of the barge are balanced by the need for a strengthened turbine.

9. Identify the best features from each concept that, when combined into a hybrid concept potentially will provide the best overall system-wide characteristics; then repeat step 1 through step 8 with the hybrid concept. This step also should assess variations in the wind turbine concept and consider unconventional features such as lightweight rotors, high power ratings, two blades instead of three or downwind rotors instead of upwind rotors.

It should be noted that not all of these steps would be applied in this research as it is not practical to do so but the process is carried out using the ones that are appropriate. The ones that are considered are steps 1, 2, 3, 5 and 6. However, not all of them are applicable as the standard turbine platforms have already been developed by NREL. This will therefore eliminate some of the steps.

Some of the specific considerations when carrying out the numerical will include the tools utilized to carry out integrated wind turbine modelling. That is, tools that integrate the aerodynamics, hydrodynamics, control system dynamics and structural dynamics of the FOWT. The design codes that are used and the applicable DLC. The hydrodynamic performance of the floater for the appropriate degrees of freedom (for example heave and pitch). Benefits and limitations of numerical modelling and the economics of the process. The hydrodynamic coefficients such as the frequency-domain hydrodynamic added mass and hydrodynamic damping matrices are also important. These are usually determined using a frequency- domain analysis tool such as WAMIT (Jonkman & Matha, 2011).

Valamanesh et al. (2015) carried out numerical analysis on a fixed-bottom OWT using the National Renewable Energy Laboratory (NREL) wind-turbine analysis code, FAST. The environmental variables were determined using a univariate and a multivariate EVA approach. The variables (H_s, T_p and wind speed) for both options were input into the FAST model to determine and compare the design response of the system for each option. The system was modelled for the parked condition using DLC 6.1 stipulated in the IEC-61400-3-1 (2019) standard. A similar numerical modelling approach is taken in this research, with the overall objective to compare the performance of a floater in the North Sea with a floater in the Caribbean Sea.

2.10 Conclusion

This literature review was done to assess some of the past work that has been done on EVA and the analysis and design of FOWT systems. It was discovered that even though EVA is one of the key methods used to deteremine the extreme sea state and wind speed which are input into wind turbine numerical models to determine their response, the process has some uncertainties. One of the uncertainties, is the environmental conditions in a particular geographical location and how this can impact on the distribution models that are used to fit data. This issue was presented in the work by Eckert-Gallup et al. (2016). It was shown that the data from the Oahu region of Hawaii, did not fit the Gaussian distribution model. Although this model was a good fit for three other locations off the US Pacific Coast. In the work by Hiles et al. (2019) at a location off the Canadian Pacific Coast, the 3P-Weibull was not a good for the marginal distirbution of H_s. A combination of an empirical distibution and the GPD model were used to fit the data. It was posited that these findings have implications for regions, like the Caribbean, which has normal conditions for a particular period of the year but are prone to hurricanes for the rest of the year. This might create a mixed distribution problem (Eckert-Gallup et al., 2016). It is one of the problems that has been identified in the literature and investigations will be carried out to see if the same situation exists in fitting a distribution model to the data from the Caribbean Sea. If the same problem exists, what is a suitable distribution that can be used to fit the data and thereby determine the extreme sea state.

The discourse on the extreme environmental conditions on a FOWT and the numerical modelling to determine the response, did not specifically consider the response of the FOWT in hurricane prone regions. The 50-year extreme sea state and wind speed determined by EVA, recommended by the wind turbine design standards, is not a suitable criteria for wind turbines in hurricane prone regions. Worsnop et al. (2017) argued that turbines deployed in regions that are prone to hurricanes are at tremendous risk of damage. Additionally, the current design criteria stipulated by the IEC wind turbine design standard does not provide design parameters for wind turbines exposed to tropical cyclones. Li et al. (2022) argued that the current research on wind turbines in hurricane regions, primarily focuses on onshore wind turbines and fixed-bottom offshore wind turbines. It was also said that few studies have been carried out on the response of FOWT in hurricane conditions. Taking these findings in the literature into consideration, the challenges in carrying out studies on FOWT in the respective hurricane region is considered to be three-fold. Firstly, it has to be determined if dsitribution models, like the 3P-Weibull is appropriate to fit the sea state data in the Caribbean Sea. Secondly, are the 50-year extreme sea state and wind speed, recommended by the wind turbine

design standards, comparable with the sea sate and wind speed that occur in hurricane conditions? Finally, is a FOWT in hurricane conditions at greater risk of damage given that it is a more complex structure which is held in place by mooring lines? These are some of the areas, upon review of the literature, that need further investigation.

This research will therefore focus on the response of a prototype FOWT in extreme environmental conditions. In particular, to test the response of one of the state-of-the-art numerical models comprising of a large wind turbine in the extreme environmental conditions of the North Sea and the Caribbean Sea. The study is also extended to include the response of the FOWT in the most extreme conditions in the Caribbean Sea, hurricane conditions. It is believed that a research of this nature will make a substantial contribution to the exiting body of knowledge for FOWT systems.

Chapter 3

Development of a Univariate Extreme Sea State and Extreme Wind Speed off the South Coast of Jamaica

3.1 Introduction

In the previous chapter, it was posited that one of the most critical factors in the development of offshore wind turbines is finding the critical design load. A precursor to finding the design load is to determine the extreme environmental conditions that is used to generate the loads. The extreme sea state (H_s, T_p) and extreme wind speed define the environmental conditions that are used for such purpose. These environmental variables are found by extreme value analysis. There are various studies that have been carried out to determine the n- year return levels for H_s, T_p and u_{10} (Palutikof et al., 1999; Caires & van Gent, 2008; Caires, 2011; Teena et al., 2012). However, none of these studies was based in the Caribbean. The purpose of this chapter is to demonstrate how to use the raw data for the Jamaica Caribbean Sea and carry out analysis to yield the extreme values. The site, shown in Figure 3.1, is located off the south coast of Jamaica, approximately 22 km from Portland Bight, St. Catherine. The latitude and longitude coordinates are 17.5, -77.00 and the water is approximately 100 m deep. There are two Port facilities near to the site namely, Port Esquivel and the Port at Rocky Point. Port Esquivel is approximately 40 km from the site and Rocky Point is approximately 32 km away. There is also a main power plant, The Jamaica Public Service Company (JPS) Old Harbour Power Station, which is approximately 41km from the site. In keeping with DNV (2010*a*), the 50-year H_s, corresponding T_p, and the 50-year wind speed were determined.

3.2 Selection of Software for Extreme Value Analysis

The carrying out of extreme value analysis is usually done using software. The extreme value analysis by Coles (2001) was carried with a program called S-Plus. This is commercial software for carrying out statistical analysis. It uses the S statistical programming language (https://www.dataone.org/software-tools/s-plus-s). Gilleland et

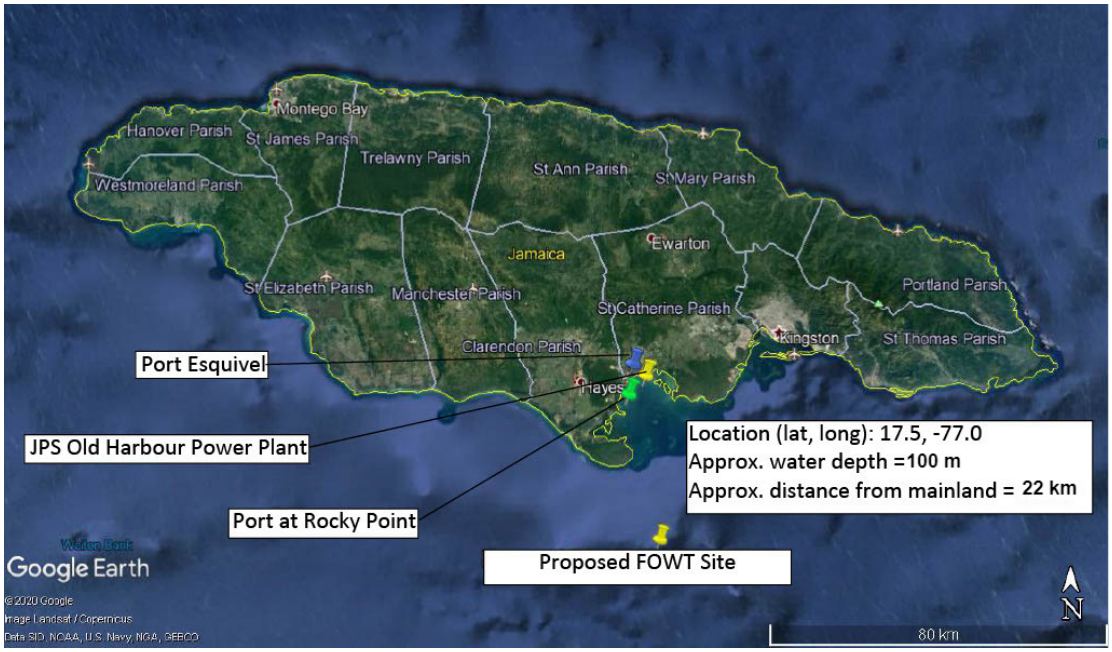

Figure 3.1: Map of Jamaica showing location of proposed FOWT site (17.5 N, 77.0 W)

al. (2012) gave an overview of a variety of software packages that were available for conducting extreme value analysis. Over 13 software packages were mentioned. Most of the programs were written in a programming language called R. It is defined as an open-source, statistical software and learning environment. Gilleland et al. (2012) posited that the R software language has become the software language that was most used by academic statisticians, because it was open-source and freely available without propriety licensing requirements.

Other programs mentioned which were not written in R but useful for carrying out extreme value analysis include EVIM (Extreme Value Analysis in Matlab), a free Matlab package(Gençay et al., 2001). It was said to contain univariate routines for inter alia block-maxima, peaks-over-threshold and extremal index estimation. However, it appeared to be no longer in development. The Matlab package, WAFO, was also mentioned. WAFO (Wave Analysis for Fatigue and Oceanography) is a toolbox of Matlab routines for statistical analysis and simulation of random waves and random loads (Brodtkorb et al., 2017). It can be used for statistical analysis of random processes, such as extreme value analysis. It contains routines for both GEV and GPD distributions. The GPD can be used for peaks over threshold analysis. There is also another Matlab toolbox which was not mentioned by Gilleland et al. (2012). It is called NEVA (Non-stationary Extreme Value Analysis). The NEVA software package has been developed to facilitate extreme value analysis under both stationary and non-stationary assumptions(Cheng &AghaKouchak, 2014). It includes two components, the GEV dis-

tribution for analysis of annual maxima (block maxima) and the GPD for analysis of extremes above a certain threshold (POT analysis). The list software presented by Gilleland et al. (2012) were perused, a shortlist was made and one was selected to carry out extreme value analysis. The criteria used for arriving at the shortlist were easily accessible, versatility in carrying out extreme value analysis & development and tutorial support. The shortlist comprised of the following:

1. WAFO
2. EVIM
3. NEVA
4. extRemes (R based software)

WAFO is relatively good to carry out GEV analysis using block maxima approach. However, it was not found to be comprehensive enough for POT analysis. The tutorial indicates that the examples illustrate how to carry out elementary extreme value analysis. This was discovered to be the nature of its applicability for POT analysis. In order for it to come to better POT functionality, it would have required modification to the structure of the Matlab scripts. It would have also required the formulation of new scripts. In particular, the modifications would have been required to generate the return level plots. In addition, for the analysis to select the threshold value, the mean residual life plot does not include the confidence intervals. Therefore, it was considered limiting.

EVIM is considered a bit more versatile than WAFO. It allowed for selecting threshold using the mean residual life plot approach as well as plot of the shape parameter against the threshold. However, the threshold range allowed is not wide enough. It also did not have a function to generate the return level plots. As indicated previously, it is no longer being developed.

NEVA is found to be the less versatile than WAFO and EVIM. It did not allow analysis to determine the threshold. It would therefore require that the threshold be determined beforehand in another program, say WAFO or EVIM, before proceeding to generate the return level plots.

extRemes version 2.0. This package is developed on the R programing platform (Gilleland & Katz, 2016). It is primarily intended for weather and climate applications, although it can be used for other applications. This new version replaces a previous version. It is used from the command line, and implements methods from univariate extreme value theory. It adopts the notation of Coles (2001). This software is considered the most versatile and apt for carrying out univariate extreme value analysis.

Although it is open-source, it has good development support and a comprehensive tutorial. This tutorial also provides good explanation, which allows for understanding the input data and interpreting the outputs. It utilizes the mean residual life plot approach as well as parameter analysis for determining the threshold. In addition, after selecting the threshold it allows for carrying out of a declustering process, supported with a corresponding plot that demarks the selected threshold value. The independent peaks generated by declustering are used to generate the return period plot. Gilleland & Katz (2016) argued that the strengths of the program include:

- Systematic and thorough treatment of univariate extremes (understood to include covariates)
- An extensive tutorial with use of real/realistic weather and climate data sets
- A large number of users who provide considerable feedback for continuing improvement and continued financial support through the Weather and Climate Impacts Assessment Science Program that allows ongoing package maintenance and user assistance. See `http://www.assessment.ucar.edu` for further information.

Because of these advantages, the ease of use of the software, and the added benefit of being open-source, it was selected for carrying out extreme value analysis. It will henceforth be referred to as extRemes.

3.3 Development of Extreme Sea State and Wind Speed at Location 17.5N, 77.0W

The data used for H_s is the European Centre for Medium-Range Weather Forecasts (ECMWF) ERA5 reanalysis data. The data from 1979 to 2018, sampled every three hours, is downloaded from `https://www.ecmwf.int/en/forecasts/datasets/browse-reanalysis-datasets`. The variable H_s only is mentioned because in carrying out extreme value analysis the extreme values of T_p are usually considered in relation to H_s. In univariate EVA, this can be done by using an appropriate relationship from an appropriate wind-turbine design standard. The values of T_p given H_s were therefore found using the following relationship from DNVGL (2016), Clause 2.4.4.2:

$$11.1\sqrt{H_{S,50-yr}/g} \leq T \leq 14.3\sqrt{H_{S,50-yr}/g} \tag{3.1}$$

where, $H_{S,50-yr}$ is the unconditional extreme significant wave height with a return period of 50-years.

3.3.1 Data preparation – checking the quality of the data

It was mentioned in the previous chapter, that the data used to carry out extreme value analysis has to be sufficiently long to get the best results. In particular, to derive the n-year event the length of the data should be at least n/3 years. Model data tends to span over long periods and is therefore suitable for developing extreme sea states. Although this is very useful for designers, model data tend to have modelling related errors. Therefore, the quality of the model data that is used to carry out extreme value analysis must first be checked before it is used to produce results for use in design. Caires (2011) outlined a process that should the carried out to check data quality and refine it, where necessary. The checks on the quality of the dataset for this research were largely carried out in accordance with these recommendations. The following checks were carried out:

1. Checking for missing data
2. Checking for repeated measurements (i.e., having the same measurement dates) and measurements for significant wave height $<$ 0.15m. These values were discarded. This is because they were not deemed to be actual storms. In addition, in general, these smaller values are not necessary to determine the extreme values.
3. Checking for outliers
4. Checking to determine if the climate can be considered stationary.

It should be noted that no outliers were identified. There were a few H_s values that appeared to be very high. However, they were real values which occurred during the passage of hurricanes Allen (Aug 5-9 1980), Gilbert (Sept 12 to 14, 1988) and Ivan (Sept 9 to 14, 2004), tropical storm Emily (Jul, 16 2005) and hurricane Dean (Aug 20 to 21, 2007). These values were retained in the dataset. These checks carried out on the ECMWF ERA5 dataset confirmed that it was of good quality. This provided a good basis for carrying out extreme value analysis.

The data for u_{10} was obtained from DHI metocean on demand portal. The 3hr-sampled data, from 1979 to 2018, was downloaded from https://www.metocean-on-demand.com/#/main. No outliers were identified.

3.3.2 Checking the accuracy of the results from extRemes

The validity of the results from extRemes was checked using data from Caires (2011). The results agreed well (Table 3.1). It can be seen that the GPD results are greater than the GEV results. This could be due to its shape factor, ξ, being greater than that of the GEV. Caires (2011) argued that a greater shape factor may be an indication that

the estimates of the GPD are more reliable than those of the GEV, due to its larger sample size.

Table 3.1: Comparison of GEV and GPD results for H_s(Caires (2011) vs Plymouth)

	Block maxima/GEV, Caires (2011)			**Block maxima/GEV, Plymouth**		
Description	**95% lower CI**	**Estimate**	**95% upper CI**	**95% lower CI**	**Estimate**	**95% upper CI**
Location(μ)	8.52	**10.57**	11.50	9.91	**10.61**	11.31
Scale(σ)	0.59	**1.46**	2.46	0.90	**1.43**	1.96
Shape(ξ)	-1.15	**-0.38**	-0.09	-0.73	**-0.37**	-0.02
Hs100(m)	10.57	**13.72**	16.76	12.68	**13.72**	14.77
Sample size	21			21		

	POT/GPD, Caires (2011)			**POT/GPD, Plymouth**		
Description	**95% lower CI**	**Estimate**	**95% upper CI**	**95% lower CI**	**Estimate**	**95% upper CI**
Location(μ)	-	-	-	-	-	-
Scale(σ)	1.110	**1.49**	1.93	1.096	**1.48**	1.87
Shape(ξ)	-0.33	**-0.15**	0.03	-0.34	**-0.145**	0.045
Hs100(m)	12.81	**14.36**	16.57	12.22	**14.39**	16.56
Sample size	119			119		
Threshold(m)	8.27			8.27		

3.3.3 Extreme Value Theory

Extreme value theory is laid out in Chapter 2. It is mentioned that two of the foundational models used in EVA are the annual maxima model and the peaks over threshold (POT) model. These models were used to determine the EVA sea states in the following sections.

3.3.4 Analysis of block maxima

Significant wave height and wind speed

The GEV analysis was carried out for H_s and u_{10}. The parameters and 50 and 100-year return levels are shown in Table 3.2. The return level plot for H_s is shown in Fig. 3.2 and the qq-plot is shown in Fig. 3.3. The GEV showed good fit to the data except for the three (3) most extreme values. This is an indication that for the most extreme values there is a greater degree of uncertainty. Like H_s, the GEV model also showed a good fit to the wind data (Figs. 3.4 and 3.5).

Table 3.2: Extreme value analysis results of H_s, T_p and u_{10} at Jamaican site(17.5N,77.0W)

	Block maxima/GEV			**POT/GPD**		
	Hs(m)			**Hs(m)**		
Description	**95% lower CI**	**Estimate**	**95% upper CI**	**95% lower CI**	**Estimate**	**95% upper CI**
Location(μ)	2.23	**2.36**	2.48	-	**-**	-
Scale(σ)	0.25	**0.37**	0.48	0.12	**0.29**	0.47
Shape(ξ)	0.15	**0.39**	0.63	0.11	**0.64**	1.18
Hs_{50}(m)	3.29	**5.83**	8.38	1.79	**6.71**	11.62
Hs_{100}(m)	3.09	**7.23**	11.37	-0.63	**9.34**	19.30
Sample size	40			37		
Threshold(m)				2.5		
	Tp(s)			**Tp(s)**		
Description	**95% lower CI**	**Estimate**	**95% upper CI**	**95% lower CI**	**Estimate**	**95% upper CI**
Tp_{50}(s)	-	**9.02 ~13.26**	-	-	**9.68 ~ 14.23**	-
Tp_{100}(s)	-	**10.04 ~ 14.77**	-	-	**11.42 ~ 16.78**	-
	u10(m/s)			**u10(m/s)**		
Description	**95% lower CI**	**Estimate**	**95% upper CI**	**95% lower CI**	**Estimate**	**95% upper CI**
Location(μ)	11.32	**11.94**	12.55	-	**-**	-
Scale(σ)	1.11	**1.67**	2.23	0.62	**1.13**	1.63
Shape(ξ)	0.08	**0.43**	0.78	0.06	**0.45**	0.83
$u10_{(50)}$(m/s)	13.55	**28.66**	43.78	13.64	**27.01**	40.39
$u10_{(100)}$(m/s)	10.01	**35.81**	61.61	10.00	**33.40**	56.80
Sample size	40			62		
Threshold(m/s)				11.92		

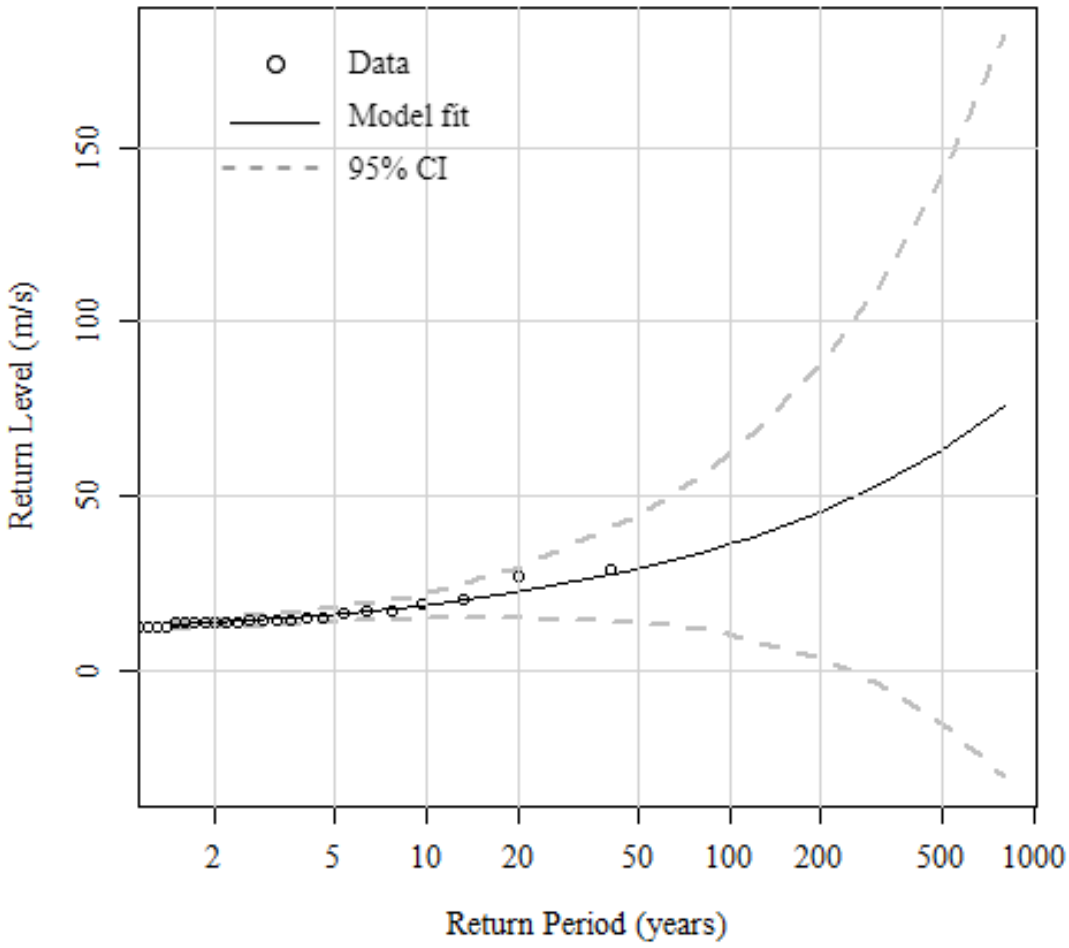

Figure 3.2: GEV return levels of H_s for site at 17.5N, 77.0W

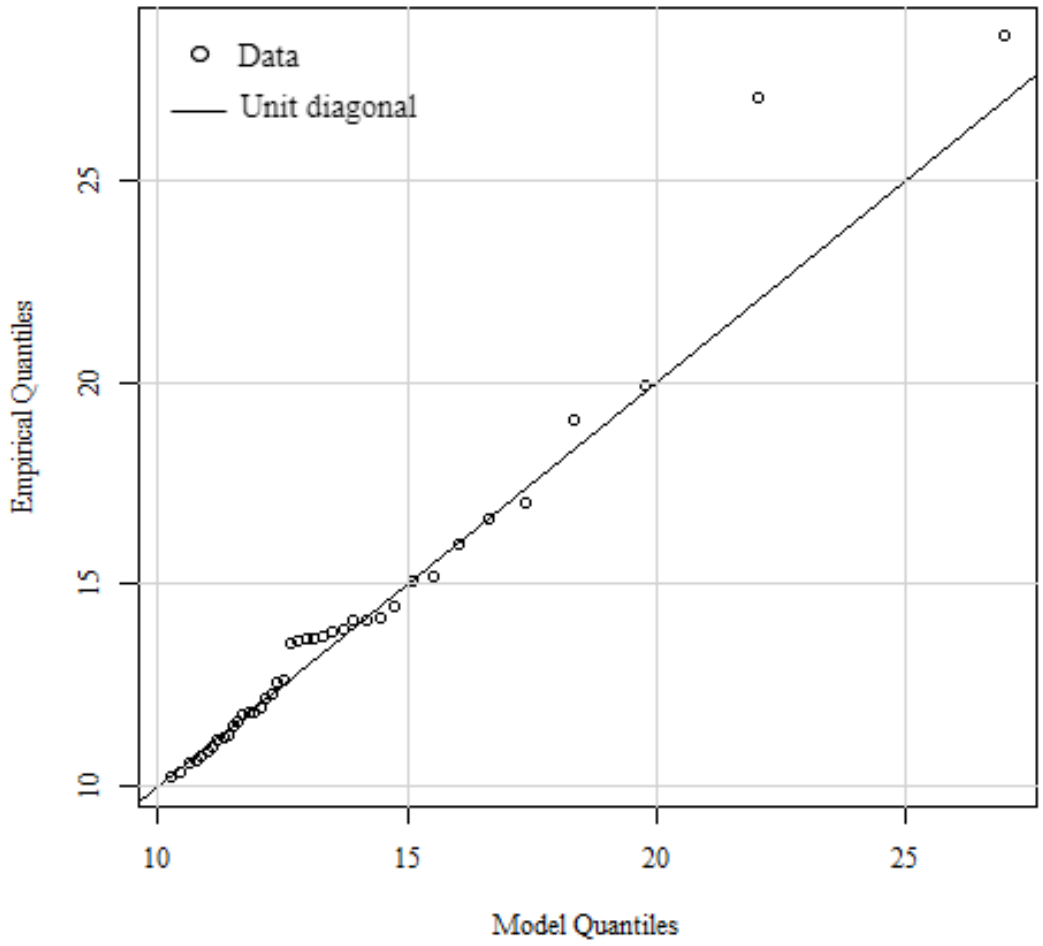

Figure 3.3: Q-Q plot of H_s for site at 17.5N, 77.0W(GEV analysis)

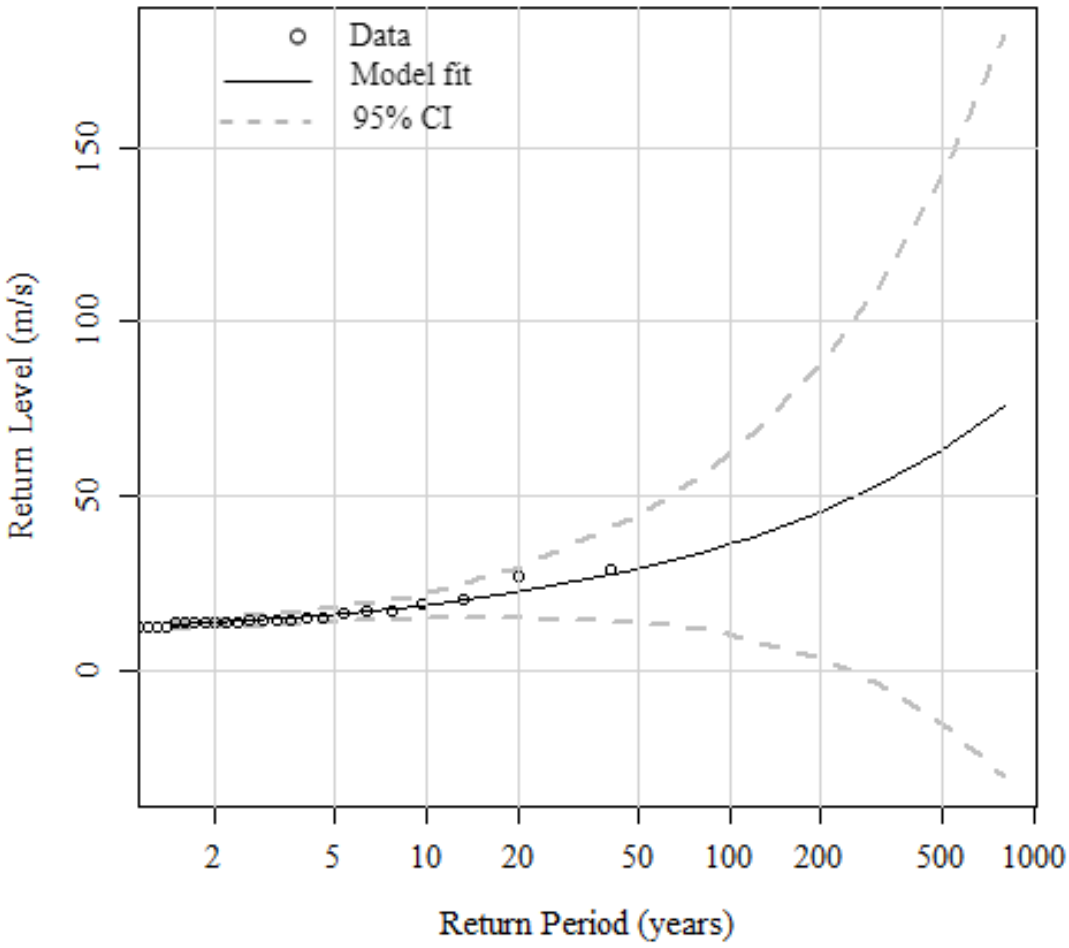

Figure 3.4: GEV return levels of u_{10} for site at 17.5N, 77.0W

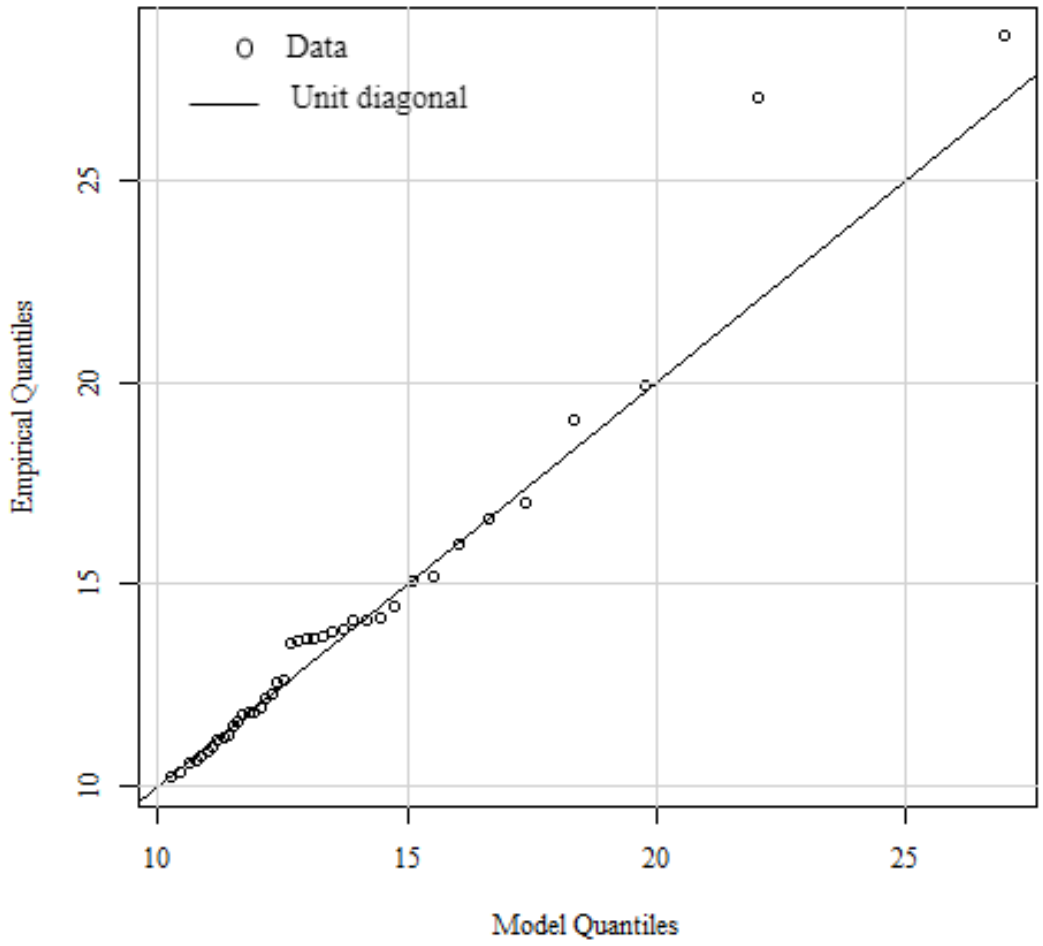

Figure 3.5: Q-Q plot of u_{10} for site at 17.5N, 77.0W(GEV analysis)

3.3.5 GPD/POT Analysis

Threshold selection

The threshold selection was done using a combination of the mean residual life plot (Fig. 3.6 for MRLP of H_s), the threshold stability parameters (Fig. 3.7 for stability parameters of H_s) and the fit of the return level plot. The mean residual life plot (MRLP) is a plot of u against the 'mean excess' (mean exceedances of u, minus u), for a range of values of u. The plot should be linear above the threshold at which the GPD model becomes valid. From the MRLP a threshold of 2.5m was selected. This value was selected since within this region the curve exhibited a linear behaviour (Gilleland & Katz, 2016). Other values within this linear range could have been selected but the value selected should maintain the balance between bias and variance. Too high a value would result in bias and fewer data points would be available. However, too low a value would result in a large variance of the estimates. Having made an initial selection of the threshold value, the threshold stability parameters were used to justify the value selected. The stability parameters plot (threshrange plot) is a plot of the parameter estimates from the GPD against u, for a range of values of u. The parameter estimates should be stable above the threshold for which the GPD is valid. This plot indicated that a threshold as low as 1.5 m might be appropriate. This was because the threshold values after 1.5 m did not change much with further increase of the threshold, that is, remained stable/constant within the confidence bounds. However, a final threshold value of 2.5 m was selected as it gave a return level plot that showed the best fit to the data. Therefore, it could be argued that in selecting the threshold, the minimum value that gives a return period plot showing the best fit to data should be selected. While at the same time giving a return level that is reasonable. In other words, for 40 years of data and a maximum H_s value of 9.0 m (the approx. value of the 1:40 year return level), the 100-year result should yield a value that is greater than 9.0 m. If the threshold value selected does not yield a return value that makes sense, a more appropriate value should be chosen regardless of the theoretical considerations. The MRLP and thresh range plots give an initial estimate of what the likely threshold value could be, but the final threshold should be based on how well the data fits the return period plot. These were the reasons for a threshold value of 2.5 m being selected. The same principle was applied to select threshold for u_{10}.

Significant wave height and wind speed

The qq-plots and return level plots for the GPD analysis are shown in Figs. 3.8 to 3.11. A threshold value of 11.92 m/s was used for u_{10}.The extremal index for $u10$ was 0.64, confirming a good degree of independence of the sample. The GPD model showed a good fit to the data for H_s, and u_{10} respectively. However, it should be noted from the

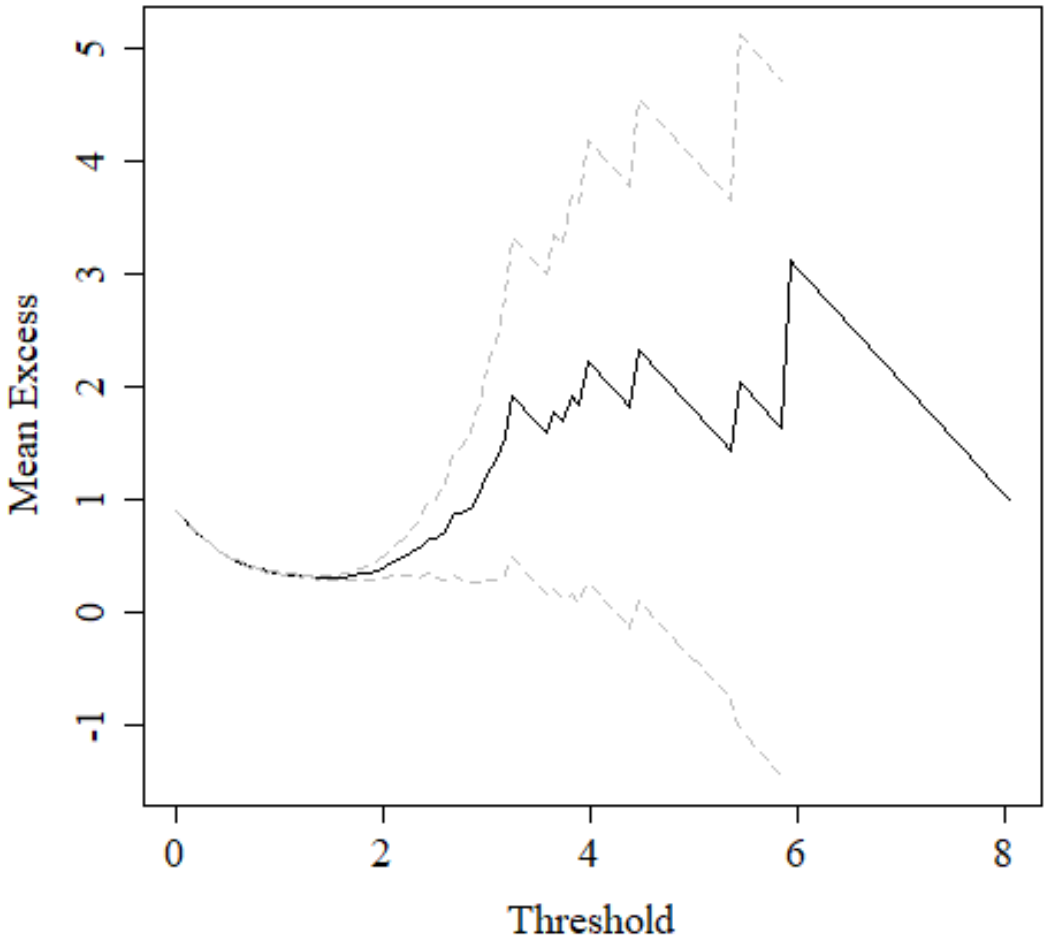

Figure 3.6: Mean residual life plot of H_s for site at 17.5N, 77.0W

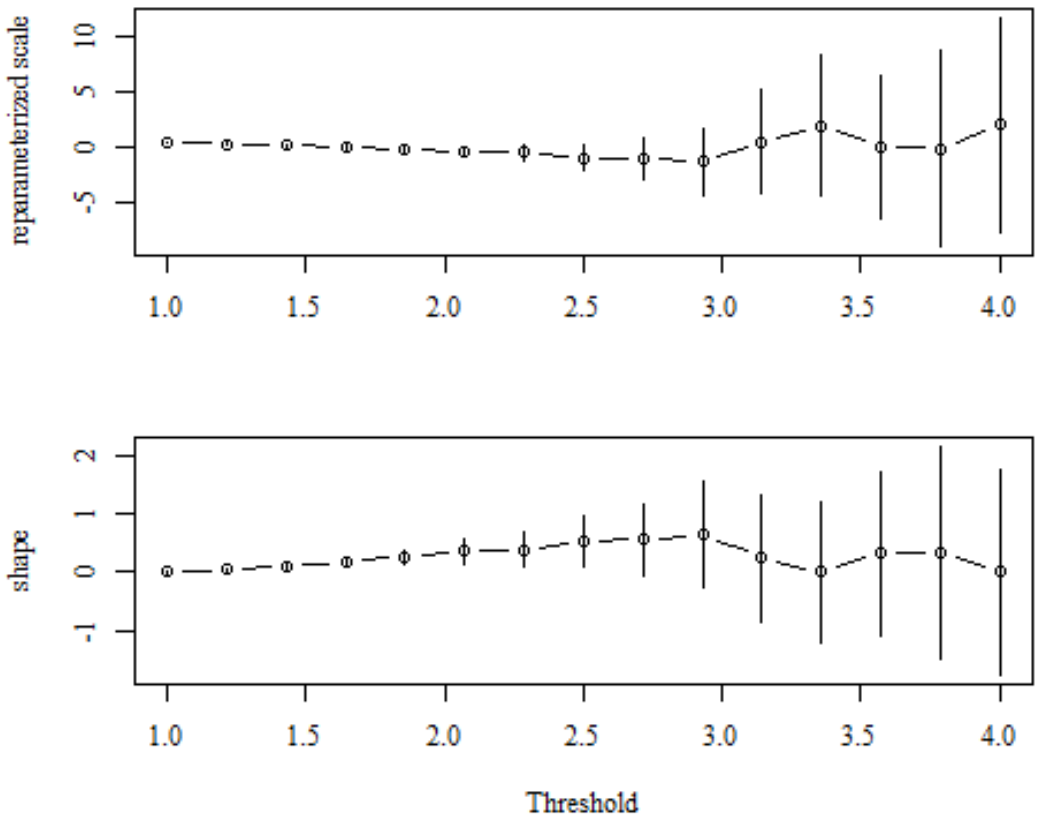

Figure 3.7: Threshold stability parameters of H_s for site at 17.5N, 77.0W(GPD analysis). Vertical lines are the width of the confidence interval band.

qq and return level plots that u_{10} showed a somewhat better fit to the data than H_s as demonstrated by the three most extreme values. Making reference to Table 3.3, it was also seen that the 50 and 100-year return levels for H_s using the GPD analysis were greater than the values using the GEV analysis. This is in keeping with the pattern that was observed by Caires (2011). It was argued that since the parameter estimates of the GPD were larger than the GEV, this may be an indication that the GEV sample was not large enough to provide reliable estimates. Therefore, the GPD return values were chosen for H_s. Unlike H_s, the return levels from the GEV model for u_{10} were greater than the values for the GPD model. Palutikof et al. (1999) argued that the distribution used most frequently in wind studies is the GEV type I, applied to a set of annual maxima. The GPD, even though it was derived from a larger sample than the GEV produced smaller return levels. This might be the reason why the GEV model is mostly used to determine the extreme values for wind speeds. The GEV model return levels were therefore selected for u_{10}.

Table 3.3: Summary of GEV and GPD 50 and 100 year design sea states and wind speeds, Jamaica(17.5N, 77.0W)

Description	**Block maxima/GEV**	**POT/GPD**
Hs_{50}(m)	5.83	6.71
Hs_{100}(m)	7.23	9.34
Tp_{50}(s)	9.02 ~ 13.26	9.68 ~ 14.23
Tp_{100}(s)	10.04 ~ 14.77	11.42 ~ 16.78
$u10_{(50)}$(m/s)	28.66	27.01
$u10_{(100)}$(m/s)	35.81	33.40

The GPD distribution is usually considered to be better suited for extreme value analysis because it uses a larger data sample in relation to the GEV distribution (Caires, 2011; Palutikof et al., 1999). However, from a design perspective, it could be argued that the choice of distribution could be based on the variable being investigated as well as the reason for carrying out the investigation. For example, if a preliminary design is being conducted, the GPD analysis might be the most appropriate for H_s. This would allow for a more conservative design so that if modifications are required later, because of cost, one could defer to the GEV analysis. On the contrary, for u_{10}, the GEV analysis would be more suited and if modifications are required subsequent, because of cost, the GPD analysis could be carried out.

When carrying out GPD/POT analysis, the threshold selection process is usually con-

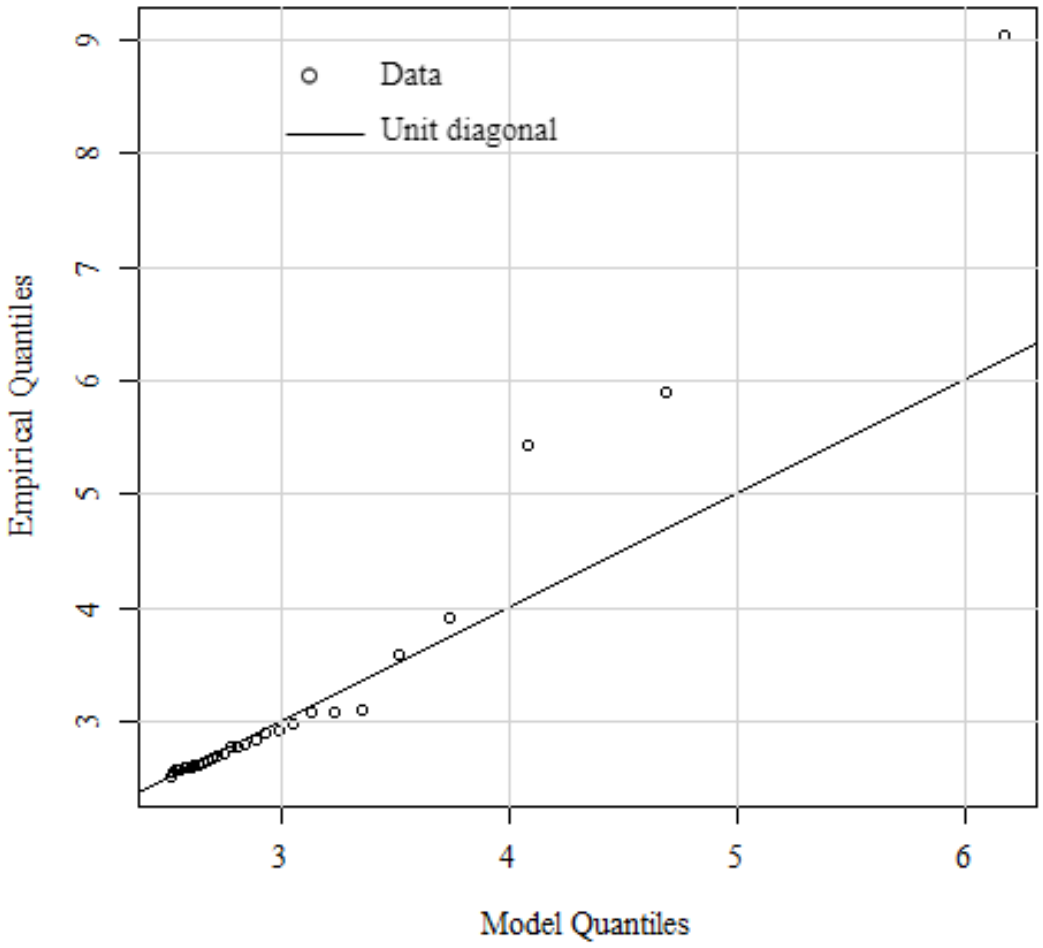

Figure 3.8: Q-Q plot of H_s for site at 17.5N, 77.0W(GPD analysis)

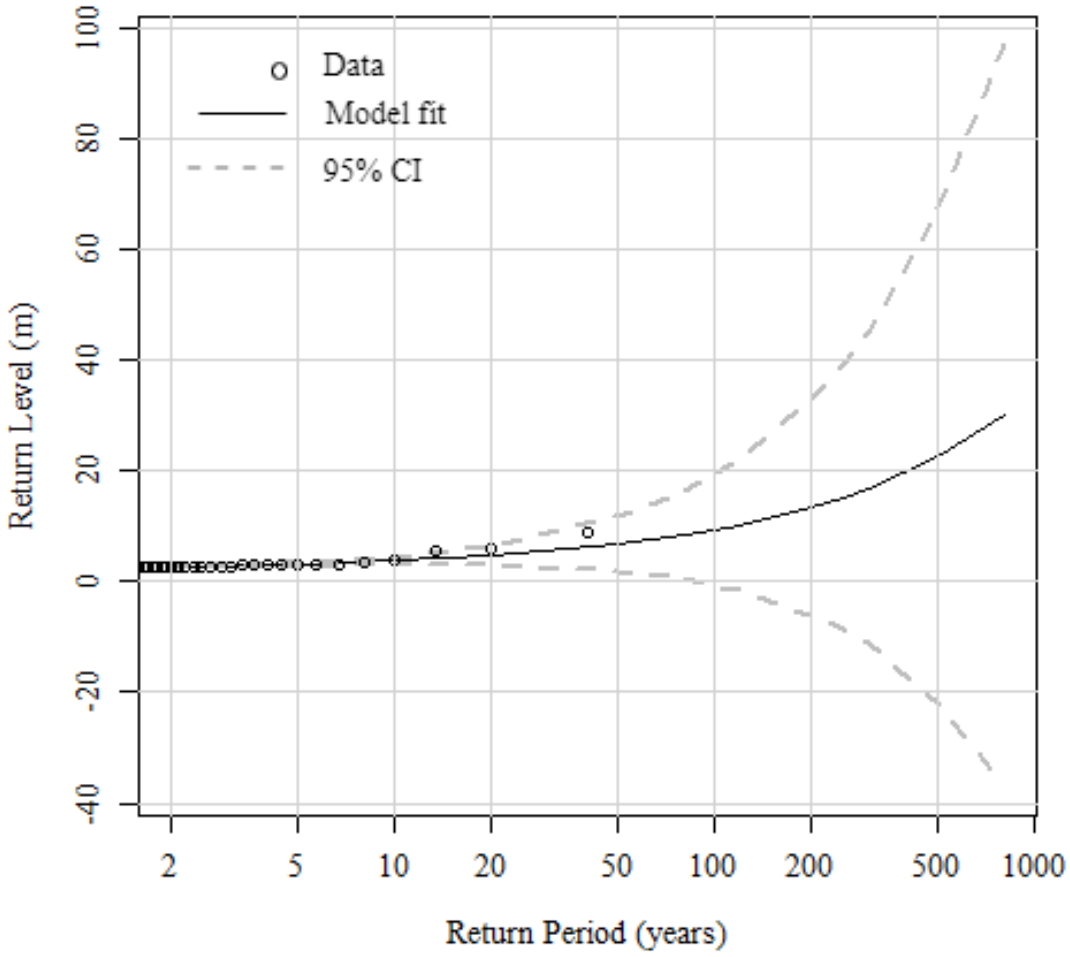

Figure 3.9: Return level plot of H_s for site at 17.5N, 77.0W(GPD analysis)

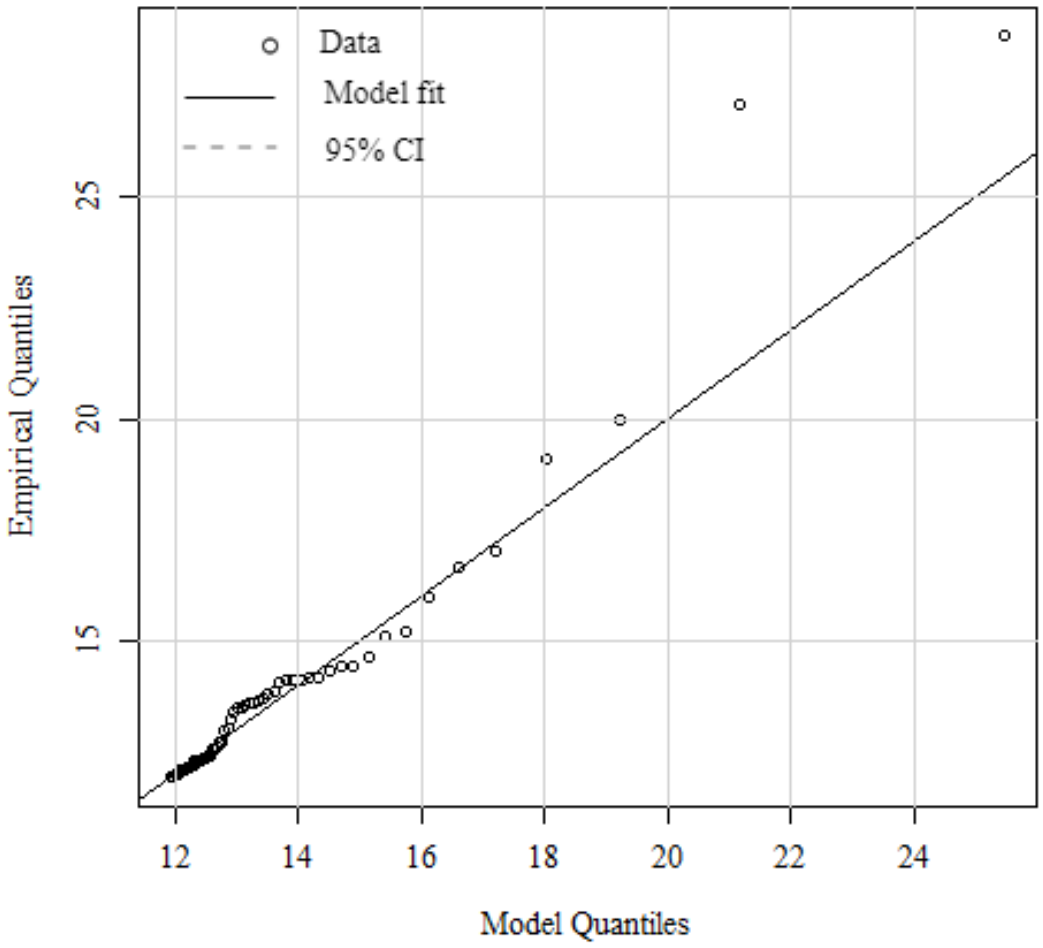

Figure 3.10: Q-Q plot of u_{10} for site at 17.5N, 77.0W(GPD analysis)

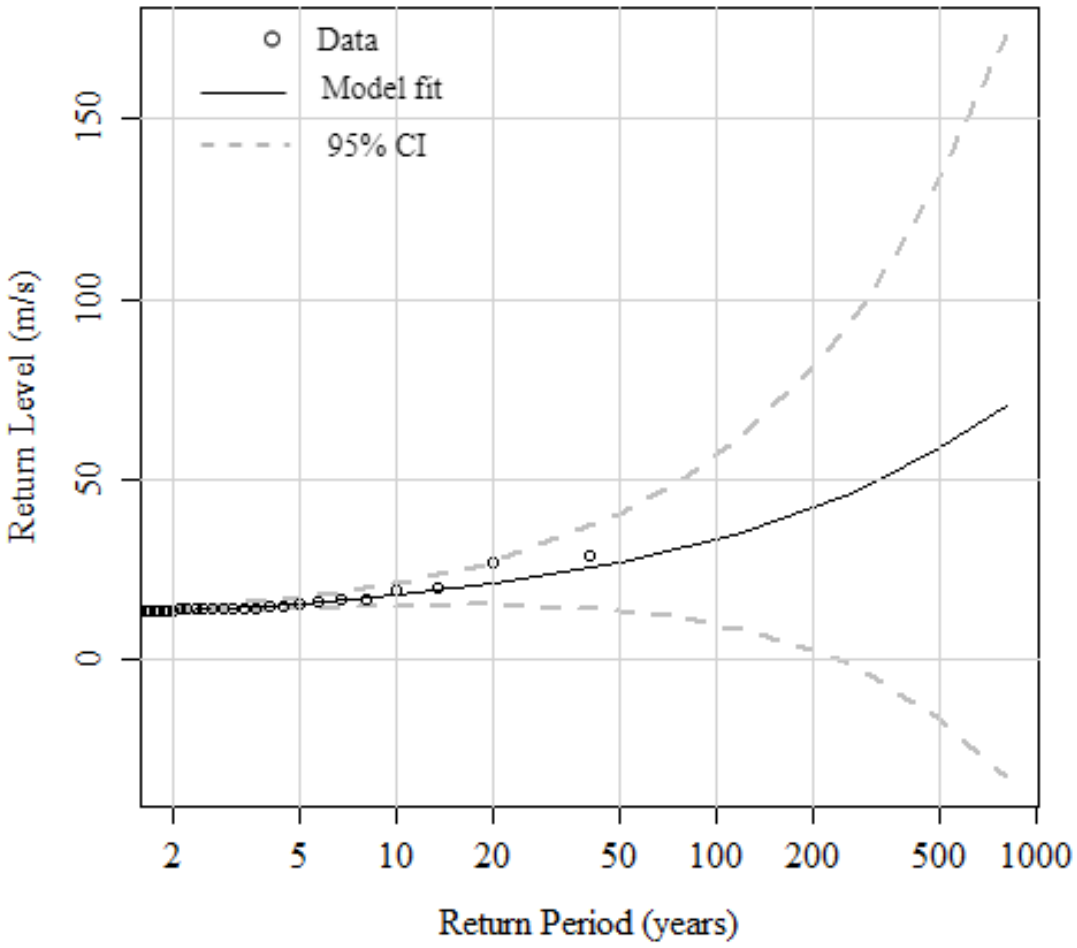

Figure 3.11: Return level plot of u_{10} for site at 17.5N, 77.0W(GPD analysis)

sidered somewhat cumbersome and complex. Palutikof et al. (1999) have indicated that determining the threshold can be a complex matter and hence the reason some designers of offshore structures tend to use block maxima. However, this process can be done iteratively by using the mean residual life plot and the threshold stability parameters plot, in tandem, to make an initial estimate of the threshold value. This initial value can be further refined, if necessary, until a return level plot that yields the best fit to the data is achieved.

3.4 Conclusion

Univariate extreme value analysis was carried out for H_s, T_p and u_{10} at a proposed offshore wind turbine site off the south coast of Jamaica (17.5N,77.0W). The data used to carry out the analyses were ECMWF reanalysis data for H_s from 1979 to 2018 and for u_{10}, DHI reanalysis data from 1979 to 2018; sampled every 3hrs. The analysis was carried out by conducting both GEV and GPD analysis on H_s and u_{10}. The tool that was used was the R based software, extRemes. T_p conditioned on H_s was determined deterministically. Table 3.3 shows the GEV and GPD 50 and 100 year return levels of H_s, T_p and u_{10} that were obtained.

It was shown that for the location considered, extreme value predictions for H_s is better suited to a GPD model, while u_{10} is better suited to a GEV distribution model. That means they were a better fit to the respective distributions (considering both the qq-plots and return period plots) and produced greater return level estimates. Further work would be required to see if this characteristic holds true for other areas off the south coast of Jamaica and subsequently other offshore areas of the Caribbean.

Chapter 4

Comparing the environmental conditions in the Scottish North Sea with the conditions in the Jamaica Caribbean Sea

4.1 Introduction

In chapter 3, a univariate extreme sea state was determined for the Jamaica Caribbean Sea, at location 17.5N, 77.0W. While this approach has been used extensively by researchers and is easy to apply, it only uses one variable to determine the extremes. To improve the validity of extreme value analysis, more data points are recommended. One of the ways to achieve this is to carry out multivariate extreme value analysis. In that case, data for more than one variable is used to determine the extreme sea state. In this chapter, the environmental conditions in the Jamaica Caribbean Sea (JCS) is compared with the environmental conditions in the Scottish North Sea (SNS). Multivariate extreme value analysis is used to determine the extreme sea state at both locations. In addition, the normal sea state conditions and wind speeds, the extreme wind speed, the wind turbulence intensity and the wave spectrums at both locations are examined. This same data is used in chapter 5 to investigate the behaviour of the turbine at both locations and to identify the variables of interest that are meaningful to the design of the FOWT system. It will help to unravel the puzzle of whether a FOWT system that has been developed for the North Sea region can be used off-the-shelf in the JCS.

4.2 An Examination of the Environmental Data from the Scottish North Sea and the Jamaica Caribbean Sea

4.2.1 Looking at some summary statistics

The location in the Scottish North Sea (SNS) that was selected is the area where the Hywind FOWT is located. It has coordinates 57.5N, 1.0W and has a water depth of between 95 m to 129 m; see https://www.equinor.com/en/what-we-do/floating-wind/hywind-scotland.html. This location was selected because it the region where one of the first FOWT demonstration projects was located. In addi-

tion, the water depth is similar to the water depth of the proposed FOWT location in Jamaica, that is, 100 m. Some of the characteristics of the data at the SNS and the JCS are first be examined to get a bird's eye view of what exists at both locations. The characteristics that are examined are the sea state (scatter plot of H_s and T_p), frequency of the data and some summary statistics. The H_s/T_p scatter plot and the histograms shown in figures 4.1, 4.2 and 4.3 indicate that for the North Sea, the significant wave heights were more evenly distributed in the H_s bins from 0 to 6 m. However, for the Jamaica Sea, most the H_s data lies between the 0 to 2.95 m range and there were a small number of H_s values in each bin above this range. These numbers were not sufficient to form proper H_s bins. As mentioned in Chapter 3, the JCS data consists of 3-hr storms (H_s and T_p) for the period 1979 to 2018. The same period was used for the respective location in the SNS. Over the respective period, Jamaica experienced five (5) hurricanes and one (1) tropical storm, see Appendix B. Hurricanes Allen (Aug 5-9, 1980), Gilbert (Sept 12 to 14, 1988), Ivan (Sept 9 to 14, 2004), Dean (Aug 20 to 21, 2007), Sandy (Oct 24 and 25, 2012 and tropical storm Emily (Jul 16, 2005). The hindcast model data seemed to predict accurately the relative increase in the value of the significant wave heights during the periods that these weather systems passed through Jamaica. However, during the period of Hurricane Allen, no significant increase was seen. A check of the data revealed that there were only thirty three (33) 3-hr storms above 2.95 m. Twenty-five (25) of these 3-hour storms were due to the severe weather systems mentioned above, not including Hurricane Allen. The remaining eight (8) 3-hr storms may have been due to severe weather events as they all occurred during the annual hurricane season, which begins on June 1 and ends on November 30. As mentioned above, the number of data points to create H_s bins after H_s of 2.95 m is very small, that is 33. This made binning the data above that range impractical. This is also one of the main things that made the JCS data very peculiar and different from the data within the SNS. The summary statistics is shown in table 4.1; the kurtosis was striking. The kurtosis for JCS is much greater than 3.0 and indicates heavy tailed data due to outliers and kurtosis less than 3, the case for SNS, indicates lighter tailed data.

4.2.2 Normal sea and wind conditions

The significant wave height of the normal sea state (HS, NSS) is defined by DNV-GL (2016) as the expected value of the significant wave height conditioned on the concurrent 10-minute mean wind speed. To determine HS,NSS the 10-minute mean wind speed at 10 m was converted to 10-minute mean wind speed at hub height, Vhub, and the data was binned for wind speeds of 3 m/s to 25 m/s (with 2 m/s time steps). The conversion of the 10-minute mean wind speed at 10 m to 10-minute mean wind speed at Vhub is done using a power law profile. The wind speed profile to convert wind speed from one reference height to another is given by (DNV, 2010*a*; DNV-GL,

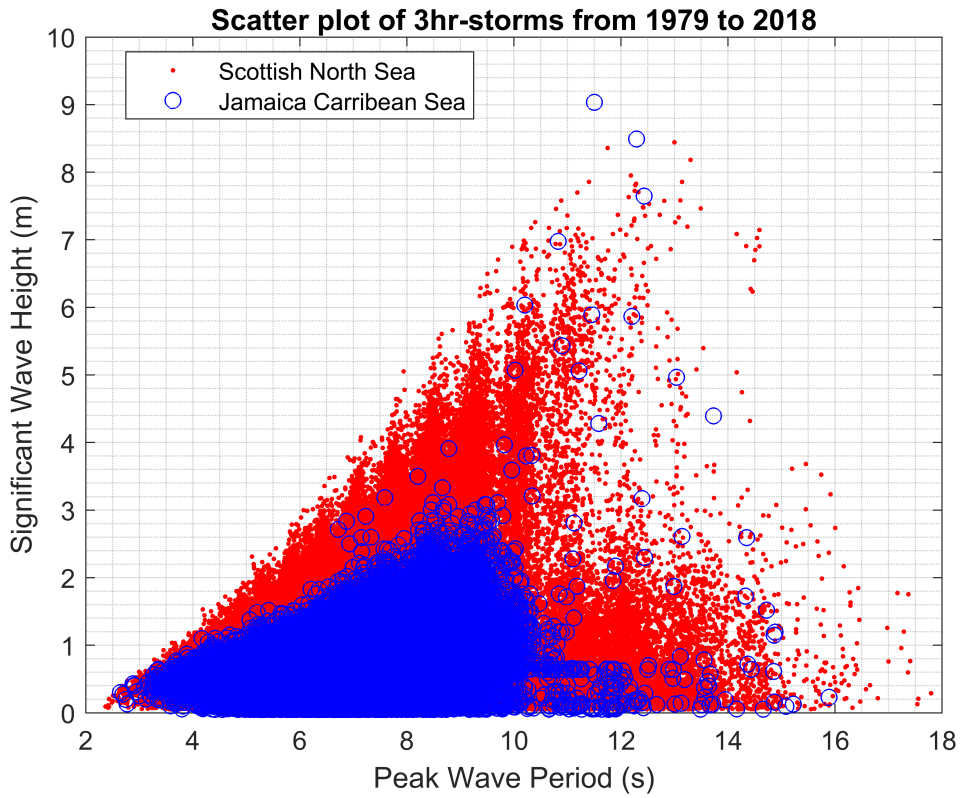

Figure 4.1: Scatter plot of 3hr-storms(H_s and T_p) for SNS and JCS from 1979 to 2018

Table 4.1: Summary Statistics of H_s (m) from 1979 to 2018 for SNS and JCS

Description	SNS	JCS
Mean	1.221	0.670
Median	0.930	0.628
Mode	0.165	0.642
Standard Deviation	1.066	0.387
Sample Variance	1.137	0.150
Kurtosis	**2.744**	**7.966**
Skewness	1.491	1.262
Minimum	0.050	0.050
Maximum	8.442	9.034
Count	112,525	107,527

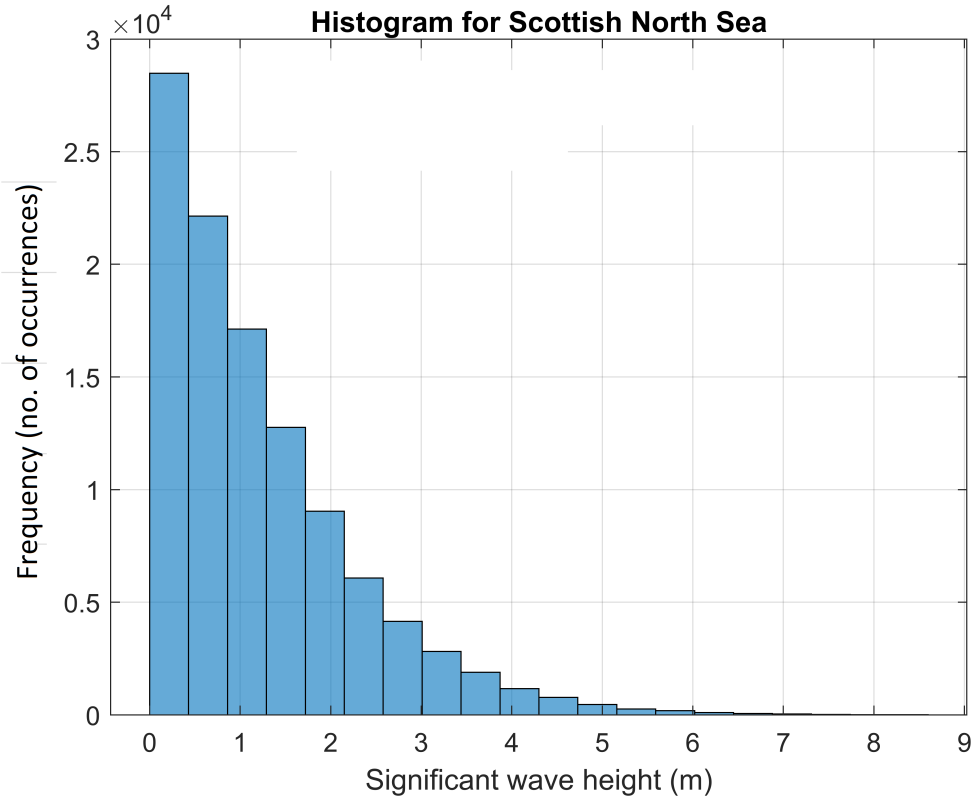

Figure 4.2: Histogram of SNS H_s from 1979 to 2018

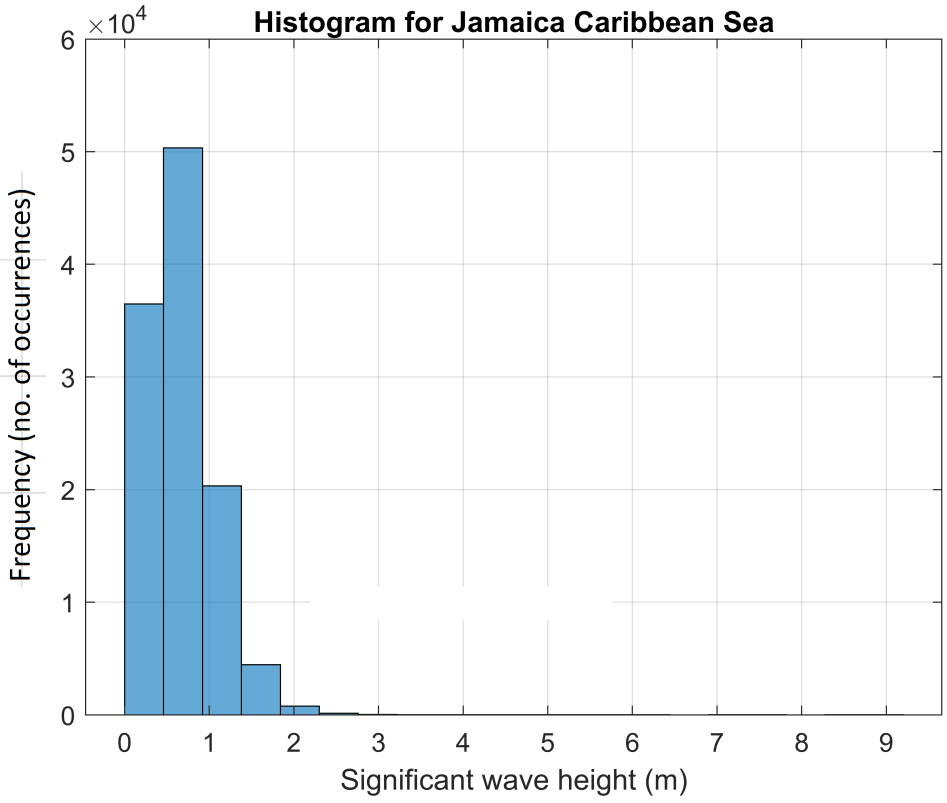

Figure 4.3: Histogram of JCS H_s from 1979 to 2018

2018):

$$U(z) = U(z_{ref}) * \left(\frac{z}{z_{ref}}\right)^{\alpha_w} \tag{4.1}$$

For offshore conditions, the wind shear exponent, α_w = 0.11. U(z_{ref}) is the 10-minute mean wind speed at reference level, z_{ref}, in this case z_{ref} is 10 m; z is the height at the hub, Vhub, which has a value of 150m. This is the 3hr-wind speed at hub height.

To convert 3-hr wind speed to 10-minute wind speed the following wind speed conversion factor from DNV-GL (2018), Clause 5.1.2, is used:

$$wind_{10min} = \frac{wind_{3hr}}{0.90} \tag{4.2}$$

This conversion is done to the full set of 3-hr wind speed data prior to binning the significant wave height data. The wind speed range of 3 m/s to 25 m/s, for the normal sea state, is as per DLC 1.1, DNVGLST0437(2016); where 3 m/s and 25 m/s are the cut-in and cut-out wind speeds respectively of IEA-15 MW reference wind turbine. To determine HS,NSS the expected values (mean) of HS, NSS in each wind speed bin is computed. The values of T_p given HS,NSS were found in the same manner as shown in section 3.3, using equation 3.1 to find the range of values of T_p. Liu et al. (2018) in their studies on a semi-sub floater argued that the wind speed around the rated wind speed is where the extreme response levels usually occur. The rated wind speed for IEA-15 MW reference wind turbine is 10.59 m/s. Therefore, taking the same approach as Liu et al (2018) the wind speeds that are considered for the normal sea states are 9 m/s to 13 m/s (2 m/s time step). The full set of load conditions for the SNS and the JCS, are shown in Table 4.3. The data shows that the normal sea conditions in the SNS appear very similar to the normal sea conditions in the JCS. This is assessed further in chapter 5 by applying both sets of data to a FOWT system to compare the responses.

4.2.3 Extreme Sea State - Joint Probability Distribution of H_s and T_p and 50 and 100 Year Environmental Contours

As was mentioned in Chapter 2, the development of the joint probability distribution includes the determination of a marginal distribution of H_s and a conditional distribution of T_p given H_s. The conditional distribution of T_p given H_s is typically modelled using a lognormal distribution, where T_p is added to bins for the given values (or classes) of H_s. The lognormal distribution is fitted to T_p in each bin and mu and sigma determined. Functions are then fitted to the plots of sigma vs H_s and mu vs H_s and coefficients of the functions are determined. These coefficients are the parameters of the conditional

distribution of T_p given H_s. The literature states that the lognormal distribution works satisfactorily for the conditional distribution of T_p given H_s. However, unlike the conditional distribution, finding a model for fitting the marginal distribution of H_s is much more challenging. This is the case for the H_s data in the JCS. This could be due to the character of the data as is mentioned above. The H_s data seemed to comprise data, which are of two separate distributions. Those that typically occur, that is all of the data below 2.95 m; and the remainder, the sparse set of data (33, 3-hr storms to be exact) which were a result of severe weather systems. Having looked at the data, the next step is to find the marginal distribution of H_s and the conditional distribution of T_p given H_s for both the SNS and the JCS. From the literature, the typical model that is used to fit H_s, in the North Sea was the three-parameter Weibull distribution (Weib3P). DNV-GL (2016) states that the wind turbine classes were developed using environmental data from the North Sea. The Weib3P also seems to work well with data from the North Atlantic. The Weib3P was therefore investigated first for both datasets.

Like the univariate EVA, the fit of the marginal distribution of H_s was checked using the qq-plot. The qq-plot gives an indication of whether the data, empirical percentiles (y-axis), is good fit for the distribution, model percentiles (x-axis). If the model is a good fit to the data, when the empirical percentiles are plotted against the model percentiles, the points should form a straight line. The more of the data points that form that line the better the fit of the model to the data. Figures 4.4 and 4.5 show the Weib3P qq-plot of the marginal distribution of H_s for the SNS and the JCS.

The Weib3P model shows a relatively good fit to the SNS H_s data. This is what is expected based on the qq-plot and what has been reported in the literature. However, the Weib3P model does not show a good fit to the JCS H_s data. To confirm this characteristic, for both the SNS and JCS datasets, the environmental contour plots were created using the Weib3P model for the marginal distribution of H_s and the lognormal model for the conditional distribution of T_p given H_s. The parameters of the Weib3P and the conditional distribution of T_p given H_s are shown in table 4.2. The bin-averaged lognormal distribution parameters, μ and σ, as a function of H_s are shown in Figure 4.6. The environmental contour plots for the SNS and the JCS are shown in Figure 4.7. The environmental contours for the 50 and 100 year events, showed that in keeping with the qq-plots, the SNS H_s data produced a relatively good contour. However, a suitable contour was not obtained with the JCS H_s data. The problem, therefore, is to find a model to fit the marginal distribution of H_s for the JCS. The two parameter Weibull (Weib2P) is considered. However, when the Weib2P is tested it produced a poorer fit to the JCS H_s data. Additionally, the Pearson Type III distribution was also tried but this also did not give a good fit to the data. The Pearson Type III is equivalent to the gener-

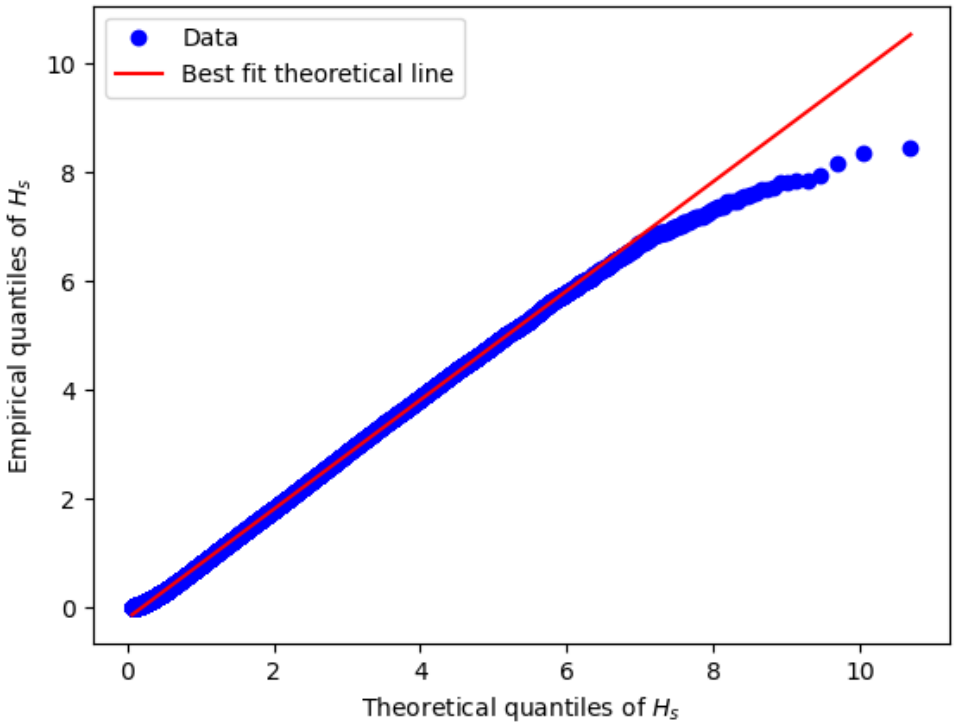

Figure 4.4: Weibull-3P q-q plot of SNS H_s from 1979 to 2018

Table 4.2: Weib3P and lognormal distribution parameters for SNS and JCS, 3h-storms from 1979 to 2018

Weib3P parameters of Hs			**Lognormal parameters of Tp given Hs**		
SNS			**SNS**		
σ	**β**	**γ**	**a1**	**a2**	**a3**
1.376	1.216	0.0698	1.332	0.465	0.447
JCS			**a4**	**a5**	**a6**
σ	**β**	**γ**	0.079	0.572	0.725
0.566	1.355	0.151	**JCS**		
σ, scale; β, shape; γ, location			**a1**	**a2**	**a3**
			1.098	0.854	0.218
			a4	**a5**	**a6**
			-0.023	0.139	0.085
			μ params; a1, a2, a3 σ params; a4, a5, a6		

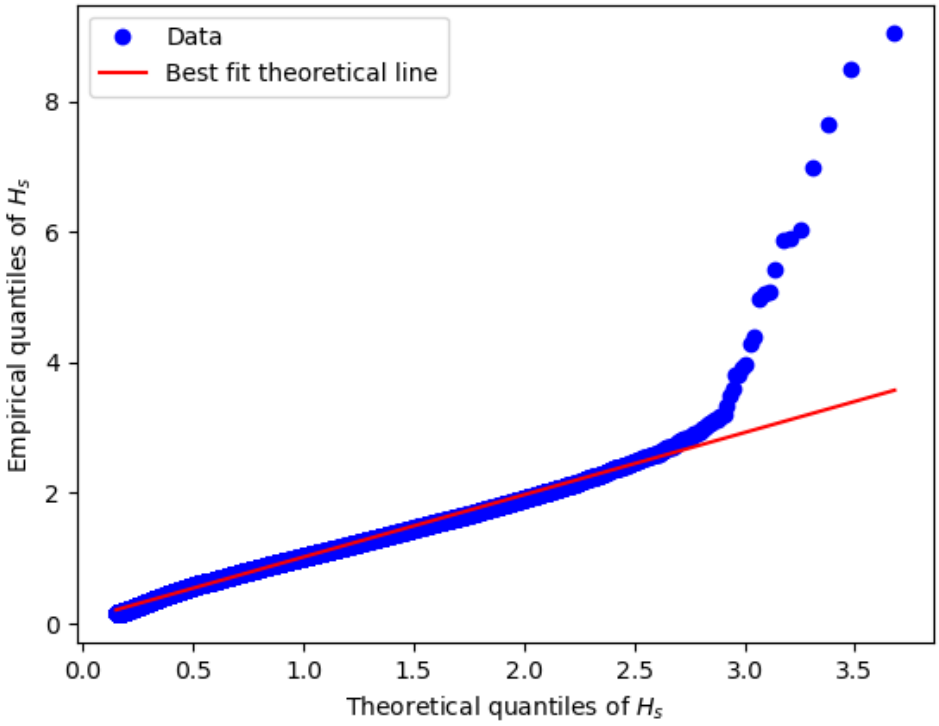

Figure 4.5: Weibull-3P q-q plot of JCS H_s from 1979 to 2018

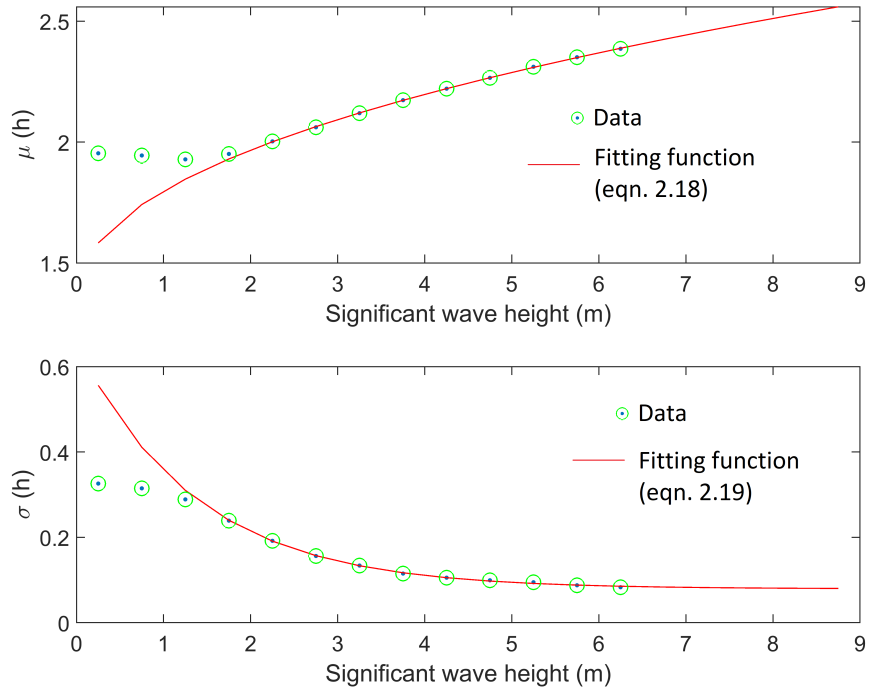

(a) SNS

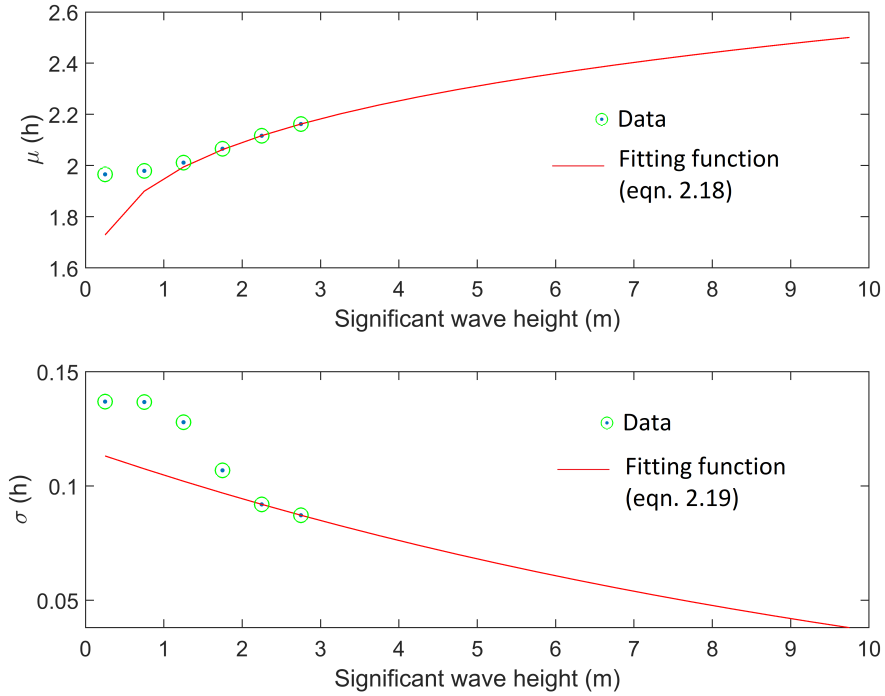

(b) JCS

Figure 4.6: Lognormal distribution parameters, μ and σ, bin-averaged, as function of H_s for (a) SNS and (b) JCS, 3hr-storms from 1979 to 2018

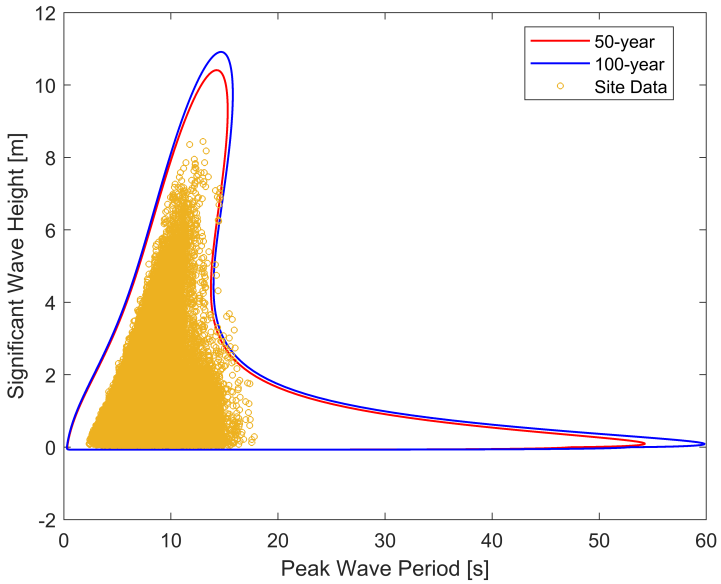

(a) SNS

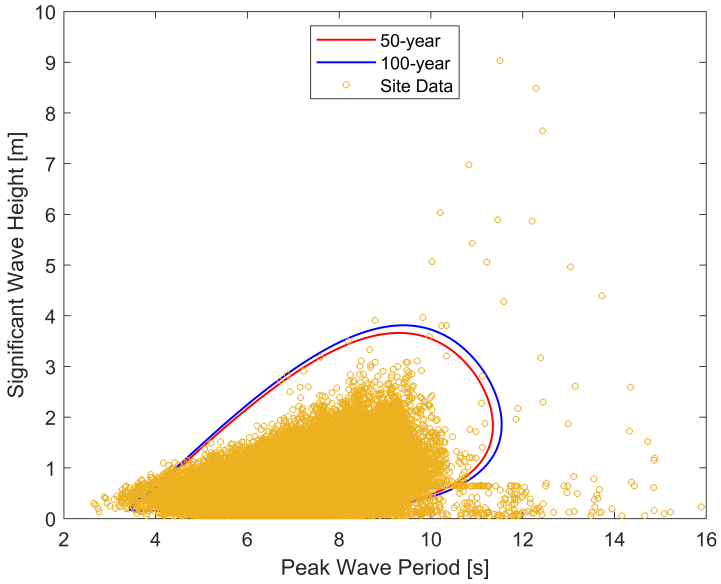

(b) JCS

Figure 4.7: Weib3P-lognormal 50-year and 100-year environmental contour for (a) SNS and (b) JCS using 3hr-storms from 1979 to 2018

alized gamma distribution. It is argued by Pasilliao (1995) that the generalized gamma can fit data from any geographical location. However, this was not found to be valid for JCS H_s data. In fact, the generalized gamma does not seem to have been utilized regularly in the literature to fit the marginal distribution of H_s; the Weib3P is mostly used. In regions where the extremes are governed by the occurrence of a few hurricanes, Haver & Winterstein (2008) argued that the POT method could be utilized . This would require the formation of a joint density function of H_s and T_p for $H_s > h_o$. This is similar to the POT method where h_o is the threshold value. Haver & Winterstein (2008) recommended that, in such a case, the Weib3P be used to fit the marginal distribution of $H_s > h_o$. This approach is considered for the JCS data but the qq-plot revealed that the Weib3P is not a good fit for $H_s > h_o$. Therefore, utilizing the principle given in Haver & Winterstein (2008) the GPD is used to fit the marginal distribution to the peak excesses (H_s-h_o). This gave a relatively satisfactory q-q plot but the environmental contour still did not capture the extreme storms. This is shown in Figure 4.8. A further approach is therefore taken for the JCS data by separating the data into normal season data and hurricane season data and fitting models to them.

Separating the JCS data according to the normal season and the hurricane season

The environmental contours produced by fitting the Weib3P and GPD models to the JCS data underestimates the extreme sea state. This may be because the data is of two different models as stated previously. To solve this problem, the first thing that is done is to look closer at the data and see how the significant wave height is affected by hurricanes. Further investigation showed that when a severe weather system, such as a hurricane, affects Jamaica it results in drastic increase in the significant wave height above the normal levels. Therefore, the data is divided into two segments, normal season data (Dec to May) and hurricane season data (June to Nov). The Weib3P and GP models are fitted to this data as appropriate. The results for the Weib3P model are shown in the Figures 4.9 and 4.10. It is seen that the Weib3P model produced a good fit to the normal sea state data. However, the same problem persisted for the hurricane season data, the model did not fit the data well and the most-extreme storms are not captured by the environmental contours. This demonstrated that the Weib3P model is not a good fit for the hurricane season data within the JCS. The investigation was continued using the GPD model. It is seen that this model produced a reasonable qq-plot but the resulting environmental contour did not capture the most extreme storms. This is shown in Figure 4.11. An attempt is also made to fit the Weib3P model to the hurricane season data for values of $H_s < 3.5$ m. Figure 4.12 shows that while the qq-plot is much improved relative to the one shown in Figure 4.10, the environmental contours

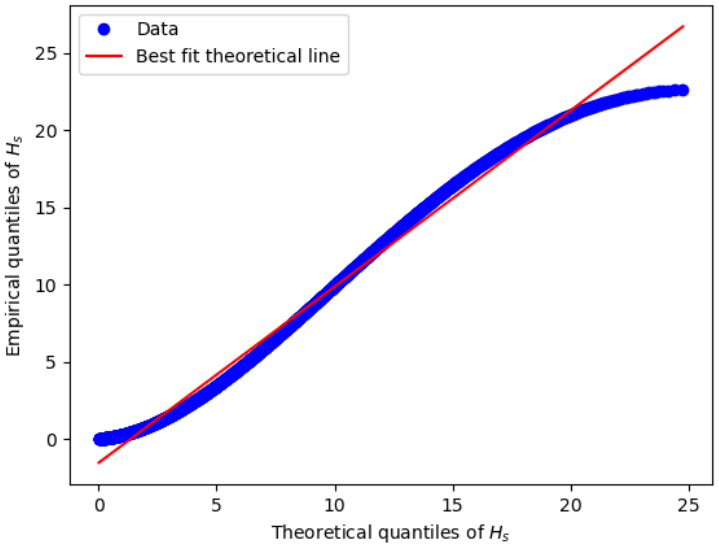

(a) GPD qq-plot

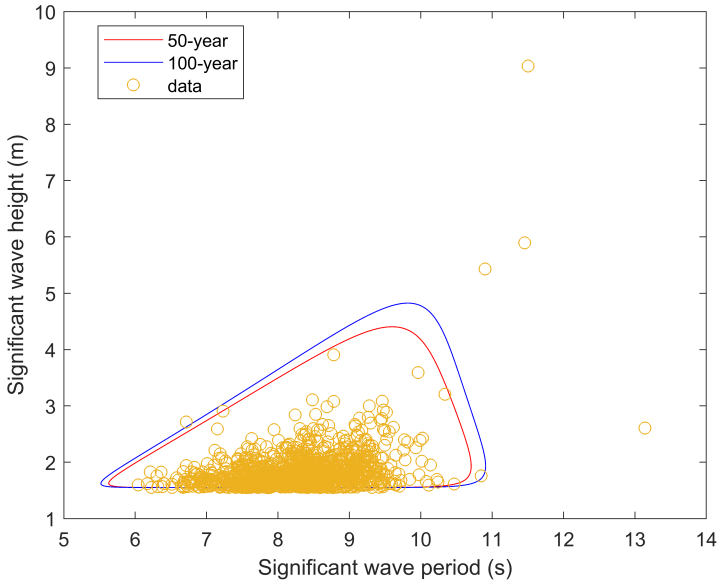

(b) GPD environmental contour

Figure 4.8: (a) GPD q-q plot of H_s for JCS, threshold =1.55 m (b) GPD 50-year and 100-year environmental contours, JCS, threshold = 1.55

did not capture the extremes of the data very well. This analysis provides sufficient evidence to show that the models, such as the Weib3P, which are typically used to produce environmental contours plots for other jurisdictions, like the North Sea, do not fit the data from the JCS very well. This may be as a result of mixing of the JCS data by the hurricanes as stated by Haver & Winterstein (2008). Therefore, the problem may be resolved by fitting models to the significant wave heights that occur during the passage of a hurricane only.

Fitting models to hurricane storms

Given that the typical models did not fit the hurricane season data from the JCS very well, the approach taken is to fit the models to hurricane storms. That is, only to significant wave heights which occur during the passage of a hurricane or other severe weather systems. Banton (2002) developed a tool called HURWave for his MSc Thesis at Delft University. It uses hurricane characteristics (peak velocity of hurricane, distance from the centre etc.) to compute the hurricane significant wave heights using a number of parametric models namely, Ross, Cooper, Young, Improved Young and Bretschneider. HURWave was developed to determine hurricane wave heights within the Caribbean Sea and is currently used as a tool within the Costal Engineering Industry in the Caribbean. Banton (2002) tested the respective wave models against actual buoy data and it was shown that all of the models overestimated the hurricane significant wave heights. However, the Improved Young was one of the models that gave the lowest RMSE. In addition, the Weib3P model fitted the data very well and therefore the hurricane significant wave heights from the Improved Young model are used to create the environmental contours for the respective site location in the JCS. The q-q plot and environmental contour are shown in Figure 4.13. The model fits the data well. The environmental contour method is used to fit hindcast data over a long period of record but it has been used here to fit hurricane wave data. Valamanesh et al. (2015) used the tails of the data to carry out EVA instead of the full dataset. This approach taken here is similar to what was done by Valamanesh et al. (2015). Further work is required to gather hurricane wave data in the relevant geographical locations, to test this application of the ECM further.

4.2.4 Selection of the normal and extreme sea state conditions for the SNS and JCS

The Weib3P model produced a reasonable 50-year environmental contour for the SNS and this same model also produced reasonable environmental contour for the JCS using the hurricane wave height data. These contours are shown in Figures 4.7 and 4.13 and are used to select the extreme sea state that are used for numerical modelling. The load conditions for both the normal and extreme sea states are shown in Table 4.3.

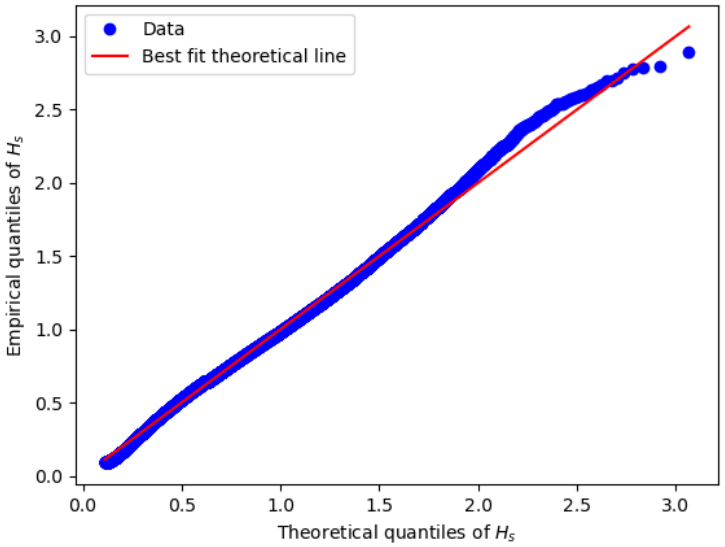

(a) Weib3P qq-plot

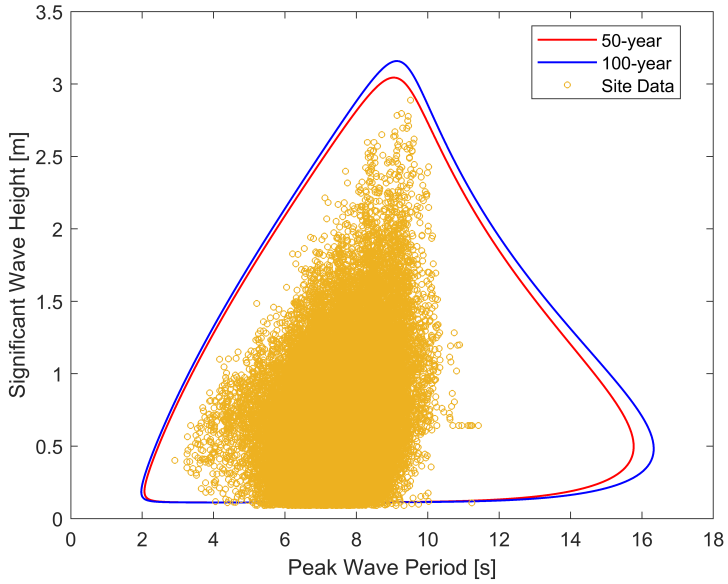

(b) Weib3P environmental contour

Figure 4.9: (a) Weib3P q-q plot of H_s for JCS normal season data, (b) Weib3P 50-year and 100-year environmental contours, JCS, normal season data

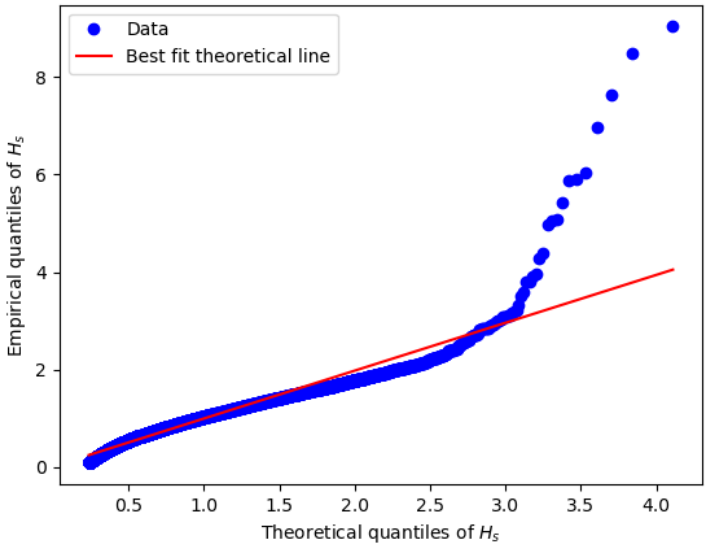

(a) Weib3P qq-plot

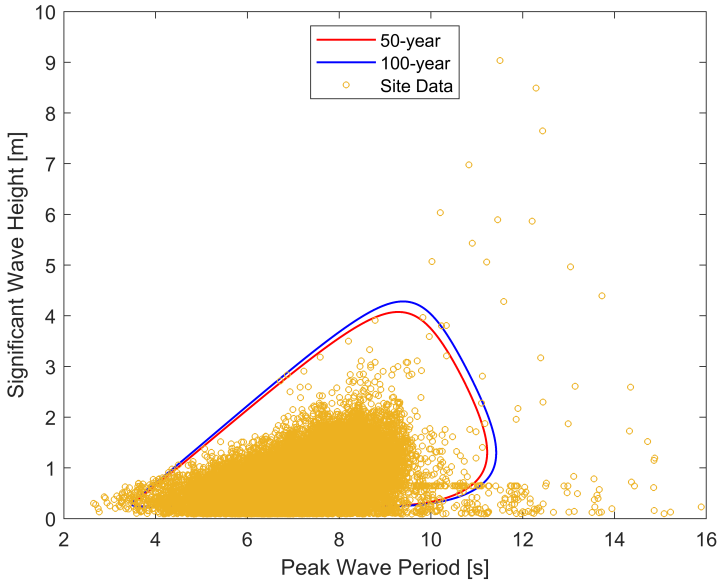

(b) Weib3P environmental contour

Figure 4.10: (a) Weib3P q-q plot of H_s for JCS hurricane season data, (b) Weib3P 50-year and 100-year environmental contours, JCS, hurricane season data

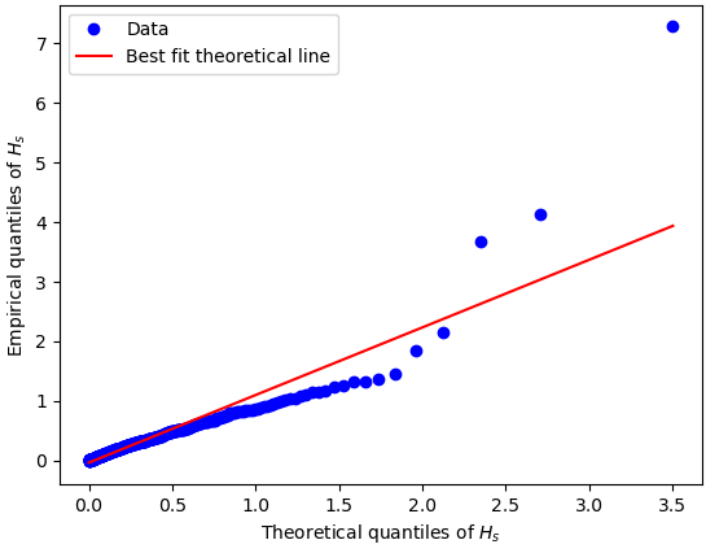

(a) GPD qq-plot, threshold = 1.75 m

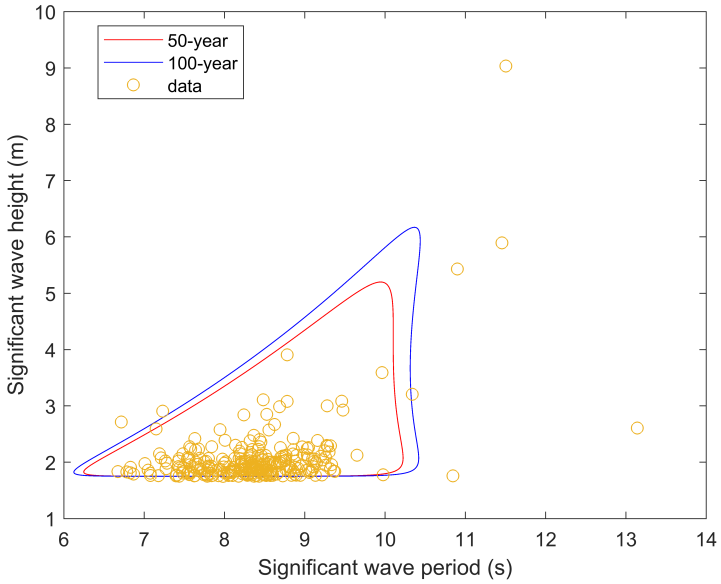

(b) GPD environmental contour, threshold = 1.75 m

Figure 4.11: (a) GPD q-q plot of H_s for JCS hurricane season data, (b) GPD 50-year and 100-year environmental contours, JCS, hurricane season data

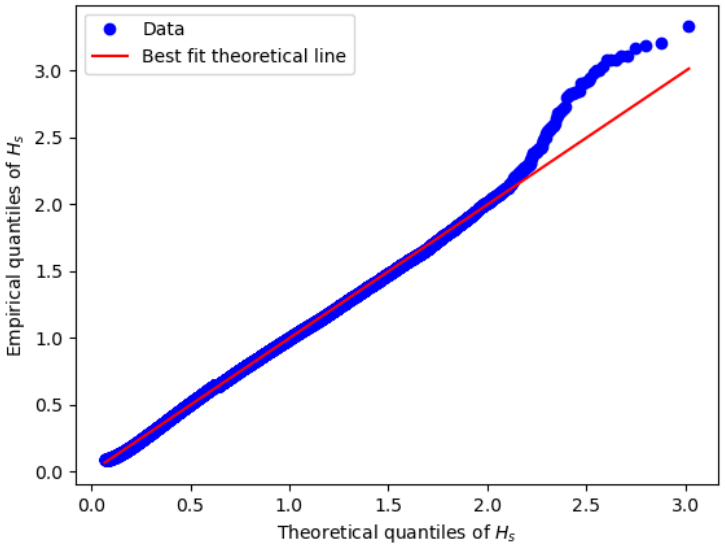

(a) Weib3P qq-plot

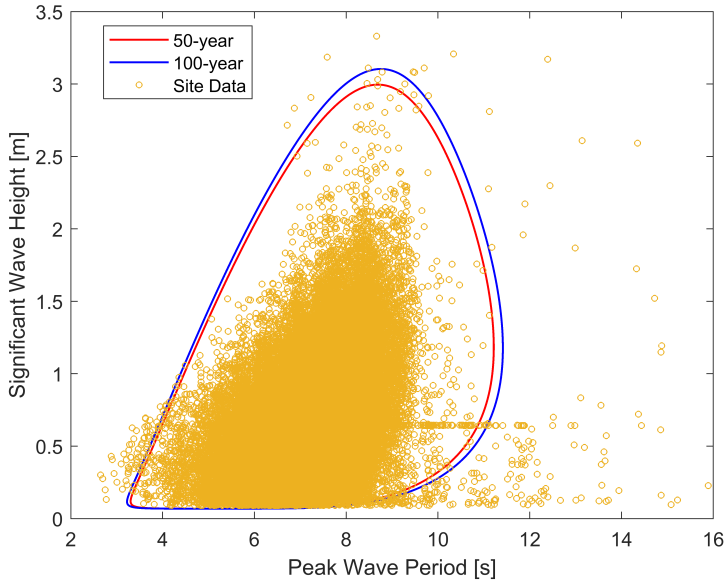

(b) Weib3P environmental contour

Figure 4.12: (a) Weib3P q-q plot of H_s < 3.5 m for JCS hurricane season data, (b) Weib3P 50-year and 100-year environmental contours, JCS, hurricane season data for H_s < 3.5 m

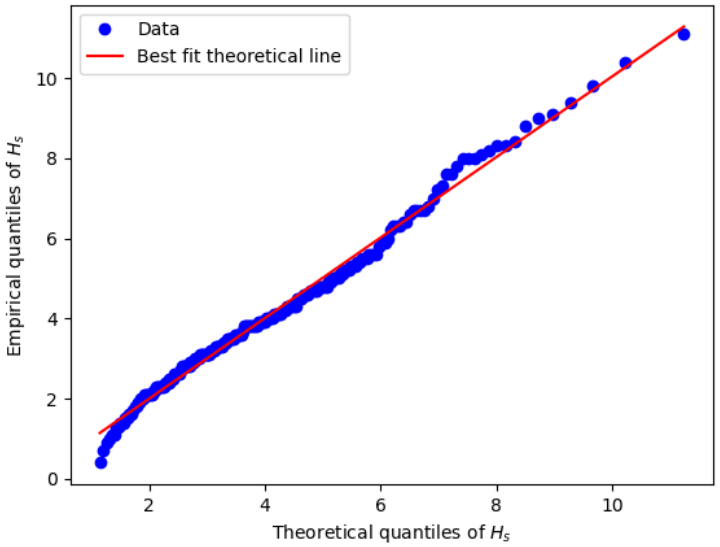

(a) Weib3P qq-plot

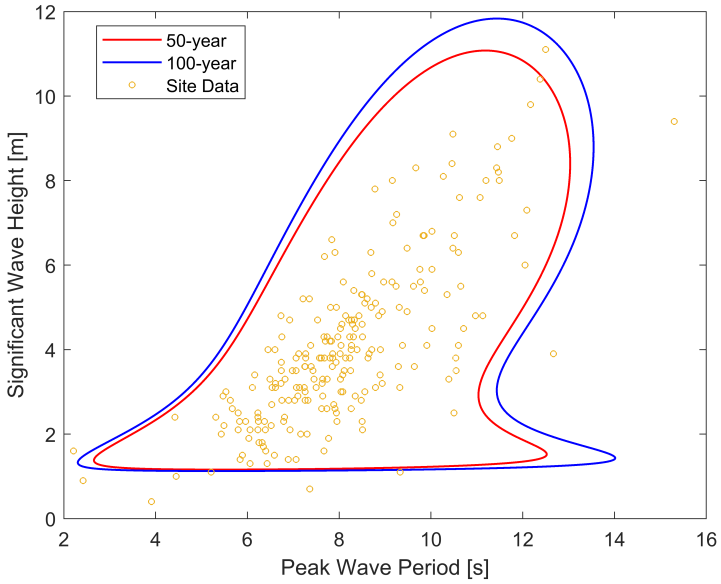

(b) Weib3P environmental contour

Figure 4.13: (a) Weib3P q-q plot of hurricane H_s for JCS, (b) Weib3P 50-year and 100-year environmental contours, JCS, hurricane H_s data

More is said about the design load conditions (DLC) in the next chapter. The extreme wind speeds for JCS are obtained from the univariate extreme sea state shown in Table 3.3 of Chapter 3. A similar analysis was done for the SNS and the results are shown in Table 4.4. The return level and qq-plots are shown in Appendix C. The normal sea state for the SNS and the JCS appear similar. The 50-year extreme sea state at both locations are comparable with H_s for the JCS being 7.3% more than H_s for the SNS. The extreme winds speeds are also comparable.

Table 4.3: Load cases for SNS and JCS

Load case	DLC	Wind condition	Sea state	Wind speed (m/s)	H_s (m)	T_p (s)	γ	Simulation time (s)	Wind Turbine
Scottish North Sea									
1	1.1	NTM	NSS	9	0.46	7.41	1.00	1800	Operating
2	1.1	NTM	NSS	11	0.74	7.24	1.00	1800	Operating
3	1.1	NTM	NSS	13	1.06	7.16	1.00	1800	Operating
4	1.1	NTM	NSS	15	1.45	7.25	1.00	1800	Operating
5	6.1	EWM (50-yr)	ESS (50-yr)	45.17	10.41	14.27	3.3	3600	Parked (Idling)
Jamaica Carribean Sea									
1	1.1	NTM	NSS	9	0.73	7.44	1.00	1800	Operating
2	1.1	NTM	NSS	11	0.97	7.74	1.00	1800	Operating
3	1.1	NTM	NSS	13	1.16	8.00	1.00	1800	Operating
4	1.1	NTM	NSS	15	1.36	8.24	1.00	1800	Operating
5	6.1	EWM (50-yr)	ESS (50-yr)	42.89	11.17	11.22	3.3	3600	Parked (Idling)

NTM - normal turbulence model; EWM - extreme wind model
NSS - normal sea state; ESS - extreme sea state

Table 4.4: Summary of GEV and GPD 50 and 100 year design sea states and wind speeds, Scottish North Sea (57.5N, 1.0W)

Description	Block maxima/GEV	POT/GPD
Hs_{50}(m)	8.35	8.72
Hs_{100}(m)	8.50	8.98
Tp_{50}(s)	10.79 ~ 15.87	11.03 ~ 16.22
Tp_{100}(s)	10.89 ~ 16.01	11.19 ~ 16.46
$u10_{(50)}$(m/s)	30.18	29.85
$u10_{(100)}$(m/s)	31.28	30.20

4.2.5 Comparing the 50-year univariate and 50-year multivariate EVA sea states

In Chapter 2, it is stated that other researchers have found that the sea state values of the univariate and multivariate EVA were comparable. For the SNS the 50-year univariate H_s is found to be 8.72 m the value of T_p is found to be 13.63 s (see Table 4.4). The 50-year multivarite EVA sea state is H_s, 10.41 m; T_p, 14.27 s. These results are comparable and agree with the findings of other researchers. For the JCS, the 50-year univariate EVA sea state is H_s, 6.71 m; T_p, 11.96 s (see Table 3.3). The 50 year multivariate EVA sea state is H_s, 11.17 m; T_p, 11.22 s. The 50-year multivariate value of H_s is found to be 64 % more than the 50-year univariate EVA value. The possible reasons for the 50-year univariate value of H_s being underestimated is due to the uncertainty in the data since it is mixed data from two different models as was discussed above. In addition, the 50-year multivariate EVA is carried out using the hurricane wave height data. The maximum values of H_s for that data are greater than the maximum values of H_s for the ECMWF hindcast data. It was also stated in Chapter 2, that there are a lot of uncertainties in EVA. This typifies that position. The multivariate EVA values of H_s at both locations are greater their univariate counterparts, therefore, for this study, the multivariate EVA results are used to develop the numerical model.

4.2.6 Steady and turbulent wind conditions in OpenFAST

The steady wind condition in OpenFAST is calculated using the power-law wind shear profile. This steady wind is applied at hub height. The turbulent wind is a full-field wind generated by TurbSim. TurbSim, developed by NREL, is a stochastic, full-field, turbulence simulator primarily for use with InflowWind based simulation tools. The wind field is represented by a 3-dimensional component of the wind inflow velocity; u, v and w. TurbSim generates an array containing all three velocity components at each point on a square grid covering the rotor area as well as points along the turbine tower. TurbSim has been widely used by others to generate turbulent wind fields for numerical FOWT models (Li et al., 2019; Jonkman & Matha, 2011). It uses a number of turbulence models, including the IEC standard turbulence models. In particular, the IEC Kaimal and von Karman spectral models. The turbulence intensity can be specified in TurbSim for a respective model, using letters A, B, C or as a percentage. The values of the turbulence intensity given in IEC-61400-1:2019 are:

- A+ - 0.18
- A - 0.16
- B - 0.14
- C - 0.12

4.2.7 Turbulent Wind Conditions

The wind in the atmospheric boundary layer (ABL) can be represented by a mean part and a turbulent part. A wind profile is used to characterize the mean wind velocity and turbulence is used to represent the turbulent part. A mathematical formulation can be used to explain the nature of the wind in the ABL. This can be done by using a Cartesian coordinate system, where the x-axis is the direction of the mean wind velocity, the y-axis the direction of the horizontal wind and the z-axis the vertical wind, with upwards being positive. The velocities at a given time are formulated as (Dyrbye & Hansen; 1997):

Longitudinal direction: $U\ (z) + u(x, y, z, t)$

Lateral direction: $v\ (x, y, z, t)$

Vertical direction: $w\ (x, y, z, t)$

where $U\ (z)$ is the mean wind velocity and only on the height above ground, (z); u, v and w are the fluctuating parts of the wind field and can be treated mathematically as a stationary, stochastic process with mean value zero (see Figure 4.14). The most important parts of the wind field are the mean wind velocity $U\ (z)$ and the turbulent part u in the wind direction. These parts are the primary contributors to the wind load on a structure. The lateral component, v, is the horizontal wind perpendicular to the wind direction and w is the vertical wind velocity. The turbulent part, in the direction of the wind, u, is what gives rise to turbulence intensity (TI). It can be considered as the degree of fluctuation of this fluctuating part of the wind from the mean wind. The greater the degree of fluctuation the greater the TI.

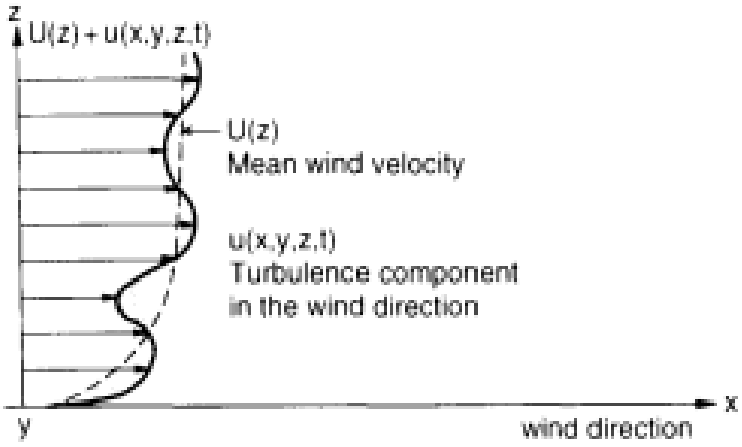

Figure 4.14: Simultaneous wind velocities in the wind direction at different heights above the ground (Source: Dyrbye & Hansen (1997))
(Permission has been granted by John Wiley and Sons to reproduce this figure)

The TI, $I_u(z)$, for the along-wind turbulence component *u* at height *z* is defined as:

$$I_u(z) = \frac{\sigma_u(z)}{U(z)} \tag{4.3}$$

where $\sigma_u(z)$ is the standard deviation of the turbulence component *u* and *U (z)* is the mean wind velocity, both at height *z*. The turbulence intensity usually lies between the ranges of 0.1 to 0.4 (Manwell et al., 2009). Low turbulence intensity has a value less than or equal to 5%, medium TI lies between 5 % and 15 % and high TI has a value greater than 15 % (Siddiqui et al.; 2015).

The TI is normally determined onsite by using a cup anemometer to measure the characteristics of the wind. The literature indicates that to capture the wind data, a cup anemometer (or other type of anemometer) is typically placed at a certain height to get the measurements over a given period. The most frequent minimum period seen in the literature is 2 years (Wang et al., 2014; Ishihara et al., 2012; Kogaki et al., 2009; Türk & Emeis, 2010; Leu et al., 2014; Donnou et al., 2020; Panofsky et al., 1977). The standard deviation of the turbulence component and the mean wind velocity can be ascertained from this wind data. The TI for the SNS and the JCS were determined using model data for each site. The data consisted of 10 min mean of the standard deviation of the turbulent wind and the related mean wind velocity from 2018 to 2019. The data was obtained from the private company, Vortex. Further information on the company and their products can be found here https://vortexfdc.com/pricing/.

When wind data is available, the 90^{th} percentile turbulence intensity, TI_{90}, can be found using the following relationship derived from equation 4.3:

$$TI_{90} = \frac{\sigma_{90}}{U} \tag{4.4}$$

where,

σ_{90} is the 90^{th} percentile of the standard deviation of the turbulent wind

U is the mean wind speed

Now σ_{90} is found from the following relationship (DNVGL, 2016; Ishihara et al., 2012; Leu et al., 2014) :

$$\sigma_{90} = \sigma_{ave} + 1.28\sigma_{\sigma} \tag{4.5}$$

where,

σ_{ave} is the mean value of the standard deviation of the turbulent wind velocity

σ_σ is the standard deviation of the standard deviation of the turbulent wind velocity

The values of σ_{ave} and σ_σ are found by utilizing the process of binning. The standard deviation of the turbulent wind was binned for wind speeds ranging from 3 m/s to 25 m/s (2 m/s intervals), that is the cut-in wind speed and cut-out wind speed of the wind turbine respectively. The values of and σ_{ave} and σ_σ were found for each wind speed bin. Values so determined were used to find σ_{90}. A lognormal distribution was assumed for each wind speed bin in a similar manner to Wang et al. (2014). However, the Gaussian (normal) distribution can also be used and was used by Leu et al. (2014). The values of TI_{90} for the SNS and the JCS are shown in Table 4.5 and the related graphs are shown in Figures 4.15 and 4.16. As mentioned previously, for the normal turbulence model, the wind speeds from 9 m/s to 13 m/s are investigated in OpenFAST.

Table 4.5: Wind turbulence intensity for SNS and JCS

Wind speed (ms)	TI90 SNS_data	TI90 JCS_data
3	0.2131	0.2443
5	0.1561	0.1665
7	0.1264	0.1286
9	**0.1092**	**0.1035**
11	**0.0990**	**0.0926**
13	**0.0955**	**0.0852**
15	**0.1057**	**0.0910**
17	0.1083	0.0966
19	0.1086	no data for bins
21	0.1030	no data for bins
23	0.1037	no data for bins
25	0.1096	no data for bins

In the absence of wind data, the value of the TI can be estimated by using one of the turbulence models from a wind-turbine design manual (Kogaki et al., 2009; Ishihara et al., 2012; Wang et al., 2014). This includes those produced by the IEC and DNV GL. These two models were fitted to the SNS and JCS TI_{90} data. This was done to check the fits of the standard models to the data at both locations. The nature of the model fits to the data will help to inform if the standard models could have been used to estimate the turbulence intensity in both locations. The DNVGL models were fitted to the data and the plots are shown in Figures 4.17. The plots show that class B

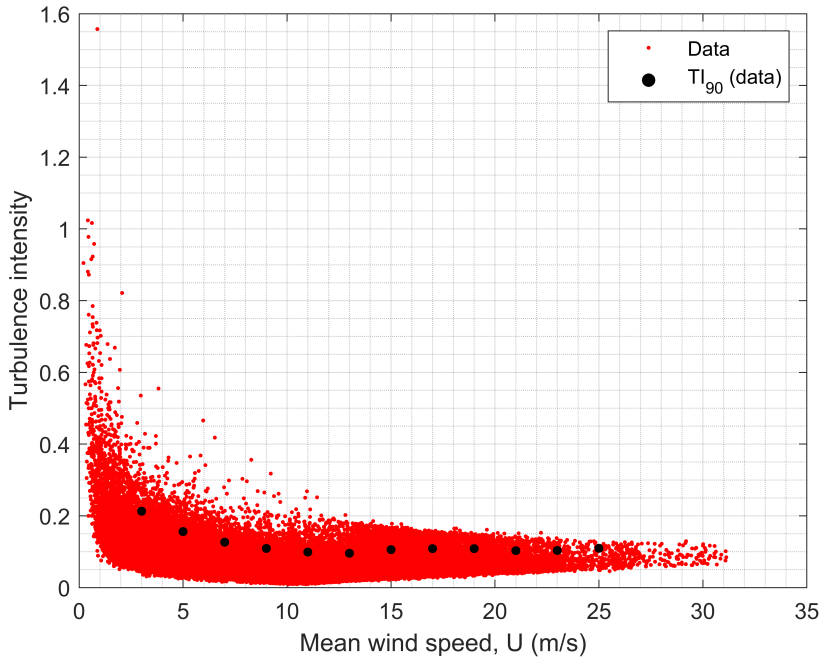

(a) SNS

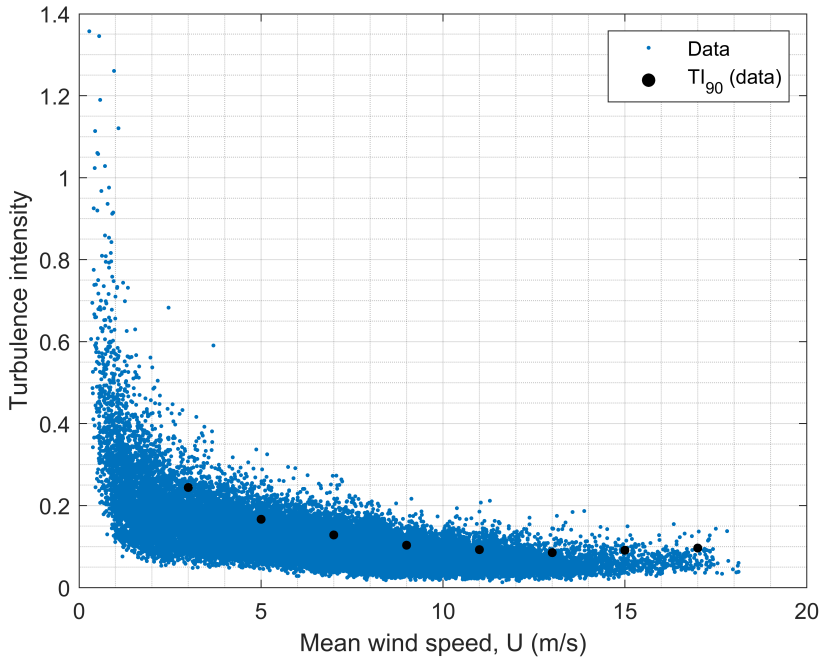

(b) JCS

Figure 4.15: Variation of turbulence intensity with wind speed (a) SNS, (b) JCS.

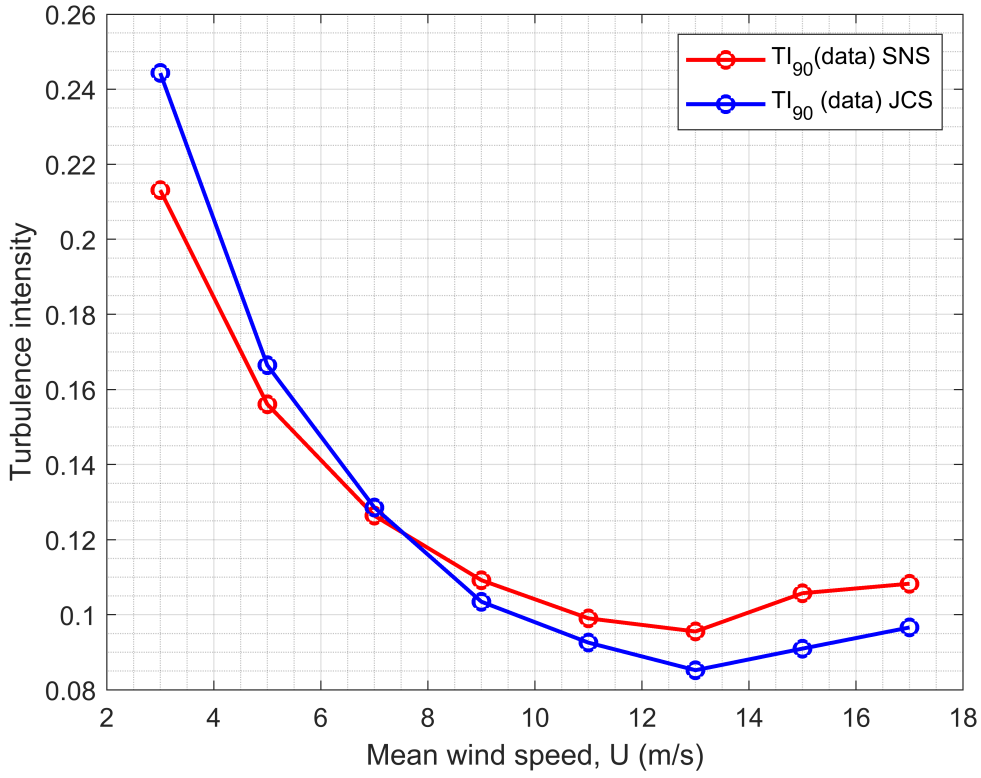

Figure 4.16: Variation of turbulence intensity with wind speed SNS vs JCS

wind turbulent model would be the most suitable for the data in both the SNS and the JCS. However, for the SNS above 13 m/s mean wind speed the TI_{90} values would be somewhat underestimated. For the JCS the values would be somewhat conservative with the class B standard turbulent model. It should be noted that the value of Iref for class B is 0.12. Iref is the expected value (mean) of the turbulence intensity at a mean wind speed of 15 m/s. It is also called the reference wind turbulence intensity. The values of Iref for SNS and the JCS are 0.064 and 0.063 respectively. The IEC-61400-1:2019 model grossly overestimated the turbulence intensity for both the SNS and the JCS (see Figure 4.18). It is stated in the literature that the standard models for IEC offshore wind turbines were done using the wind data for onshore wind turbines. The wind characteristics on land are much different from offshore and the difference is demonstrated in the results. The model shown in Figure 4.17 is IEC turbulence class C. The lowest class of turbulence model. The TI for both class A and B models would be even greater. Two of the variables contained in the relationship used to compute TI_{90} in IEC-61400-1:2019 are I_{ref} and a constant *b*; the value of these variables for turbulence class C are 0.12 and 5.6 respectively. If these values are changed to 0.10 and 3.8, respectively, better fits to the SNS and JCS data would be produced (see Figure 4.19). It was shown in the literature that a value of 3.8 was used in earlier versions of the IEC manual. Therefore, if the IEC model is used at both locations the standard model would have to be altered to a turbulence category lower than category C to fit the data.

4.2.8 Wave spectrum

Short-term irregular sea states can be represented by a wave spectrum. The distribution of the energy of the wave when plotted against frequency is known as the wave frequency spectrum (DNV, 2010*a*; Goda, 2000). There are several spectrums that are used to represent the irregular wave. The Pierson-Moskowitz (PM) spectrum and the JONSWAP spectrum are the ones that are most widely used (Chakrabarti, 1987; Reeve et al., 2004). The PM spectrum was developed using wind and wave data from the North Atlantic for fully developed seas (Reeve et al., 2004). The JONSWAP spectrum was formulated as an extension of the PM spectrum for a developing sea state in fetch limited conditions (DNV, 2010*a*). The magnitude of the peak enhancement factor, γ, for the JONSWAP spectrum lies between 1 and 7, with an average value of 3.3. A JOSNWAP model with γ = 3.3 is typically used in the North Sea (Goda, 2000; Chakrabarti, 1987). Therefore, for the extreme sea state in the SNS a JONSWAP spectrum was used to describe the irregular sea state with a peakedness factor of 3.3. A factor of 1.0 was used for the normal sea state as was done by Allen et al. (2020).

The JONSWAP spectrum was also selected for the JCS. Chakrabarti (1987) argued

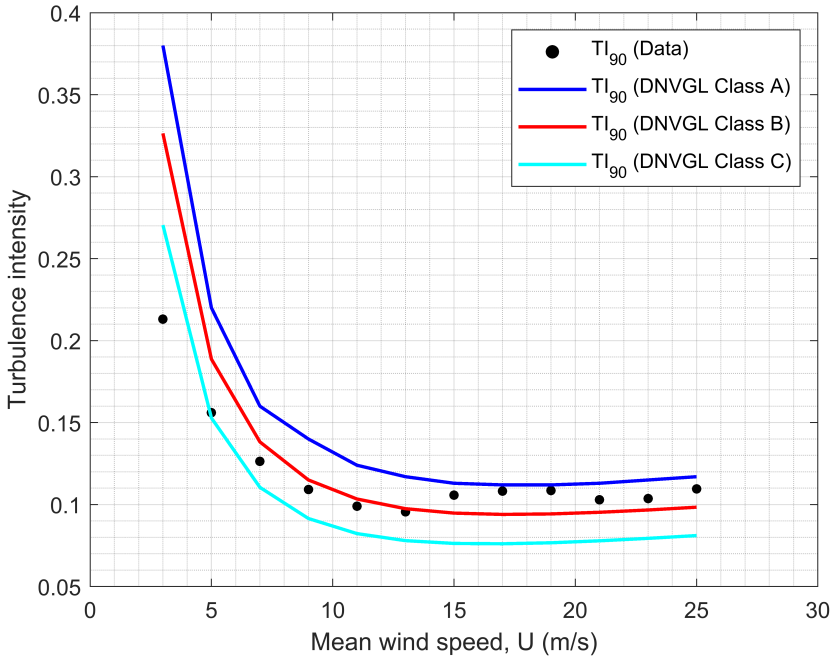

(a) SNS

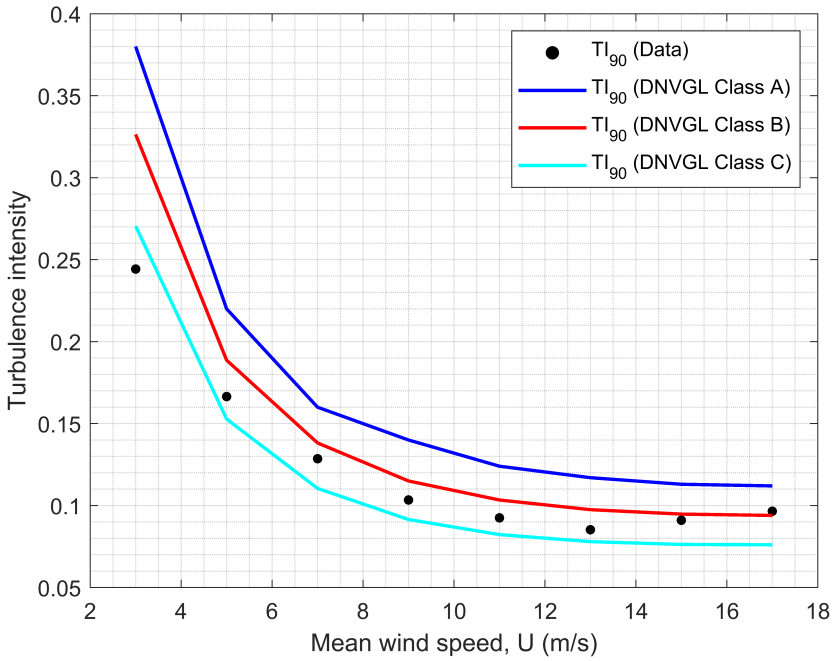

(b) JCS

Figure 4.17: Variation of turbulence intensity with wind speed (Comparison with DNVGL offshore turbulence model) (a) SNS, (b) JCS.

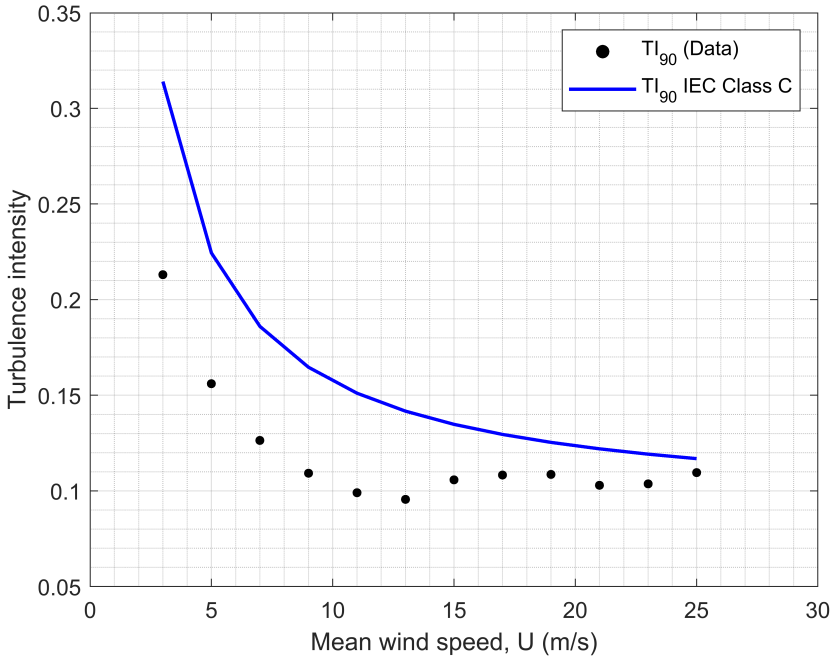

(a) SNS

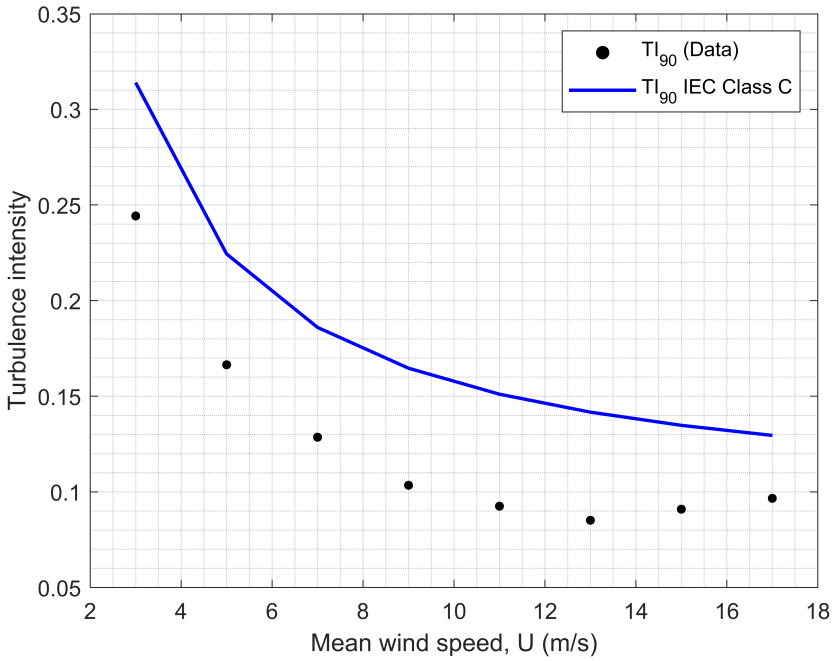

(b) JCS

Figure 4.18: Variation of turbulence intensity with wind speed (Comparison with IEC-61400-1:2019) (a) SNS, (b) JCS.

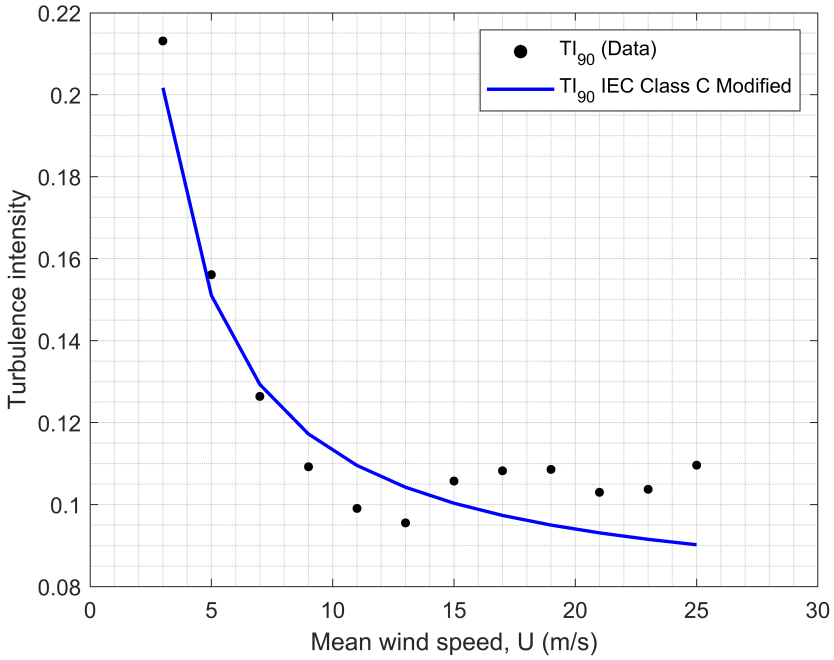

(a) SNS

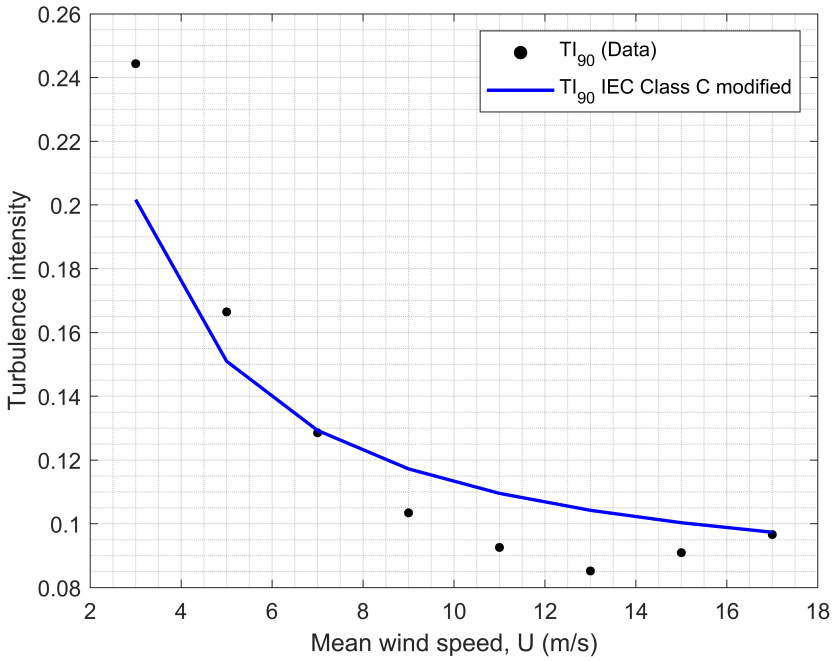

(b) JCS

Figure 4.19: Variation of turbulence intensity with wind speed (Comparison with IEC-61400 modified) (a) SNS, (b) JCS.

that the JONSWAP spectrum with a peakedness factor between 1.0 and 4 is usually used as the representative form of a design storm wave. Reeve et al. (2004) argued that the JONSWAP spectrum is one of the most widely used spectrums both in design and for lab experiments. DNV-GL (2016) recommends a JONSWAP spectrum unless the data indicates otherwise. This is an indication that the JOSWAP, which is widely used, was a reasonable choice of spectrum at both site locations. However, the SNS is characterized by winter storms whereas the JCS is characterized by hurricanes, which typically occur during the hurricane season as mentioned in Chapter 4. This difference in the characteristic of the environment might have an effect on the peakedness factor that is used for the JONSWAP spectrum. This was argued by Liu et al. (2017b), who carried out studies on an appropriate peakedness factor to use for environmental conditions in the South China Sea. An area characterized by hurricanes. However, for the purpose of this study, the same peakedness factors for the SNS were used for the JCS. Further studies could be done to investigate the behaviour of the FOWT system for the JCS using the formulations in Liu et al. (2017b) to determine the peakedness factor.

4.3 Conclusion

A comprehensive view of the data for the SNS and the JCS is taken. The data is viewed by looking at the normal sea state and normal wind speed, the extreme sea state and wind speed, the wind turbulence intensity and applicable wave spectrums. This study indicates that the normal sea and wind speed data for the SNS and the JCS are quite similar. The extreme wind speeds and wind turbulence intensity are also quite similar. Concerning the 50-year extreme sea state, the environmental contour method (ECM) is found to be suitable for the data in the North Sea. However, it is not appropriate for the data in the JCS. This was due to the presence of hurricane and other weather systems during the hurricane season. The data is therefore separated into normal season data and hurricane season data. The ECM using the Weib3P-lognormal model is suitable for the normal season data. However, the ECM did not yield good results for the hurricane season data regardless of whether the Weib3P or GPD models are used. It should be noted that Haver & Winterstein (2008), recommended that a GPD model could be used to fit the peaks of $H_s > h_o$ where the data was from a region that is affected by hurricanes. However, the fit of the GPD to the hurricane season data for the JCS using this methodology did not yield good results. Given that this problem existed, another approach is tried utilizing the ECM. The model is fitted to hurricane wave data. The significant wave data generated during the passage of a hurricane or other severe weather system. This data is obtained using a tool called HURWave developed by Banton (2002) at Delft University of Technology. The tool is still used

today by coastal engineers in the Caribbean to predict the hurricane wave height. The Weib3P fitted the hurricane data produced by Improved Young model very well and the resulting environmental contours are satisfactory. This solved the problem where the ECM used on the hurricane season data, resulted in an underestimation of the extreme sea state. This approach was only utilized for data from HURWave and data from other tools or models would be required to see if this approach is satisfactory for the hurricane wave data from other models in the JCS.

On balance, the environmental data for the SNS and the JCS appear quite similar. The next Chapter will examine this further by using the data in a FOWT numerical model and observing the response.

Chapter 5

Definition of a FOWT Numerical Model to Assess Its Performance in the SNS and the JCS

5.1 Introduction

In the previous chapter, multivariate extreme sea states were developed for the Scottish North Sea (SNS) and the Jamaica Caribbean Sea (JCS). The aim of this Chapter is to assess the behaviour of a large FOWT system in normal sea conditions and extreme environmental conditions at both site locations. The wind turbine that is studied regularly in the literature is NREL 5MW baseline wind turbine. However, the sizes of wind turbines are increasing and the wind turbines of the future will utilize large wind turbines (ORECatapult, 2018). IRENA (2019*a*) reported that it was expected that by 2025 the projects to be commissioned will consist of turbines of 12 MW and above. It was posited that with increased research and development in the future wind turbine ratings could range between 15 to 20 MW.

The projected increase in wind turbines means that wind turbine systems being studied now must consider the technology advance that will occur in the future. Therefore, although more data is available to carry out a study on the 5MW FOWT system, because of the increasing demands of the future a large wind turbine system is studied at both project locations. One of the state-of-the-art large wind turbine systems that is currently being studied in the IEA-15 MW wind turbine supported on the UMaine VolturnUS-S semi-submersible floater (Allen et al., 2020). This FOWT system is employed to carry out this study. It will help to delve deeper into understanding if a FOWT system in the North Sea is suitable for use in the Caribbean Sea. In the next section, a description of the respective FOWT system is given.

5.2 Description of the FOWT system

The FOWT that is used in this study is the UMaine VolturnUS-S semi-submersible floater, which has been designed to support the IEA-15MW reference wind turbine. It consists of a chain catenary mooring system, a steel tower and a controller (Allen et al.,

2020). The controller has been customized for the IEA-15 MW wind turbine.

5.2.1 IEA-15 MW Reference Wind Turbine and Controller

The key properties of the IEA-15MW turbine were given by Gaertner et al. (2020) and are shown in Table 5.1. The turbine has a 240 m rotor diameter, a hub height of 150 m and is a direct-drive machine. The controller that is utilized is NREL Reference Open Source Controller (ROSCOE), with a minimum rotor speed of 5 rpm and rated rotor speed of 7.55 rpm.

5.2.2 UMaine VolturnUS-S Semi-Submersible Floater

The properties of UMaine VolturnUS-S semi-submersible floater, shown in Table 5.2 and Figure 5.1, are given by Allen et al. (2020). It is a steel semi-submersible floater. VolturnUS-S consists of four columns, three external and one central column. The central column is connected at the top and bottom to the external columns. Three pontoons of 12.5 m wide x 7.0 m high rectangular cross-section connect the bottom and three 0.9 m diameter radial struts connect the top. Three cross bracing (not shown in the drawing), each 0.9 m in diameter are also connected at the top and bottom. The transition piece and the tower rest on the central column. The floater is held in position by a three line catenary mooring system in 200 m deep water. When viewed in plan, the radius from the centre of the tower to point where each mooring line connects to the anchor is 837.6 m. The mooring lines are each spread at an angle of 120 degrees. The floater has a draft of 20 m and the freeboard to the top of each of the four columns is 15 m.

5.2.3 Mooring system

The mooring system consists of a three chain catenary mooring system each of unstretched length 850 m. Each mooring chain connects to one of the fairleads, which is attached to each outer column at a depth of 14 m below SWL. The mooring system properties, shown in Figure 5.2 and Table 5.3, were given by Allen et al. (2020).

5.2.4 The Tower

The tower comprises a steel tubular section, the outer diameter at the top is 6.5 m and the outer diameter at the base is 10 m. The wall thickness varies from top to bottom, with the top being 21.21 mm thick and the bottom being 82.95 mm thick. The key properties of the tower are shown in Table 5.4. Further information on the properties of the tower is given in Allen et al. (2020).

Table 5.1: Properties of IEA-15MW Wind Turbine

Description	Unit	Value
Power rating	MW	15
Turbine class	-	IEC Class 1B
Specific rating	W/m^2	332
Rotor orientation	-	Upwind
Number of blades	No.	3
Control	-	Variable speed, collective pitch
Cut-in wind speed	m/s	3
Rated wind speed	m/s	10.59
Cut-out wind speed	m/s	25
Rotor diamater	m	240
Airfoil series	-	FFA-W3
Hub height	m	150
Hub diameter	m	7.94
Hub overhang	m	11.35
Drivetrain	-	Low speed, direct drive
Design tip-speed ratio	-	9.0
Minimum rotor speed	rpm	5
Maximum rotor speed	rpm	7.56
Maximum tip speed	m/s	95
Gearbox ratio	-	-
Shaft tilt angle	deg	6
Rotor precone angle	deg	-4
Blade prebend	m	4
Blade mass	ton	65
Rotor nacelle assembly mass	ton	1,017

Table 5.2: Properties of UMaine VolturnUS-S Semi-Sub

Description	Unit	Value
Power rating	MW	15
Hub height	m	150
Excursion[1] (Length, Width, Height)	m	90.1, 102.1, 290.0
Water depth	m	200
Freeboard	m	15
Draft	m	20
Total system mass	t	20,093
Platform mass	t	17,839
Tower mass	t	1,263
Rotor nacelle assembly mass	t	991
Tower top diameter	m	6.5
Tower base diamater	m	10
Transition piece height	m	15
Tower interface mass	t	100
Ballast mass (fixed/fluid)	t	2,540/11,300
Hull displacement	m^3	20,206
Hull steel mass	t	3,914
Vertical centre of gravity from SWL	m	-14.94
Vertical centre of buoyancy from SWL	m	-13.63
Roll inertia about centre of gravity	kg/m^2	1.251E+10
Pitch inertia about centre of gravity	kg/m^2	1.251E+10
Yaw inertia about centre of gravity	kg/m^2	2.367E+10
Mooring system	-	Three line chain catenary

[1] *The system's excursion describes the volume encompassed by the complete structure.*

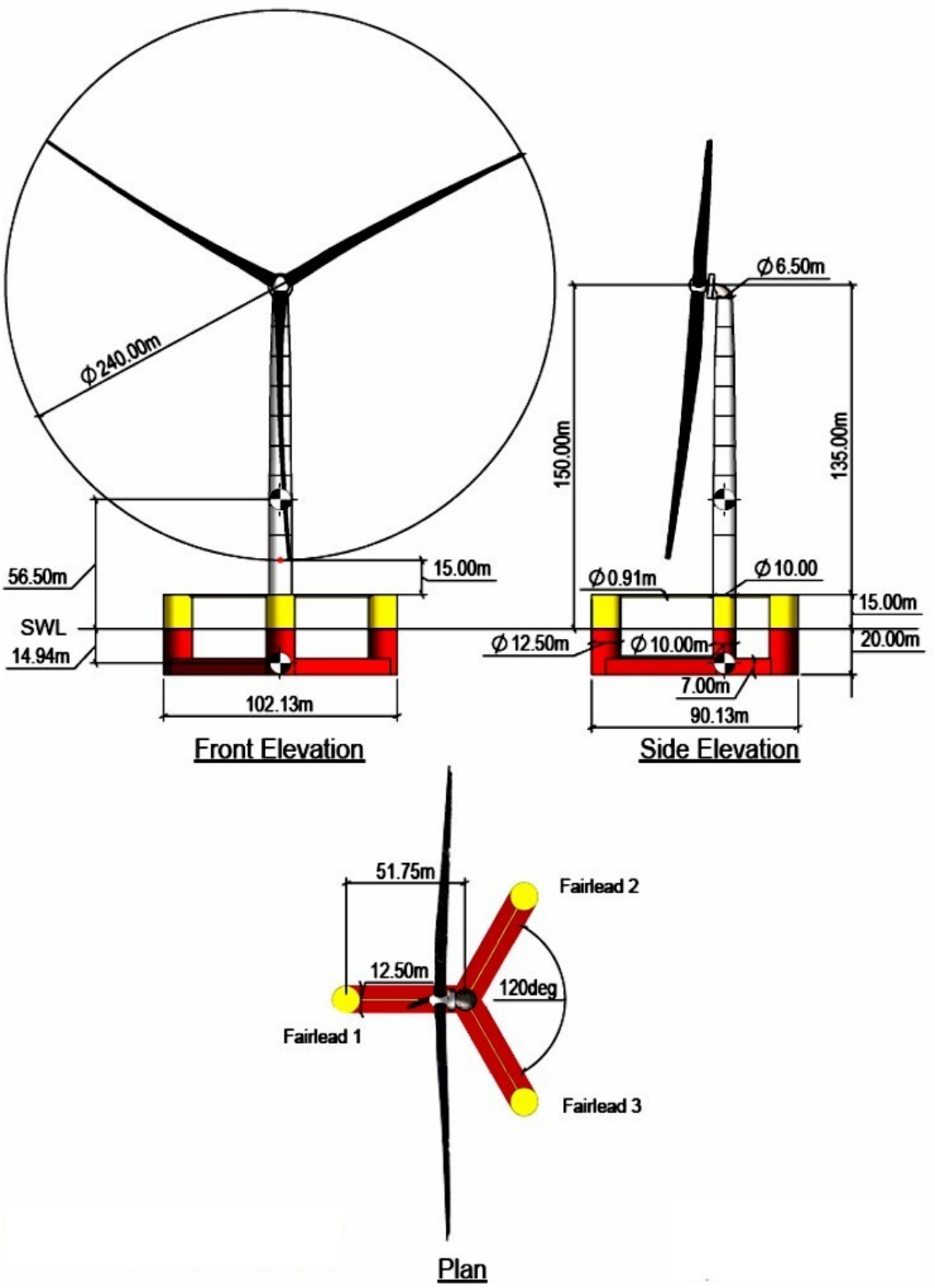

Figure 5.1: Layout Plan and Section UMaine VolturnUS-S Semi-sub Floater (Source: Allen et al. (2020))
(Permission has been granted by Garrett Barter of NREL to reproduce this figure)

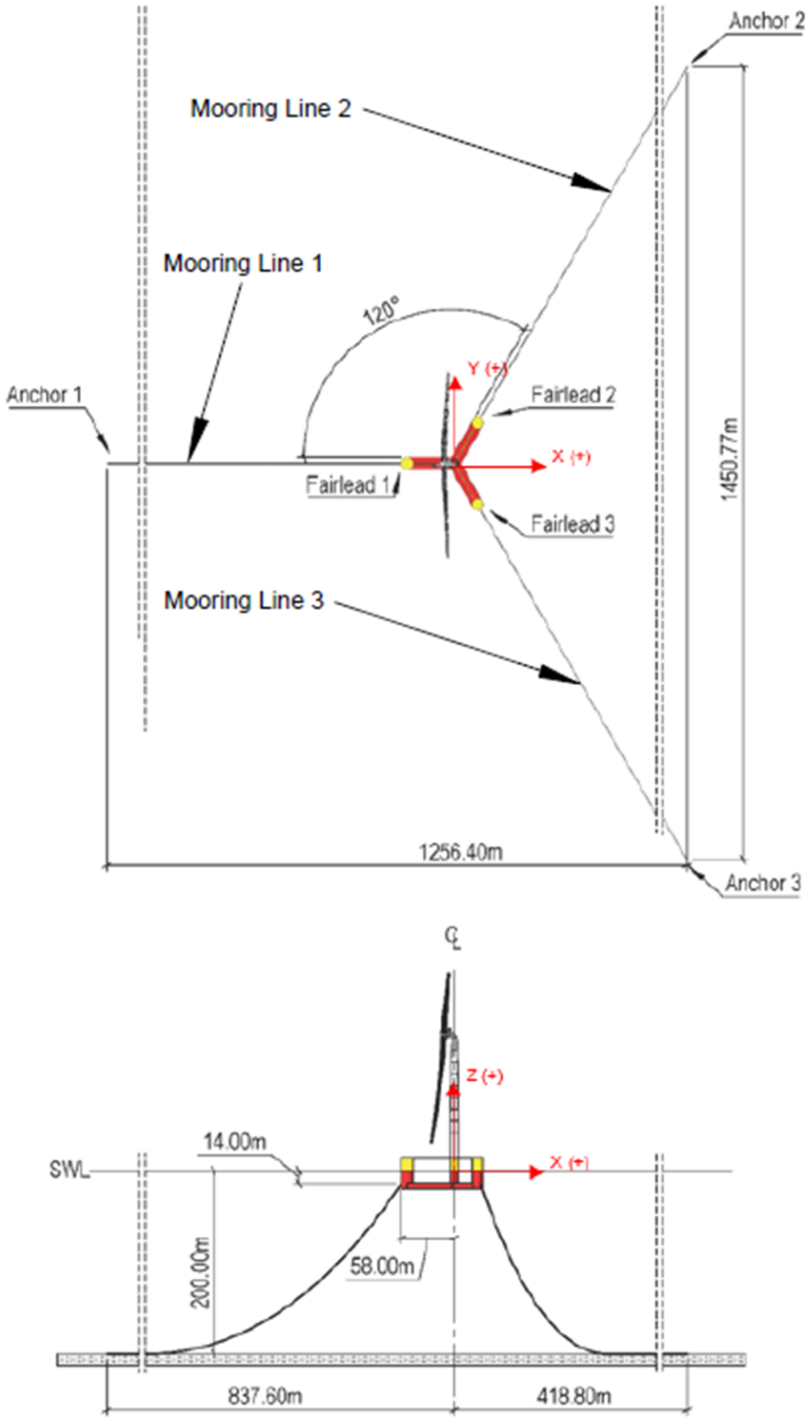

Figure 5.2: Mooring System Arrargement UMaine VolturnUS-S Semi-sub Floater (Adapted from: Allen et al. (2020))
(Permission has been granted by Garrett Barter of NREL to reproduce this figure)

Table 5.3: Properties of UMaine VolturnUS-S Mooring Line

Description	Unit	Value
Mooring system type	-	Chain catenary
Line type	-	R3 studless mooring chain
Line breaking strength	kN	22,286
Number of lines	-	3
Angle between adjacent mooring lines	deg	120
Anchor depth	m	200
Fairlead depth	m	14
Radius of anchors from platform centreline	m	837.6
Radius of fairleads from platform centreline	m	58
Nominal chain diameter	mm	185
Dry line linear density	kg/m	685
Extensional stiffness	MN	3,270
Line unstretched length	m	850

Table 5.4: Tower Properties - UMaine VolturnUS-S Semi-Sub

Description	Unit	Value
Mass	ton	1,263
Length	m	129.495
Base outer diamater	m	10
Top outer diameter	m	6.5
1st Fore-Aft bending mode	Hz	0.496
1st Side-Side bending mode	Hz	0.483

5.3 Numerical Model Set Up and Description

The standard 15 MW VolturnUS-S FOWT OpenFAST model is available for download on GitHub (Allen et al., 2020). This model is used for analysis of the 15MW FOWT system with modifications made to the mooring line to accommodate other water depths as appropriate. The reference coordinate system is shown in Figure 5.3. The first step in setting up the numerical model is to carry out a verification exercise. The tests done to verify the model are a static equilibrium test and a free decay test. These tests are described in the following sections.

5.3.1 Numerical Model Verification

Static equilibrium test of VolturnUS-S FOWT system

A static equilibrium test is done to check the balance between the hydrostatic forces, the mooring forces, and the gravitational forces. This is done in the absence of wind and waves, that is, in a still wind and still water environment (Mahfouz et al., 2021; Liu et al. 2022). In the static state, the full system weight of the FOWT (floater + tower + rotor nacelle assembly (RNA)) and the vertical mooring pretension should balance the undisplaced buoyant forces (upward forces). To achieve this, the FOWT system is set up such that when the platform floats the mean heave is 0 metres about the SWL as shown in Figure 5.1.

The static equilibrium check of the VolturnUS-S FOWT system is done at the original water depth of 200 m given in Allen et al. (2020). The simulation time is set in the main OpenFAST file to 1800 s with a time step of 0.025 s. This simulation time is in accordance with the times given in the DTU wind turbine document (Natarajan et al., 2016) and is similar to the time used by Liu et al. (2022) when carrying out a static equilibrium check for the VolturnUS-S FOWT. The output of the results is started after 600 s to eliminate transients that occur during startup (Liu et al., (2022). Static equilibrium is verified by calculating the mean heave of the FOWT system over the entire simulation period (600 to 1800 s). The mean heave is found to be 0.001 m (min = 0.0002 m; max = 0.0020 m). This shows that there is negible movement in heave as the platform floats about the SWL. An indication that the downward forces due to weight are balanced by the buoyancy forces and the FOWT system is thus in a state of static equilibrium.

Verification of the Natural frequency of VolturnUS-S FOWT system

Similar to Allen et al. (2020) and Mahfouz et al. (2021), a free decay test is conducted for each of the rigid-body degrees of freedom to determine the natural frequency of the FOWT system. This is done by giving the system a perturbation for each degree of freedom of interest and allowing the system to oscillate freely. The objective is to

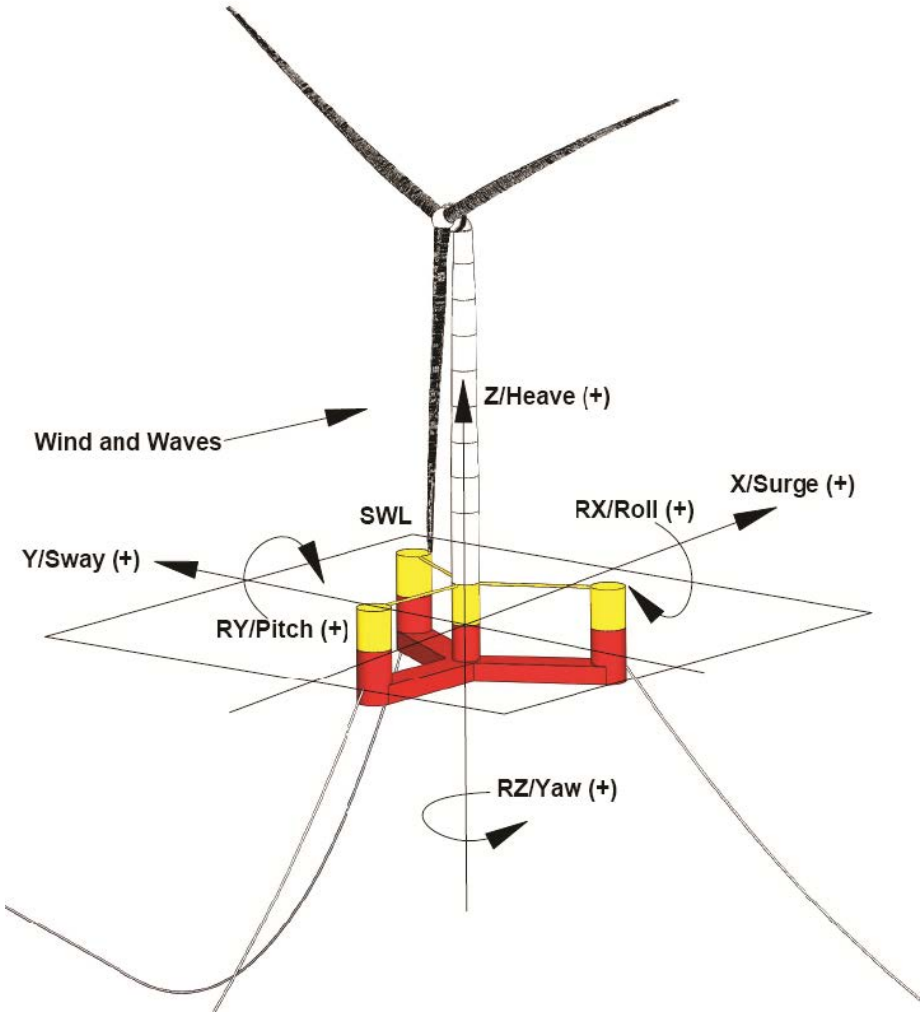

Figure 5.3: Reference Coordinate System UMaine VolturnUS-S Semi-sub (Source: Allen et al. (2020))
(Permission has been granted by Garrett Barter of NREL to reproduce this figure)

verify that the natural frequencies used in this study are similar to the ones given by Allen et al. (2020). Therefore, the perturbations used by them is used for this exercise. An initial displacement of 20 m is used for the surge and sway DOFs, 5m is used for the heave DOF, 10 deg is used for roll and pitch DOFs and 15 deg is used for the yaw DOF. The smiluation times are 500 s, 130 s, 100 s and 425 s respectively as given by Allen et al. (2020). The simulations are carried out in still water conditions and a still wind environment in the same manner as the static equilibrium test. Table 5.5, shows the system natural frequencies and Figure 5.4 shows the free decay motions in the 6-DOFs that are produced from the free decay test. The natural frequencies (Hz) are computed by using the relationship *f = 1/wave period*. The wave period is the time taken to complete one wavelength. Each decay time series shown in Figure 5.4 is divided into a specific number of wave lengths and the natural frequency is computed for each wavelength. The natural frequencies are added and the averages taken to yield the values in Table 5.5. The tower's fore- aft and side-side natural frequencies were also determined. This was done by running OpenFAST with the linearization functionality set to TRUE (Jonkman et al., 2018). The natural frequencies are found to be in good agreement with the values given by Allen et al. (2020). The results of the natural frequency check and that from the static equilibrium test verify that the numerical model of the VolturnUS-S FOWT system has been properly set up and the results that are obtained from subsequent analyses should be credible.

Table 5.5: System natural frequency UMaine VolturnUS-S FOWT

Description	Unit	Allen et al (2020)	This study
Surge	Hz	0.007	0.007
Sway	Hz	0.007	0.007
Heave	Hz	0.049	0.049
Roll	Hz	0.036	0.035
Pitch	Hz	0.036	0.034
Yaw	Hz	0.011	0.011
Tower 1st Fore-Aft bending mode	Hz	0.496	0.491
Tower 1st Side-Side bending mode	Hz	0.483	0.466

5.4 Proposed Wind Turbine for the SNS and the JCS

5.4.1 Modification to the mooring line

The verification case study set up in section 5.3.1 for the UMaine VolturnUS-S FOWT was set up for 200 m deep water. The water depth at both site locations as mentioned in Chapter 4 is 100 m. Therefore, the original mooring system for the VolturnUS-S

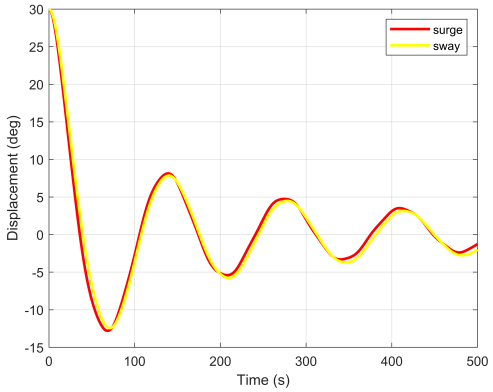

(a) Surge and Sway

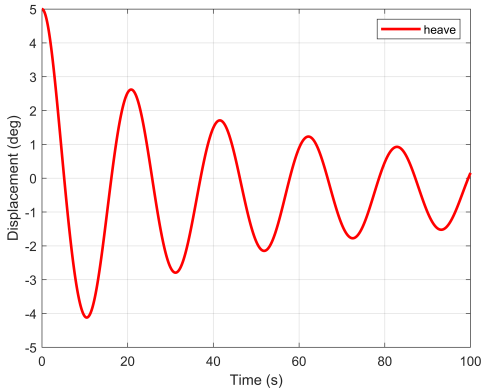

(b) Heave

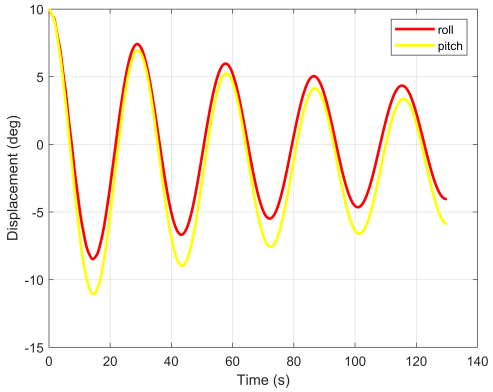

(c) Roll and Pitch

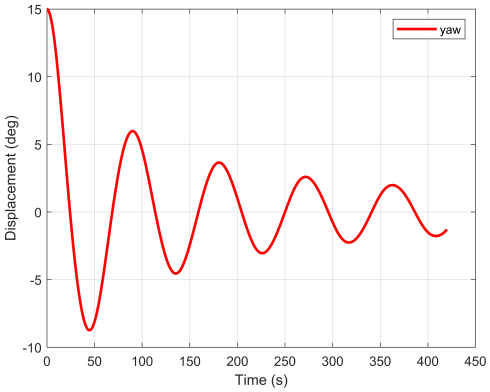

(d) Yaw

Figure 5.4: UMaine VolturnUS-S free decay time histories(a) Surge and Sway (b) Heave (c) Roll and Pitch (d)Yaw

FOWT is modified for water depth of 100 m. Rather than carrying out a full mooring system design, the moorings were scaled to the shallower water depth. This is done by starting with the original 200 m deep mooring line and using the method of similar triangles to determine the geometrical properties of the 100 m deep-water mooring line. The properties of the mooring line for 100 m deep water are shown in Table 5.6. A similar modification of a mooring line in water shallower than 200 m was carried out by Shin et al. (2019). However, they did not indicate what calculations were done to modify the mooring line.

Table 5.6: Properties of UoP Mooring Line for 100m Deep Water

Description	Unit	Value
Mooring system type	-	Chain catenary
Line type	-	ORQ stud link mooring chain
Line breaking strength	kN	37,980
Number of lines	-	3
Angle between adjacent mooring lines	deg	120
Anchor depth	m	100
Fairlead depth	m	14
Radius of anchors from platform centreline	m	418.5
Radius of fairleads from platform centreline	m	58
Nominal chain diameter	mm	300
Dry line linear density	kg/m	1,971
Extensional stiffness	MN	8,100
Line unstretched length	m	415

The primary consideration for the mooring line modification is to ensure that for the no wave and no wind condition (static equilibrium test) the average heave of the wind turbine is zero. In addition, the mooring lines are checked to ensure that the minimum breaking load (MBL) conditions are satisfied. The computation of MBL is done in accordance with Chryssostomidis & Liu (2011). The axial stiffness per unit length (AE) and breaking strength (BS) of the mooring chain are given as follows:

$$AE = 90000D^2 \tag{5.1}$$

where D is the diameter of the mooring chain in mm and AE is in N.

$$BS = c(44 - 0.08D)D^2 \tag{5.2}$$

where c is a corrosion factor and BS is in N. For the ORQ grade mooring chain shown

in Table 5.6, c=21.1 (If *BS* is given in kN, c = 0.0211).

The static equilibrium test is carried out in a similar manner to the above in still wind and water conditions. The simulation is run for 1800 s and the average heave is determined for the last 1200 s of the simulation. The average heave of the FOWT system is found to be 0.03 m (min = -0.01; max = 0.042). Hence the FOWT system has mean heave of zero and the static equilibrium test is satisfactory. In addition, the modified mooring line satisfied the MBL condition. The MBL of the mooring line (computed using equation 5.2) is 37,980 kN and the maximum fairlead tension (obtained from OpenFAST output) is 6,590 kN, which gives a factor of safety of 5.8 (> required FOS of 2.7 shown in Chrysostomidis & Liu (2011). With this condition satisfied, a free decay test is carried out for the FOWT system in 100 m deep water and the natural frequencies are determined in the same manner as above. The natural frequencies are shown in Table 5.7.

Table 5.7: System Natural Frequency of the 100 m Deep Water FOWT System alongside the solution for the 200 m water depth condition

Description	**Unit**	**This study 100 m deep**	**Allen et al (2020) 200 m deep**
Surge	Hz	0.010	0.007
Sway	Hz	0.013	0.007
Heave	Hz	0.049	0.049
Roll	Hz	0.035	0.036
Pitch	Hz	0.034	0.036
Yaw	Hz	0.007	0.011
Tower 1st Fore-Aft bending mode	Hz	0.491	0.496
Tower 1st Side-Side bending mode	Hz	0.466	0.483

It is observed that the heave, roll and pitch natural frequencies are in good agreement with the values of the 200 m deep system. This is because the hydrostatic stiffness of the system is unchanged and the respective motions are affected by hydrostatic stiffness. Surge, sway and yaw motions are affected by the stiffness of the mooring line. The difference in the stiffness of both lines is the reason for the difference in the natural frequencies of both systems. This agreed with Mahfouz et al. (2021) where the difference in the stiffnes of the mooring lines affected the natural frequencies of the FOWT in the surge, sway and yaw DOFs.

5.4.2 Design load conditions

The FOWT systems at both the SNS and JCS are investigated for normal operating conditions and extreme conditions. These conditions are set referring to the design

load conditions (DLC) for FOWT turbines design given in DNV-GL (2016). The conditions considered are DLC 1.1 and DLC 6.1 and are presented in Table 4.3. DLC 1.1 considers the turbine operating in normal sea and wind conditions, whereas DLC 6.1 considers the turbine in extreme sea and wind conditions. These sets of conditions would define in practical terms the conditions that might affect the wind turbine. They would therefore allow for proper assessment of the behaviour of the wind turbine at both locations.

Normal sea and wind conditions. The load conditions for the normal sea state and extreme sea state are given in Table 4.3 of Chapter 4. It was observed that the sea state and turbulence intensity for the JCS and the SNS are comparable. Therefore, two conditions are investigated, at the normal sea state (DLC 1.1):

1. The wave only condition
2. The wind and wave condition, assuming a turbulent wind condition using the TI values shown in Table 4.3.

Extreme sea and wind conditions. The extreme sea states are determined using multivariate extreme value analysis as outlined in Chapter 4. In accordance with DNV-GL (2016) the extreme sea state is used for a return period of 50-years and 1-year and the corresponding significant wave heights denoted by H_s, 50-yr and $H_{s,1-yr}$, respectively. For the purpose of this study, the maximum value of $H_{s,50-yr}$ and the corresponding value of T_p are used for the extreme sea state values. The values are shown in Table 4.3, Chapter 4. The 50-year wind speed that is determined in Chapter 3 is used as the extreme wind for the JCS. The 50-year wind speed for the SNS is determined in the same manner.

Six random seeds are run for each sea state at each of the site locations. A total of 36 simulations in total at both locations. This was done in accordance with IEA (2019) and DTU (2016). Each seed represents one wave realization and the response for each wave realiztion is different as the process is random. Therefore the maximum response occurs for different wave realizations. The maximum value from each of the six seeds are determined. The mean of these maximum values is used as the critical design load. IEC-61400-3-1 (2019) indicated that the characteristic value can be the mean of the worst case computed load effect. The following responses of the FOWT system are investigated:

1. Surge motion
2. Heave motion

3. Pitch motion
4. Tension at fairlead 1
5. Tension at fairlead 2
6. Tension at fairlead 3
7. Blade root resultant moment
8. Fore-aft tower base moment
9. Side-side tower base moment
10. Resultant moment at tower base

A floater has motions in 6 DOF but the DOFs that were studied by others for a semi-submersible type floater are the heave, surge and pitch motions. DNV (2010*b*) stated that the fundamental differences among floaters are related to their motions in the vertical plane that is heave, pitch. Zhou et al. (2017) only considered the surge and pitch motions in their study on a semi-submersible floater. Shi et al. (2019) and Mahfouz et al. (2021) considered heave, surge and pitch motions in their study. It is on this basis that the heave, surge, pitch motions of the floater are considered.

5.5 Comparing the response of the FOWT in the SNS and the JCS

The following sections examine the response of the FOWT in the JCS and the SNS in both the normal sea environment and an extreme sea environment. The mean values of the response are shown in Table 5.8 and Table 5.9. The response is divided into three categories, the dynamic motion of the platform, the tensions in the fairleads and the bending moments (on the blades and at the base of the tower). The motion of the turbine in the normal sea state considering the wave loading condition only is examined next.

5.5.1 FOWT respose for the normal sea state, SNS and the JCS - wave only condition

Surge motion. Referring to figure 5.5 and Table 5.8, the surge motion is responsive to the wave climate in both the JCS and the SNS under normal sea conditions. When the surge motion for the JCS is compared to the motion for the SNS, for the three sea states investigated, the motion for the JCS is very close to the motion for the SNS. In particular, for SS9, the surge motion of the SNS is 1.2 m and 1.3 m for the JCS. For SS11, the surge motion is 1.4 m for the SNS and 1.5 m for the JCS. For SS13, the surge motion is 1.65 m for the SNS and 1.65 m for the JCS. The results in surge

indicate that the normal sea state of the JCS and the SNS have a similar influence on the longitudinal motion of the platform. This is because the normal sea states appear quite similar as shown in Table 4.3. For exmaple, for SS9, SNS, H_s = 0.46 m and T_p = 7.41 s; JCS, H_s = 0.73 m and T_p = 7.44 s. The motion in surge reflects these results.

Table 5.8: Mean responses of VolturnUS-S FOWT - SNS and the JCS, normal wave conditions (SNS9, JCS9, etc., are the sea states in Table 4.3 and notes below)

Description	SNS9	JCS9	Scale Factor, SF = JCS9/SNS9	SNS11	JCS11	Scale Factor, SF = JCS11/SNS11	SNS13	JCS13	Scale Factor, SF = JCS13/SNS13
Surge (m)	1.20	1.34	1.11	1.35	1.50	1.11	1.65	1.65	1.00
Heave (m)	0.46	0.48	1.02	0.47	0.49	1.04	0.48	0.51	1.06
Pitch (m)	2.42	2.42	1.00	2.42	2.44	1.00	2.44	2.46	1.01
Tension in fairlead1 (N)	2.04E+06	2.05E+06	1.00	2.05E+06	2.06E+06	1.01	2.07E+06	2.07E+06	1.00
Tension in fairlead2 (N)]	2.07E+06	2.07E+06	1.00	2.07E+06	2.07E+06	1.00	2.07E+06	2073500	1.00
Tension in fairlead3 (N)	2.07E+06	2.07E+06	1.00	2.07E+06	2.07E+06	1.00	2.07E+06	2073500	1.00
Blade root resultant bending moment (kNm)	1.80E+04	1.80E+04	1.00	1.80E+04	1.80E+04	1.00	1.80E+04	1.79E+04	0.99
FA tower base moment (kNm)	1.80E+05	1.89E+05	1.05	1.89E+05	1.99E+05	1.05	2.00E+05	2.06E+05	1.03
SS tower base moment (kNm)	44.24	48.64	1.10	48.66	53.43	1.10	55.41	59.10	1.07
Tower base resultant moment (kNm)	1.80E+05	1.89E+05	1.05	1.89E+05	1.99E+05	1.05	2.00E+05	2.06E+05	1.03

Notes:

- SNS9: H_s = 0.46 m, T_p = 7.41 s; JCS9: H_s = 0.73 m, T_p = 7.44 s
- SNS11: H_s = 0.74 m, T_p = 7.24 s; JCS11: H_s = 0.97 m, T_p = 7.74 s
- SNS13: H_s = 1.06 m, T_p = 7.16 s; JCS13: H_s = 1.16 m, T_p = 8.00 s

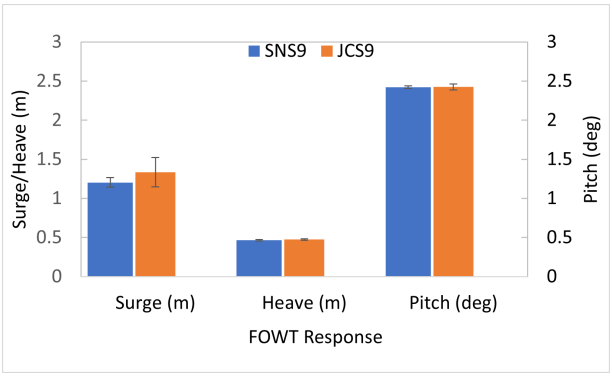

(a) Sea state 9

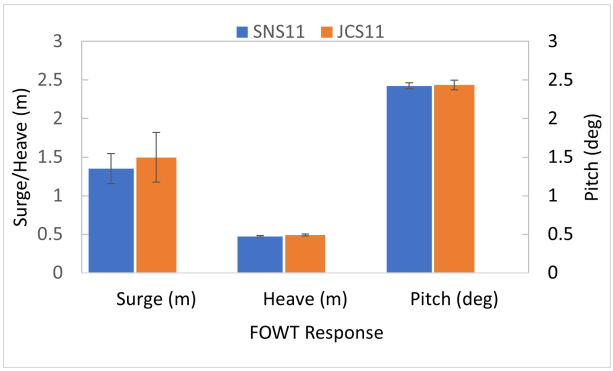

(b) Sea state 11

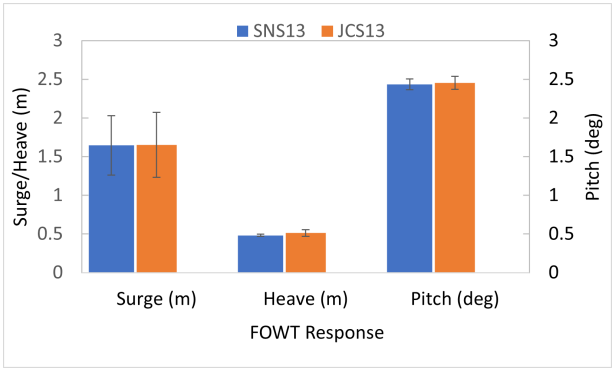

(c) Sea state 13

Figure 5.5: Comparison of the magnitude of the motion of the VolturnUS-S platform in surge, heave and pitch during three different normal sea conditions, for wave only, SNS vs JCS.

Heave motion. Referring to 5.5 and Table 5.8, the motion in heave for the JCS and the SNS are quite similar for SS9, SS11. That is, for SS9 the heave motion is 0.48 m for the JCS and 0.46 m for the SNS; for SS11 the heave motion is 0.49 m for the JCS and 0.47 m for the SNS. For SS13 the heave motion in the JCS is 1.06 times the motion in the SNS, with a value of 0.51 m for the JCS and 0.48 m for the SNS. These results show that the heave amplitudes do not show significant change for the increased normal sea states. They also show that the magnitude of the heave motions can be considered very close at both locations. In the study by Liu et al. (2019a), there was also very small increase in heave amplitudes for increased sea states. For example, for load condition 1 with H_s of 2.51 m and T_p of 9.86 s, the maximum heave motion is 0.49 m and for H_s = 4.74 m and T_p = 11.81 s, the maximum heave motion is 0.86 m. In addition, these values in heave for the JCS and the SNS are similar in magnitude to the value obtained by Allen et al. (2020) for the VolturnUS-S FOWT at normal sea state conditions. In particular, a mean heave motion of 0.3 m was shown for normal sea state conditions (where at 10 m/s, H_s =1.54 m and T_p = 7.65 s).

Pitch motion. Referring to 5.5 and Table 5.8, the motion in pitch is quite similar for the JCS and the SNS. For example, for SS9, JCS, the pitch is 2.42 deg and 2.42 deg for the SNS. For SS11, the pitch is 2.42 deg for the SNS and 2.44 deg for the JCS. For SS13, the pitch is 2.44 deg for the JCS and 2.46 deg for the SNS. These values are similar to the value obtained at the normal sea state by Allen et al. (2020). A mean value of 2.3 deg is given as the pitch motion during normal sea state conditions.

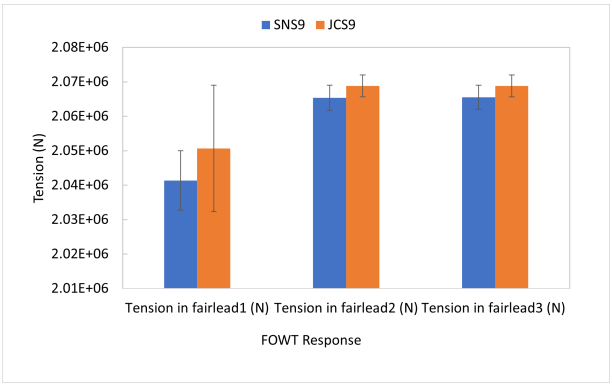

(a) Sea state 9

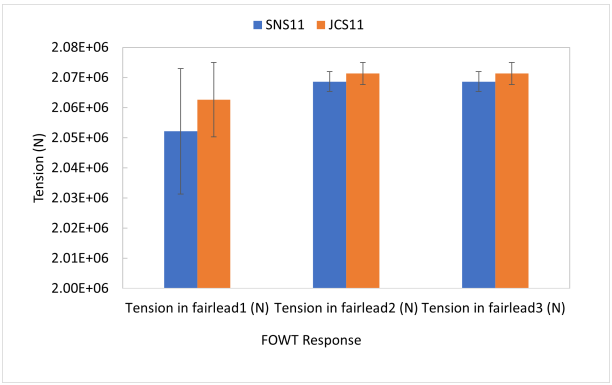

(b) Sea state 11

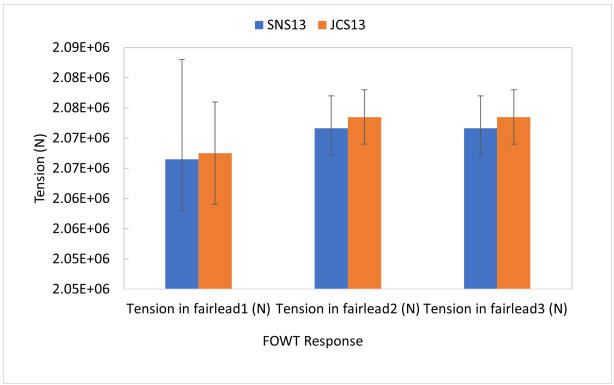

(c) Sea state 13

Figure 5.6: Comparison of the magnitude of the tensions in the fairleads for the VolturnUS-S platform during three different normal sea conditions, for wave only, SNS vs JCS.

Fairlead tensions. Figure 5.6 and Table 5.8 show the magnitude of the tensions in the fairleads at both the JCS and the SNS during normal sea conditions, assuming that the wind is negligible. The results show that the tensions in fairleads 1 to 3 are similar at both locations, with a value of 2.1 E+06 N. This is because the wave climate is similar at both locations for normal sea conditions and would therefore cause similar displacements of the platform. This is also evidenced by the nearness of the motions in surge, the value are very close at both locations and hence the displacements at the

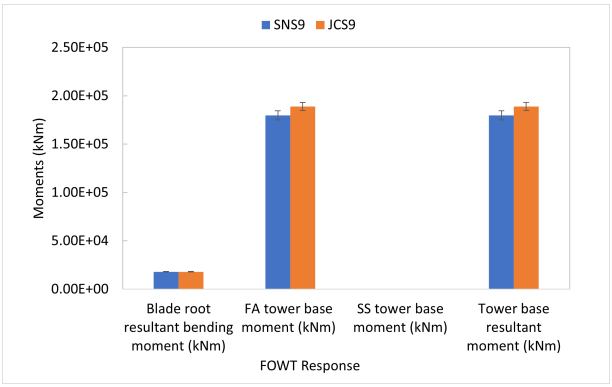

(a) Sea state 9

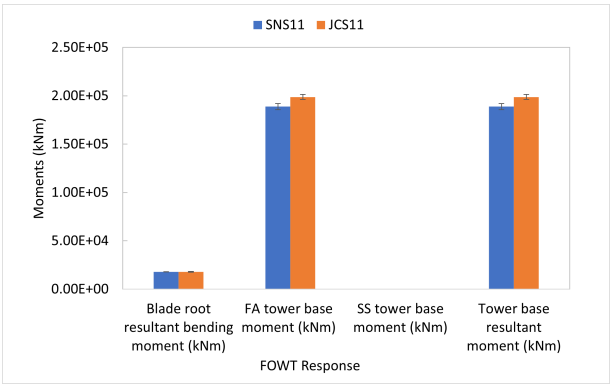

(b) Sea state 11

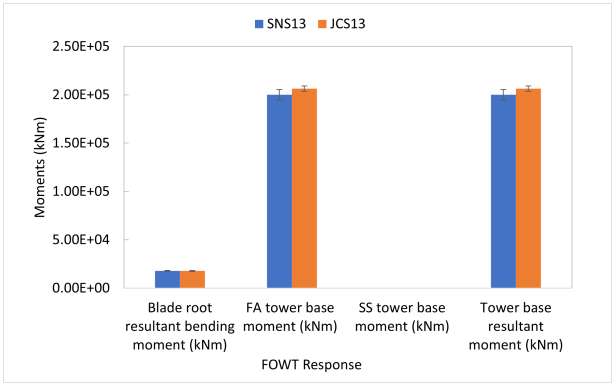

(c) Sea state 13

Figure 5.7: Comparison of the magnitude of the bending moment at the blade root and at the base of the tower for the VolturnUS-S platform during three different normal sea conditions, for wave only, SNS vs JCS.

platform would be similar, resulting in similar tensions in the fairleads.

Bending moments. The structural response of the FOWT system in normal sea conditions (see Table 4.3) is investigated. The results are comparable at both locations. Figure 5.7 and Table 5.8 show the magnitude of the response of the blade root moments and the bending moments at the base of the tower. It is very clear that the moments at the blade root are the same at the JCS and the SNS and the moments at the base of the tower are very close at both locations. For SS9 to SS13, SNS and the JCS, the resultant blade root moment is 1.8E+06 N. The fore-aft moment at the base of the tower, for SS9 and SS11, JCS is 1.1 times the fore-aft moment in the SNS. That is, for SS9, the fore-aft moment is 1.8E+05 kNm for the SNS and 1.89E+05 kNm for the JCS. For SS11, the fore-aft moment for the SNS is 1.89E+05 kNm and 1.99E+05 kNm for the JCS. For SS13, the fore-aft moment in the JCS and the SNS are very close, with a value of 2.0E+05 kNm for the SNS and 2.1E+05 kNm for the JCS.

Closing remarks normal wave condition. Table 4.3 shows the normal sea conditions for the JCS and the SNS. The nearness of the dynamic motions of the platform in surge, heave and pitch at both locations confirms that the normal sea states shown in the Table are quite similar.The magnitude of the tensions in the fairleads and the structural responses also indicate that the wave climate at the SNS and the JCS is similar with the responses being very close. The next section will investigate the effect of wind on the platform and is called the wind and wave condition. This condition equates to what occurs in reality. It is significant to note that the difference in the wind condition at both locations occurs because of the variation in the turbulence intensity. Please refer to Table 4.5 for the turbulence intensities at normal sea conditions for the three states considered in the SNS and the JCS.

5.5.2 FOWT response for the normal sea state, SNS and JCS - wind and wave condition

Although this section deals with the motion of the platform in wave and wind conditions, the nomenclature, SS9, SS11 and SS13 have been retained. For SS9, this is the wind and wave conditions at a wind speed of 9 m/s. Similarly, for SS11 and SS13.

Surge motion. Referring to Figure 5.8 and Table 5.9, when wind is applied to the FOWT system (Table 4.3) the platform motions at both the SNS and the JCS increase drastically. This is because the turbine in now operating and the wind blowing on the blades activates the rotor thrust force. This causes an increase in the longitudial movement of the platform. In particular, for SS9, SNS, the surge is 1.27 m for the wave only condition and 23 m for the wind and wave condition. Similarly for the JCS, the surge is 1.5 m for the wave only condition and 27.9 m for the wind and wave condition.

Considering the motion of the floater during normal wind and wave condition in the SNS and the JCS; the surge motion, SS9, in the SNS is 1.03 times the surge for the JCS. For SS11, the surge motion within the SNS and the JCS are very close, with values of 30.76 m and 30.24 m respectively. For SS13, the surge motion in the SNS is 5.1 m and 3.0 m in the JCS. That is, the surge motion in the SNS is 1.7 times the motion in the JCS. The larger surge motion within the SNS for SS9 to SS13 is due to the larger values of the turbulence intensity within the SNS. Referring to Table 4.5, for SS9, TI for SNS is 10.92 % and 10.35 for JCS; SS11, SNS, TI of 9.90 % and 9.26 % for the JCS ; SS13, 9.55 % for SNS and 8.52 % for JCS. Li et al. (2019) in their study on turbulent flow on offshore wind turbines, indicated that the increase in the turbulence intensity results in greater surge motion for the FOWT.

Table 5.9: Mean responses of VolturnUS-S FOWT - SNS and the JCS, normal wind and wave conditions (SNS9, JCS9, etc., are the sea and wind conditions in Table 4.3 and notes below)

Description	SNS9	JCS9	Scale Factor, SF = JCS9/SNS9	SNS11	JCS11	Scale Factor, SF = JCS11/SNS11	SNS13	JCS13	Scale Factor, SF = JCS13/SNS13
Surge (m)	28.76	27.86	0.97	30.76	30.24	0.98	5.141	3.045	0.59
Heave (m)	0.87	0.87	1.00	1.12	1.12	1.00	0.52	0.5716	1.11
Pitch (deg)	7.73	7.62	0.99	11.28	11.10	0.98	1.76	2.083	1.19
Tension in fairlead1 (N)	5.60E+06	5.31E+06	0.95	6.83E+06	6.79E+06	0.99	2.22E+06	2.08E+06	0.94
Tension in fairlead2 (N)	1.82E+06	2.08E+06	1.15	1.82E+06	1.84E+06	1.01	2.19E+06	2.12E+06	0.97
Tension in fairlead3 (N)	1.85E+06	2.06E+06	1.12	1.82E+06	1.75E+06	0.96	2.07E+06	2.14E+06	1.03
Blade root resultant bending moment (kNm)	1.01E+05	9.98E+04	0.99	1.32E+05	1.31E+05	0.99	2.52E+04	2.12E+04	0.84
FA tower base moment (kNm)	6.68E+05	6.63E+05	0.99	9.80E+05	9.66E+05	0.99	1.69E+05	2.05E+05	1.21
SS tower base moment (kNm)	2.67E+04	2.75E+04	1.03	3.43E+04	3.10E+04	0.94	5.32E+04	1.70E+04	0.32
Tower base resultant moment (kNm)	6.68E+05	6.63E+05	0.99	9.82E+05	9.66E+05	0.98	1.77E+05	2.06E+05	1.16

Notes:

- SNS9: H_s = 0.46 m, T_p = 7.41 s; JCS9: H_s = 0.73 m, T_p = 7.44 s, windspeed = 9 m/s
- SNS11: H_s = 0.74 m, T_p = 7.24 s; JCS11: H_s = 0.97 m, T_p = 7.74 s, windspeed = 11 m/s
- SNS13: H_s = 1.06 m, T_p = 7.16 s; JCS13: H_s = 1.16 m, T_p = 8.00 s, windspeed = 13 m/s

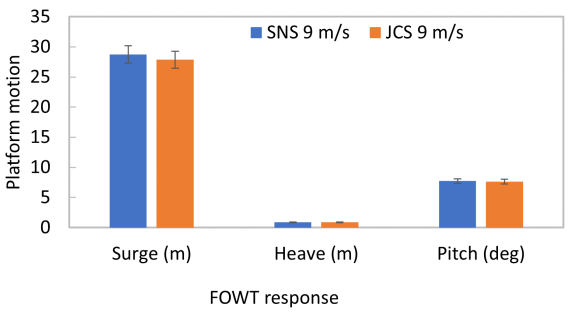

(a) Sea state 9

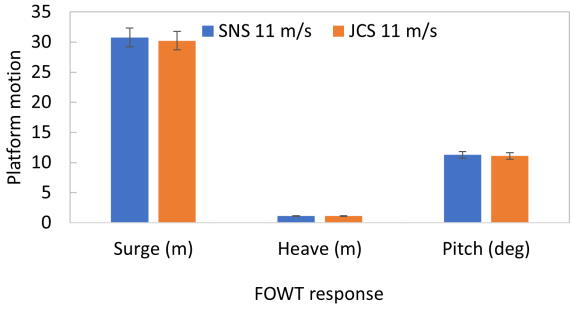

(b) Sea state 11

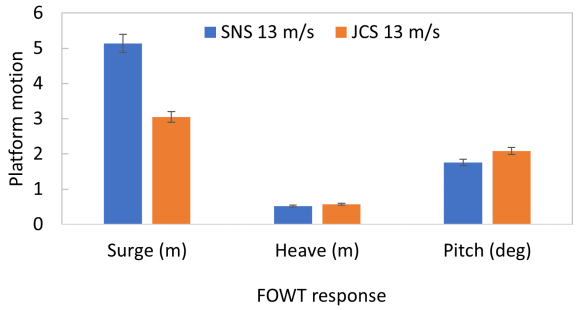

(c) Sea state 13

Figure 5.8: Comparison of the magnitude of the motion of the VolturnUS-S platform in surge, heave and pitch during three different normal wind and sea conditions, SNS vs JCS.

Heave motion. Referring to Figure 5.8 and Table 5.9, addition of the wind causes the values of the heave motion to increase for the respective sea states at both locations. This is because the motion of the wind on the blades causes motion on the tower and this causes the waves to be agitated resulting in greater up and down motion of the platform. For example, for SS9, SNS, the heave is 0.46 m for the wave only condition and 0.87 m for the wind and wave condition. This phenomenon also exists for SS11 and SS13. Comparing the response to the normal wind and wave condition at both locations, for SS9 the heave is 0.87 m for the SNS and 0.87 m for the JCS. For SS11 the heave motion is 1.12 m for the SNS and 1.12 m for the JCS. For SS13 the heave motion is 0.52 m for the SNS and 0.57 m for the JCS. For SS13, the heave motion for the JCS is slightly greater than the heave motion for the SNS. These values are very close but it was expected that the heave motion in the SNS would be marginally greater than in the JCS based on the higher TI values.

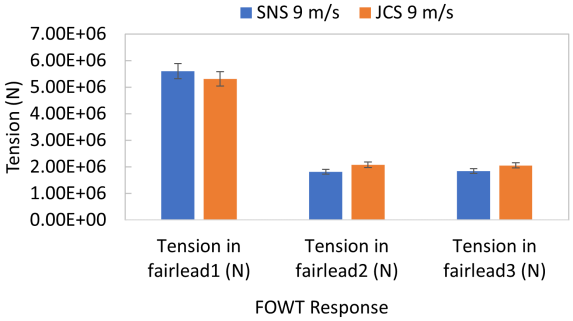

(a) Sea state 9

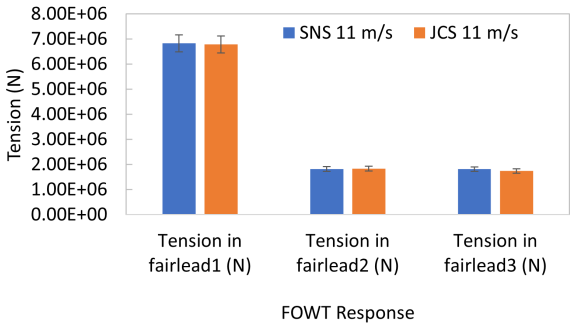

(b) Sea state 11

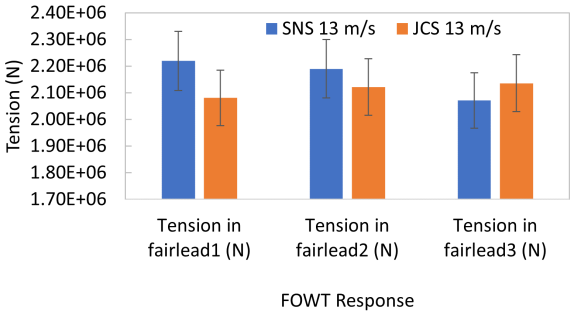

(c) Sea state 13

Figure 5.9: Comparison of the magnitude of the motion of the VolturnUS-S platform fairlead tensions during three different normal wind and sea conditions, SNS vs JCS.

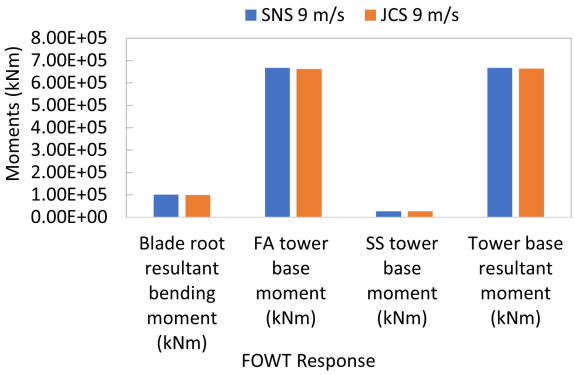

(a) Sea state 9

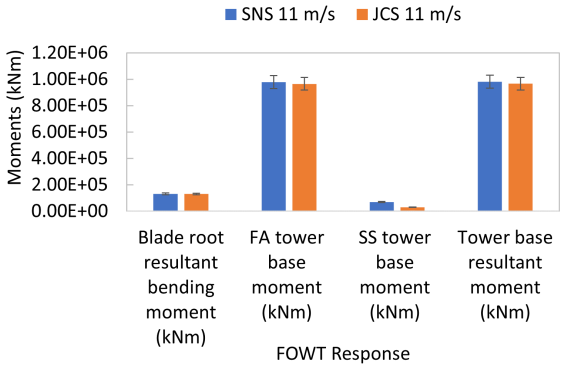

(b) Sea state 11

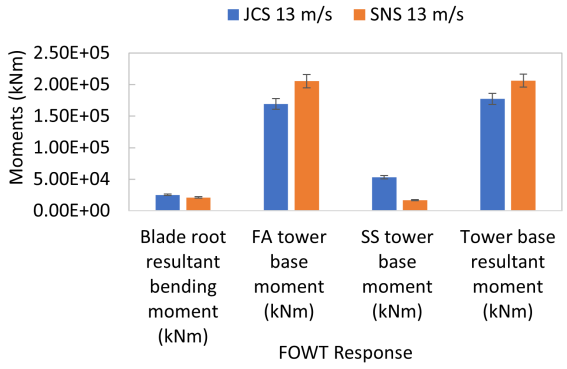

(c) Sea state 13

Figure 5.10: Comparison of the magnitude of the VolturnUS-S moments during three different normal wind and sea conditions, SNS vs JCS.

Pitch motion. The pitch motions for JCS and SNS follow the same trend as the heave motion (See Figure 5.8 and Table 5.9). For SS9, the pitch motion for the SNS is 7.73 deg and 7.62 deg for the JCS. For SS11, the pitch motion is 11.28 deg for the SNS and 11.10 deg for the JCS. For SS13, the pitch motion is 1.76 deg for the SNS and 2.08 deg for the JCS. For SS9 and SS11, the greater TI for the SNS would have resulted in greater pitch motions. However, SS13 represents an anomaly as the JCS yields greater motion in pitch than the SNS, even though the TI for the SNS is greater.

Fairlead tensions. Referring to Figure 5.9 and Table 5.9, the fairlead tensions are very close for the SNS and the JCS for all three sea states. For SS9, the tension in fairlead 1 for the SNS is 1.1 times the tension in the JCS, with a value of 5.60E+06 N and 5.31E+06 N for JCS. The tension in fairlead2 for the SNS 1.82E+06 N and 2.08E+06 N for the JCS. The tension in farilead3 is 1.85E+06 N for the SNS and 2.06E+06 N for the JCS. For SS11, the tension in fairlead1 for SNS is 6.83E+06 N and 6.79E+06 N for the JCS. For farilead2, the tension is nearly the same for the SNS and the JCS with values of 1.82E+06 N and 1.84E+06 N respectively. The tension in fairlead3 for the SNS is 1.82E+06 N and the JCS has a value of 1.75E+06 N. For SS13, the tension in fairlead1 for SNS is 2.22E+06 N and 2.08E+06 N for the JCS. The tension in fairlead2 are nearly the same for the SNS and the JCS with values of 2.19E+06 N and 2.12E+06 N respectively. The same holds for fairlead3 with values of 2.07E+06 N and 2.14E+06 N respectively for the SNS and the JCS. The greatest mooring load occurs on mooring line 1 for SS9 and SS11 for both the JCS and the SNS. This is because the greater surge motion result in a greater displacement on mooring line 1, which is directly in the path of the incoming wave. This phenomenon was pointed out by Shin et al. (2019). It should be noted that the tension in the fairlead decreases after SS11, that is, after the rated wind speed of 11 m/s. For example, for the SNS, SS9 the tension in fairlead1 is 5.60E+06 N, for SS11 it is 6.83E+06 N and for SS13 the tension is 2.22E+06 N. For the JCS, SS9, tension in fairlead1 is 5.31E+06 N, for SS11 it is 6.79E+06 N and 2.08E+06 N for SS13. This is because after the rated wind speed, blade pitch control causes the loads on the turbine to decrease, this includes the tension the fairleads. This is the same phenomenon that was reported by Liu et al. (2018).

Moments. Referring to Figure 5.10 and Table 5.9, the blade root moment for the SNS and the JCS are close. For SS9, the mean blade root moment is 1.01E+05 kNm for the SNS and 1.00E+05 kNm for the JCS. For SS11 the mean blade root moment is 1.32E+05 kNm for the SNS and 1.31E+05 kNm for the JCS. For SS13, the mean blade root moment for the SNS is 2.52E+04 kNm and 2.12E+04 kNm for the JCS. This is due to the greater TI value for the SNS causing greater turbine response. This same characteristic was reported by Li et al. (2019), who indicated that greater TI values

resulted in greater platform responses.

The fore-aft moments at the base of the tower for the SNS and the JCS are very close. For SS9, the fore-aft moment for the SNS is 1.03 times the fore-aft moment for the JCS, with values of 6.68E+05 kNm and 6.63E+05 kNm respectively. This is due to the greater TI for the SNS. For SS11, the fore-aft moment for the SNS and the JCS are very close, with values of 9.80E+05 kNm and 9.66E+05 kNm respectively. For SS13, the fore-aft moment for the JCS is 1.2 times the fore-aft moment in the SNS, with a value of 1.69E+05 kNm for the SNS and 2.05E+05 kNm for the JCS. The values for SS13 represent an anomaly. The TI for the SNS is greater and hence it was expected that its fore-aft moments would have been greater than the fore-aft moment for the JCS. The side-side moment at the base of the tower demonstrates this characteristic. The side-side moments for SS9 for the SNS and the JCS are nearly the same with values of 2.67E+04 kNm and 2.75E+04 kNm respectively. For SS11 the side-side moments for the SNS is 1.1 times the side-side moments for the JCS; for SS13 the side-side moment for the SNS is 3.13 times the side-side moment for the JCS. The responses for SS11 ad SS13 are in keeping with what was expected, that is, the response for the SNS is greater due to the greater values of the TI.

Closing remarks normal wind and wave condition. The response of the FOWT in normal sea and wind conditions of the SNS and the JCS are usually very close or the same. The dynamic motions of the platform, the resultant tensions in the fairlead and the moments for SS9, SNS, are predominantly greater than the values in the JCS. Where the values are not greater for the SNS, they are very close or the same. For SS11 and SS13, there are instances where the FOWT responses are greater for the JCS than the SNS. This is so, even though the magnitude of the TI for the SNS are greater than the JCS (see Table 4.5 for TI values). However, except for the side-side moments at the base for SS11 and SS13, the magnitude of the responses at both locations is never greater than 21 %, hence the reason these responses are considered close.

5.5.3 FOWT response for the extreme sea state, SNS and the JCS - wind and wave condition

Having investigated the response of the FOWT system under normal sea and wind conditions, this section will investigate the response of the FOWT for the extreme 50-year condition which is presented in Table 4.3. For this case the turbine is in idling mode with the blades feathered at a pitch angle of 90 degrees. The wind field is generated using TurbSim and setting the wind speed at hub height to 43 m/s for the JCS and 45 m/s for the SNS at the respective TI. The power law profile is used to determine mean wind speed profile with a power law exponent of 0.14, the value which is used

for offshore wind turbines. The maximum values of the response are shown in Table 5.10.

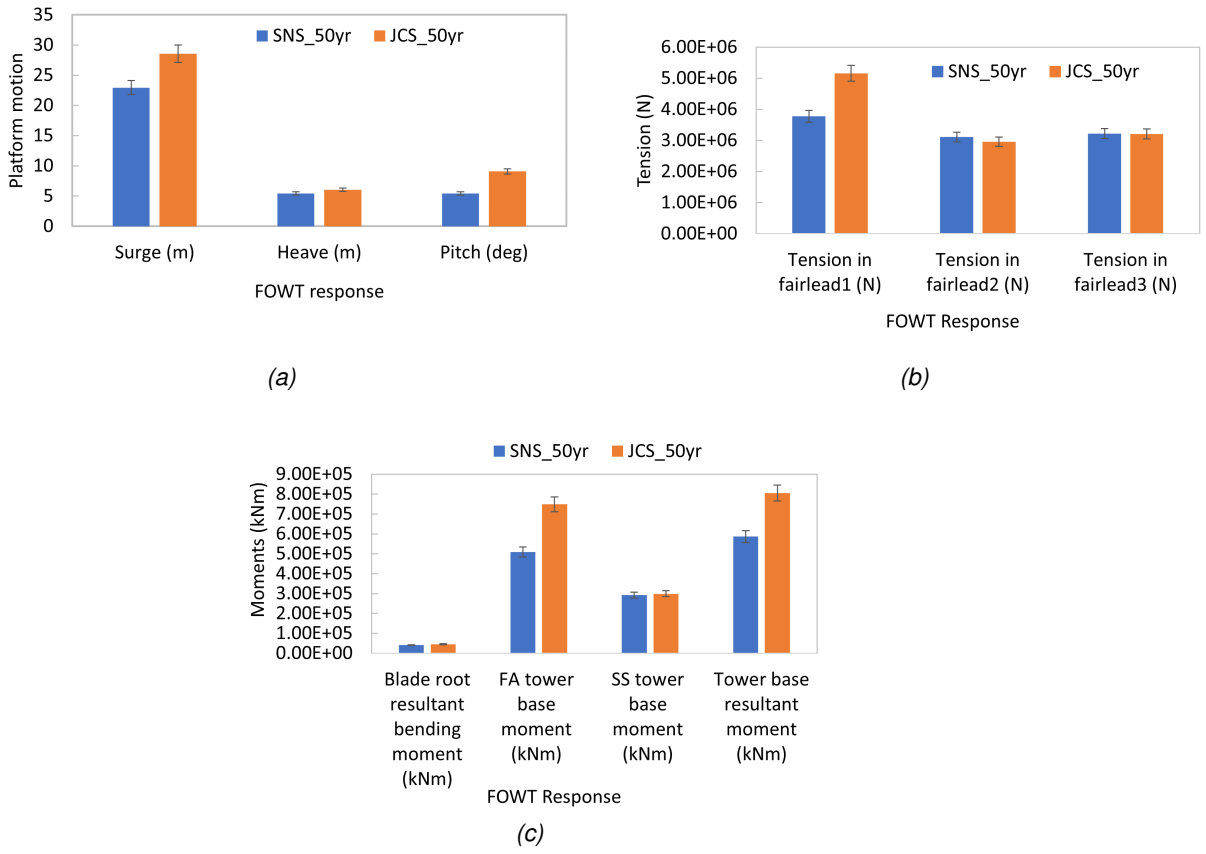

Figure 5.11: Comparison of the magnitude of the motion of the VolturnUS-S platform in surge, heave and pitch; fairlead tensions and moments for 50-year extreme wind and wave conditions, SNS vs JCS

Platform motions, tensions and selected moments. Referring to Figure 5.11 and Table 5.10, for the platform motions, surge motion for the JCS is 1.2 times the motion for the SNS, with values of 28.6 m and 23.0 m respectively; the heave motion for the JCS is 1.1 times the motion for the SNS, with values of 6.0 m and 5.4 m respectively. The pitch motion for the JCS is 1.7 times the motion for the SNS, with values of 9.1 deg and 5.4 deg respectively. The 50-year wind load for the SNS is 45 m/s and the 50-year wind load for the JCS is 43 m/s. Therefore, it is expected that the responses of the FOWT in the SNS would have been greater than the responses in the JCS. However, the responses in the JCS are greater. The greater motion responses for the JCS as compared to the SNS is due to the greater 50-year sea state for the JCS. This is shown in the wave power spectral density plot in Figure 5.12. It shows that the wave in the JCS has greater energy than the wave in the SNS.

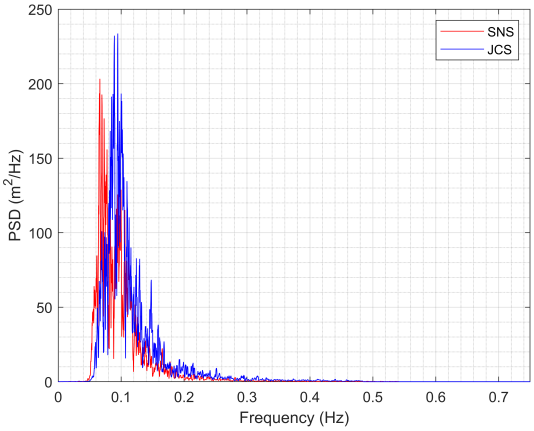

Figure 5.12: Power spectral density of the 50-year wave, SNS vs JCS.

Table 5.10: Maximum responses of VolturnUS-S FOWT - SNS and the JCS, 50-year wind and wave conditions (the sea and wind conditions are in Table 4.3 and notes below)

Description	**SNS50-year**	**JCS50-year**	**Scale Factor, SF = JCS50/SNS50**
Surge (m)	22.95	28.55	1.2
Heave (m)	5.42	6.04	1.1
Pitch (deg)	5.42	9.07	1.7
Tension in fairlead1 (N)	3.78E+06	5.16E+06	1.4
Tension in fairlead2 (N)	3.11E+06	2.96E+06	0.9
Tension in fairlead3 (N)	3.22E+06	3.21E+06	1.0
Blade root resultant bending moment (kNm)	4.10E+04	4.48E+04	1.1
FA tower base moment (kNm)	5.09E+05	7.48E+05	1.5
SS tower base moment (kNm)	2.92E+05	2.99E+05	1.0
Tower base resultant moment (kNm)	5.87E+05	8.06E+05	1.4

Notes:
- SNS50-year: H_s = 10.41 m, T_p = 14.27 s, windspeed = 45 m/s
- JCS50-year: H_s = 11.17 m, T_p = 11.22 s, windspeed = 43 m/s

Looking at the tensions in the fairleads, the tension in fairlead1 for the JCS is 1.4 times the tension in the fairlead for the SNS, with values of 5.2E+06 N and 3.8E+06 N respectively. The tension in fairlead2 for the SNS is 1.1 times the tension for the JCS, with values of 3.22E+06 N and 2.96E+06 N respectively. The tension in fairlead3 is 3.2E+06 N for the SNS and 3.2E+06 N for the JCS. The resultant tension on the fairleads for JCS is greater than the value for the SNS, with a value of 6.8E+06 N for the JCS and 5.9E+06 for the SNS. The surge in the JCS is 1.7 times the surge in the SNS, resulting in greater distribution of the forces on mooring lines 1 and 2 for the JCS. For the moments in the blade and at the base of the tower, the blade root resultant bending moment for the JCS is 1.1 times the moment in the SNS, with values of 4.5E+04 kNm and 4.1E+04 kNm respectively. The fore-aft moment at the base of the tower for the JCS is 1.5 times the fore-aft moment for the SNS, with values of 7.5+E05 kNm and 5.1E+05 kNm respectively; the resultant moment at the base of the tower for the JCS is 1.4 time the moment at the base of the tower for the SNS, with values of 8.1E+05 kNm and 5.9E+05 kNm respectively. The greater moments on the blade and at the base of the tower for the JCS is also due to the greater energy of the 50-year extreme wave. This resulted in greater motion and hence greater forces on the turbine. It can therefore be said that unlike the normal wind and sea conditions, for the extreme 50-year wind and wave condition, the respective platform motions and structural responses of the VoluturnUS-S FOWT system for the JCS are greater than the responses for the SNS.

5.6 Conclusion

In chapter 4, the environmental conditions (normal and extreme) in the SNS and the JCS were determined. These are shown in Table 4.3 and Table 4.4. This chapter examines the response of a FOWT to see how a FOWT responds to these normal and extreme conditions. This is done by examining the dynamics of the floater, namely, surge, heave and pitch motions and selected structural respones of the VolturnUS-S FOWT system. The structural responses included the blade root resultant moment and the fore-aft and side-side moments at the base of the tower. The investigation revealed that for the normal sea conditions, the floater motions for the JCS and the SNS are similar. In particular, the surge, heave and pitch motions are similar for sea state 9 (SS9), sea state 11 (SS11) and sea state 13 (SS13). The tensions in the platform are very similar for the normal sea conditions of the SNS and the JCS. In particular, for fairlead 1, SS9, the tension is 2.0 E+06 N for both the SNS and the JCS; for SS11 the tension is 2.1E+06 N for both the SNS and the JCS; for SS13, the tension is 2.1 E+06 in both the SNS and the JCS. For the moments, the responses of the turbine in the SNS are the same or very close to the responses in the JCS. In particular, the blade

root moment for SS9, SS11 and SS13 are the same for the SNS and the JCS with a value of 1.8 E+04 kNm. The fore-aft moment at the base of the tower for the SNS and the JCS are also very close; for SS9 the fore-aft moment for the SNS is 1.8E+05 kNm and 1.89E+05 kNm for the JCS; for SS11 the fore-aft moment for the SNS is 1.89E+05 kNm and 1.99E+05 kNm for the JCS; for SS13 the fore-aft moment is 2.0E+05 kNm for the JCS and 2.1E+05 kNm for the JCS. The magnitude of the sea states for the JCS and the SNS are very similar and is the primary reason for these responses being similar. Specifically, for SS9, SNS, H_s = 0.46 m and T_p = 7.41 s; for the JCS, SS9, H_s = 0.73 m and T_p = 7.44 s. These values confirm that the normal sea conditions for the JCS are similar to the normal sea conditions for the SNS. Hence producing responses which are similar or very close.

The responses of the FOWT are also investigated during normal sea and wind conditions. It is shown that the addition of wind resulted in tremendous increase in the floater motions for both the SNS and the JCS. For SS9, the surge for the SNS is 28.76 m and 27.86 m for the JCS. These values were 1.2 m and 1.34 m respectively, without wind. For SS11, the surge for the SNS is 30.76 m for the SNS and 30.24 m for the JCS. The values were 1.35 m and 1.5 m respectively without wind. For SS13, the surge is 5.14 m for the SNS and 3.05 m for the JCS. These values were 1.65 m for both the SNS and the JCS without wind. The reason for the drastic increase in the surge motion is due to the thrust force on the operating turbine. This results in increased longitudinal motion of the floater. For the comparison of the SNS and JCS responses for normal sea and wind conditions, for SS9, 60 % of the responses of the FOWT in the SNS are marginally greater than the responses in the JCS and one response (the heave motion) is the same at both locations. It should be noted that the other three responses veer away from what was expected. That is, fairlead tensions 2 and 3, and the side-side moments at the base of the tower were marginally greater for the JCS than the SNS. For SS11, 80 % of the responses for the SNS are greater than the responses for the JCS, with one response (the heave motion) being the same. For SS13, 50 % of the responses for the SNS are greater than the responses for the JCS. The other responses for the JCS are greater than for the SNS, with the greatest being the fore-aft moment at the base, which is 1.21 times the response in the SNS. In general, it is observed that most of the responses (say, 90 %) of the FOWT for the SNS and the JCS are very close. For example, SS9, for fairlead1, the tension for the SNS is 6.83E+06 N and 6.79E+06 N for the JCS. This phenomenon also holds for the other fairlead tensions. The blade root moments, fore-aft and the side-side moments at the base. For SS11, the blade root moment is 1.32E+05 kNm for the SNS and 1.31E+05 kNm for the JCS. For the side-side moment the SNS value was 1.1 times the value for the JCS. For SS13, the heave motion in the JCS is 1.1 times the motion in the SNS

and the pitch motion in the JCS is 1.2 times the pitch motion in the SNS. The blade root moment for the SNS is 1.2 times the value for the JCS and the fore-aft moment for the JCS is 1.2 times the values for the SNS. It was expected that all of the responses for the SNS would have been greater than the JCS for the wind and wave condition due to the greater TI for the SNS. This anomaly could be due to numerical modelling errors but further work would be required to determine if this is conclusive. It should be noted that where the responses of the JCS are greater, they are only greater by 10% to maximum of 21%. The key finding though is that the responses of the FOWT for normal sea and wind conditions for the SNS and the JCS are quite similar.

The assessment of the turbine for the 50-year wind and wave condition showed that the responses in the JCS are greater than the responses in the SNS. Despite the fact that the 50-year wind speed for the SNS is 45 m/s and the 50-year wind speed for the JCS is 43 m/s. It was therefore assessed if the reason for the greater responses in the JCS is due to a more severe sea state. The psd of the 50-year wave is computed and the JCS is shown to have greater wave energy than the SNS. The surge motion in the JCS is 1.2 times the surge motion in the SNS, the heave motion in the JCS is 1.1 times the motion in the SNS and the pitch motion in the JCS is 1.7 times the pitch motion in the SNS. For the resultant tension in the fairleads, JCS is 1.2 times the value in the SNS. The blade root moment in the JCS is 1.1 times the moment in the SNS. The fore-aft moment in the JCS is 1.5 times the moment in the SNS and the resultant moment at the base of the tower for the JCS is 1.4 times the moment for the SNS. The 50-year wind and wave condition is the criteria set for the design of FOWT systems in wind turbine design standards produced by the IEC and DNV (Worsnop et al., 2017; Roddier et al., 2010). Worsnop et al. (2017) argued that the data for offshore wind turbine design is derived from the data and experience in the European region (which includes the North Sea). In this region, hurricanes are non-existent. This is, unlike the Caribbean Sea, where the strongest hurricanes can have wind speeds as high as 70 m/s. It was mentioned in Chapter 4 that Jamaica experienced 5 hurricanes between 1979 and 2018. Three of these hurricanes were category 4 (58 m/s to 70 m/s 1 min mean maximum sustained winds at 10m.), one was category 3 (50-58 m/s 1 min mean maximum sustained winds at 10m) and the other was a category 1 (33-42 m/s 1 min mean maximum sustained winds at 10m). A turbine that is developed for the Caribbean region must therefore be investigated for the extreme conditions of a hurricane, which could be more onerous than the conditions that exist in the North Sea Region. It cannot therefore be said with any certainty that the 50-year extreme wind and wave conditions from the wind turbine design standards give a good indication of how a FOWT responds in hurricane prone regions. The FOWT system is therefore further investigated in hurricane conditions to see how the responses compare to the

responses caused by the 50-year extreme wind and wave loads.

Finally, it is shown in this chapter that the normal sea and normal sea and wind conditions of the SNS and the JCS are quite close and therefore the floater dynamic and structural responses of the VolturnUS-S FOWT system at those locations are similar or very close. In the case of extreme conditions, the 50-year extreme sea state in the JCS is greater than the extreme sea state in the SNS and the responses of the VolturnUS-S FOWT system in the JCS are more severe than in the SNS.

Chapter 6

Investigation of the response of a FOWT in the JCS for Selected Characteristics of a Hurricane

6.1 Introduction

The response of the floating offshore wind turbine in extreme wind and sea conditions was assessed in the previous chapter. It was discovered that the extreme sea states and wind speeds in the JCS and the SNS are very similar. One could therefore infer that a turbine that is suitable for the SNS could be used off-the-shelf in the JCS. However, the Caribbean region is susceptible to severe weather systems such as hurricanes. Therefore, a true measure of the suitability of a wind turbine system in the Caribbean Sea should include an examination of how it behaves in hurricane conditions. Kapoor et al. (2020) argued that studies have been done on the exposure of wind farms off the US East Coast to hurricane conditions. However, those works did not investigate the magnitude of the response for specific and intense hurricane wind-field characteristics. Worsnop et al. (2017) argued that hurricanes pose a significant risk to turbines deployed in hurricane prone regions and that the current design standards do not provide design parameters that account for extreme wind conditions caused by a tropical cyclone. Kim & Manuel (2014) stated that offshore wind farm sites along the Atlantic seaboard and in the Gulf of Mexico should be designed for the conditions induced by a hurricane.

The objective of this chapter is to assess the response of a floating offshore wind turbine in hurricane conditions. This is the benchmark set of extreme conditions to test the suitability of a wind turbine in the Caribbean. The computation of extreme wind and sea conditions that is done in Chapters 3 to 5 is for the 50-year return period as recommended by the wind design codes (DNV-GL, 2016). Worsnop et al. (2017) argued that the criteria in the wind turbine standards are not adequate for regions that are prone to tropical cyclones such as hurricanes. Worsnop et al. (2017) also stated that the IEC design criteria does not encompass extreme wind speeds and directional shifts greater than those seen in a category 2 hurricane. Hence, this study also includes

the response of the FOWT within the hurricane conditions of the Caribbean Sea. After the passage of hurricane Ivan in 2004, commercial clients started requesting that their new buildings and other important structures be designed to resist category 4 hurricanes (58 m/s to 70 m/s 1-min mean maximum sustained winds). The author believes that these clients and other key stakeholders would also consider a wind farm with the same degree of significance. A very important aspect of the assessment of the FOWT system for hurricane conditions is determining the wind field characteristics that represent those conditions. Worsnop et al. (2017) proposed a model that can be used to simulate the conditions of a category 5 hurricane (> 70 m/s 1-min mean maximum sustained winds). The model is a compressible nonhydrostatic model developed for axisymmetric simulation of tropical cyclones. It is used to evaluate the maximum possible intensity of tropical cyclones. This model would therefore adequately represent the hurricane conditions that have been experienced in Jamaica and could likely impact her in the future. In addition, since this is a floating turbine, this work extends to determining the sea state of the respective hurricane conditions.

Kapoor et al. (2020) carried out a study to assess the response of a 10 MW onshore wind turbine in category 5 hurricane conditions. They simulated the hurricane wind field characteristics using the output results of the large eddy simulation (LES) model developed by Worsnop et al. (2017). The characteristics of the hurricane were derived from Hurricane Felix, which made landfall in Mexico after travelling across the southern Caribbean in August 2007. The wind field that was generated was inputted to a numerical model of the wind turbine to determine the structural responses. In their study Kapoor et al. (2020) used TurbSim to simulate the hurricane wind field. TurbSim, a full field, turbulent wind field simulator, was already introduced in Chapter 2. This wind field was input to the FAST (now called OpenFAST, see section 2.7.3) wind turbine software code and used to determine relevant structural responses of the wind turbine system. This same approach used by Kapoor et al. (2020) is used in this study to generate the hurricane wind field and assess the response of the FOWT wind turbine. Before assessing the response of the FOWT, the process is first applied to the 10 MW onshore wind turbine model to reproduce the results obtained by Kapoor et al. (2020). This to provide a basis for the credibility of the results produced from assessing the FOWT. The process is carried out using a three (3) step approach, shown in the flow chart in Figure 6.1, and is outlined as follows:

- Step one - obtain the characteristics of the hurricane from Kapoor et al. (2020). This includes the mean wind speed at hub height (where HRef is the hub height) at selected distances from the centre of the hurricane, the wind shear profile, the wind veer profile, the wind turbulence intensity (TI) and the coherence exponent

(CohExp). The wind shear profile, wind veer profile and the choherence exponent are defined in sections 6.3 and 6.4.

- Step two - input the hurricane wind characteristics in TurbSim to generate the wind field for each distance from the hurricane centre.
- Step three - Use the wind fields in the OpenFAST numerical model to carry out simulations and determine the respective structural responses of the 10 MW wind turbine.

The next section describes the characteristics of the DTU 10 MW reference wind turbine, which was used by Kapoor et al. (2020).

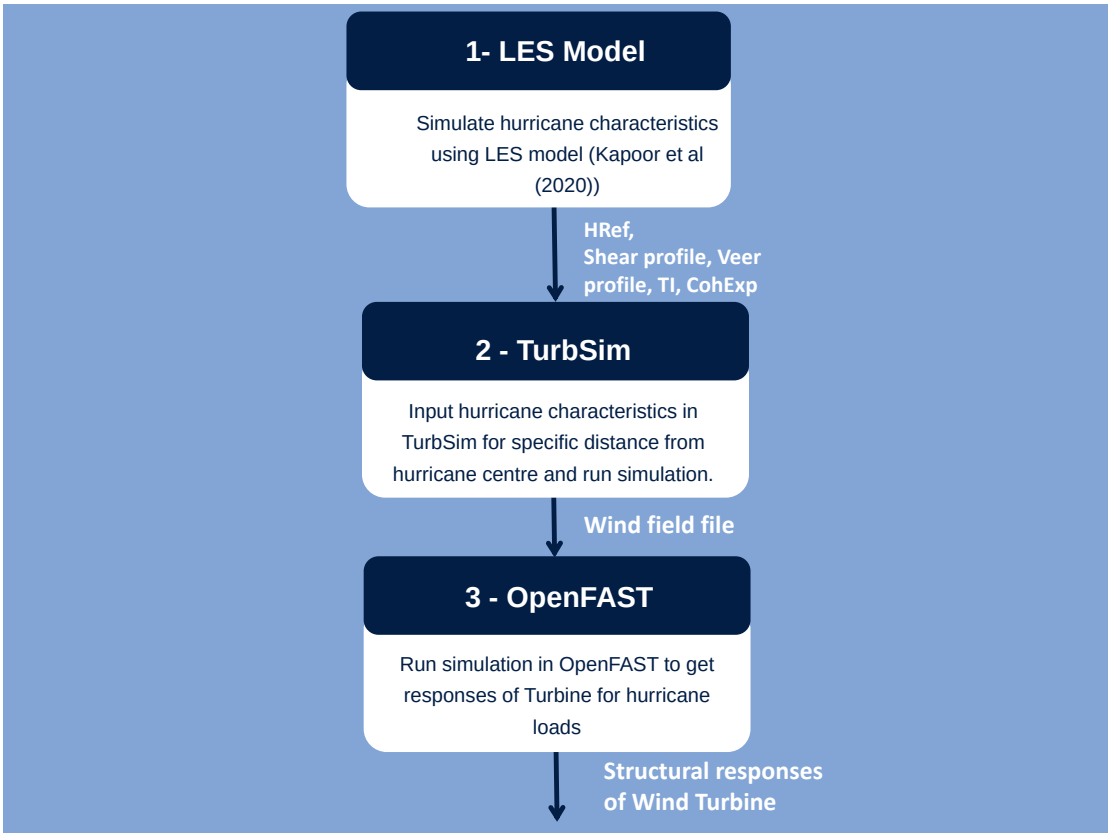

Figure 6.1: Process of assessing wind turbine for hurricane conditions using TurbSim and OpenFAST

6.2 DTU 10MW Wind Turbine Properties

The DTU 10 MW reference wind turbine is a fixed-bottom wind turbine with a hub height of 119 m. The tower base diameter is 8.3 m and the diameter at the top of the tower is 5.5 m (Quancard et al., 2019). The full set of characteristics of this wind turbine are

shown in Table 6.1 (Bak et al., 2013; Saint-Drenan et al., 2020). An illustration of the turbine is given in Bak et al. (2013).

Table 6.1: Properties of DTU 10 MW Reference Wind Turbine (Bak et al., 2013)

Description	**Unit**	**Value**
Power rating	MW	10.0
Drive-train	-	Medium speed, multiple stage gearbox
Rotor orientation	-	Upwind
Number of blades	No.	3.0
Control	-	Variable speed, collective pitch
Cut-in wind speed	m/s	4.0
Rated wind speed	m/s	11.4
Cut-out wind speed	m/s	25.0
Rated tip speed	m/s	90.0
Rotor diamater	m	178.3
Hub height	m	119.0
Hub diameter	m	5.6
Minimum rotor speed	rpm	6.0
Maximum rotor speed	rpm	9.6
Maximum tip speed	m/s	95.0
Hub overhang	m	7.1
Shaft tilt angle	deg	5.0
Pre-cone	deg	2.5
Blade prebend	m	3.3
Rotor mass	ton	228.0
Nacelle mass	ton	446.0
Tower mass	ton	628.4

6.3 Characteristics of the Hurricane Wind Field

Figure 6.2 shows the characteristics of the structure of a hurricane. A distinctive feature of a hurricane is that it consists of a calm central location known as the eye. The eye is usually 30 to 65 km in diameter (https://www.britannica.com/science/tropical-cyclone#ref848886). Surrounding the eye is a region known as the eyewall. It is usually 15 to 30 km in diameter. It is the region where the winds are strongest and the rainfall is heaviest. Surrounding the eyewall are secondary cells arranged in bands. These bands are called rainbands and spiral into the centre of the storm. The rainbands can be stationary relative to the storm or rotating. The rotating bands cause a wobbling of the storm track, resulting in a difference between the acutual landfall position and the forecast landfall position. Further information on the features of a hurricane can be found at https://www.britannica.com/science/tropical-cyclone#ref848886.

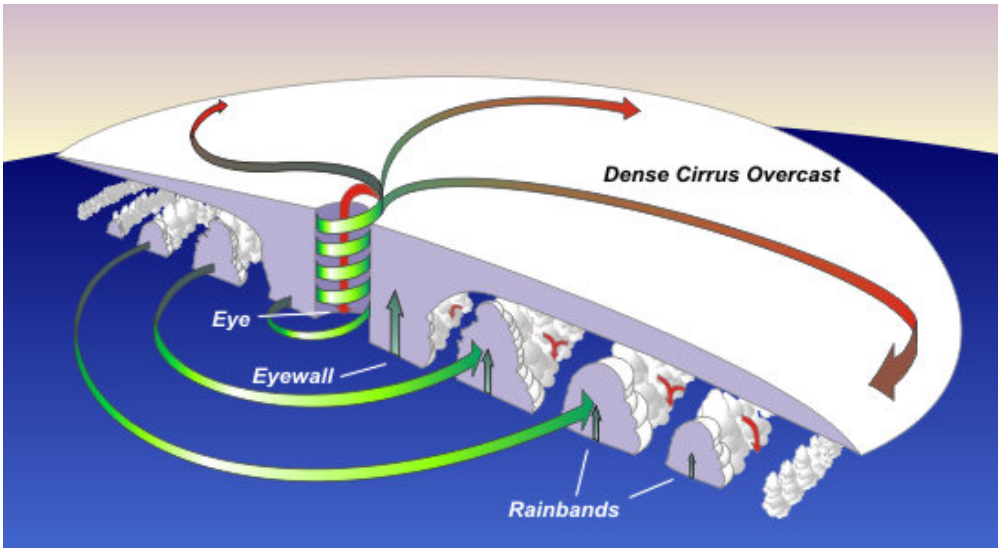

Figure 6.2: Structure of a mature tropical cyclone (Source: NOAA, National Weather Service)
(Permission has been granted by NOAA's National Weather Service's Online School for Weather, JetStream, to reproduce this figure)

The study of hurricane conditions experienced by any system, in this case an offshore wind turbine system, requires wind data. This data includes the wind speed, turbulence intensity, coherence exponent, wind shear profile etc. This data is not readily available because it is difficult to set up equipment, such as an anemometer, to capture data during a hurricane (Worsnop et al., (2017). This was also reported by Stern et al. (2012), Stern et al., (2016), Cione et al., (2016), French et al., (2007) and Archer et al., (2014). Offshore wind turbines are usually high above sea level, say, just below 200 m

ASL, making it difficult to get wind data (Worsnop et al., 2017). It was further stated that where data is available they are not adequate. Because hurricane wind data is not readily available, large eddy simulation (LES) is one of the methods to simulate hurricane data. Worsnop et al., (2017) stated that LES could be used to simulate the winds within the eyewall at turbine heights with high spatial (approx. 30 m) and temporal (approx. 0.2 s) resolution. In particular, LES is used to simulate the turbulent processes within the hurricane boundary layer (Bryan et al., 2017).

Worsnop et al., (2017) set out in detail how a LES model was used to simulate a category 5 hurricane, hurricane Felix. The LES model that was used was the 3-D, nonhydrostatic, time-dependent numerical model, Cloud Model 1[CM1]. The simulation consists of two different size meshes, the outer domain (3000 km x 3000 km x 25 km) and a smaller domain - (80 km x 80 km x 3 km) with horizontal grid spacing of 31.25 m and vertical grid spacing of 15.625 m) - which sits inside the larger domain. The outer domain captures the entire hurricane (eye, eyewall and, rainbands), while the inner domain captures the turbulent conditions within the inner core, that is, the eye and the eyewall. The data was output in 0.1875 s time steps at points called virtual towers, spaced 1 km apart in the x and y direction and 7.81 m to 507.81 m ASL. The simulation is run and after it gets to the steady state (4 hr), wind fields are analyzed for a 10 min period. The following variables are determined at each virtual tower location; 10 min mean wind speed, 3 s gusts, gust factors (defined by Worsnop et al. (2017) as the ratio between the peak 3s mean gust and the mean wind speed that occurs within 10 min), directional shifts at hub height and veer. The data is divided into 1 km radial bins to get a sample at each radius. Having done this, the maximum value of the variables at each radius is determined. This gives the strongest wind conditions that a turbine at the respective locations would experience. Further information on the LES model can be found in Worsnop et al. (2017).

Kapoor et al. (2020) analyzed a subset of the complete LES simulation data that covered a domain of 60 km x 60 km x 508 m using virtual towers 1 km x 1km x 119 m (hub height). The simulated hurricane included the eye, the turbulent eyewalls, and the outer rainbands. To carry out the wind turbine analysis, which includes simulation of the hurricane wind fields in TurbSim, the characteristics of the LES wind fields were determined at discrete radii from the hurricane centre. The turbine is considered to be located at each of these discrete locations. The locations from the hurricane centre considered are: 10 km (inner edge of the eyewall), 12 km (within the eyewall), 15km (outer edge of the eyewall) and 20 km (outside the eyewall). The hurricane wind field characteristics were used to determine the effects of mean wind speed (wind shear), veer, and direction change or misalignment on the structural response of a wind turbine.

The wind shear, wind veer and change in wind direction for the category 5 hurricane are given in Kapoor et al. (2020). These characteristics change with distance from the hurricane centre. As mentioned previously, the wind shear shows the variation of the wind speed with height and is represented by a wind shear profile. For the respective hurricane, it shows that the wind shear is at its highest within the turbulent eyewall and decreases as the distance from the centre of the hurricane increases. The wind veer refers to the change in wind direction with height in a clockwise direction (Gao et al., 2021; Kapoor et al., 2020; Worsnop et al., 2017) and is represented by a wind veer profile. For a wind turbine, the veer from the base of the tower rotor to the top tip of the blade would be of importance. See Figures 6.3 and 6.4 for the shear and veer profiles considered for the category 5 hurricane. The misalignment deals with the change in alignment between the axis of the nacelle and the direction of the wind. In hurricane conditions, the wind frequently changes direction and this causes a misalignment between the wind direction, and the axis of the nacelle and is given by an angle. Figure 6.5 d is an illustration of yaw misalignment. Turbines are designed to automatically yaw in the direction that the wind is blowing, however, because of the frequent changes in the wind direction, there is a period of time when the wind direction and the nacelle axis are out of alignment (Kim & Manuel, 2014). Finally, the wind turbulence intensity is another important feature used to define the hurricane. This was already discussed in Section 4.7.3 as well as above.

These wind field characteristics from Kapoor et al. (2020) are used to define a set of wind load simulation cases which are used to assess the structural responses of the turbine. The characteristics are defined for the turbine 10 km,12 km, 15 km and 20 km from the hurricane centre. The hurricane load cases are defined as Base, Veer and Misal for each of these four distances. The Base case is the baseline hurricane winds that uses each of the wind shear profiles shown in Figure 6.3. The Veer case considers hurricane winds with veer and uses the predominant veer profile from each of the profiles shown in Figure 6.3. The Misal case uses the baseline hurricane with yaw misalignment for each of the four distances from the hurricane centre considered. For each of these hurricane load cases, the wind turbine blades are pitched to feather, the rotor is set to idle and the generator is turned off. A Rated case was used to generate loads to compare with the loads from the hurricane load cases. The Rated case considers the operating turbine with a mean wind speed of 11.4 m/s, a turbulence intensity of 10% and a power law exponent of 0.1. The wind field characteristics are shown in Table 6.2 and the related illustration of each case in Figure 6.5. Referring to Figure 6.6, it is shown that the most turbulent winds are within the eyewall and the outer edge of the eyewall. At the inner edge of the eyewall, which is closer to the eye and far away from the outer edge of the eyewall the wind speeds are less than in the

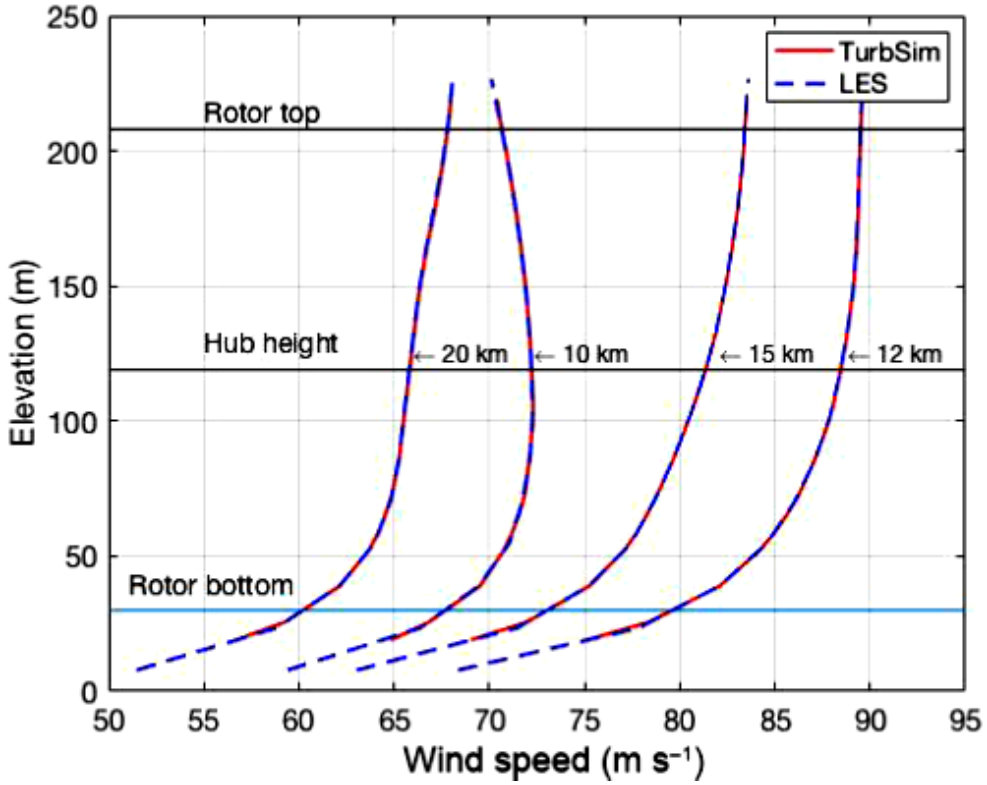

Figure 6.3: Shear profile a) 10 km, b) 12 km, c) 15km and d) 20 km from the hurricane centre (Source: Kapoor et al. (2020))
(Permission has been granted by Sanjay Arwade of University of Massachusetts, Amherst to reproduce this figure)

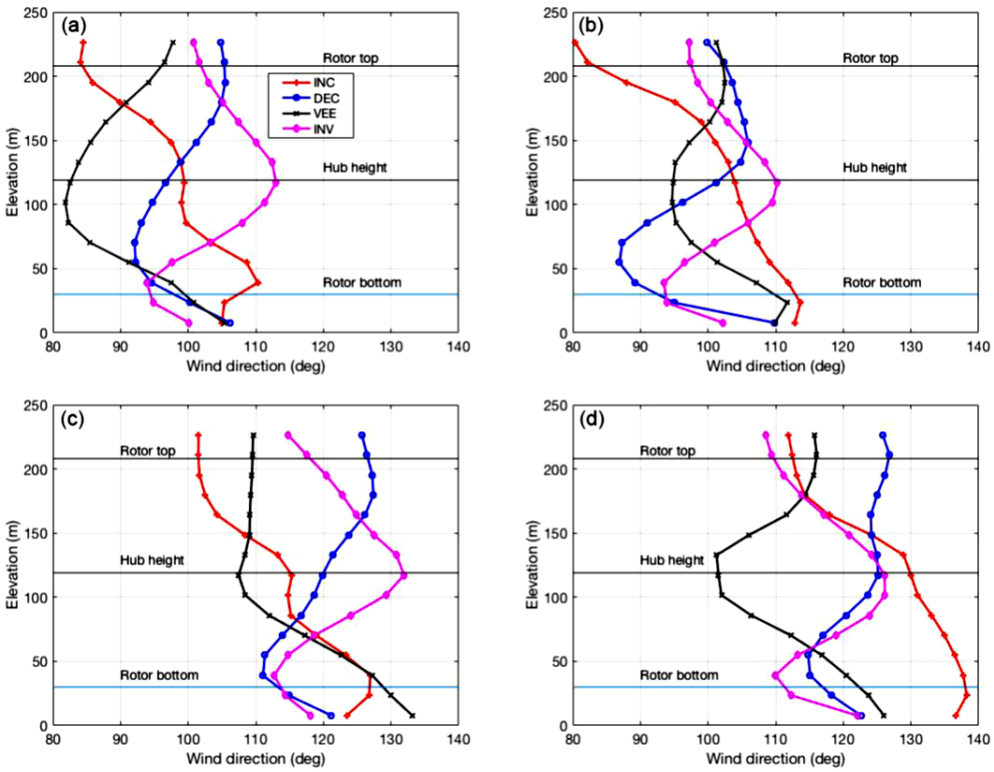

Figure 6.4: Veer profile a) 10 km, b) 12 km, c) 15km and d) 20 km from the hurricane centre (Source: Kapoor et al. (2020))
(Permission has been granted by Sanjay Arwade of University of Massachusetts, Amherst to reproduce this figure)

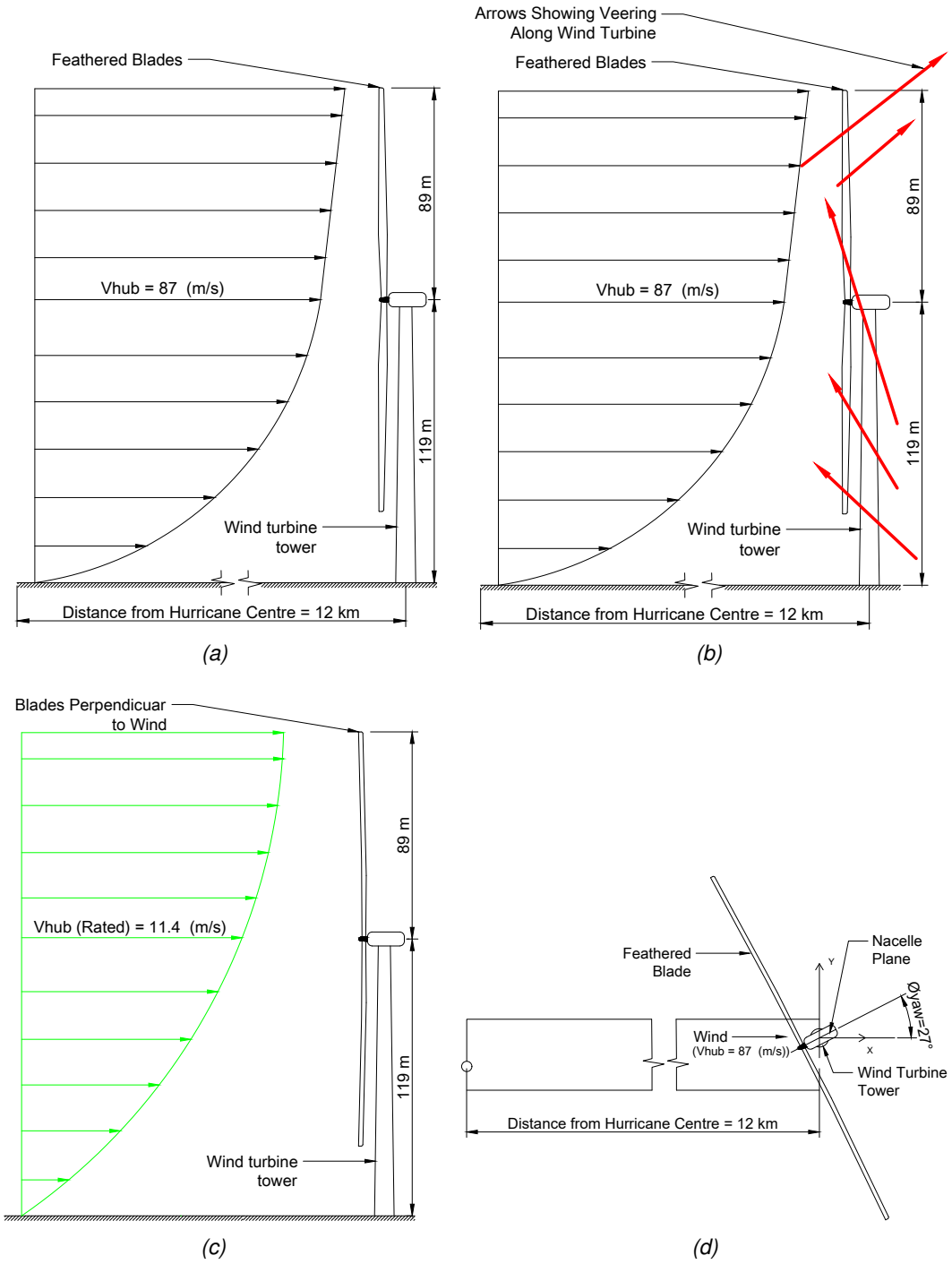

Figure 6.5: Illustration of (a) Base (b) Veer (c) Rated (d) Misal(Plan View) Load Cases. Base, Veer and Misal are the hurricane load cases for a respective distance from the hurricane centre; 12 km is shown here.

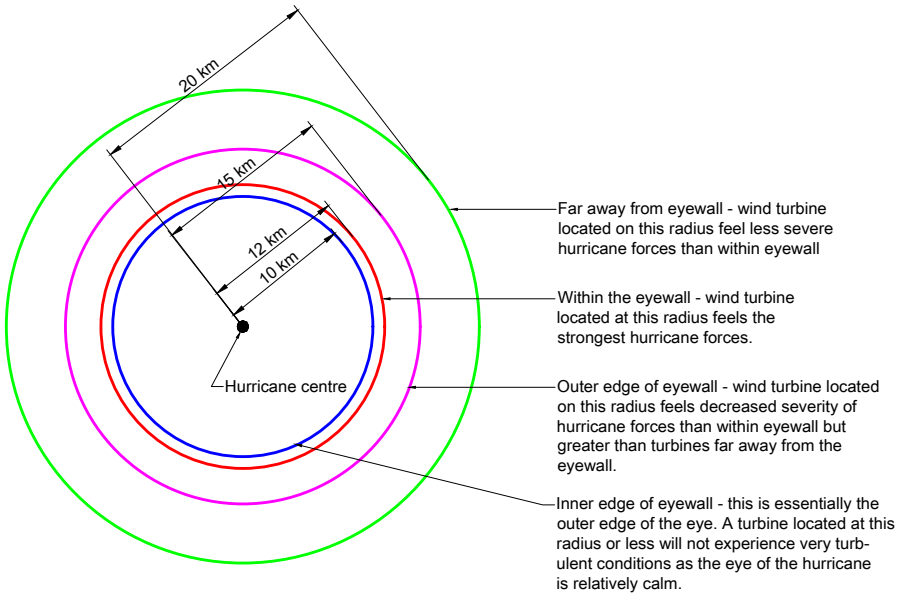

Figure 6.6: Potential locations of the FOWT at distances of 10 km, 12 km, 15 km and 20 km from the hurricane centre.

turbulent eyewall region.

6.4 Reproducing the Hurricane Wind Fields from Kapoor et al. (2020) using TurbSim

The hurricane wind field shown in Table 6.2 is set up in TurbSim for each of the distances from the hurricane centre but the results of the 10 km distance are excluded. These results are excluded because it is shown in the work by Kapoor et al. (2020) that they have the least adverse effect on the wind turbine and for the purpose of this study are not considered significant. Inputs are made for the mean wind speed at hub height, the wind turbulence intensity, the wind shear profile, the wind veer profile, the coherence exponent, the rectangular grid size in m, the time step (0.05 s). The coherence exponent is a function of the wind speed and is given in the following relationship in the TurbSim users guide (Jonkman & Buhl, 2006):

$$Coh_{i,j} = exp\left(-a\left(\frac{r}{z_m}\right)^{CohExp}\sqrt{\left(\frac{fr}{\bar{u}_m}\right)^2 + (br)^2}\right), \tag{6.1}$$

where,

Table 6.2: Wind Field Characteristics of Simulation Cases (Source: Kapoor et al., 2020)

Condition	Reference radius, R (km)	Wind speed (m/s) (turbulence intensity, %)	Wind shear profile or power law exponent	Coherence exponent	Veer	Yaw misalignment	Operating state
Base (baseline hurricane)	10	72.2 (9.27)	Figure 6.1	0.85			Idle
	12	88.4 (7.38)					
	15	81.3 (7.97)					
	20	66.8 (8.25)					
Veer (hurricane w/ veer)	10	72.2(9.27)	Figure 6.1	0.85			Idle
	12	88.4 (7.38)					
	15	81.3 (7.97)					
	20	66.8 (8.25)					
Misal (misaligned hurricane)	10	72.2(9.27)	Figure 6.1	0.85	Figure 6.1	28.4	Idle
	12	88.4 (7.38)				27.1	
	15	81.3 (7.97)				19.9	
	20	66.8 (8.25)				20.6	
Rated	n/a	11.4 (10)	0.10				Operating

r is the vertical distance between the points *i* and *j*

f is the cyclic frequency

CohExp is the coherence exponent input parameter

z_m is the mean height of points *i* and *j*

$\bar{u}_m$ is the mean wind speed of points *i* and*j*

a and *b* are the input coherence decrement and offset parameter, respectively

Kapoor et al. (2020) argued that an increase in the coherence exponent could lead to increasing loads on the wind turbine blades. Capturing coherence of the wind field to the greatest degree possible is thus necessary for estimating the variability in structural loads. The coherence captures the turbulent flow experienced by the turbine in the rotor swept area (Worsnop et al., 2017b). The value ranges from 0 to 1 and indicates how well two spatially separated time series are correlated. This therefore suggests that the greater the coherence the more robust the wind field, causing greater loads on the turbine.

The simulations are run for 1 hr, which is in keeping with the DNV GL wind turbine design standard (DNV-GL, 2016). They are carried out for six random seeds as is done in Chapter 5. The mean correlation coefficient of the wind speed at different levels of the wind turbine to the mean wind speed at hub height are determined using the values from the six random seeds and plots are done and compared with the correlation coefficients in Kapoor et al. (2020). See Figure 6.7. The plots show that for the random seeds considered, the correlation coefficient from Kapoor et al. (2020) fits within

the range of values produced by this study for 12km, 15 km and 20 km away from the hurricane centre respectively. The hub- height wind speeds are also reproduced satisfactorily; the mean wind speed at hub height for the respective wind shear profiles are found to be the same results as given by Kapoor et al. (2020) in Table 6.2. The satisfactory results obtained for the hub-height wind speed and the correlation coefficients showed the wind fields were simulated accurately in TurbSim and that TurbSim can be used to create hurricane wind fields once the characteristics of the hurricane are known. In the following section simulations of the wind turbine are carried out in OpenFAST using the wind field from TurbSim and compared with the responses from Kapoor et al. (2020).

6.5 Using the output from TurbSim to reproduce Kapoor et al (2020) wind turbine responses in OpenFAST

The wind field from TurbSim is input into OpenFAST and simulations carried out. Six structural responses of the DTU 10 MW turbine are investigated by Kapoor et al. (2020). The same is done for this study and the results are compared with the results shown in Kapoor et al. (2020) in order to verify the modelling approach used in the present work.

6.5.1 Turbine responses 20 km from hurricane centre

Six turbine responses are compared for different hurricane load conditions (namely, Base, Veer and Misal) with the Rated load condition, that is, when the turbine is operating normally. The responses are assessed using graphs and tables. Figures 6.8 and 6.9 give a graphical representation of the responses of the turbine, the error bar is a measure of the variability of a response, where a greater bar would indicate a greater variability of a response. The root mean square logarithmic error (RMSLE) values from Table 6.3 provide a good metric for comparing the results, to better understand if the result is poor or satisfactory. A smaller value of RMSLE (say closer to zero) is a better agreement between the actual and the predicted results. For this study, a RMSLE of 0.5 or less is considered to be close to zero and hence shows a good agreement between the actual and the predicted results.

Rated case, 20 km. The responses for this work are in good agreement with the values obtained by Kapoor et al. (2020). The blade out of plane and in plane deflections, compare well with RMSLE of 0.06 and 0.04 respectively. The moments at the blade root and the base moments at the tower also compare with the results obtained by Kapoor et al. (2020) with RMSLE ranging from 0.08 to 0.22. This shows that the Rated wind speed case is modelled accurately and provide a sound basis for comparing with the results from the hurricane load cases.

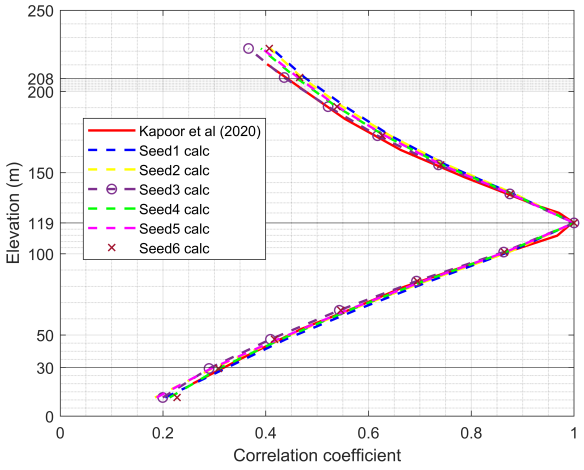

(a) 12 km

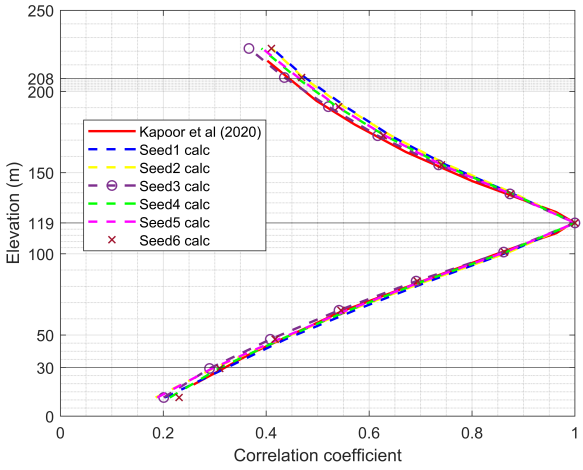

(b) 15 km

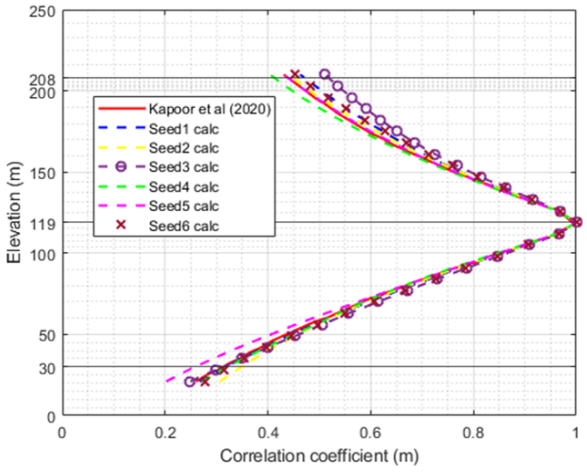

(c) 20 km

Figure 6.7: Correlation coefficient of the wind velocity at each elevation to the velocity at hub height, Kapoor et al (2020) vs computed for 6 random seeds from TurbSim. (a) 12 km from hurricane centre (b) 15 km from hurricane centre and (c) 20 km from hurricane centre

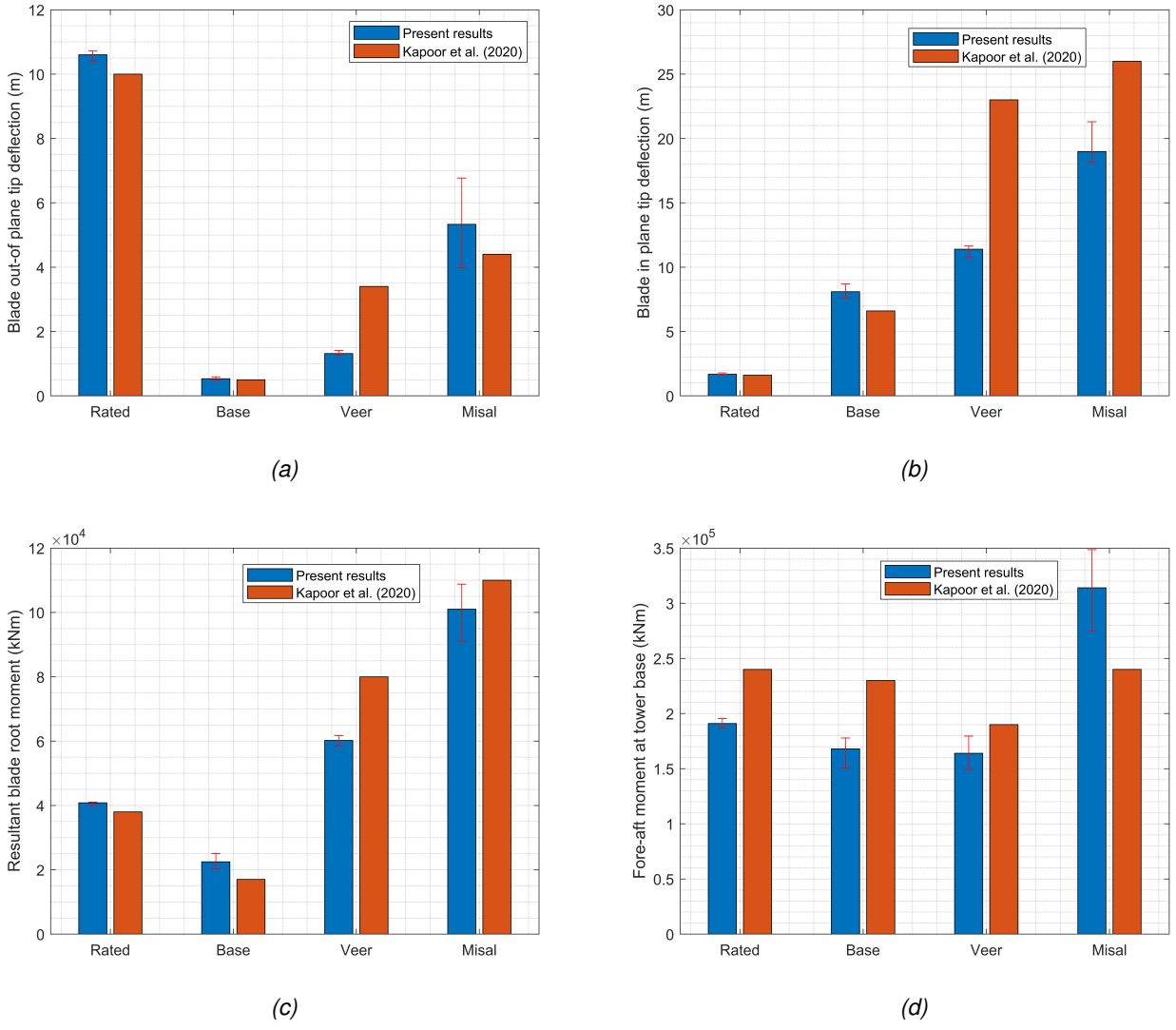

Figure 6.8: (a) Blade out-of-plane tip deflection (b) Blade in-plane tip deflection (c) Resultant blade root moment (d) Fore-aft moment at tower base - 20 km from hurricane centre, Kapoor et al (2020) vs present results.

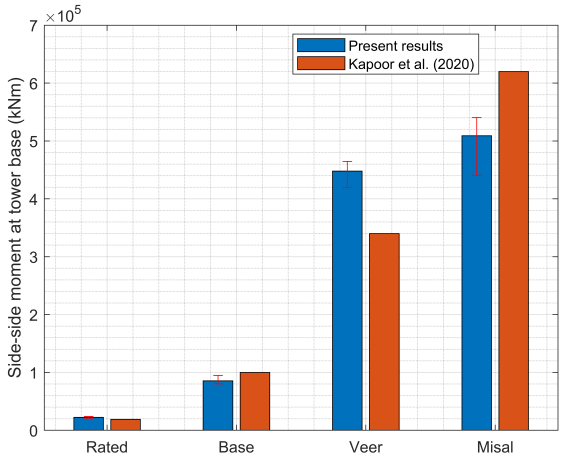

(a)

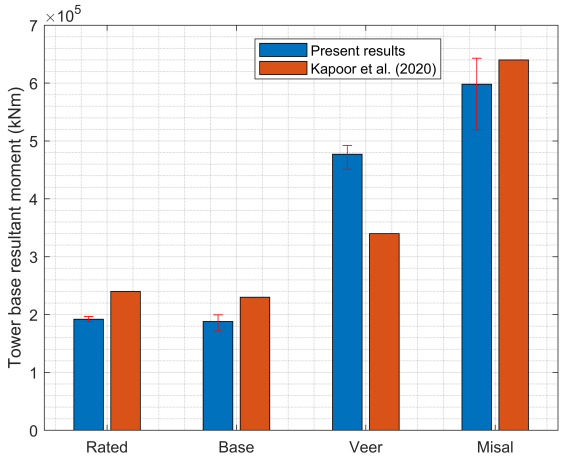

(b)

Figure 6.9: (a) Side-side moment at tower base (b) Tower base resultant moment - 20 km from hurricane centre, Kapoor et al (2020) vs present results.

Table 6.3: Responses of DTU 10 MW wind turbine for Rated, Base, Veer and Misal load cases, Kapoor et al. (2020) vs present results, 20 km from the hurricane centre

Property	**Rated (Kapoor et al. (2020)**	**Rated**	**RMSLE**
Out-of-plane blade tip deflection (m)	10	10.65	0.06
In-plane blade tip deflection (m)	1.6	1.71	0.04
Blade root resultant bending moment (kNm)	3.80E+04	4.10E+04	0.08
FA tower base moment (kNm)	2.40E+05	1.96E+05	0.20
SS tower base moment (kNm)	1.90E+04	2.37E+04	0.22
Tower base resultant moment (kNm)	2.40E+05	1.96E+05	0.20

Property	**Base (Kapoor et al. (2020)**	**Base**	**RMSLE**
Out-of-plane blade tip deflection (m)	0.5	0.59	0.06
In-plane blade tip deflection (m)	6.6	8.69	0.24
Blade root resultant bending moment (kNm)	1.70E+04	2.59E+04	0.42
FA tower base moment (kNm)	2.30E+05	1.78E+05	0.26
SS tower base moment (kNm)	1.00E+05	9.49E+04	0.05
Tower base resultant moment (kNm)	2.30E+05	2.01E+05	0.13

Property	**Veer (Kapoor et al. (2020)**	**Veer**	**RMSLE**
Out-of-plane blade tip deflection (m)	3.4	1.4	0.61
In-plane blade tip deflection (m)	23	11.65	0.64
Blade root resultant bending moment (kNm)	8.00E+04	6.18E+04	0.26
FA tower base moment (kNm)	1.90E+05	1.80E+05	0.05
SS tower base moment (kNm)	3.40E+05	4.65E+05	0.31
Tower base resultant moment (kNm)	3.50E+05	4.99E+05	0.35

Property	**Misal (Kapoor et al. (2020)**	**Misal**	**RMSLE**
Out-of-plane blade tip deflection (m)	4.4	6.8	0.37
In-plane blade tip deflection (m)	26	21.3	0.19
Blade root resultant bending moment (kNm)	1.10E+05	1.09E+05	0.01
FA tower base moment (kNm)	2.40E+05	3.48E+05	0.37
SS tower base moment (kNm)	6.20E+05	5.40E+05	0.14
Tower base resultant moment (kNm)	6.40E+05	6.43E+05	0.00

Base case, 20 km. The blade deflections show good comparison with the results of Kapoor et al. (2020) with RMSLEs of 0.06 and 0.24 for the out of plane and in plane deflections respectively. The moments also compare well, with RMSLEs ranging from 0.05 to 0.42. This shows that the Base case is modelled accurately.

Veer case, 20 km. All of the loads except the blade tip deflections are in good agreement with the results of Kapoor et al. (2020). The blade root resultant bending moment has a RMSLE of 0.26 and the side-side moment has a RMSLE of 0.31. The fore-aft moment is also in good agreement with a RMSLE of 0.05. The blade deflections were underestimated with RMSLE of 0.61 and 0.64 respectively. A possible reason for this might be the stiffness of the blade used in the OpenFAST model that may be different from those used by Kapoor et al. (2020). The OpenFAST blade properties file indicates that the average blade edgewise stiffness used in this model is 1.57E+10 N/m^2 and the average blade flapwise stiffness is 4.14E+09 N/m^2. However, blade stiffness values were not quoted by Kapoor et al (2020).

Misal case, 20 km. The moments are in good agreement with Kapoor et al. (2020) with the blade root resultant moment and the resultant moment at the base of the tower being practically the same as those quoted by Kapoor et al (2020). That is, they both registered a RMSLE of 0.00. The blade deflections were in good agreement with RMSLEs of 0.37 and 0.19 for the out-of-plane and in-plane blade tip deflections respectively. On balance, the Misal condition is modelled satisfactorily.

Although not all the responses were in agreement for the Veer case, the Rated, Base and Misal cases produced satisfactory results relative to the results from Kapoor et al. (2020). In addition, the general trend of the hurricane load case when compared to the Rated case, is the same as shown by Kapoor et al. (2020). That is, there are responses that are shown by Kapoor et al. (2020) to be relatively higher or lower for the hurricane load cases in comparison to the Rated case. This same characteristic is shown in this study and Figure 6.8 shows that although there are some differences in individual values for each case, the trend between cases is similar in the present work to that presented by Kapoor et al. (2020). For the blade in-plane tip deflection, the hurricane loads result in greater deflections when compared to the Rated case. This same trend is depicted by Kapoor et al. (2020).

6.5.2 Turbine responses 15 km from hurricane centre

Rated case. It was already shown that the Rated case can be modelled satisfactorily, using the wind field from TurbSim to model turbine responses in OpenFAST.

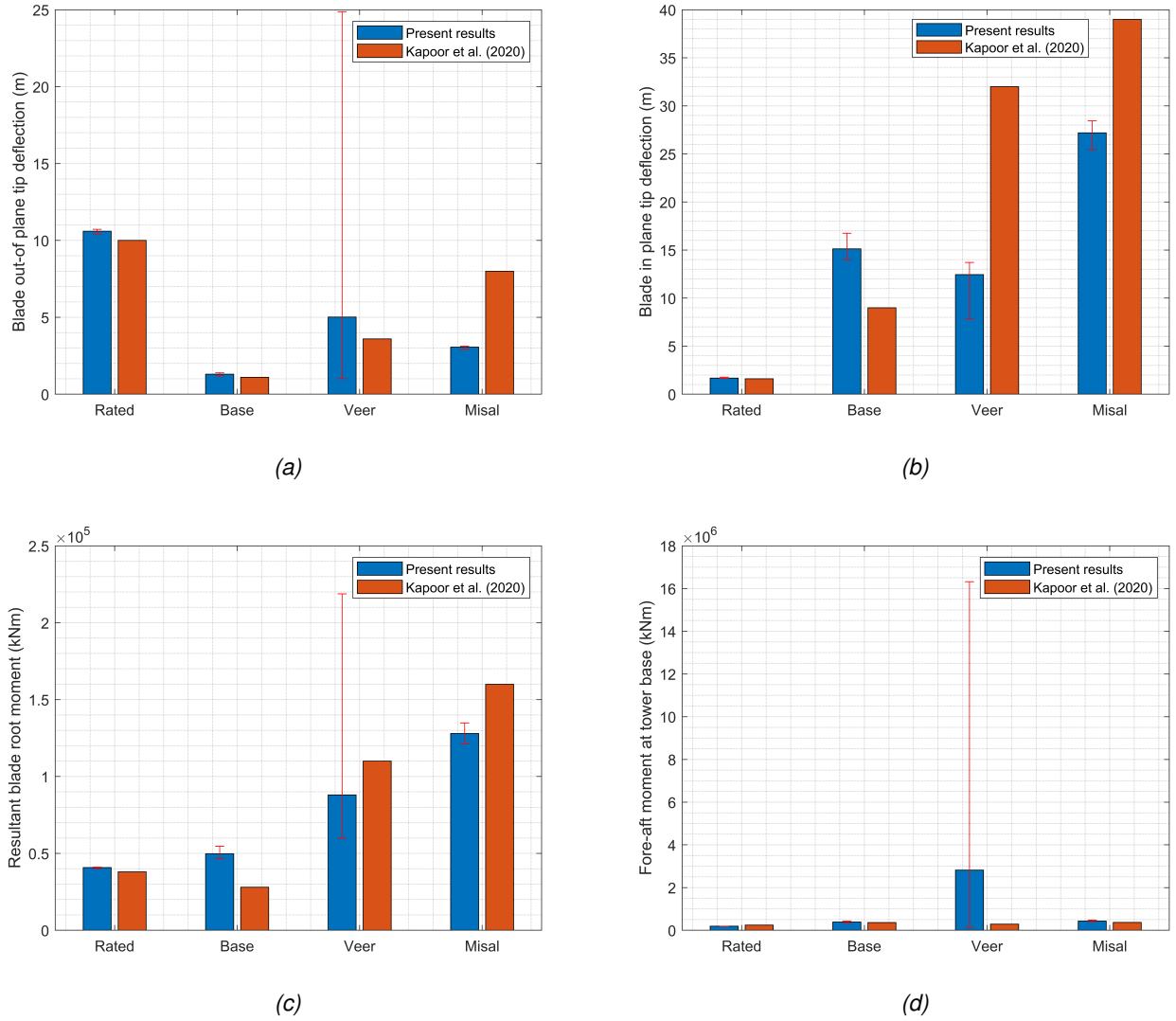

Figure 6.10: (a) Blade out-of-plane tip deflection (b) Blade in-plane tip deflection (c) Resultant blade root moment (d) Fore-aft moment at tower base - 15 km from hurricane centre, Kapoor et al (2020) vs present results.

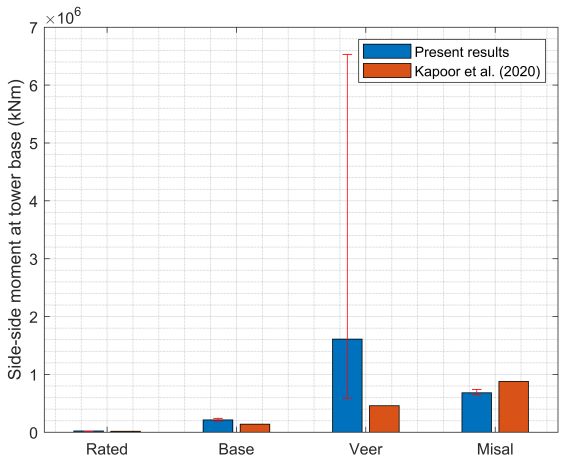

(a)

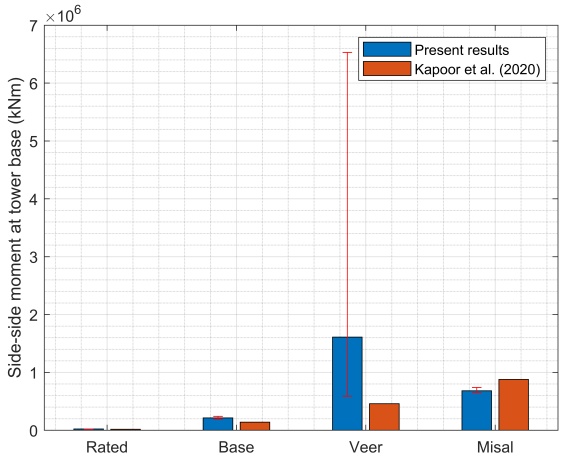

(b)

Figure 6.11: (a) Side-side moment at tower base (b) Tower base resultant moment - 15 km from hurricane centre, Kapoor et al (2020) vs present results.

Table 6.4: Responses of DTU 10 MW wind turbine for Rated, Base, Veer and Misal load cases, Kapoor et al. (2020) vs present results, 15 km from the hurricane centre

Property	**Rated (Kapoor et al. (2020)**	**Rated**	**RMSLE**
Out-of-plane blade tip deflection (m)	10	10.65	0.06
In-plane blade tip deflection (m)	1.6	1.71	0.04
Blade root resultant bending moment (kNm)	3.80E+04	4.10E+04	0.08
FA tower base moment (kNm)	2.40E+05	1.96E+05	0.20
SS tower base moment (kNm)	1.90E+04	2.37E+04	0.22
Tower base resultant moment (kNm)	2.40E+05	1.96E+05	0.20

Property	**Base (Kapoor et al. (2020)**	**Base**	**RMSLE**
Out-of-plane blade tip deflection (m)	1.1	1.386	0.13
In-plane blade tip deflection (m)	9	16.75	0.57
Blade root resultant bending moment (kNm)	2.80E+04	5.47E+04	0.67
FA tower base moment (kNm)	3.60E+05	4.40E+05	0.20
SS tower base moment (kNm)	1.40E+05	2.43E+05	0.55
Tower base resultant moment (kNm)	3.60E+05	5.03E+05	0.33

Property	**Veer (Kapoor et al. (2020)**	**Veer**	**RMSLE**
Out-of-plane blade tip deflection (m)	3.6	24.9	1.73
In-plane blade tip deflection (m)	32	13.7	0.81
Blade root resultant bending moment (kNm)	1.10E+05	2.19E+05	0.69
FA tower base moment (kNm)	2.90E+05	1.63E+07	4.03
SS tower base moment (kNm)	4.60E+05	6.53E+06	2.65
Tower base resultant moment (kNm)	4.80E+05	1.76E+07	3.60

Property	**Misal (Kapoor et al. (2020)**	**Misal**	**RMSLE**
Out-of-plane blade tip deflection (m)	8	3.121	0.78
In-plane blade tip deflection (m)	39	28.44	0.31
Blade root resultant bending moment (kNm)	1.60E+05	1.35E+05	0.17
FA tower base moment (kNm)	3.70E+05	4.75E+05	0.25
SS tower base moment (kNm)	8.80E+05	7.40E+05	0.17
Tower base resultant moment (kNm)	9.10E+05	8.80E+05	0.03

Base case, 15 km. The out of plane blade tip deflection showed good agreement with the results of Kapoor et al. (2020) with RMSLEs of 0.13. However, the in-plane tip deflection was overestimated, having a RMSLE of 0.57. The resulting blade root moment was also overestimated with a RMSLE of 0.67. The moments at the base of the tower are also greater than those in Kapoor et al. (2020), with RMSLE ranging from 0.20 to 0.55. The pattern that is shown here is that for all but one case, the turbine responses are greater than the values obtained by Kapoor et al. (2020). Notwithstanding the overestimation, if the results in Tables 6.3 and 6.4 are compared, it is shown that when the turbine is closer to the eyewall the conditions are more onerous than when it is outside of the eyewall, the case for the turbine 20 km from the hurricane centre. This clearly demonstrates what was expected, that is, the hurricane conditions at the edge of the eyewall are greater than those outside of the eyewall. It therefore shows that the hurricane conditions 15 km from the hurricane centre, have greater intensity than the conditions 20 km from the hurricane centre. This means that for a turbine situated at the edge of the eyewall, the ratio of the Base Case Loads/Rated Case Loads would be greater than when the turbine is located outside the eyewall. This same trend is shown in the results by Kapoor et al. (2020).

Veer case, 15 km. All but one response (the blade in-plane tip deflection) is overestimated in relation to the results in Kapoor et al. (2020). This is similar to the Base case. In addition, these Veer case results (at the outer edge of the eyewall) are also greater than the values when the turbine is outside the eyewall. It should be noted, however, that the magnitude of the loads for the Veer Case are greater than the Base case with RMSLEs ranging from 2.65 to 4.03 for the moments at the base of the tower, and RMSLEs of 1.73 and 0.81 for the blade out-of-plane tip deflection and in-plane tip deflections respectively. This same trend was shown in the results of Kapoor et al. (2020).

Misal case, 15 km. From the graphs in Figures 6.10 and 6.11 it is shown that all the responses of the turbine, except the blade out-of-plane tip deflection, are in good agreement with the results of Kapoor et al. (2020). The tower base resultant moment giving the best response with an RMSLE of 0.03. The results also demonstrate what is expected when the turbine is situated at the edge of the eyewall as compared to outside of the eyewall. That is, all the responses at the location of the edge of the eyewall are greater.

Although not all the responses are in agreement with the values shown by Kapoor et al. (2020), one important characteristic that is demonstrated is that the responses of the wind field at the outer edge of the eyewall are more severe than the response for the turbine situated outside the eyewall. This replicated what happens in a real

hurricane. An indication that the TurbSim model produced the correct behaviour based on the relative location to the eyewall. It is therefore shown that the hurricane loads can be modelled in TurbSim, the wind field is then input to OpenFAST to determine its structural responses.

6.5.3 Turbine responses 12 km from hurricane centre

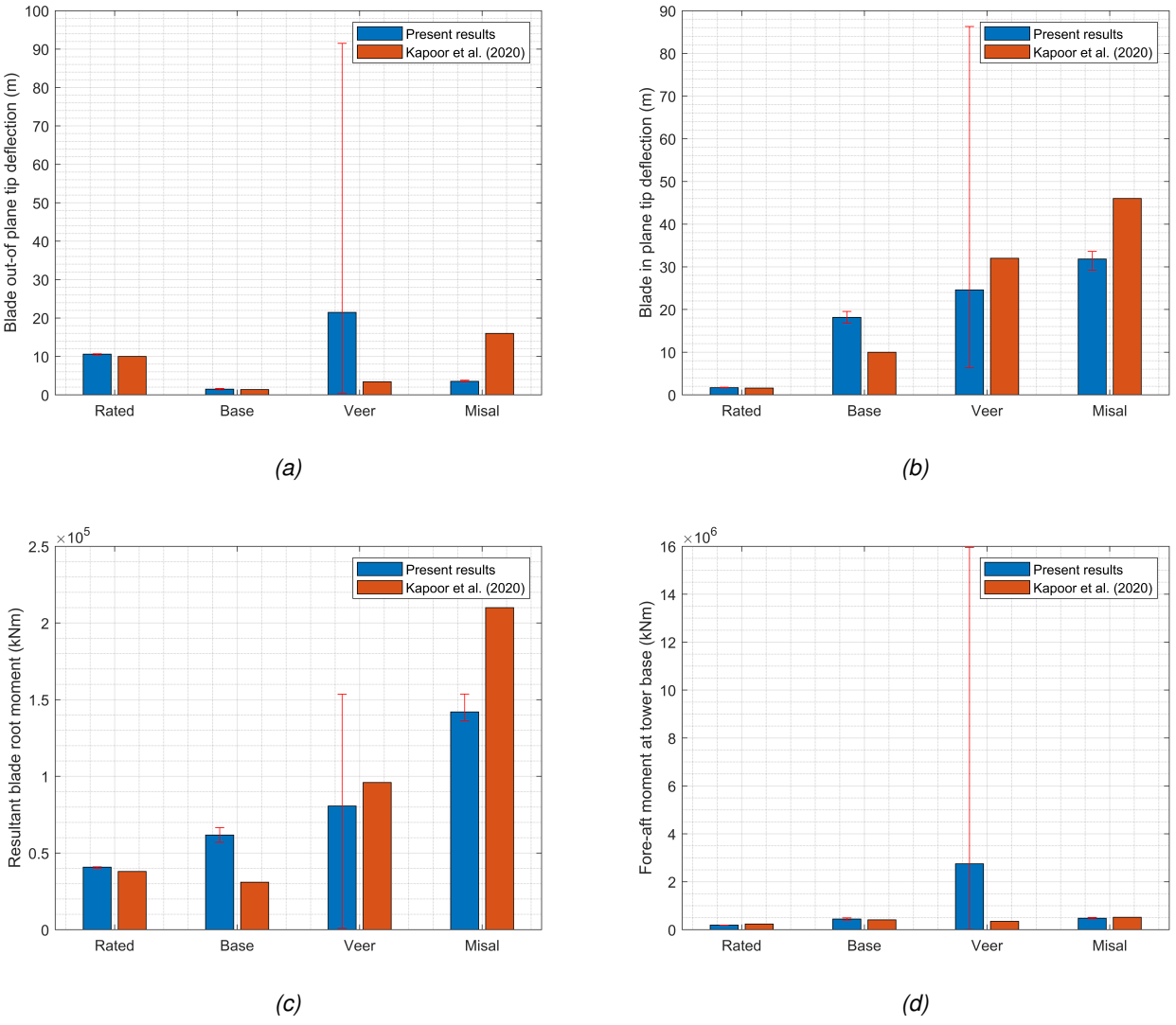

Figure 6.12: (a) Blade out-of-plane tip deflection (b) Blade in-plane tip deflection (c) Resultant blade root moment (d) Fore-aft moment at tower base - 12 km from hurricane centre, Kapoor et al. (2020) vs present results.

Base case, 12 km. The out of plane blade tip deflection is overestimated but showed fairly good agreement with the results of Kapoor et al. (2020) with RMSLEs of 0.50. Similarly, the in-plane tip deflection is also overestimated, having a RMSLE of 0.62.

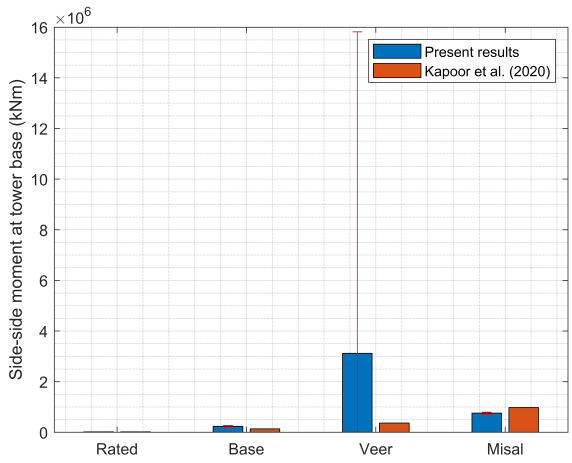

(a)

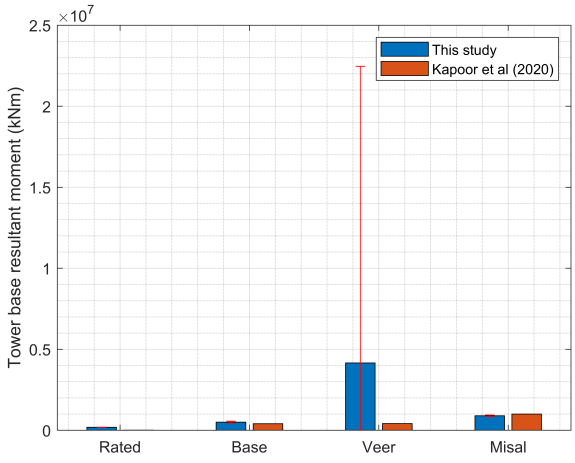

(b)

Figure 6.13: (a) Side-side moment at tower base (b) Tower base resultant moment - 12 km from hurricane centre, Kapoor et al. (2020) vs present results.

Table 6.5: Responses of DTU 10 MW wind turbine for Rated, Base, Veer and Misal load cases, Kapoor et al. (2020) vs present results, 12 km from the hurricane centre

Property	**Rated (Kapoor et al. (2020)**	**Rated**	**RMSLE**
Out-of-plane blade tip deflection (m)	10.0	10.65	0.06
In-plane blade tip deflection (m)	1.6	1.71	0.04
Blade root resultant bending moment (kNm)	3.80E+04	4.10E+04	0.08
FA tower base moment (kNm)	2.40E+05	1.96E+05	0.20
SS tower base moment (kNm)	1.90E+04	2.37E+04	0.22
Tower base resultant moment (kNm)	2.40E+05	1.96E+05	0.20

Property	**Base (Kapoor et al. (2020)**	**Base**	**RMSLE**
Out-of-plane blade tip deflection (m)	3.4	1.659	0.50
In-plane blade tip deflection (m)	10.0	19.55	0.62
Blade root resultant bending moment (kNm)	3.10E+04	6.65E+04	0.76
FA tower base moment (kNm)	4.10E+05	4.97E+05	0.19
SS tower base moment (kNm)	1.40E+05	2.70E+05	0.66
Tower base resultant moment (kNm)	4.10E+05	5.66E+05	0.32

Property	**Veer (Kapoor et al. (2020)**	**Veer**	**RMSLE**
Out-of-plane blade tip deflection (m)	3.4	91.5	3.05
In-plane blade tip deflection (m)	32.0	86.3	0.97
Blade root resultant bending moment (kNm)	9.60E+04	1.54E+05	0.47
FA tower base moment (kNm)	3.50E+05	1.59E+07	3.82
SS tower base moment (kNm)	3.70E+05	1.59E+07	3.76
Tower base resultant moment (kNm)	4.20E+05	2.25E+07	3.98

Property	**Misal (Kapoor et al. (2020)**	**Misal**	**RMSLE**
Out-of-plane blade tip deflection (m)	16.0	3.80	1.27
In-plane blade tip deflection (m)	46.0	33.6	0.31
Blade root resultant bending moment (kNm)	2.10E+05	1.53E+05	0.32
FA tower base moment (kNm)	5.20E+05	5.16E+05	0.01
SS tower base moment (kNm)	9.80E+05	7.91E+05	0.21
Tower base resultant moment (kNm)	1.00E+06	9.45E+05	0.06

The resulting blade root moment is also overestimated with a RMSLE of 0.76. The moments at the base of the tower are also greater than those in Kapoor et al. (2020), with RMSLE ranging from 0.19 to 0.66 (see Table 6.5 for full set of results). Like the case 15 km from the hurricane centre, this shows that the results would be conservative where design and costing are concerned. In addition, the magnitude of the responses when the wind turbine is 12 km away from the centre of the hurricane are greater than the responses 15 km from the hurricane centre. This again demonstrates what was expected, that is, the hurricane conditions within the eyewall are greater than those at the outer edge of the eyewall. Comparing the Base case versus the Rated case the ratio of the loads would be greatest when the turbine is inside the eyewall. This is what was shown by Kapoor et al. (2020).

Veer case, 12 km. All responses were overestimated in relation to the results in Kapoor et al. (2020). In addition, all six responses for the turbine inside the eyewall were greater than the responses at the outer edge of the eyewall, except the blade root moment and the fore-aft moment at the base of the tower. It should be noted that like the case for the turbine 15 km from the hurricane centre (Veer case), the blade root moment, and fore-aft and side-side moments at the base of the tower are much greater than the values shown in Kapoor et al. (2020). The RMSLEs range from 3.82 to 3.98. It is also seen that the Veer case results in more onerous responses when the turbine is inside of the eyewall, as well as at the outer edge of the eyewall in comparison to when the turbine is outside the eyewall. See Figures 6.12 and 6.13 for clarification. On balance, the wind forces within eyewall result in greater turbine response. However, these responses increase significantly for the Veer case. The greatest effect being on the moments at the base of the tower.

Misal case, 12 km. From the graphs in figures 6.12 and 6.13 it is shown that all the moments are in good agreement with Kapoor et al. (2020) with RMSLE ranging from 0.01 to 0.32. However, the blade tip deflections are underestimated with RMSLE of 1.27 for the out-of-plane tip deflection and 0.31 for the in-plane tip deflection. The results also demonstrate what is expected when the turbine is situated within the eyewall relative to outside or at the edge of the eyewall, that is, all the forces are greater.

6.5.4 Concluding remarks on reproducing of TurbSim hurricane wind fields and OpenFAST wind turbine responses given by Kapoor et al. (2020)

The objective of the work above is to reproduce the wind fields of the LES of the category 5 hurricane using TurbSim and to input the wind fields in OpenFAST to calculate the wind turbine structural responses. This is done for the turbine located outside the eyewall (20 km radius), the outer edge of the eyewall (15 km radius) and inside the

eyewall (12 km radius) for Base, Veer and Misal load conditions. The results compare well with Kapoor et al. (2020) in the following ways:

1. The majority of the responses have a RMSLE within the range $0.00 \leq \text{RMSLE} \leq 0.50$. In particular, for the Base case, this applies to all of the responses, that is the blade tip deflections (in-plane and out-of-plane), the blade root moments, the fore-aft and side-side moments at the base of the tower and the resultant moment at the tower base (20km radius).The out-of-plane tip deflection, fore-aft moment and resultant moment at the tower base (12 km radius and 15 km radius). For the Veer case, this applies to all the moments, moments on the blade and the moments at the base of the tower (20 km radius). For the Misal case, this applies to the all of the responses as for the Base case at 20 km radius outlined above (20 km radius). The blade in-plane tip deflection, the blade root moments, the fore-aft and side-side moments at the base of the tower and the resultant moment at the tower base (12 km radius and 15km radius).
2. The trend in the hurricane loads relative to the loads at rated wind speed is the same; Figures 6.8 to 6.13
3. The loads on the wind turbine are greater when it is located within the eyewall relative to outside the eyewall or the outer edge of the eyewall
4. The Veer case produces the most immense structural responses of the wind turbine
5. The Misal case tends to show good agreement with Kapoor et al. (2020) for all wind turbine responses

The results did not compare well (RMSLE > 0.5) with Kapoor et al. (2020) for:

1. The Base case, blade in-plane tip deflection, blade root resultant moment and the side-side moment at the base of the tower (12km and 15 km radius).
2. The Veer case, all of the responses, that is the blade out-of-plane tip and in-plane tip deflections, the fore-aft and side-side moments at the base of the tower and the resultant moment at the tower base (12 km and 15km radius).
3. The Misal case, the out-of-plane blade tip deflections (12 km and 15km).

It should be noted that all the responses were not the same magnitude as the responses for Kapoor et al. (2020). This could be due to the random nature of wind loads and the change in response for the change in random seed. Kapoor et al. (2020)

did not indicate the specific numbers that were used for the random seed in either the TurbSim or OpenFAST models. From the graphs in Figures 6.9 to 6.14, the results from Kapoor et al. (2020) do not always fit within the range of the response of the error bars. In Figures 6.9 to 6.10, turbine 20 km from the hurricane centre, only three of these responses fit within the range of the responses given. They are the blade out-of-plane tip deflection, the resultant blade root moment and the tower base resultant moment for the Misal case. In Figure 6.11 to 6.12, turbine 15 km from the hurricane centre, the resultant balde root moment for the Veer case only fits within the range of value of the error bar. In Figures 6.13 to 6.14, 12 km from the hurricane centre, the blade in-plane deflection and the resultant blade root moment fits within the range of value of the error bar. This difference in values could be attributed to the difference in random seeds used. In addition, there is very little information provided by Kapoor et al. (2020)about the material properties of the wind turbine and so it was difficult to ensure that the exact properties are used. These two characteristics might have resulted in the magnitudes of some of the loads being different. Notwithstanding this, items 2 to 5 provide a good basis to say that the model that is developed for this study reproduces the results of Kapoor et al. (2020) satisfactorily. This gives confidence that the methodology used for the fixed-bottom 10MW turbine in hurricane conditions can be applied to a floating offshore wind turbine to determine the response in hurricane load conditions.

As was mentioned in the Introduction, the effect of hurricane conditions on a FOWT system is not well studied. The author is of the view that this is one of the things that sets this work apart in relation to the studies done on other wind turbine systems in hurricanes. The previous works have dealt with fixed-bottom wind turbines. This provides a good segue to investigate the behaviour of a FOWT system in hurricane conditions. It should be interesting to further investigate the effects of the hurricane forces on the structural response of the wind turbine, the dynamic motions of the platform as well as the loads on the mooring lines. In particular, for the mooring line, it would be a good to investigate if the minimum breaking load of the mooring line would be exceeded during hurricane conditions. Kim & Manuel (2014) indicated that the parked-standstill case leads to greater side-side moments than for the parked-idle case. This study will therefore be extended to include forces on the FOWT for the parked-standstill condition. The response of the floater in hurricane conditions is investigated in the next section.

6.6 Assessing the behaviour of a FOWT during hurricane conditions

6.6.1 Description of FOWT system

The response of a fixed-bottom onshore wind turbine was previously assessed for hurricane conditions. The same hurricane conditions used by Kapoor et al. (2020) are

used to assess the behaviour of a FOWT system. NREL's 5MW baseline wind turbine is used to assess the behaviour of a FOWT system in a hurricane. This turbine is supported by the DeepCwind semi-sub and fits within the boundaries of the wind field of the hurricane. The properties of NREL's 5MW baseline wind turbine are given by Robertson et al. (2014) and are shown in Table 6.6. The properties of the DeepCwind floater and related mooring system are shown in Tables 6.7 and 6.8 respectively. Figure 6.14, is an illustration of the FOWT system, showing the geometrical properties.

Table 6.6: Properties of NREL's 5MW Baseline Wind Turbine (Jonkman & Matha (2011))

Description	**Quantity/Property**
Rating	5MW
Rotor orientation and configuration	Upwind, 3 blades
Control	Variable speed, collective pitch
Drivetrain	High speed, multiple-stage gearbox
Rotor and hub diameter	126m, 3m
Hub height	90m
Cut-in, rated and cut-out wind speeds	3m/s, 11.4m/s and 25m/s
Cut-in and rated rotor speeds	6.9rpm, 12.1rpm
Rotor tip speed	80m/s
Hub overhang, shaft tilt and precone	5m, 5º and 2.5º
Rotor mass	110,000kg
Nacelle Mass	240,000 kg
Tower Mass	347,500kg
Location of overall CM of rotor, nacelle and tower combined	0.2m upwind of tower centreline, 64.0m above SWL

6.7 Numerical Model Set Up and Verification

The numerical model of the DeepCwind FOWT system is set up in OpenFAST in a similar manner to the VolturnUS-S FOWT system described in Chapter 5. The first step in setting up the numerical model is to carry out a verification exercise. This is done to make sure that the results being output from OpenFAST are credible. It is done by comparing the results from the DeepDwind numerical model in this study with the results from the DeepCwind model given in offshore code comparison within IEA

Table 6.7: Properties of DeepCwind Semi-submersible Floater (Robertson et al. (2014))

Description	Quantity
Full Draft	20m
Elevation of main column above still water level(SWL)	10m
Spacing between offset columns	50m
Length of upper columns	26m
Length of base columns	6m
Depth to top of base columns below SWL	14m
Diameter of main column	6.5m
Diameter of offset (upper) columns	12m
Diameter of base columns	24m
Diameter of pontoons and cross braces	1.6m
Platform mass, including ballast	1.3473E +7 kg
CM location below SWL	13.46m
Platform roll inertia about centre of mass(CM)	6.827E +9 kg/m^2
Platform pitch inertia about CM	6.827E + 9 kg/m^2
Platform yaw inertia about CM	1.226 E + 10kg/m^2
Centre of buoyancy below SWL	13.15m
Displaced volume in undisplaced position	13,917 m^3

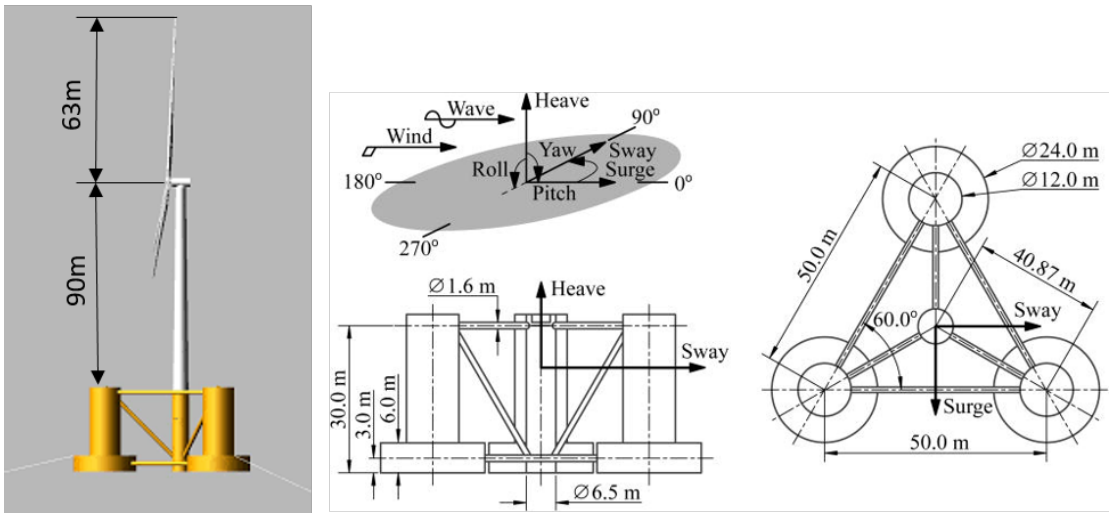

Figure 6.14: DeepCWind Floating Wind Turbine System (Li et al. (2019))
(Permission has been granted by Zhiming Yuan to reproduce this figure)

Table 6.8: Properties of DeepCwind Mooring System (Robertson et al. (2014))

Description	Quantity
Number of mooring lines	3
Angle between adjacent mooring lines	120 º
Depth of Anchors Below SWL	200m
Depth to fairleads below SWL	14m
Radius of anchors from platform centreline	836.7m
Radius of fairleads from platform centreline	40.868m
Unstretched mooring line length	835.5m
Mooring line diameter	0.0766m
Equivalent mooring line mass density	113.35kg/m
Equivalent mooring line mass in water	108.63kg/m
Equivalent mooring line extensional stiffness	753.6MN

Wind Task 30 by Robertson et al. (2014b). The tests done to verify the model are a static equilibrium test and a free decay test, this includes determining the system natural frequency.

6.7.1 Numerical Model Verificationon

Static equilibrium test of DeepCwind FOWT system

A static equilibrium test is carried out to ensure that the average heave of the FOWT was zero. It is performed in the absence of wind and waves (still water condition). In this state, the full system weight of the FOWT (floater + tower + rotor nacelle assembley) and the vertical mooring pretension should be equal to the buoyant forces (upward forces). A static equilibrium test is conducted and average heave was found to be 0.0 m, satisfying the static equilibrium for the FOWT system.

Natural frequency of DeepCwind FOWT system

Similar to Robertson et al. (2014b) the natural frequency of the system is determined and a surge and heave free decay test is carried out. This is done by setting the respective DOFs to a specific value and allowing the system to oscillate freely. In addition, as customary (Mahfouz et al., (2021), the wind, current and wave loads are set to zero. Table 6.9 shows the system natural frequencies and Figure 6.15 shows the surge and heave free decay motions respectively. The free decay test shows that

the system oscillates freely, and the natural frequencies are in good agreement with the values given by Robertson et al. (2014b). The results of this test and that from the static equilibrium test indicate that the numerical model of the DeepCwind FOWT system is properly set up and the results that are obtained from subsequent analyses are credible.

Table 6.9: System natural frequency NREL's DeepCwind FOWT

Platform motion	Nat frequency (Hz)	Nat frequency computed (Hz)
Surge	0.009	0.009
Sway	0.009	0.009
Heave	0.058	0.058
Roll	0.039	0.039
Pitch	0.039	0.039
Yaw	0.013	0.013

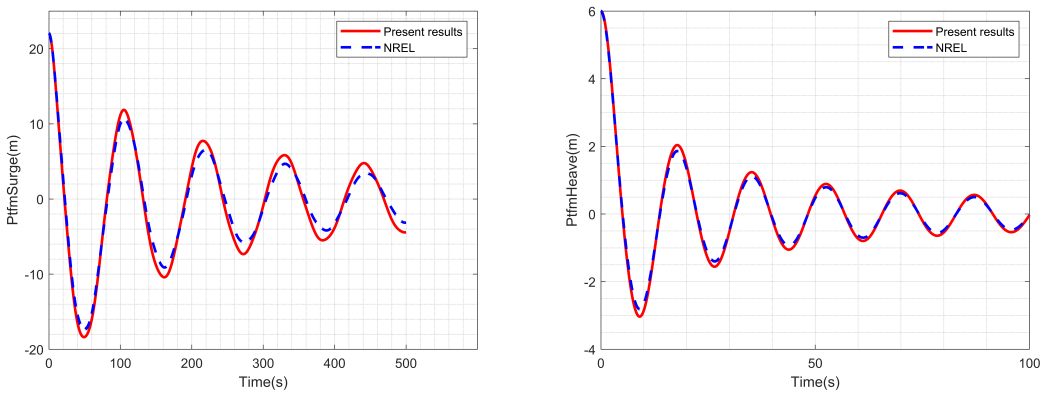

(a) *(b)*

Figure 6.15: a) Surge Free Decay and b) Heave Free Decay, DeepCwind Motion Response

6.8 Response of DeepCwind FOWT 12 km from the hurricane centre

6.8.1 Responses investigated for the FOWT system.

The responses that are investigated for the FOWT system are, all the structural responses that were previously investigated plus some additional responses:

1. Surge
2. Heave

3. Pitch
4. Tension in fairlead 1
5. Tension in fairlead 2
6. Tension in fairlead 3
7. Out-of-plane blade tip deflection
8. In-plane blade tip deflection
9. Blade root resultant bending moment
10. FA tower base moment
11. SS tower base moment
12. Tower base resultant moment

6.8.2 Modifications of the mooring line.

Similar to what was done in Chapter 5, the mooring line was redesigned for 100 m depth of water by scaling the dimensions of the mooring line from the 200 m to the 100 m deep water condition. A similar modification was made by Shi et al. (2019) in ajusting the dimension of a mooring line to suit shallower water depths. The properties of the mooring line at 100 m water depth are shown in Table 6.10.

Table 6.10: Properties of mooring line for DeepCwind at 100 m water depth

Description	Unit	Value
Mooring system type	-	Chain catenary
Line type		3S stud link mooring chain
Line breaking strength	kN	8964
Number of lines	-	3
Angle between adjacent mooring lines	deg	120
Anchor depth	m	100
Fairlead depth	m	14
Radius of anchors from platform centreline	m	450
Radius of fairleads from platform centreline	m	40.87
Nominal chain diameter	mm	100
Dry line linear density	kg/m	219
Extensional stiffness	MN	900
Line unstretched length	m	426

6.8.3 Hurricane Wind Field and Sea State.

From Kapoor et al. (2020) and the DTU turbine that is modelled above, it is shown that the location of the turbine 12 km from the hurricane centre (within the eyewall) produced the most onerous results. The DeepCwind model is therefore assessed for the turbine located 12 km from the hurricane centre. It is also assessed for the turbine at the rated wind speed to investigate the variation of the responses for the hurricane conditions relative to the rated wind speed conditions. As was done previously, the turbine responses are compared for different hurricane load conditions (namely, Base, Veer and Misal) with the Rated load condition.

The wind turbine codes and standards recommend that wind turbine systems be designed to withstand 50-year return period loads. Worsnop et al. (2017) argued that the maximum loads computed with the code equate to category 2 hurricane conditions. The 50-year 3hr-mean wind speed at 10m (shown in Chapter 4) for the JCS is 28.7 m/s. This equates to a 10-min mean wind speed of 31.84 m/s. The Saffir Simpson hurricane winds mentioned in the Introduction are 1-min mean wind speeds. Therefore, to make the 50-year EVA wind speed comparable with the hurricane winds, the 10-min mean winds are converted to 1-min mean wind speeds. This is done by the following relationship (Harper et al., 2010):

$$U_{1-min} = \alpha U_{10-min} \tag{6.2}$$

where, the conversion factor α is 1.16.

The 50-year extreme value analysis (EVA) wind at 10 m is therefore 37 m/s. This is equivalent to a category 1 hurricane. The wind speed at hub height (90 m) is 47 m/s.

The hurricane sea state is determined from a relationship between hurricane wind speed and hurricane significant wave height that is given in Ochi (1993b). This relationship was developed using hurricane data from NOAA data buoys. It states that the significant wave height, H_s, during the growing stage of a hurricane can be obtained as a function of the mean wind speed at a 10 m level by:

$$H_s = 0.235\bar{U}_{10} \tag{6.3}$$

where, $\bar{U}_{10}$ is the mean wind speed at 10 m.

The mean wind speed at 10 m is found by carrying out a simulation in TurbSim using the hurricane wind speed 12 km from the hurricane centre and setting the reference height as 10 m. The mean wind speed at 10 m is found to be 69.32 m/s. From equation

6.3 H_s is 16.29 m. Equation 3.1, given in Chapter 3, is used to find the corresponding peak wave period, T_p. The sea state at 11 m/s that is given in Table 4.3 of Chapter 4, is used as the sea state for the Rated case. The wind field characteristics and sea state for the turbine 12 km from the hurricane centre are shown in Table 6.11.

Table 6.11: Wind Field Characteristics and Sea State of Simulation Cases for DeepCwind

Condition	**Reference radius, R (km)**	**Wind speed (m/s) (Turbulence intensity, %)**	**Wind shear profile or power law exponent**	**Coherence exponent**	**Veer**	**Yaw misalignment**	**Sea State**		**Operating state**
							Hs (m)	**Tp (s)**	
Base (baseline hurricane)	12	87.3 (7.38)	Figure 6.1	0.85	-	-	16.29	18.62	Idle
Veer (hurricane w/ veer)	12	87.3 (7.38)	Figure 6.1	0.85	-	-	16.29	18.62	Idle
Misal	12	87.3 (7.38)	Figure 6.1	0.85	Figure 6.1	27.1	16.29	18.62	Idle
Extreme 50-year*	n/a	47.0 (9.70)	0.11				11.17	11.22	Idle
Rated*	n/a	11.4 (10)	0.11				0.74	7.24	Operating

* The sea states for the Extreme 50-year and Rated cases are taken from table 4.3.

6.8.4 DeepCwind FOWT in Idle conditions, hurricane loads compared to 50-year extreme loads.

To investigate the impact of the category 5 hurricane loads on the FOWT system, the 47 m/s 50-year EVA load is applied to the system and compared with the results of the category 5 hurricane loads. The results are shown in Figures 6.16 to 6.18 and Table 6.12.

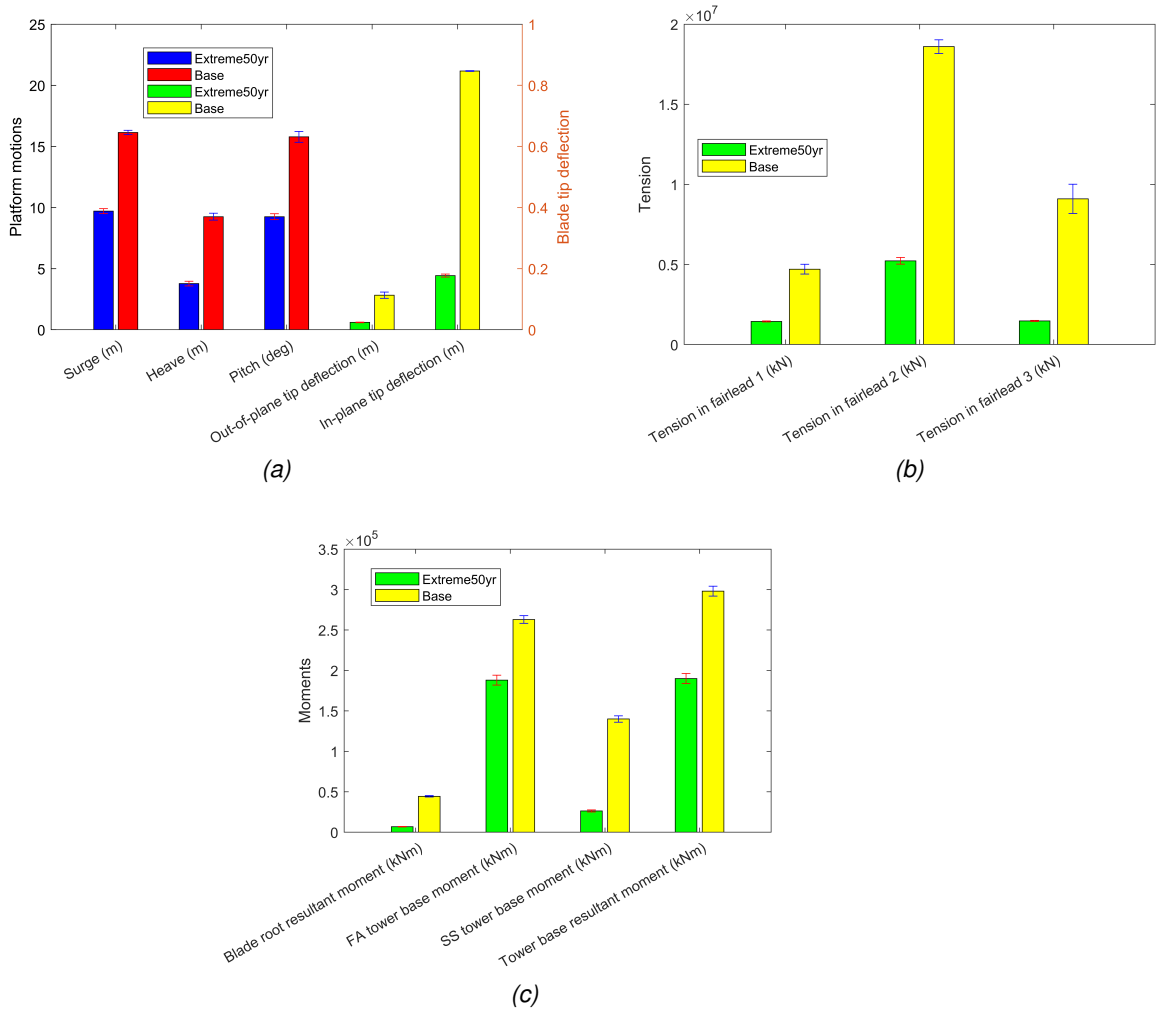

Figure 6.16: FOWT wind turbine response for Base Case compared with the 50-year extreme loads: (a) Platform motions and blade tip deflections (b) Tension in the fairleads (c) Moments.

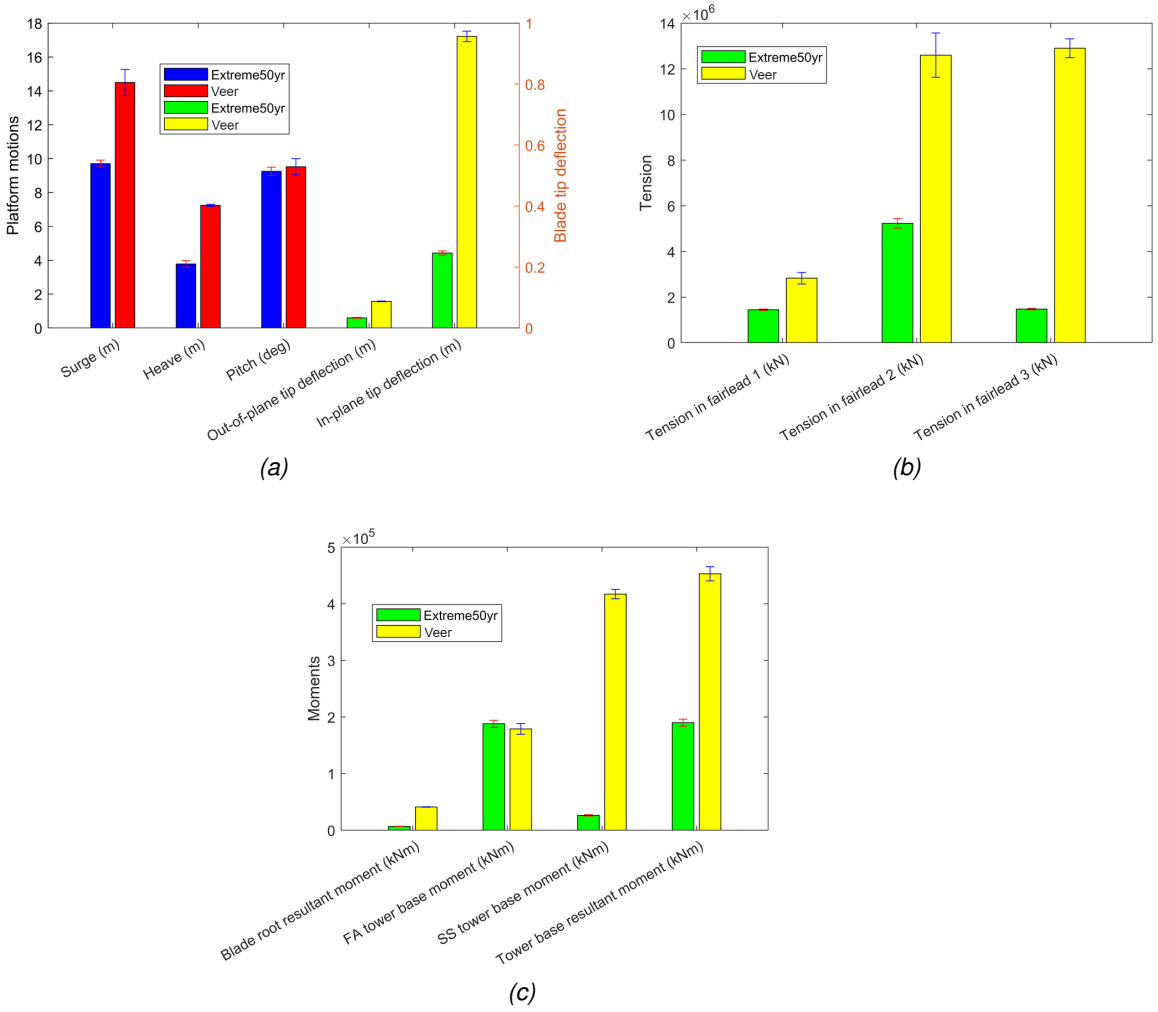

Figure 6.17: FOWT wind turbine response for Veer Case compared with the 50-year extreme loads: (a) Platform motions and blade tip deflections (b) Tension in the fairleads (c) Moments.

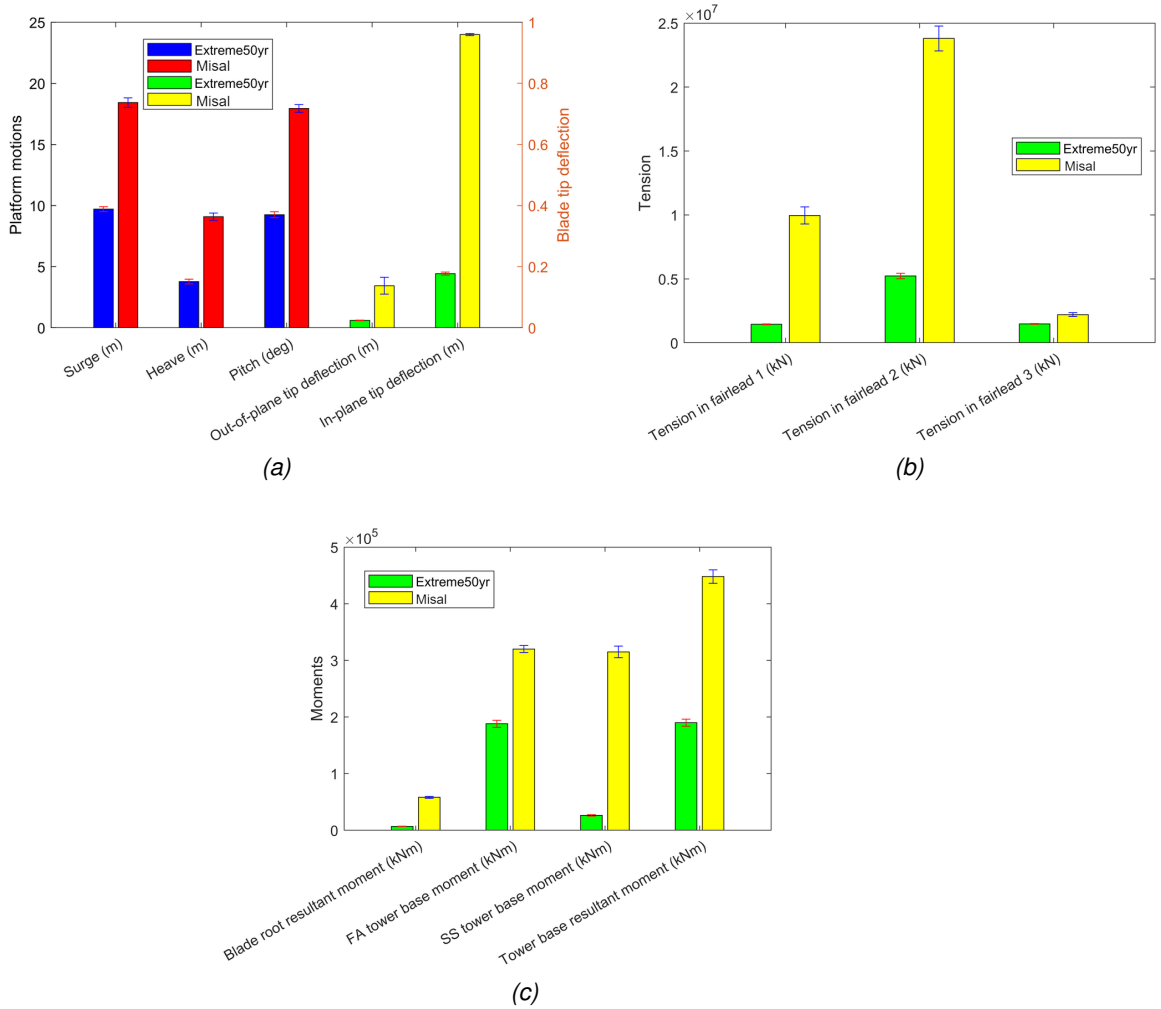

Figure 6.18: FOWT wind turbine response for Misal Case compared with the 50-year extreme loads: (a) Platform motions and blade tip deflections (b) Tension in the fairleads (c) Moments.

Table 6.12: Response of the DeepCwind FOWT in the JCS, Extreme 50-year vs Category 5 Hurricane: a) Base b)Veer c) Misal Load Cases

Property	Extreme 50-year	Base	Scale Factor, SF (= Base/E50-year)	Extreme 50-year	Veer	SF (= Veer/E50-year)	Extreme 50-year	Misal	SF (= Misal/E50-year)
Surge (m)	9.71	16.14	1.66	9.71	14.49	1.49	9.71	18.42	1.90
Heave (m)	3.78	9.25	2.45	3.78	7.24	1.91	3.78	9.09	2.40
Pitch (deg)	9.25	15.78	1.71	9.25	9.52	1.03	9.25	17.94	1.94
Out-of-plane blade tip deflection (m)	0.60	2.83	4.73	0.60	1.57	2.62	0.60	3.44	5.74
In-plane blade tip deflection (m)	4.43	21.17	4.78	4.43	17.22	3.89	4.43	23.99	5.42
Tension in fairlead1 (N)	1.45E+06	4.71E+06	3.25	1.45E+06	2.83E+06	1.95	1.45E+06	9.96E+06	6.87
Tension in fairlead2 (N)	5.23E+06	1.86E+07	3.56	5.23E+06	1.26E+07	2.41	5.23E+06	2.38E+07	4.55
Tension in fairlead3 (N)	1.48E+06	9.10E+06	6.15	1.48E+06	1.29E+07	8.72	1.48E+06	2.21E+06	1.49
Blade root resultant bending moment (kNm)	6.85E+03	4.44E+04	6.48	6.85E+03	4.11E+04	6.00	6.85E+03	5.80E+04	8.47
FA tower base moment (kNm)	1.88E+05	2.63E+05	1.40	1.88E+05	1.79E+05	0.95	1.88E+05	3.20E+05	1.70
SS tower base moment (kNm)	2.63E+04	1.40E+05	5.32	2.63E+04	4.17E+05	15.86	2.63E+04	3.15E+05	11.98
Tower base resultant moment (kNm)	1.90E+05	2.98E+05	1.57	1.90E+05	4.53E+05	2.38	1.90E+05	4.48E+05	2.36

It is seen that in all cases the hurricane loads due to the category 5 hurricane are significantly greater than the 50-year extreme loads. Considering the Base case, the resultant blade root moment, and the tension in fairlead number 3 for the hurricane loads were more than 6 times the moment for the 50-year extreme loads. In addition, the side-side moment at the tower base was more than 5 times the value for the 50-year extreme condition. For the Veer case, Figure 6.17, the resultant blade root moment is 6 times the 50-year value, the tension in fairlead number 3 is more than 8 times the 50-year value and the side-side moment at the base is more than 16 times the 50-year value. For the Misal case, the blade root resultant moment is more than 8 times the 50- year value, the tension in fairlead 1 is about 7 times the 50-year value. The shift in wind direction caused the displacement of mooring line 1 to increase resulting in a greater tensile force. Notwithstanding this increase in tension of fairlead 1, it is mooring line 2 that has the largest tensile force. Increasing from 5.37E+06 N for the 50-year load to 2.38E+07 N for the Misal hurricane load. The greater loads from the hurricane conditions compared to the 50-year extreme conditions is because of the greater wind speed for the hurricane conditions, from Table 6.11 the 50-year wind speed is 47.0 m/s and the hurricane wind speed is 87.3 m/s. The force emitted on the blades and the rest of the wind turbine system are therefore greater for the hurricane wind case. In Chapter 2, equation 2.4.1 shows that the power varies according to the wind speed cubed. The power on the turbine would therefore be due to the cube of the 87.3 m/s wind speed for the hurricane case and the cube of 47.0 m/s for the 50-year case. This explains the significantly greater forces for the hurricane loads.

Impact of the hurricane conditions on the minimum breaking load (MBL) of the mooring line. It should be noted that both the 50-year and the hurricane case result in a drastic increase in the tension in the fairlead when compared to the Rated case. Therefore, the mooring line has to be checked to ensure that it is able to withstand these increased loads. To do this, the minimum breaking load (MBL) is computed to make sure it is not exceeded. For the Rated case, the tension in fairlead 2 is 2.11E+06 N, therefore the 50-year value of 5.23E+06 N, is 2.5 times the Rated case. The factor of safety (FOS) of the mooring line is the ratio of the minimum breaking load (MBL) to the fairlead tension (where the fairlead tension is multiplied by a load factor of 1.35 to get the ultimate load as per DNV (2010*a*)). The MBL from Table 6.10 is 8.96E+06 N. The FOS on the mooring line for the 50-year is found to be 1.27. This is less than the required factor of safety for survival conditions of 1.80 (Chryssostomidis & Liu, 2011). To get the required FOS, the mooring line diameter or the grade of steel (or both) should be increased. If the diameter is increased from 100 mm to 125 mm the MBL of the mooring line is 13, 228 kN. This gives a FOS of 1.87, which is greater than the required FOS of 1.80. The Misal hurricane load results in even more severe conditions

on the mooring line. For the MBL to not be exceeded and the FOS satisfied, both the grade of steel and the mooring line diameter are modified. A very high steel grade, say with a c value of 32, is required, together with a mooring line diameter of 350 mm. The MBL of this mooring line is 62,720 kN and the tension of fairlead 2 is 23,800 kN. This gives a FOS of 1.95, which is greater than the required FOS of 1.80. This demonstrates that the mooring line loads can increase significantly in the event of a hurricane. This puts the offshore wind turbine at risk.

It can be seen from the response of the turbine to category 5 hurricane loads, relative to the extreme 50-year loads that the moments on the blade, the side-side moments at the base of the tower and the tensions in the fairleads are critical for the design of a FOWT in the most severe hurricane conditions that affect the Caribbean.

Proposed estimating of the category 5 hurricane wind speed using EVA. The category 5 hurricane loads being greater than the 50-year extreme loads indicate that wind turbines in the Jamaica Caribbean Sea should be designed for wind speeds greater than the 50-year return period that is recommended by the wind turbine design manuals. The 50-year EVA wind speed is equivalent to a category 1 hurricane. To get a value that closer equates to a category 5 hurricane, the EVA wind speed has to be computed for a higher return period. This was carried out and it was discovered that at least a 450-year return period would be required to produce a wind speed equivalent to category 5 hurricane winds. In this case, a wind speed of 87.3 m/s. This is a factor of 1.86 times the 50-year EVA wind speed of 47 m/s. Therefore, in the absence of LES data, hindcast data and EVA can be used to estimate the hurricane loads in the JCS. This can be done by altering the return period until a wind speed equivalent to the required hurricane category (4 or 5, say) is obtained. The corresponding hurricane sea state can be estimated using equation 6.3. This approach is not as sophisticated as LES but would provide a preliminary estimation of the structural and dynamic response of a FOWT system before more sophisticated methods, which would be more numerically expensive, are used to refine the design.

6.8.5 DeepCwind FOWT in Idle vs Standstill conditions, hurricane loads.

So far, the turbine has been investigated in a hurricane when it is set to idle i.e., allowed to rotate. If the turbine is set to the standstill condition, that is, not allowed to rotate, Kim & Manuel (2014) argued that some of the loads on the wind turbine system could vary. The turbine is set to the standstill condition for the respective hurricane load cases and responses of the FOWT system during idle and standstill conditions compared. Some of the loads are similar for both the idle and standstill conditions. However, there are some loads that are greater for the standstill condition when compared to the idle condition. If we look at Figures 6.19 to 6.21 and 6.13, we see that the blade out of

plane tip deflection can be as much as 3.5 times greater for the standstill condition. In addition, the side-side moment at the tower base, can be as much as twice the amount that is produced in the idling case. This indicates that a FOWT should be modelled for both idle and standstill criteria to determine the worst case scenario when hurricane conditions are considered.

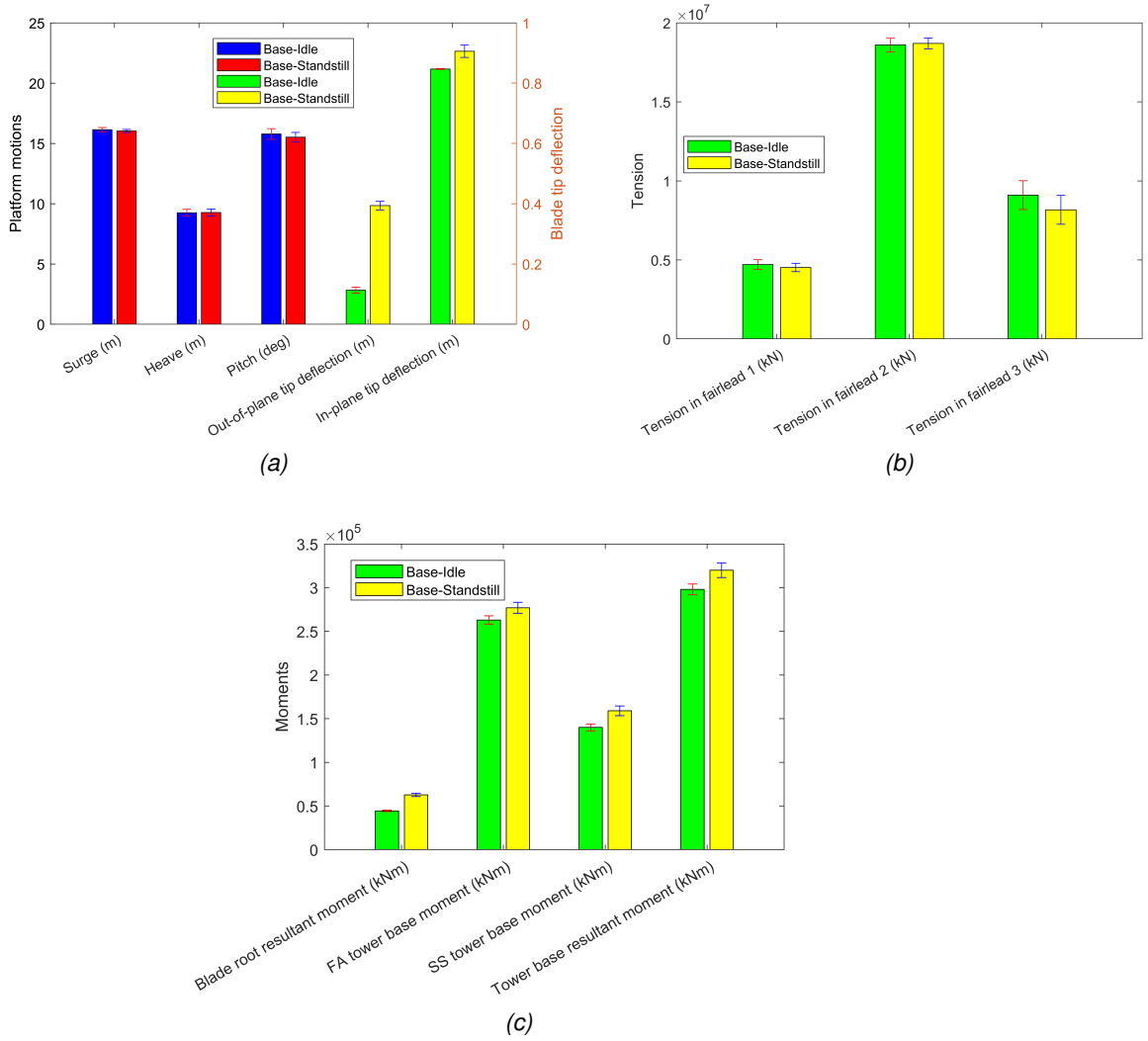

Figure 6.19: FOWT wind turbine response for standstill vs idling conditions. Base Case: a) Platform motions and blade tip deflections (b) Tensions in fairleads (c)Bending moments.

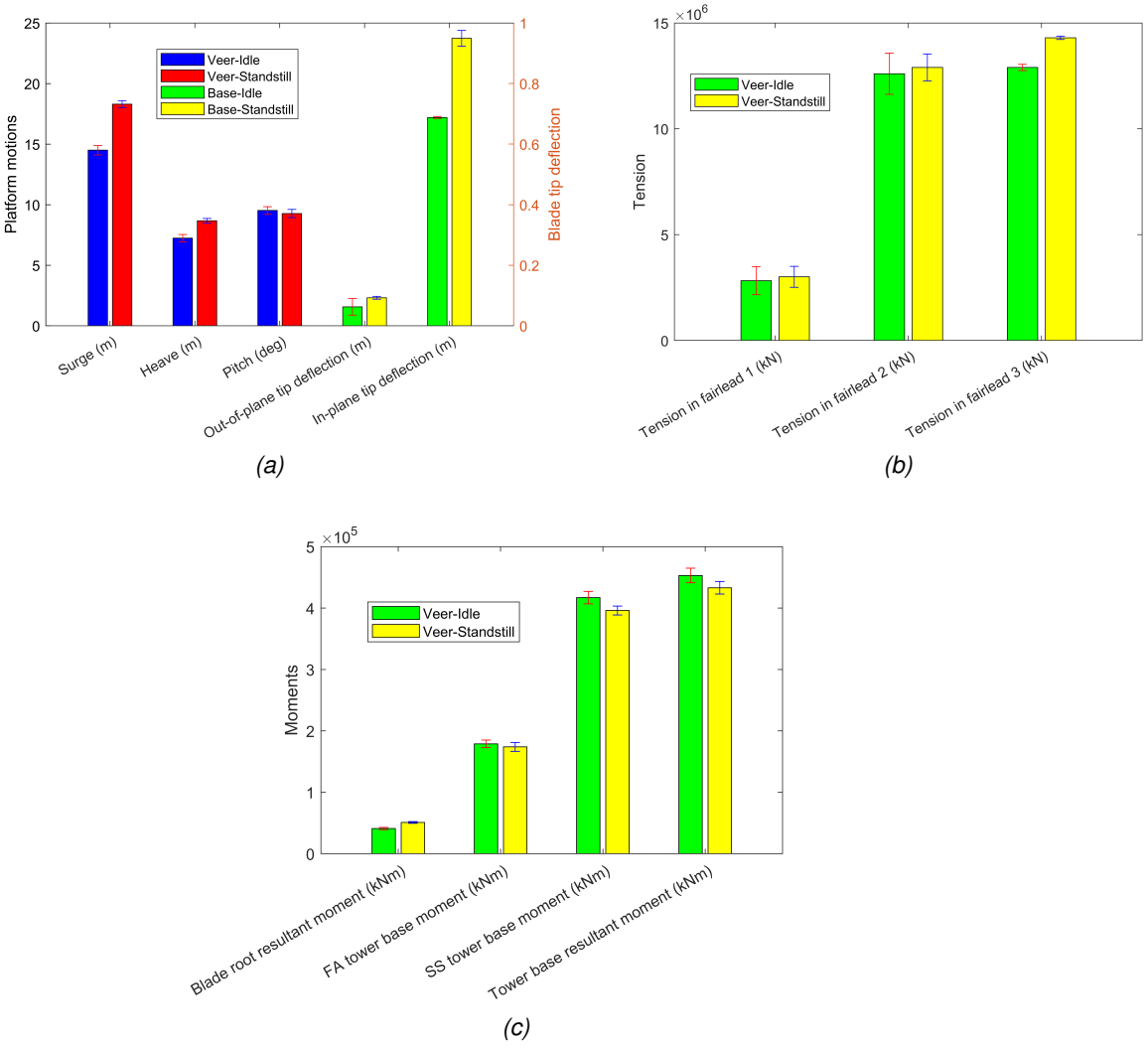

Figure 6.20: FOWT wind turbine response for standstill vs idling conditions. Veer Case: a) Platform motions and blade tip deflections (b) Tensions in fairleads (c)Bending moments.

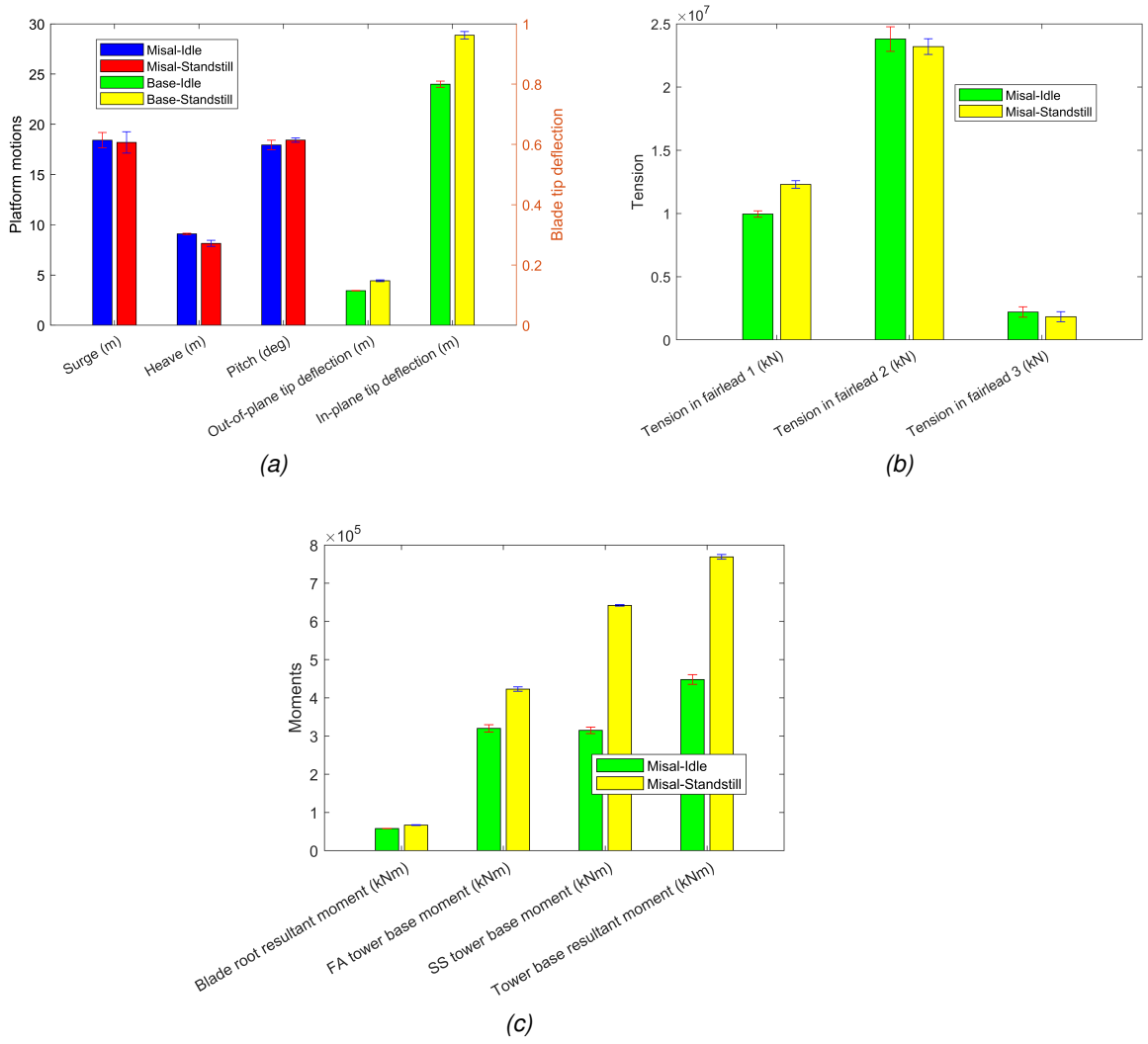

Figure 6.21: FOWT wind turbine response for standstill vs idling conditions. Misal Case: a) Platform motions and blade tip deflections (b) Tensions in fairleads (c)Bending moments.

Table 6.13: Response of DeepCwind FOWT in the JCS to Category 5 Hurricane Winds: a) Base b)Veer c) Load Cases - Idle vs Standstill Conditions

Property	Base-Idle	Base-Standstill	Scale Factor, SF (= Standstill/Idle)	Veer-Idle	Veer-Standstill	SF (= Standstill/Idle)	Misal-Idle	Misal-Standstill	SF (= Misal/E50-year)
Surge (m)	16.14	16.03	0.99	14.50	18.30	1.26	18.42	18.2	0.99
Heave (m)	9.25	9.27	1.00	7.24	8.67	1.20	9.09	8.15	0.90
Pitch (deg)	15.78	15.51	0.98	9.52	9.27	0.97	17.94	18.43	1.03
Out-of-plane blade tip deflection (m)	2.83	9.84	3.48	1.57	2.31	1.47	3.44	4.43	1.29
In-plane blade tip deflection (m)	21.17	22.65	1.07	17.22	23.73	1.38	23.99	28.87	1.20
Tension in fairlead1 (N)	4.71E+06	4.52E+06	0.96	2.83E+06	3.01E+06	1.06	9.96E+06	1.23E+07	1.23
Tension in fairlead2 (N)	1.86E+07	1.87E+07	1.01	1.26E+07	1.29E+07	1.02	2.38E+07	2.32E+07	0.97
Tension in fairlead3 (N)	9.10E+06	8.17E+06	0.90	1.29E+07	1.43E+07	1.11	2.21E+06	1.84E+06	0.83
Blade root resultant bending moment (kNm)	4.44E+04	6.28E+04	1.41	4.11E+04	5.10E+04	1.24	5.80E+04	6.70E+04	1.16
FA tower base moment (kNm)	2.63E+05	2.77E+05	1.05	1.79E+05	1.74E+05	0.97	3.20E+05	4.23E+05	1.32
SS tower base moment (kNm)	1.40E+05	1.59E+05	1.14	4.17E+05	3.96E+05	0.95	3.15E+05	6.42E+05	2.04
Tower base resultant moment (kNm)	2.98E+05	3.20E+05	1.07	4.53E+05	4.33E+05	0.96	4.48E+05	7.69E+05	1.72

6.9 Conclusion

The purpose of this chapter is to extend the work done in chapter 5 beyond the 50-year extreme loads that are recommended by the wind turbine design manuals, to also include the extreme conditions caused by hurricanes. This is because, the JCS is prone to hurricanes and those hurricanes can create more extreme conditions than those experienced in regions such as the North Sea. The wind turbine design manuals were developed using data from regions like the North Sea, a region that usually experiences winter storms and where hurricane conditions are non-existent. The 50-year return period stipulation was arrived at using data from this same region. It is shown that the 50-year extreme value analysis (EVA) results in the JCS is equivalent to a category 1 hurricane and Jamaica has experienced hurricanes as high as category 4. The FOWT system is assessed under category 5 hurricane conditions derived from a LES model. The hurricane conditions are for the FOWT system positioned 12 km from the hurricane centre. It is demonstrated that the floater and structural responses of the idle FOWT in hurricane conditions is greater than the responses for the 50-year extreme load conditions. For example, the blade root moment under hurricane conditions, can be as much as 8 times that for the 50-year conditions; and the side-side moment at the base can be 16 times the value for the 50-year conditions. This side-side moment is even greater if the turbine is in the parked-standstill mode. It is further shown that the tension in the fairleads can increase tremendously under hurricane conditions, causing the mooring line to exceed its MBL. A mooring line consisting of a higher-grade material (for example, steel of c value 32) and a large diameter (350 mm) is required to withstand the most severe hurricane conditions. A FOWT system that is exposed to these severe conditions is at a greater risk of damage. A system that is more resistant to such high category hurricanes would be appropriate for the JCS.

In the absence of LES models with hurricane chracteristics, hindcast data and EVA can be used to estimate the hurricane wind speed and sea state that a FOWT in the JCS would experience. The 50-year extreme wind speed obtained for the JCS by EVA is equivalent to a category 1 hurricane. To get a wind speed that equates to the highest category hurricane in the JCS, EVA is used but for a higher return period than 50 years. It is shown that a return period of 450-years gives a wind speed that is equivalent to the category 5 hurricane that can be expected in the JCS. The hurricane sea state is estimated using the hurricane wind speed. It is demonstrated that the 50-year wind speed times a factor of 1.86 gives the category 5 hurricane wind speed. This factor is only for one area in the JCS, further checks are needed to determine if this holds true for other locations.

A turbine that is designed to satisfy the hurricane conditions in the JCS needs to be

more robust to achieve the required factors of safety. However, there must be a balance between risk tolerance and economic viability. Although a FOWT system can be designed to be resistant to a 450-year return period wind speeds (that is the strongest hurricane, say, that could occur in a region), it may not be financially feasible. Further work would be required to determine, the highest category hurricane that can be designed for in the JCS that fulfills the criteria of achieving technical soundness while being economically viable.

An importance criteria is required in the design of FOWT systems. In the design of building structures, for example, the importance of the structure determines the magnitude of the risk factors that are applied. This done by using what is called an importance factor. Depending on the importance of the structure the design requirement could be to ensure that lives are not lost and hence the building should not collapse. However, there are structures, for example hospitals, that are of greater importance. The requirement for those structures would be that the building experiences as minimal a downtime as possible after a natural disaster. These buildings would be designed for higher return periods. A similar type of importance criteria is required for FOWT structures in hurricane regions. In this case, the kind of importance that is placed on a FOWT system has to be determined. It is very unlikely that persons would be at the location of the FOWT during a hurricane and hence the risk of loss of life is non-existent. Therefore, the importance of such a structure would not be based on lives lost but how critical it is to the supply of power in a region. If the power from the FOWT system is required to supply a hospital with power, it would be considered to have a high importance factor. In that case, clients and by extension designers would want the wind turbine to experience as little downtime as possible after a natural disaster. However, in the final analysis, there would still be a balance between the magnitude of the risk factor and the economic viability.

It must be mentioned that the matter of designing a wind turbine for hurricane conditions is one that still requires considerable research. A holistic approach should be taken to design a wind turbine in regions that are susceptible to hurricanes. Researchers are taking this approach as they seek to gain better understanding about this area.

Chapter 7

Conclusion and Recommendations

7.1 Conclusion

THe purpose of this study is to investigate if a FOWT in the Scottish North Sea (SNS) can be used off -the-shelf in the Jamaica Caribbean Sea (JCS). To the best of the authors knowledge this is the first time that the behaviour of a floating offshore wind turbine (FOWT) is investigated using the environmental conditions in the JCS. It is also the first time that the extreme sea and wind conditions (50-year return levels) in the JCS is determined using extreme value analysis and the environmental contour method. In addition, it is the first time that hurricane wave height data of the JCS is used to determine the extreme sea state using multivariate EVA. Furthermore, the utilization of hindcast data for the JCS to determine extreme sea and wind conditions was not found in the literature. There are numerous studies that have been carried out to determine the extreme sea and wind conditions, for example, in the United States and Europe but no work is found in the literature where hindcast data is used to determine the extreme sea and wind conditions in the JCS. While there are works investigating the behaviour of a FOWT in the North Sea, for example, there is no work found in the literature which compares the behaviour of a FOWT in the North Sea with the behaviour in the Jamaica Caribbean Sea. Neither is any literature found that specifically compares the normal and extreme wind and sea conditions of the North Sea with the Caribbean Sea. Further, the behaviour of a FOWT or even a fixed-bottom wind turbine has not been investigated using the hurricane conditions of the JCS. Liu et al. (2022) investigated the dynamic performance of the VolturnUS-S 15 MW FOWT under typhoon conditions but the extreme wind values were determined using the American Petroleum Institute (API) and IEC 61400-1 codes. This work in the JCS uses hurricane wind values which are found to be more extreme than the 50-year wind conditions stipulated in the wind turbine design standards. Instead of using extreme data that have been developed for other jurisdictions, it develops extreme environmental data that characterizes the conditions in the JCS. Before now, a FOWT study to determine extreme sea states using hindcast data from the JCS was non-existent. However, this extreme environmental data can be used as a basis for carrying out further studies on wind turbines within the JCS.

To carry out this FOWT study, the first thing that was done is to determine the environmental conditions in the SNS and the JCS. Extreme value analysis (EVA) was used to determine the 50-year extreme sea state (H_s and T_p) and extreme wind speed (50-year) at both locations. The 50-year wind speed is determined by univariate EVA, in which the GEV model is used to fit 40 years of hindcast data at both locations. The sea state was determined using multivariate extreme value analysis, in which statistical distributions are fitted to hindcast data of H_s and T_p. The distribution parameters are then extrapolated to determine the n-year return levels of Hs and Tp. It is discovered that the Weibull-3P model together with a lognormal distribution fitted the data in the SNS well. However, the data in the JCS was not well suited for the Weib3P lognormal model. In fact, the JCS data was separated in two categories; the first category contained data during the normal season and the second category contained data for the hurricane season. The Weib3P lognormal model fitted the normal season data well. However, this model did not fit the hurricane season data well and H_s 50-year was underestimated.

Referring to Haver & Winterstein (2008), it is recommended that a GPD model could be used to fit the peaks of Hs > h_o where the data is from a region that is affected by hurricanes. However, the fit of the GPD to the hurricane season data for the JCS using this methodology did not yield good results. Therefore, the approach to use the EVA/ECM method to fit to hurricane wave heights. The problem here is to get sufficient wave heights to fit the distribution models. The data is obtained using a tool called HURWave which was developed by Banton (2002) at Delft University of Technology. The tool is used to predict hurricane wave heights in the JCS, creating a sufficient dataset to fit the Weib3P model. The fit is satisfactory and hence the Weib3P lognormal model is used to determine the extreme sea state for the JCS. In summary the primary findings when carrying out EVA are:

- The Weib3P lognormal model does not fit the data from the JCS very well as the data consist of a mixture of predominantly normal sea state data and a balance of sea states that are due to hurricanes.
- The Weib3P lognormal model fits the hurricane wave data from the JCS well.
- The environmental data from the SNS and the JCS appear to be quite similar during normal sea conditions. This is also true for the 50-year sea state data. Hs 50-year for the JCS is 11.17 m and Tp 50-year is 11.22 s. Hs-50 year for the SNS is 10.41 m and Tp 50-year is 14.27 s.

The VolturnUS-S FOWT model is used to assess the responses of a FOWT system in normal sea and wind conditions and extreme sea and wind conditions of the JCS and

the SNS. TurbSim is used to model the turbulent wind field and OpenFAST is used to model the FOWT. It is shown that the response of the FOWT in the SNS and the JCS are the same under normal sea and wind conditions. However, for extreme sea and wind conditions, the responses within the JCS are predominantly greater. In particular, the following responses of the FOWT in extreme sea and wind conditions are much greater in the JCS than the SNS:

1. The platform surge in the JCS is 1.2 times the surge in the SNS
2. The platform pitch in the JCS is 1.7 times the pitch in the SNS
3. The fairlead tension in mooring line 1 (mooring line in the direct path of the incoming wave, see Fig 5.1) in the JCS is 1.4 times the tension in the SNS
4. The fore-aft moment at the tower base for the JCS is 1.5 times the moment in the SNS
5. The tower base resultant moment in the JCS is 1.4 times the moment in the SNS

The most extreme conditions for the JCS occur during hurricanes and therefore, category 5 hurricane wind data from a LES model given by Worsnop et al. (2017) is used to simulate hurricane wind fields. The related hurricane significant wave height is determined using a methodology proposed by Ochi (1993b). The responses of NREL's 5MW reference wind turbine on the DeepCwind floater in hurricane sea and wind conditions are compared to the responses from the 50-year sea and wind conditions. The findings are as follows:

- For all FOWT turbine responses that are assessed, the hurricane load conditions resulted in greater response than the 50-year extreme conditions stipulated in wind turbine design manuals
- The blade root moment for the hurricane conditions can be as much as 8 times the blade root moment for the 50-year extreme conditions
- The side-side moment at the base for the hurricane conditions can be as much as 16 times the value for the 50-year extreme conditions
- The tension in the mooring line 1 for the hurricane conditions can be as much as 16 times the value for the 50-year extreme conditions.
- The tension in the fairlead due to hurricane conditions can cause the minimum breaking load (MBL) of the mooring line to be exceeded. In particular, for mooring line 2 (seperated from mooring line 1 by 120 degrees in clockwise direction),

which experiences the largest tension, a very large diameter (350 mm) and very high steel grade (grade dependent constant, c, value of 32) mooring line are required to withstand the hurricane loads.

- The wind turbines in the JCS should be designed for greater wind speeds than the 50-year wind speeds stipulated in the wind turbine design manuals.
- The blades, the steel tower and the mooring lines are affected greatly during hurricanes and these should be sized such that they are hurricane resistant
- The 50-year wind speed recommended by wind turbine design manuals is equivalent to a category 1 hurricane in the JCS. This is the lowest category hurricane that is experienced. Jamaica has previously experienced category 4 hurricanes.
- The 50-year EVA wind conditions can be scaled up to category 4 and 5 hurricane winds, by computing the 450-year return levels. Multiplying the 50-year wind speed by a factor of 1.86 yields the category 5 hurricane wind speed. The related hurricane sea state can be determined from this wind speed. This is a crude method of a using hindcast data to estimate hurricane wind and sea data in the absence of LES simulation model data.
- When the standstill parking conditions are considered there are some loads on the FOWT which are greater than the idle parked conditions. For example, the blade tip deflection can be 3.5 times the value for the idle parked condition and the side-side moment at the base can be twice the value for the idle conditions. Therefore, the turbine should be simulated for both idle and standstill parked conditions during a hurricane.
- Notwithstanding that hurricane conditions require a FOWT to be more robust than extreme 50-year conditions stipulated in wind turbine design manuals, a balance between economic and technical viability should be reached. It appears as if this 50-year condition that is set in wind turbine design manuals is what achieves this balance in the North Sea (Myers et al., 2013). A balance has to be found for the hurricane conditions in the JCS, as designing to withstand category 5 hurricanes may not be economically viable.
- A FOWT in the most severe hurricane conditions of the JCS would be at a greater risk of damage than one in the 50-year extreme conditions of the SNS. Therefore, a more robust FOWT system would be appropriate for the JCS.

7.2 Recommendations

There are some limitations with the current study and on this basis a number of recommendations are made:

1. A multivariate EVA can be used to determine the 50-year wind speed values by considering a joint distribution of H_s and wind speed. A univariate EVA process was used to determine the 50-year wind speed. The most sophisticated assessment, though, would be to use of three variables, H_s, T_p and wind speed together to determine the 50-year H_s, T_p and wind speed.

2. The data used for the hurricane sea state was determined using the HURWave tool. It is thought that maybe another tool could be investigated that gives more adequate hurricane wave data to fit a distribution model.

3. The LES model data for the category 5 hurricane was obtained from Kapoor et al. (2020), a LES model of lower category hurricanes could be developed to investigate the effects on a FOWT system.

4. The FOWT system investigated for hurricane loads was NREL's 5 MW baseline wind turbine. This is due to a limitation in the extent of the LES simulation data that was obtained from Kapoor et al. (2020). The larger FOWT system, VolturnUS-S was too large to fit in the size of the LES domain. A larger FOWT system in the hurricane conditions of the JCS should be considered.

5. The turbine tower and blades should be investigated in a design tool to determine the optimum thickness that would be required to withstand category 5 hurricane conditions

6. The cost of the selected FOWT system in hurricane conditions should be determined to investigate economic viability. It is believed that there is a limiting category of hurricane for which a FOWT in the JCS should be designed and beyond this category, a FOWT system is no longer economically viable.

7. The wind and wave were acting in the same direction. Further work could include carrying out the same analysis but for wind and wave misalignment

8. There was no LES model available to simulate the winter storm conditions in the SNS. This would have made the comparison with the JCS hurricane conditions more complete.

9. OpenFAST uses potential flow theory and is therefore a potential flow solver. Yang et al. (2023) argued that potential flow based engineering tools can underpredict by more than 10 % extreme and fatigue loads, because they do not take

into account non-linear behaviour that exist at lower frequencies. Therefore, this analysis should be conducted using a computational fluid dynamics (CFD) solver as some of the extreme loads on the model could be higher than those predicted by OpenFAST. However, it is known that high-fidelty solvers such as CFD are computationally expensive and require significant computer time as compared to potential flow solvers. The CFD solvers also need to be tested against experimental results (Otter et al., 2022).

Appendix A

The History of Offshore Wind

A.1 Brief overview of the history of offshore wind

THe use of wind energy dates back to more than 2,000 years ago when it was used to power sailboats. The use of wind turbines date back to the 1st century AD in which a wind wheel was used to power a machine. This technology was developed by a Greek engineer (Shahan, 2014). Between the 7th and 9th century AD wind power was used for practical activities such as the grinding of corn and flour and the pumping of water. By 1,000AD, windmills were used for pumping seawater to make salt in China and Sicily; and in the 1880s, vertical windmills were first used for grinding flour in Northern Europe.

In 1887, the first wind turbine used to produce electricity was developed in Scotland. This was done by Professor James Blyth of Anderson's College, Glasgow (which is today known as the University of Strathclyde). This cloth-sailed wind turbine was used to power Blyth's holiday cottage (the first house in the world to be supplied with electricity from wind turbines) and generated enough power to supply the streetlights with electricity. The following year, in the United States of America (USA), the first wind turbine for the production of electricity was developed by inventor Charles Brush. It was a 12kW slow speed, high solidity wind turbine (Kaldellis & Zafirakis, 2011) and provided electricity to his home in Ohio.

In 1891, an electricity-generating wind turbine was developed by Danish scientist, Paul La Cour. This included the development of the technology to supply a steady stream of power from the wind turbine by use of a regulator. In 1895, La Cour developed a prototype electrical power plant from the wind turbine. The electricity from the plant was used to provide lighting for a village in the urban area called Askov. By 1900, 2,500 windmills with a combined power of 30MW were used (in Denmark) for mechanical purposes such as the grinding of grains and pumping of water. This could be classified as one of the first wind farms.

In 1927, the brothers Joe and Marcellus Jacobs developed a wind turbine-manufacturing factory in Minneapolis, Minnesota, USA. The wind turbines were used primarily used to charge batteries and power streetlights, as the technology to use wind turbine to

supply power to the electrical grid was not yet developed. In 1931, a French aeronautical engineer, George Jean Marie Darrieus developed and patented a vertical-axis wind turbine. In the same year, a horizontal axis wind turbine was developed in Yalta, a resort city off the south coast of Crimea. This turbine was 32m high and had a capacity of 100 kW and load capacity of 32%.The technology for the horizontal axis wind turbine was perfected by the Germans in the 1960s (Kaldellis & Zafirakis, 2011).

The connection of a wind turbine to the electrical grid first occurred in 1941. It was a Smith-Puttman wind turbine in Castleton, Vermont, USA. The turbines had a capacity of 1.25MW and length of 75 feet. This was the genesis of MW sized wind turbines. In 1957, Jacobs Wind produced and sold about 30,000 wind turbines, this included customers in Africa and Antarctica (Shahan, 2014). In addition, Johannes Juul, a former student of Paul La Cour developed a 3-bladed horizontal axis wind turbine. It was a 20kW turbine, which employed a new technology, aerodynamic tip brakes. This turbine formed the basis for the 3-bladed wind turbines that are in use today.

In 1975, The National Aeronautics and Space Administration (NASA) established a program to develop utility scale wind turbines (Shahan, 2014). In 1980, the first wind farm was put on the electrical grid. It was located in New Hampshire, USA, had a capacity of 0.6MW, and consisted of 20 turbines (www.awea.org/wind-101/history-of-wind/1980s). In this same year, Denmark started siting offshore wind turbines. In addition, Zond (later known as GE Wind Energy) was established; Danregn Vindcraft (later known as Bonus Energy and eventually Siemens Wind Power) was formed; and Enertech began to make 1.8kW turbines that connect to the electrical grid.

In 1981, US established their second wind farm with a capacity of 10MW; this generated enough power for approximately 8,575 homes. In this same year, the first European wind farm was established on the Greek island of Kythnos. It had a capacity of 100MW and consisted of 5.0 x 20kW turbines. Wind turbine development in the US continued and between 1982 and 1984, 27 wind turbines were established with the capacity to power 286,500 homes. In 1984, Enercon became Germany's largest wind turbine manufacturer and Vestas, out of Denmark started production of 75kW three-bladed turbines.

In 1986, a nuclear reactor exploded in Chernobyl, Ukraine (Brennan, 2019). This accident resulted in the loss of many lives and to date there is still uncertainty about the number of people who died because of this disaster. A report by the UN Scientific Committee stated that 54 persons died, including those who died afterwards because of trauma and radiation. A Chernobyl Forum Group consisting of representatives from the nuclear energy sector, UN and related governments reported that 4,000 to 9,000 persons had died considering cancers that were caused due to environmental impacts

afterwards. The Union of Concerned Scientists reported that 27,000 persons died including those who died of cancer and the environmental group, Greenpeace, proposed that over 200,000 persons had died. The UN estimated that 3.5million people were affected and about 20,000 sq. miles of land (Croatia is 21,851 sq. miles and Jamaica is 4,244 sq. miles) was contaminated.

In 1987, NASA developed a 3.2MW wind turbine with the first large-scale drivetrain and a sectioned two-bladed rotor allowing for easier transportation. In 1988, two years after the disaster in Chernobyl, the Danish government passed a law abolishing the construction of nuclear power plants (Wind-Europe, 2019). In 1989, Danish Bonus Company started production of 450kW three-bladed turbines with a 35m rotor diameter.

The period of the first and largest wind farms, and the birth of the offshore wind farm (1990 to 1996) In 1990, Europe's largest wind farm was installed in Jutland, Denmark. It consisted of 42 x 300kW Nordtank turbines. In 1991, the first offshore wind farm in the world was constructed in Vindeby, off the southern coast of Denmark. It consisted of 11 x 450kW Bonus energy wind turbines. In this same year, the first onshore wind farm was constructed in the United Kingdom (UK), in Delabole, Cornwall. It consisted of 10 x 400kW wind turbines and had the capacity to power 2,700 homes. In addition, a wind farm was installed on Sijiao Island, off the Shanghai coast of China. It consisted of 10 x 30kW wind turbines. In 1992, UK constructed its first wind farm to supply power to the electrical grid. It was a 1.1MW wind farm located in Haverigg Hill, Cumbria. In addition, the first Spanish wind farm was established in Tarifa, Andalusia. In 1993, the largest wind farm in Europe was constructed in Llandinam, Wales. It consisted of 103 x 300kW Mitsubishi wind turbines. In 1994, France installed its first wind farm in the Tramonte wind corridor. It consisted of 4.0 x 500kW Vestas wind turbines. In 1995, Vestas produced its first offshore wind turbine and Suzlon Energy was established in India to manufacture, install and operate wind turbines. In 1996, Iran, the fifth largest oil producer in the world, created its first wind farm. It consisted of 300kW Nordtank turbines. It should be stated that the developments in wind energy was also taking place in the developing world and India reached 800MW of wind energy in 1996. The development of wind energy in India was driven by the need to reduce CO2 emissions into the atmosphere and to reduce the dependence of fossil fuels as their primary source of energy (Sharma & Sinha, 2019).

In 1997 (10 years after the publication of Our Common Future) the UN, Koyoto Protocol was adopted in Japan on December 11, with a target to reduce GHG emissions by 5% of their 1990 levels by 2012 (UNFCC, 2019). The second commitment period, was adopted in Doha, Qatar on December 8, 2012. In this period, Parties committed to reduce GHG emissions to 18% below 1990 levels in the eight-year period from 2013

to 2020. In this same year, the European Union (EU) set a target to increase the amount of electricity that was produced from renewables, from 14% to 22% by 2020. In addition, new firms continued to be created to produce wind turbines. Enron acquired Zond and German wind turbine manufacturer Tackle; while Nordtank Energy Group and Micon of Denmark, merged to form NEG Micon.

In 1998, the Chinese firm Goldwind was formed to manufacture wind turbines. In the year 2000, 97 wind farms were established in the US providing enough power for up to 592,000 homes. In this same year, the first of five offshore 150MW wind power demonstration projects, went to tender in Denmark. In addition, the first large-scale offshore wind farm, Middelgrunden, was constructed off the coast of Copenhagen. The wind farm consisted of 20 x 2MW Bonus Energy wind turbines.

In 2002, the Horns Rev wind farm was established in the Danish North Sea. It consisted of 80 x 20MW Vestas wind turbines. In addition, Alaiz wind farm was established in Spain. In this same year, General Electric (GE) purchased both the US and EU bases from Enron Wind Corp. GE went on to become the # 1 wind turbine manufacturer in the world by 2012. In 2003, Vestas and NEG Micon merged to form the world's largest wind turbine manufacturer, called Vestas. In addition, the UK commissioned its first offshore wind farm in North Hoyle, Wales. It consisted of 30 wind turbines each with a capacity of 2MW.

In 2004, Siemens purchased Bonus Energy of Denmark and became the fifth largest wind turbine manufacturer in the world. In this same year, the German turbine manufacturer Repower installed a prototype 5MW wind turbine and the Danish blade manufacturer LM Glasfiber produced its longest wind turbine blade. The blade was 61.5m long. In 2005, Siemens started installing its 3.75MW turbine.

In 2006, France set a target to make twice as much wind power compared to nuclear and coal generated power over the following 10 years. In 2007, the largest wind turbine, a 7MW Enercon E126 was installed in Embden, Germany. In 2008, there were almost 2,000 wind farms in operation in the UK. These wind farms produced electricity for 1.5million homes, which is 7% of the homes in the UK (UKSTATS, 2010). In this same year, the UK identified nine (9) zones for the development of 25GW of wind farms.

The birth of floating offshore wind turbines (2009) In September 2009, Statoil (now called Equinor) started the operation of the first large capacity floating wind turbine off the coast of Norway. This wind farm was called Hywind. It consisted of a spar type floater supporting a 2.3MW Siemens wind turbine. It should be noted that up to this point only fixed-bottom offshore wind farms were being installed. The monopile was the predominant foundation type. In this same year, The US installed the world's largest onshore wind farm in, Rascoe, Texas. It consisted of 634 wind turbines with an overall

capacity of 781.5MW. It should be noted that up to this point only onshore wind farms were being developed in the US.

In 2010, ten (10) North Sea countries (Belgium, Denmark, France, Germany, Ireland, Netherlands, Norway, Sweden, Luxembourg and the UK) agreed to work together to develop an offshore electricity grid. This North Sea offshore grid would serve to interconnect wind power systems in Northern Europe and to connect offshore wind power to onshore wind power systems (Gorenstein Dedecca and Hakvoort, 2016). In addition, in 2010, China surpassed the US and became the country with the most cumulatively installed wind capacity in the world.

Floating offshore wind turbine projects continued to gather momentum (2011) In March 2011, the Fukushima nuclear plant failure occurred in Fukushima, Japan. In this same year, Japan had planned to construct a multi-unit floating wind farm. The wind farm would consist of six (6) wind turbines, each with 2MW of capacity. The country has also planned to have up to 80 floating wind turbines off the coast of Japan by 2020. This represented a policy shift by the Japanese government to focus on the development of renewable energy, this included offshore wind energy (Carbon-Trust, 2019). In addition, as a result of the disaster Germany took a policy position to shut down all nuclear power plants by the year 2022 and to double the amount of energy that comes from renewables, including wind energy (Wind-Europe, 2019*a*). Wind turbine technology continued to improve and rotors went up to a diameter of 126m and wind turbines got up to a capacity of 7,500kW. This is 100 times the capacity of a wind turbine in the 1980s. Two years after the installation of the Hywind, another floating offshore wind-turbine demonstration project was launched by Principle Power in Portugal. This project was called WindFloat and consisted of a semi-submersible floater supporting a 2MW wind turbine.

In 2012, the US installed the world's largest wind farm, The Alta Wind Energy Centre in California. It had a capacity of 1,320MW. In this same year, the world's largest offshore wind farm was established off the coast of Cumbria, England. It had a capacity of 367MW.

In 2013, the London Array became the largest offshore windfarm in the world. It consisted of 175 x 3.6MW wind turbines, a capacity of 630MW. This was practically twice the capacity of the Cumbria offshore wind farm. In this same year, wind power became the third largest source of energy in China, more than nuclear power.

In December 2015, the United Nations Framework Convention on Climate Change (UNFCC) adopted the Paris agreement. This is a universal agreement, which aims to keep the global rise in temperature for this century well below 2.0 ℃, with the goal to drive efforts to limit the temperature rise to 1.5 ℃ above pre-industrial levels (IPCC,

2018). This agreement brought into clearer focus the effects of climate change. In this same year, a number of companies started to use wind energy to provide power for their daily operations (Wind-Europe, 2015). The companies include, BMW, General Motors, CEMEX, Heineken, LEGO, IKEA, Facebook, Google, Amazon, Apple and Microsoft. In addition, IKEA made a commitment of 1 billion Euros to wind and solar development and climate action.

In 2016, the US installed its first offshore wind farm, off the coast of Block Island, Rhode Island (www.awea.org/policy-and-issues/u-s-offshore-wind). It was a 30MW wind farm, which consisted of 50 x 6MW Alstom Haliade 150 turbines. At the end of 2018, this was still the only commercially operating wind farm in the United States.

Commissioning of the world's first floating offshore wind farm (2017) In 2017, Denmark reached a milestone as wind energy had the capacity to cover their entire power demand on 22nd of February. In addition, the world's first floating wind farm, Hywind Scotland was commissioned on 18th of October 2017. The wind farm consisted of 5.0 turbines each with a capacity of 6MW. In this same year, the longest wind turbine blade in the world is produced by LM Wind Power. The blade was 88.4m long and created for an 8.8MW offshore turbine.

In 2018, it was announced by the Netherlands that the first operational offshore wind farm without subsidies is to be built. The 700MW wind farm, the Kust Zuid (I & II) is to be built by Vattenfall and should be fully commissioned by 2022. In addition, the world's largest operational offshore wind farm, Orsted's Walney Extension, was built in the Irish Sea. It was an 87-turbine wind farm, had a capacity of 695MW and was able to power nearly 600,000 homes (https://walneyextension.co.uk/About-the-project#0). It surpassed the London Array as the largest operational offshore wind farm. In Germany, Mercedes-Benz made the first corporate power purchase agreement (PPA) for wind farm power of 46MW.

The aim of this discourse is to answer the question, why wind energy. It is shown that wind energy is a mature technology. Improvements in the technology being made from windmills of AD1 to the first onshore wind farm connecting to the grid in the US in 1980; the first fixed-bottom offshore wind farm in 1991, in Denmark, and the early stages of the development of a floating offshore wind farm by Equinor in September 2009. In addition, wind turbine manufacturing companies have evolved over the years and the wind turbines have grown from kW capacity turbines to MW capacity turbines of larger rotor diameters and blade length. Three important factors have driven the development of wind energy. Two of them were already mentioned. The three factors are, the climate change effect due to the emission of GHGs such as CO2, the nuclear power disasters in Chernobyl (1986) and Fukushima (2011); and the oil crisis of 1973

and 1986, which saw wind turbines evolve from domestic and agricultural applications to utility interconnected wind farm applications (Kaldellis & Zafirakis, 2011). These factors continue to drive the development of wind energy today.

Further information on the history of wind energy is described by Shahan (2014) and Wind-Europe (2019*a*).

Appendix B

List of major hurricanes in Jamaica by category from 1900 to 2018

Table B.1: List of major hurricanes and tropical storms in Jamaica, 1900 to 2018

Name	Category	Category in Jamaica	Month	Year	Location
Galveston (1915)	4	3	Aug	1915	Jamaica
Charlie	4	2	Aug	1951	Jamaica
Gustav	4	T.S.	Aug	2008	Jamaica
"Cuba"	5	T.S.	Nov	1932	Lesser Antilles, **Jamaica**, Cayman Islands, Cuba, The Bahamas, Bermuda.
"Tampico"	5	T.S.	Sept	1933	**Jamaica**, Yucatán Peninsula
Allen	5	4	Aug	1980	**The Caribbean**, Yucatán Peninsula, Mexico, South Texas.
Gilbert	5	3	Sept	1988	**Jamaica**, Venezuela, Central America, Hispaniola, Mexico.
Ivan	5	4	Sept	2004	**The Caribbean**, Venezuela, United States Gulf Coast.
Emily	5	T.S.	July	2005	Windward Islands, **Jamaica,** Mexico, Texas.
Dean	5	4	Aug	2007	**The Caribbean**, Central America.
Sandy	1	1	Oct	2012	**Jamaica**, Greater Antilles.

Data from Wikipedia and The National Hurricane Centre.

Appendix C

Return level and qq-plots of significant wave height and wind speed for the Scottish North Sea (SNS), location 57.5 N, 1.0 W

C.1 GPD Plots of H_s and Wind Speed, SNS

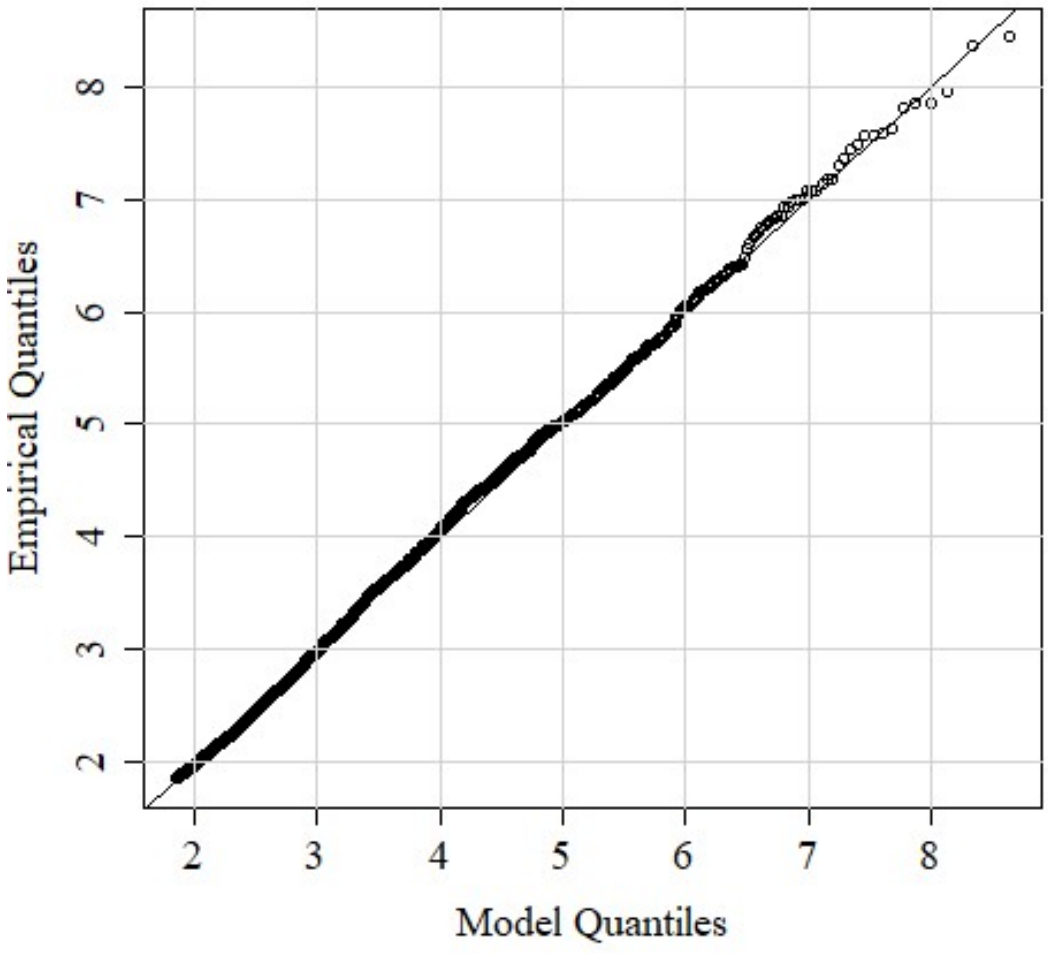

Figure C.1: Q-Q plot of H_s for SNS site, 57.5N, 1.0W (GPD analysis)

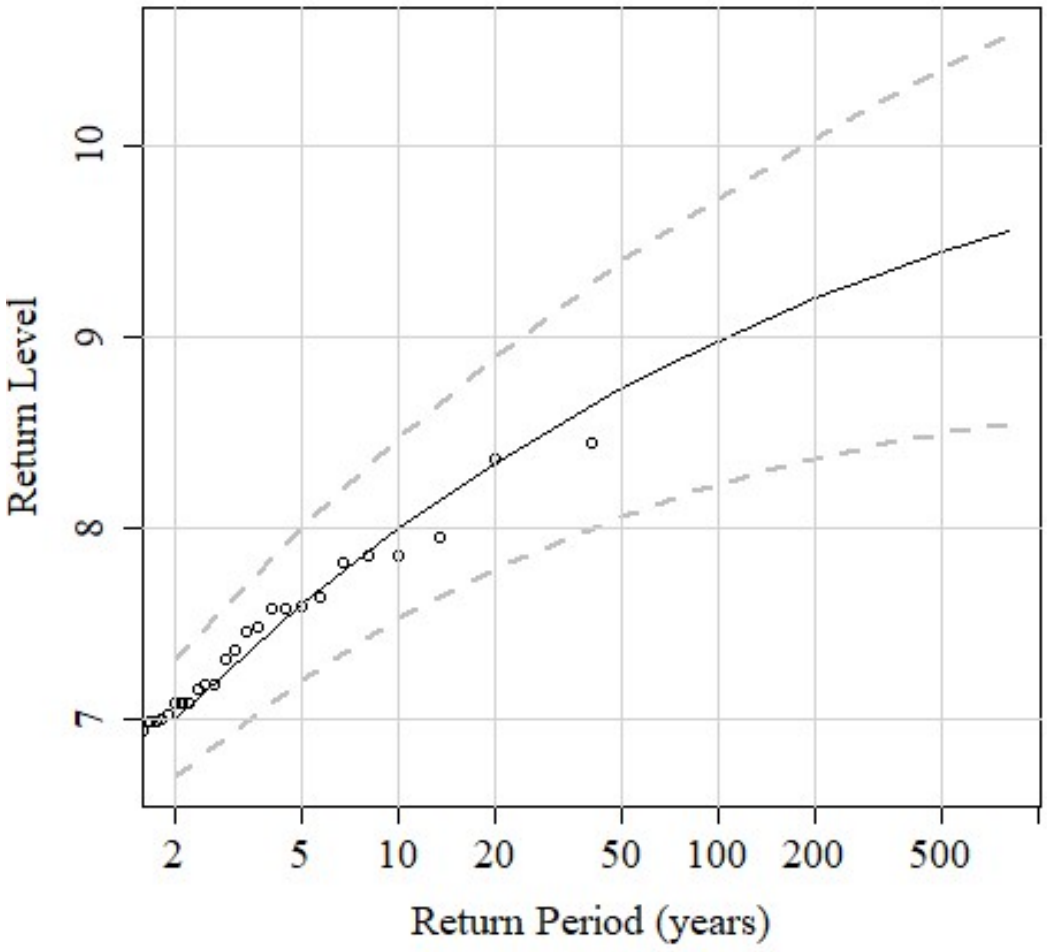

Figure C.2: Return level plot of H_s for SNS site, 57.5N, 1.0W (GPD analysis)

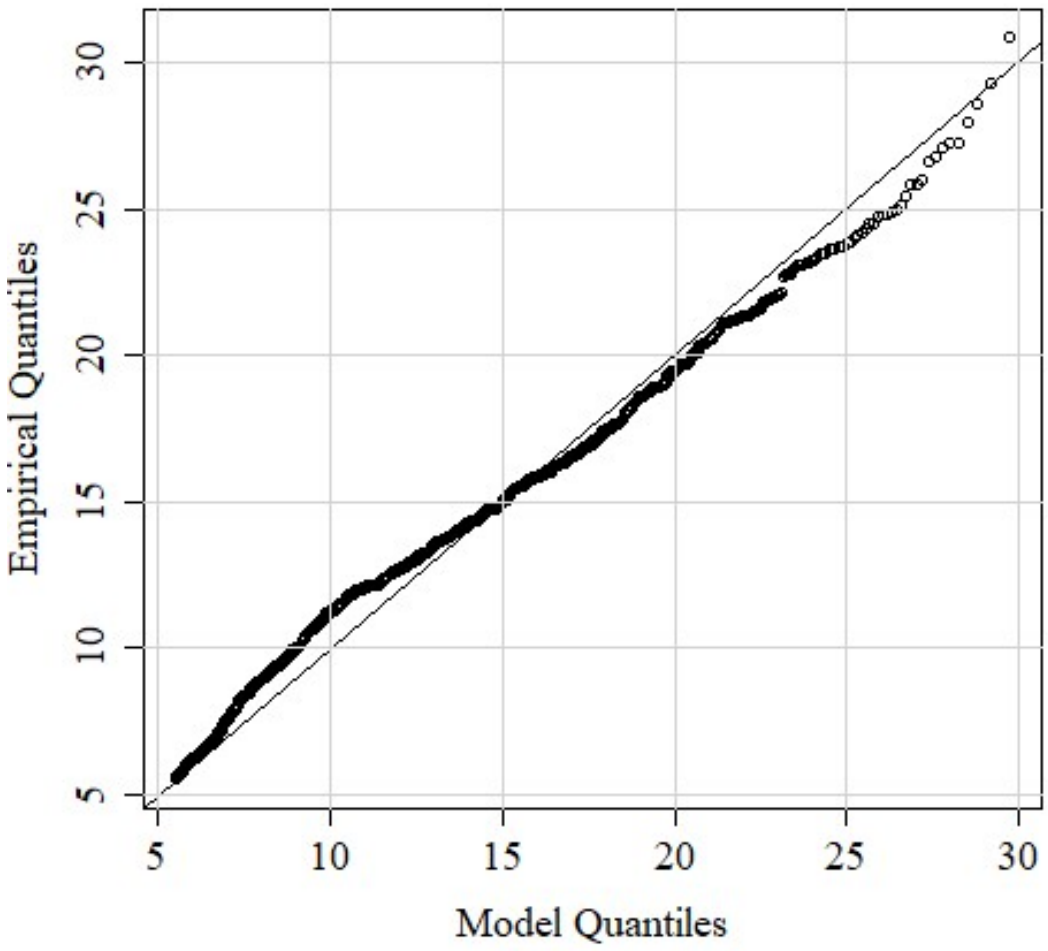

Figure C.3: Q-Q plot of wind speed for SNS site, 57.5N, 1.0W (GPD analysis)

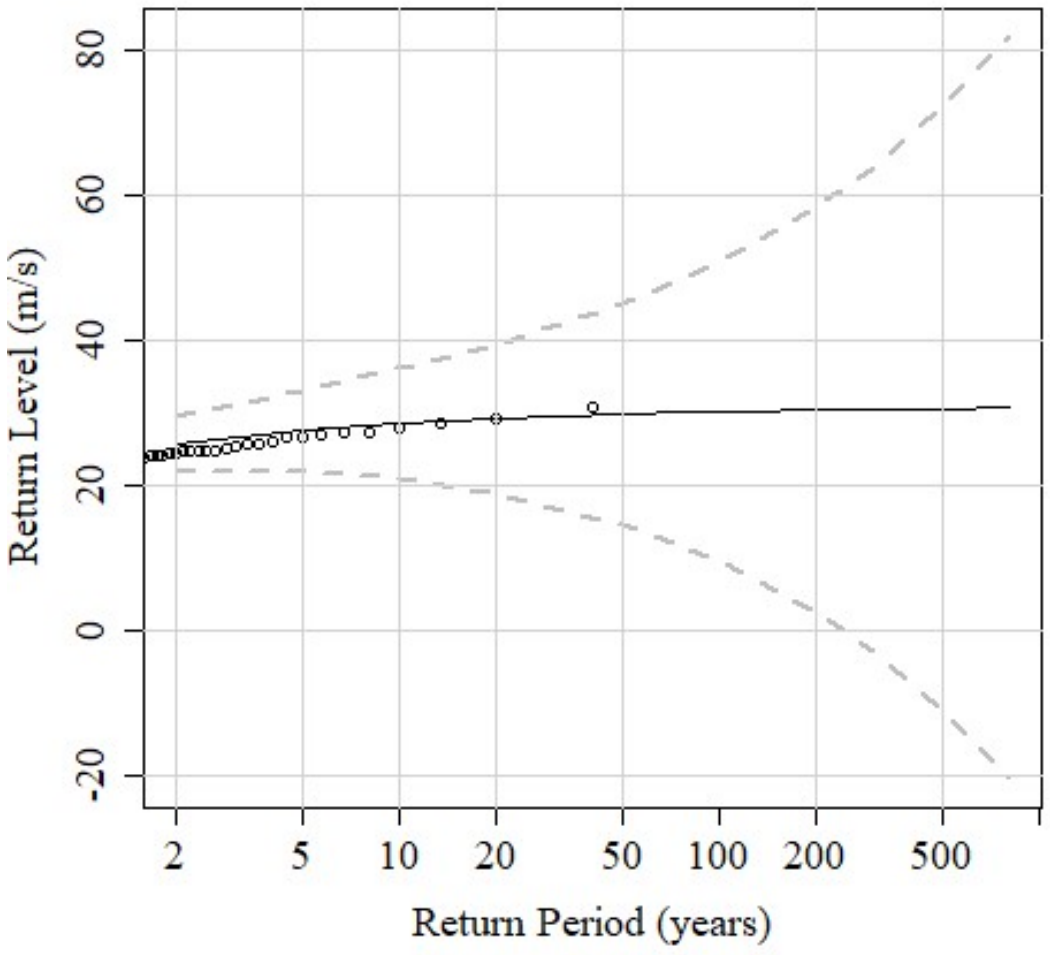

Figure C.4: Return level plot of wind speed for SNS site, 57.5N, 1.0W (GPD analysis)

C.2 GEV Plots of H_s and Wind Speed, SNS

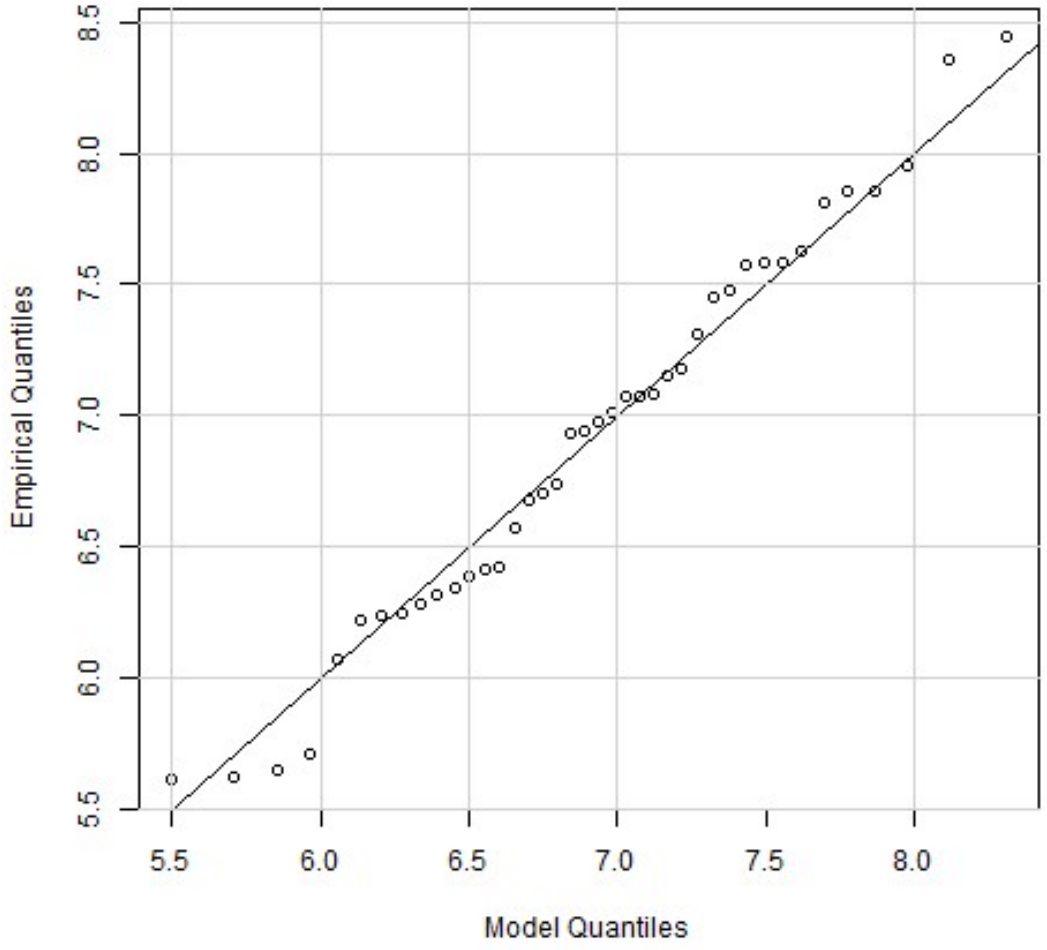

Figure C.5: Q-Q plot of H_s for SNS site, 57.5N, 1.0W (GEV analysis)

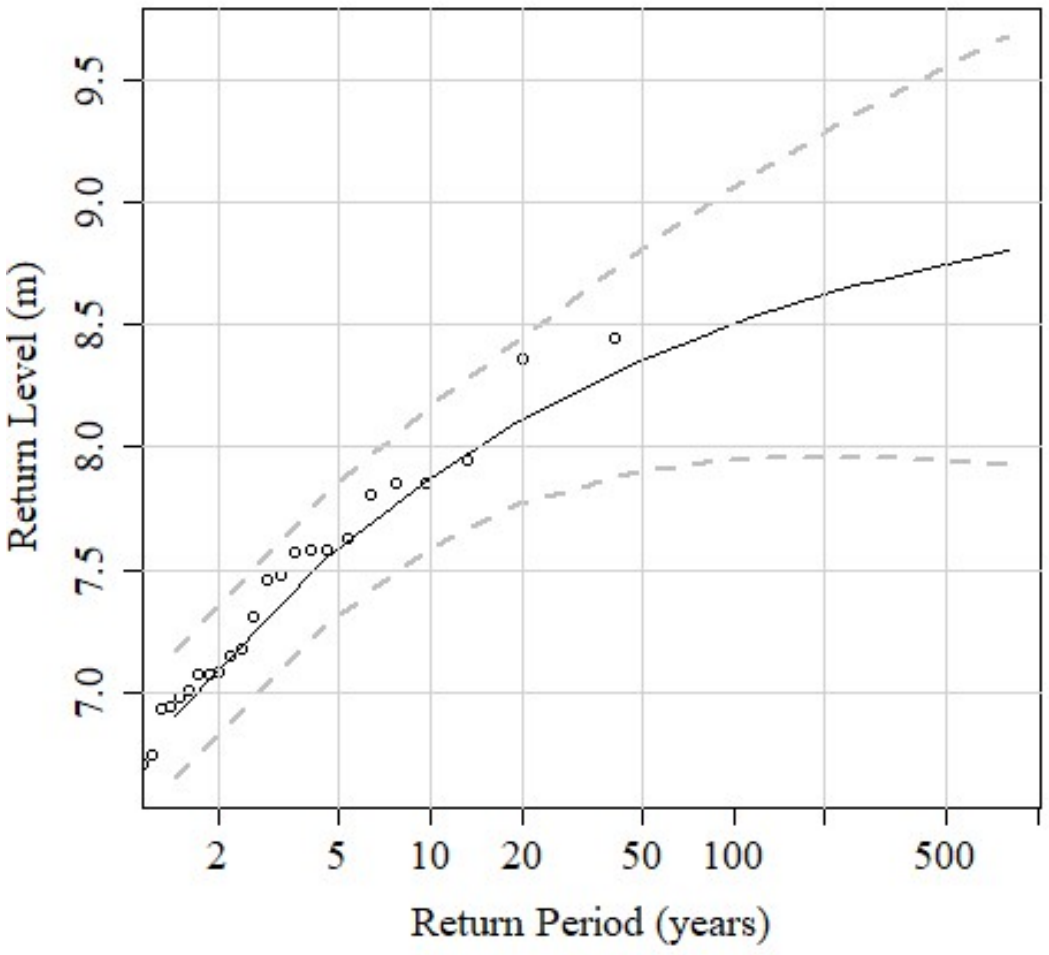

Figure C.6: Return level plot of H_s for SNS site, 57.5N, 1.0W (GEV analysis)

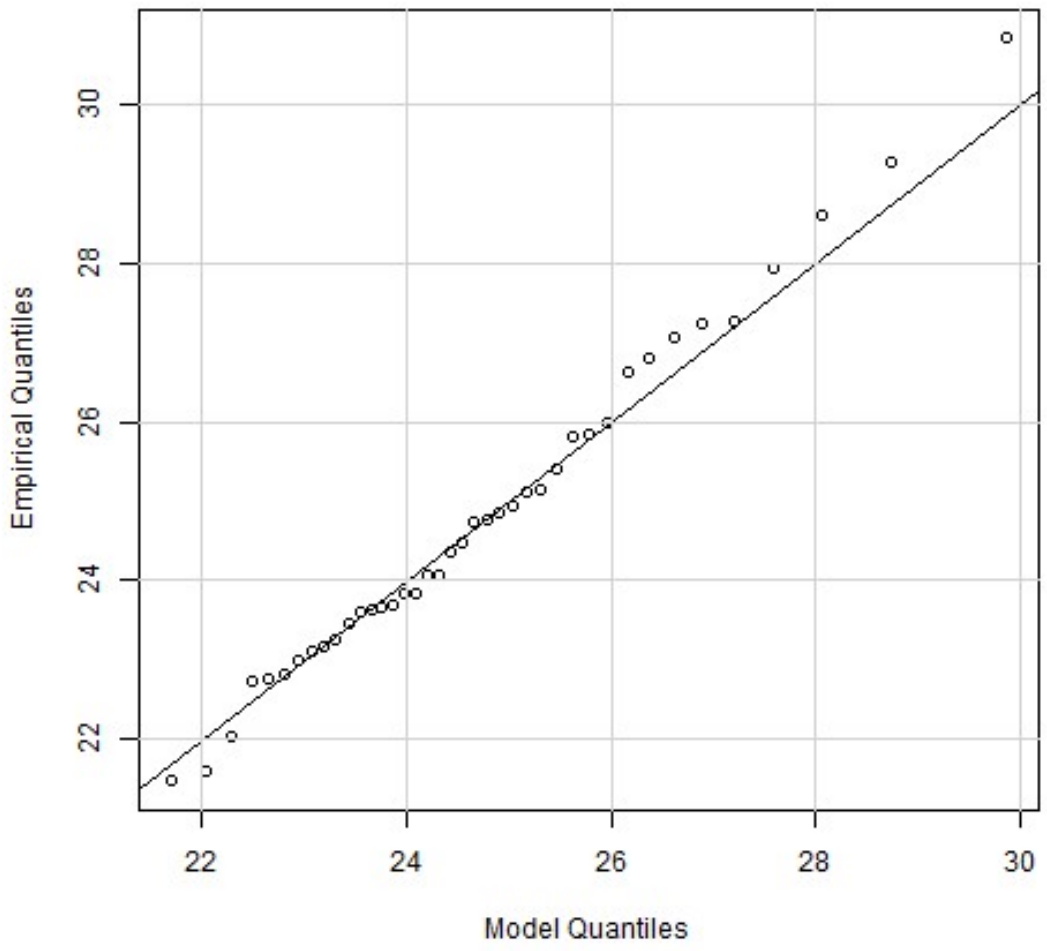

Figure C.7: Q-Q plot of wind speed for SNS site, 57.5N, 1.0W (GEV analysis)

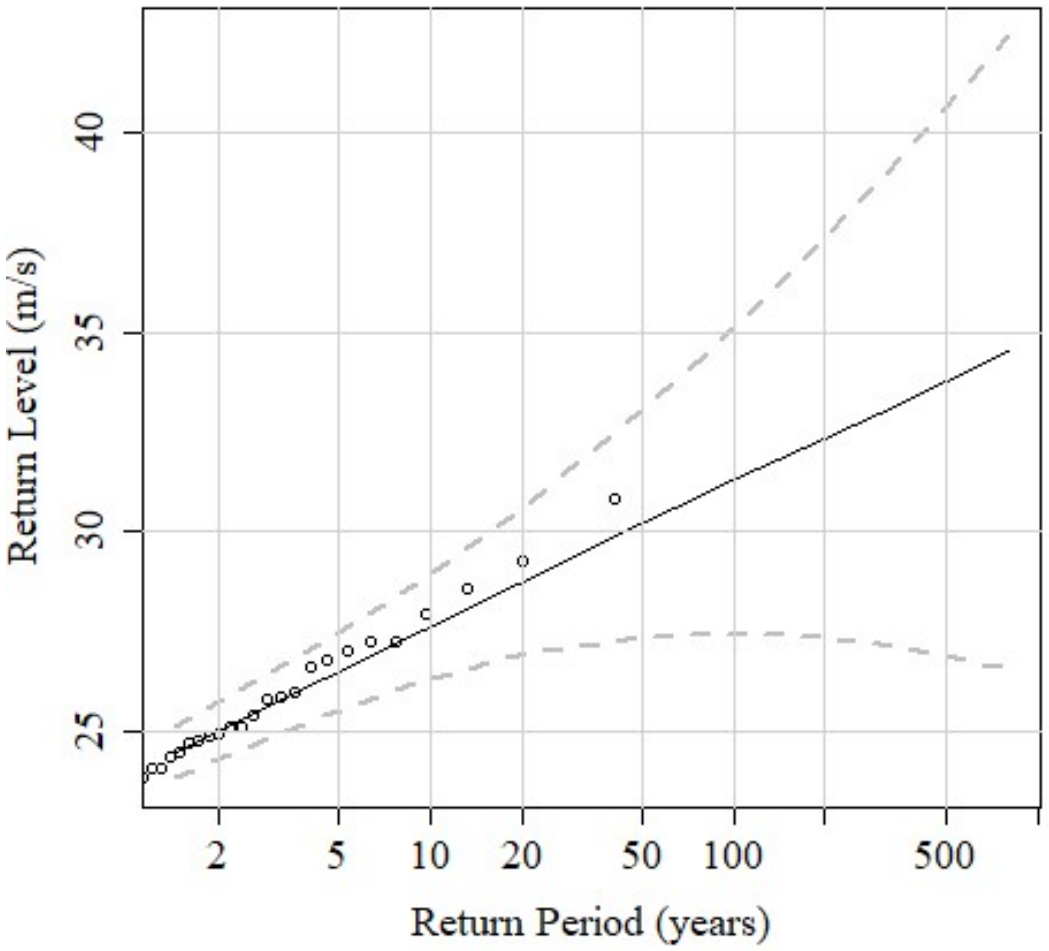

Figure C.8: Return level plot of wind speed for SNS site, 57.5N, 1.0W (GEV analysis)

Appendix D

Request to authors to include their figures in my work

Re: Request to use VolturnUS image in my PhD Thesis

Andre White <andre.white@plymouth.ac.uk>
Sat 17/02/2024 12:10
To:Taylor Ward <taylor.ward@composites.maine.edu>

Thank you.

Regards,
AOAW

From: Taylor Ward <taylor.ward@composites.maine.edu>
Sent: 16 February 2024 18:40
To: Andre White <andre.white@plymouth.ac.uk>
Subject: Re: Request to use VolturnUS image in my PhD Thesis

Please see attached!

Taylor Ward
Communications Manager

University of Maine | Advanced Structures & Composites Center
mobile: +1.207.852.4530 | **office:** +1.207.581.2230
taylor.ward@composites.maine.edu | www.composites.umaine.edu

From: Andre White <andre.white@plymouth.ac.uk>
Sent: Friday, February 16, 2024 12:21 PM
To: Taylor Ward <taylor.ward@composites.maine.edu>
Subject: RE: Request to use VolturnUS image in my PhD Thesis

Hi Taylor:
Just giving you a reminder about the higher resolution image.
Thank you.

Regards,
AOAW

From: Andre White
Sent: 16 February 2024 14:35
To: Taylor Ward <taylor.ward@composites.maine.edu>
Subject: RE: Request to use VolturnUS image in my PhD Thesis

Yes. Thank you.
Please provide higher resolution version.

Regards,
AOAW

From: Taylor Ward <taylor.ward@composites.maine.edu>
Sent: 16 February 2024 14:13
To: Andre White <andre.white@plymouth.ac.uk>
Subject: Fw: Request to use VolturnUS image in my PhD Thesis

Hi Andre,
You can absolutely use the photo and I can provide a higher res version if you'd like. Please credit "University of Maine, Advanced Structures and Composites Center"

With that, I wanted to share with you some info on an upcoming conference we host called, open call for abstracts. We have an open call for abstracts right now!

Kindly,
Taylor

Taylor Ward
Communications Manager

University of Maine | Advanced Structures & Composites Center
mobile: +1.207.852.4530 | **office:** +1.207.581.2230
taylor.ward@composites.maine.edu | www.composites.umaine.edu

From: Front Office <frontoffice@composites.maine.edu>
Sent: Friday, February 16, 2024 7:43 AM
To: Taylor Ward <taylor.ward@composites.maine.edu>
Subject: FW: Request to use VolturnUS image in my PhD Thesis

Communications.

Tracy Porter
Administrative Assistant

University of Maine | Advanced Structures & Composites Center
office: +1.207.581.2123
frontoffice@composites.maine.edu | www.composites.umaine.edu

From: Andre White <andre.white@plymouth.ac.uk>
Sent: Friday, February 16, 2024 5:56 AM
To: Front Office <frontoffice@composites.maine.edu>
Subject: Request to use VolturnUS image in my PhD Thesis

Dear Sir or Madam:
I am requesting your permission to use the following image in my PhD Thesis on the assessment of FOWT in extreme conditions. The image was taken from a Carbon Trust report entitled, "Floating offshore wind - market and technology review: Prepared for the Scottish government."

Regards,
Andre White
University of Plymouth

This email and any files with it are confidential and intended solely for the use of the recipient to whom it is addressed. If you are not the intended recipient then copying, distribution or other use of the information contained is strictly prohibited and you should not rely on it. If you have received this email in error please let the sender know immediately and delete it from your system(s). Internet emails are not necessarily secure. While we take every care, University of Plymouth accepts no responsibility for viruses and it is your responsibility to scan emails and their attachments. University of Plymouth does not accept responsibility for any changes made after it was sent. Nothing in this email or its attachments constitutes an order for goods or services unless accompanied by an official order form.
The content of this email is confidential and intended for the recipient specified in message only. It is strictly forbidden to share any part of this message with any third party, without a written consent of the sender. If you received this message by mistake, please reply to this message and follow with its deletion, so that we can ensure such a mistake does not occur in the future.

To: Fábio Espírito Santo <fsanto@principlepowerinc.com>
Subject: RE: General Inquiry - University of Plymouth

From: Fábio Espírito Santo <fsanto@principlepowerinc.com>
Sent: 16 February 2024 17:20
To: Andre White <andre.white@plymouth.ac.uk>
Subject: RE: General Inquiry - University of Plymouth

Dear Andre,

Thank you for your interest and for following up.

You are free to use the image for the sole purposes of your thesis, and under the agreed conditions.

Thank you for your understanding. Have a nice work!

Kind Regards,

Principle Power
A planet powered by floating offshore wind

Fabio Espirito Santo
Marketing and Communications Coordinator

M +351 910 394 022
E fsanto@principlepowerinc.com
W principlepower.com

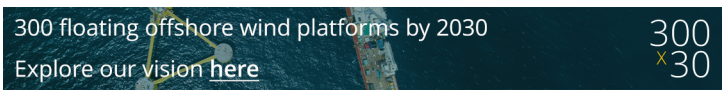

Dear André,

Thank you for your e-mail and interest.

I believe we can support you. Could you please let me know what image are you referring to?

Thank you in advance.

Principle Power
A planet powered by floating offshore wind

Fabio Espirito Santo
Marketing and Communications Coordinator

M +351 910 394 022
E fsanto@principlepowerinc.com
W principlepower.com

From: notifications@typeform.com <notifications@typeform.com>
Sent: Friday, 16 February, 2024 11:01 AM
To: PPI Web Admin <webadmin@principlepowerinc.com>; General Information <info@principlepowerinc.com>; Fábio Espírito Santo <fsanto@principlepowerinc.com>
Subject: Typeform: New response for General Inquiry

Your typeform General Inquiry has a new response:

- **What is your name?**
  Andre White

- **Nice to meet you, Andre White.**
  What is your email address?
  andre.white@plymouth.ac.uk

- **Andre White, what company do you work for?**
  University of Plymouth (Student)

- **What is University of Plymouth (Student)'s website?**
  https://plymouth.ac.uk/

- **How can we help?**
  I would like to use an image of the Windfloat semi-submersible in my PhD Thesis. The image was taken from a Carbon Trust report entitled, “Floating offshore wind - market and technology review: Prepared for the Scottish government.”

- **Almost there!**
  Would you like to subscribe to our newsletter?
  Yes

- **All done!**
  I understand.

Log in to view or download your responses at
https://admin.typeform.com/form/zsoEJ3m4/results
020ep6amwvz9f5mlrdu020ep8mywkc5i

This email and any files with it are confidential and intended solely for the use of the recipient to whom it is addressed. If you are not the intended recipient then copying, distribution or other use of the information contained is strictly prohibited and you should not rely on it. If you have received this email in error please let the sender know immediately and delete it from your system(s). Internet emails are not necessarily secure. While we take every care, University of Plymouth accepts no responsibility for viruses and it is your responsibility to scan emails and their attachments. University of Plymouth does not accept responsibility for

RE: Request to use figure in my PhD Thesis

From: Info at Pelastar <info@pelastar.com>
Sent: 19 February 2024 20:45
To: Andre White <andre.white@plymouth.ac.uk>
Cc: Kris Volpenhein <kevolpenhein@glosten.com>
Subject: RE: Request to use figure in my PhD Thesis

Hello Andre,

You are welcome to use that image. Thank you for asking. However, it's about twelve years old.

You are also welcome to use the newer attached image, so long as you include the simple credit, "Courtesy PelaStar, LLC"

With Best Regards,
Ben Ackers

BENJAMIN B. ACKERS, PE | CEO

T +1 206.624.7850 | D +1 206.812.6056 | M +1 206.850.9162

1201 WESTERN AVENUE, SUITE 200
SEATTLE, WA 98101

PELASTAR
A GLOSTEN COMPANY

From: Andre White <andre.white@plymouth.ac.uk>
Sent: Friday, February 16, 2024 2:42 AM
To: Info at Pelastar <info@pelastar.com>
Subject: Request to use figure in my PhD Thesis

Dear Sir or Madam:
I am requesting your permission to use the following image in my PhD Thesis on the assessment of FOWT in extreme conditions. The image was taken from a Carbon Trust report entitled, "Floating offshore wind - market and technology review: Prepared for the Scottish government."

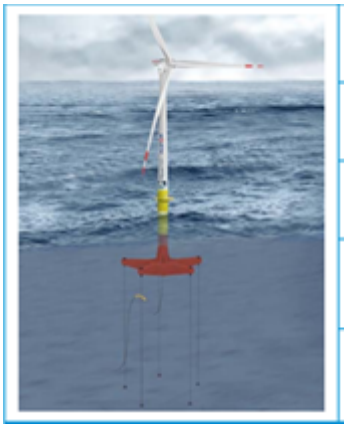

Regards,
Andre White
University of Plymouth

RE: Request to use the Blue H TLP in my PhD Thesis

Nico C.F. Bolleman <nico.bolleman@bluehengineering.com>
Sent: 18 February 2024 16:59
To: Andre White <andre.white@plymouth.ac.uk>
Subject: Re: Request to use the Blue H TLP in my PhD Thesis

Dear Andre,

Feel free to use the image in your PhD thesis.

Would appreciate that you could share a summary of your thesis.

Best Regards,

Nico

Ir. ing Nico C.F. Bolleman

Blue H Engineering BV
Ter Moere 1
4504SC Nieuwvliet
The Netherlands

M +31 651 621 123

On 16 Feb 2024, at 12:18, Andre White <andre.white@plymouth.ac.uk> wrote:

Dear Sir or Madam:
I would like to use an image of the Blue H TLP in my PhD Thesis. The image was taken from a Carbon Trust report entitled, “Floating offshore wind - market and technology review: Prepared for the Scottish government.”
<image001.png>

Thank you.

Regards,
Andre White
University of Plymouth

Re: Request to use figure from report "Floating foundations: A game changer for offshore wind power"

Andre White <andre.white@plymouth.ac.uk>
Thu 08/02/2024 15:52
To:Bauer, Joshua <Joshua.Bauer@nrel.gov>

Thanks Josh.

Regards,
AOAW

From: Bauer, Joshua <Joshua.Bauer@nrel.gov>
Sent: 08 February 2024 15:35
To: Andre White <andre.white@plymouth.ac.uk>
Subject: Re: Request to use figure from report "Floating foundations: A game changer for offshore wind power"

Hi Andre,

Thank you for the email.

Absolutely!

You may use the illustration just as long you give proper credit.

Please use Josh Bauer/NREL.

Thanks,
Josh

From: Andre White <andre.white@plymouth.ac.uk>
Date: Thursday, February 8, 2024 at 9:10 AM
To: Bauer, Joshua <Joshua.Bauer@nrel.gov>
Subject: Request to use figure from report "Floating foundations: A game changer for offshore wind power"

Hi Joshua:
Can I use the attached figure in my PhD Thesis. See correspondence below.

Regards,
AOAW

From: Publications <publications@irena.org>
Sent: 08 February 2024 12:34
To: Andre White <andre.white@plymouth.ac.uk>
Subject: RE: Request to use figure from report "Floating foundations: A game changer for offshore wind power"

Hi
I have looked at the actual image, it has the following text under it '**Illustration by Joshua Bauer, National Renewable Energy Laboratory (US Department of Energy)** '. So, despite the fact it is in an IRENA publication. It would be best to reach out to Joshua Bauer and ask permission to use his image. He works at NREL and his LinkedIn profile is active. You could always check to see where it is used in an NREL report and cite that instead? You still need to credit Mr Bauer.

Alternatively, add the credit as in the figure provided and in the IRENA *report Illustration by Joshua Bauer, National Renewable Energy Laboratory (US Department of Energy)* ; put **Source: IRENA (2016)** under the image and add the IRENA citation to the reference section.
Citation: IRENA (2016), Floating Foundations: a Game Changer for Offshore Wind Power, International Renewable Energy Agency, Abu Dhabi

Requested image is attached. Do let me know if I can help further.

Kind regards
Stephanie

IRENA Publications

IRENA Headquarters, Masdar City | P.O. Box 236 | Abu Dhabi, United Arab Emirates | Tel: +97124179000 | Publications@irena.org | www.irena.org

Follow us

From: Andre White <andre.white@plymouth.ac.uk>
Sent: Thursday, February 8, 2024 2:14 PM
To: Publications <publications@irena.org>
Cc: Collaborative Framework on Offshore Renewables <CFOffshore@irena.org>
Subject: Re: Request to use figure from report "Floating foundations: A game changer for offshore wind power"

Dear IRENA Publications:
Thank you very much. Yes I would be grateful for the high resolution images. Do those images have the notation of copyright and year of copyright or is that something I should write in when labelling the figure.
As you can see in the labelling I only stated Source : IRENA (year). But it seems like this is not sufficient. Please clarify.

Thank you.

Regards,
AOAW

From: Publications <publications@irena.org>
Sent: 08 February 2024 08:55
To: Andre White <andre.white@plymouth.ac.uk>
Cc: Collaborative Framework on Offshore Renewables <CFOffshore@irena.org>
Subject: RE: Request to use figure from report "Floating foundations: A game changer for offshore wind power"

Dear Dr White
Thank you for your email and your interest in IRENA.

Consistent with the copyright notice contained in the reports, we confirm that you are able to freely use, share, copy, reproduce, print and/or store material in the publications entitled “Floating Foundations: a Game Changer for Offshore Wind Power”, provided that all such material is clearly attributed to IRENA and bears a notation of copyright (© IRENA) with the year of copyright (2016).

If you need high res. images, please get in touch.

Regards
IRENA Publications

IRENA Publications

IRENA Headquarters, Masdar City | P.O. Box 236 | Abu Dhabi, United Arab Emirates | Tel: +97124179000 | Publications@irena.org | www.irena.org

Follow us

From: Andre White <andre.white@plymouth.ac.uk>
Sent: Wednesday, February 7, 2024 8:38 PM
To: IRENA Info <info@irena.org>; Collaborative Framework on Offshore Renewables <CFOffshore@irena.org>
Subject: Request to use figure from report "Floating foundations: A game changer for offshore wind power"

Hello:
I recently passed my PhD (University of Plymouth)but I have a few issues with Copyright for some of my figures. I would like to ask your permission to use the figure below from the captioned report in my Thesis.

Re: Request for permission to use figure from WPED website

Andre White <andre.white@plymouth.ac.uk>

Thu 08/02/2024 17:46

To:Kelly Pickerel <kpickerel@wtwhmedia.com>
Cc:cnagle@wtwhmedia.com <cnagle@wtwhmedia.com>

Thank you.

Regards,
AOAW

From: Kelly Pickerel <kpickerel@wtwhmedia.com>
Sent: 08 February 2024 17:45
To: Andre White <andre.white@plymouth.ac.uk>
Cc: cnagle@wtwhmedia.com <cnagle@wtwhmedia.com>
Subject: Re: Request for permission to use figure from WPED website

Permission granted!
Please just cite/credit where relevant: Lloyd's Register/Windpower Engineering & Development

Willing to Work Harder,

Kelly Pickerel
Editor in Chief, Solar Power World
Renewables Editorial Director, WTWH Media
WTWH Media LLC / Solar Power World / Windpower Engineering & Development
Cleveland, Ohio
(216) 860-5259

On Thu, Feb 8, 2024 at 12:41 PM Andre White <andre.white@plymouth.ac.uk> wrote:

> Hello:
> I am requesting permission to use this image found on the wind power engineering website (https://www.windpowerengineering.com/factoring-six-degrees-freedom-floating-offshore-wind-turbines/) in my PhD Thesis.

Andre White

From: Dimitris Manolas <manolasd@fluid.mech.ntua.gr>
Sent: 21 December 2023 14:02
To: Andre White
Subject: Re: Request to use figure from paper

Dear Andre,

Sure you can use the figures.

I wish you all the best.

Kind regards,

Dimitris

Dimitris Manolas

Mechanical Engineer, PhD
National Technical University of Athens
Department of Mechanical Engineering
Laboratory of Aerodynamics, Fluids Section
No. 9, Heroon Polytechniou str., GR 15780, Athens, Greece
Tel: +30-210-7721097; Mob: +30-693-8376558
E-mail: manolasd@fluid.mech.ntua.gr

Στις 21/12/2023 15:55, Andre White έγραψε:

> Hi Dimitris,
>
> I am just completing my PhD in offshore wind and would like to know if it is possible to use some of the figures from your paper entitled, "Hydro-Servo-Aero-Elastic Analysis of Floating Offshore Wind Turbines." I will make sure that the figures are properly referenced.
>
> Thank you.
>
> Regards,
>
> AOAW

From: Andre White
To: Steve Winterstein
Subject: RE: Paper on Environmental contour line method Winterstein 2008
Date: 18 December 2023 13:13:00
Attachments: image006.png

Hi Steve,
Thank you very much. Good to know that you are doing well. I think I will stay in industry.
I will try and keep in touch and yes I would welcome the collab to publish papers.

Thanks again.

Regards,
AOAW

From: Steve Winterstein <stevewinterstein@alum.mit.edu>
Sent: 15 December 2023 22:08
To: Andre White <andre.white@plymouth.ac.uk>
Subject: Re: Paper on Environmental contour line method Winterstein 2008

Hi Andre! Great to hear from you again. Glad to see you approaching the end of your dissertation. That's great news.

You are of course welcome, and encouraged, to cite any of my work and/or figures. I think my Google Scholar page has pdf versions of a fair number of them. I hold a few more personally… let me know if I can help dig out any more info you'd find helpful.

Have you future plans, in academia or industry? Any interest in a follow-up paper on a related topic? This could be fun to continue a little further, and maybe a published paper might be a helpful resume item in your future career? I will meet with Sverre Haver next month, and he may have knowledge of a practical problem or two that might benefit from our analysis methods. If you happen to have interest and a little time, it could be fun to involve you in this.

Finally, you are to be congratulated for all your PhD efforts, overcoming hurdles like our long-distance collaborations. I imagine COVID didn't help either. In any case, please try to stay in touch. I'd be happy to see a copy of the final thesis at some point. And again, I'm available if you need any last-minute help with any of this.

With all best wishes…. Steve

Website: http://alum.mit.edu/www/stevewinterstein
LinkedIn: https://www.linkedin.com/in/steve-winterstein-91a0b8234
Citations: https://scholar.google.com/citations?user=dRM-gA0AAAAJ&hl=en
Music: https://www.youtube.com/@rachmaninov03/videos

On Fri, Dec 15, 2023 at 12:14 PM Andre White <andre.white@plymouth.ac.uk> wrote:

> Hi Steve:
> It's been a long time.
> I am just completing my PhD; would like to know if I can use one of the figures from your paper entitled, "Environmental contour lines: A method for estimating long term extremes by a short term analysis."
> Thank you.
>
> Regards,
> AOAW

Andre White

From: Andre White
Sent: 15 December 2023 20:25
To: acecker@sandia.gov
Subject: Request to use figure from your paper

Dear Aubrey:
I am just completing my PhD and would like to know if it is possible to use a figure from your paper entitled, "Modified inverse first order reliability method (I-FORM) for predicting extreme sea states."

Thank you.

Regards,
AOAW

JOHN WILEY AND SONS LICENSE
TERMS AND CONDITIONS

Feb 08, 2024

This Agreement between University of Plymouth -- Andre White ("You") and John Wiley and Sons ("John Wiley and Sons") consists of your license details and the terms and conditions provided by John Wiley and Sons and Copyright Clearance Center.

License Number	5724280746055
License date	Feb 08, 2024
Licensed Content Publisher	John Wiley and Sons
Licensed Content Publication	Wiley Books
Licensed Content Title	Introduction: Modern Wind Energy and its Origins
Licensed Content Date	Dec 28, 2010
Licensed Content Pages	22
Type of use	Dissertation/Thesis
Requestor type	University/Academic
Format	Electronic
Portion	Figure/table
Number of figures/tables	6
Will you be translating?	No
Title of new work	Assessment of floating offshore wind turbines in extreme conditions

Institution name	University of Plymouth
Expected presentation date	Mar 2024
Order reference number	1
Portions	Figures 1.2, 1.3, 3.1,3.4,3.22, 3.24
Requestor Location	Andre White 8 Waverley Avenue Twickenham, TW2 6DW United Kingdom Attn: Andre White
Publisher Tax ID	EU826007151
Billing Type	Invoice
Billing Address	University of Plymouth 8 Waverley Avenue Twickenham, United Kingdom tw2 6dw Attn: Andre O. White
Total	0.00 GBP
Terms and Conditions	

TERMS AND CONDITIONS

This copyrighted material is owned by or exclusively licensed to John Wiley & Sons, Inc. or one of its group companies (each a"Wiley Company") or handled on behalf of a society with which a Wiley Company has exclusive publishing rights in relation to a particular work (collectively "WILEY"). By clicking "accept" in connection with completing this licensing transaction, you agree that the following terms and conditions apply to this transaction (along with the billing and payment terms and conditions established by the Copyright Clearance Center Inc., ("CCC's Billing and Payment terms and conditions"), at the time that you opened your RightsLink account (these are available at any time at http://myaccount.copyright.com).

Terms and Conditions

- The materials you have requested permission to reproduce or reuse (the "Wiley Materials") are protected by copyright.

- You are hereby granted a personal, non-exclusive, non-sub licensable (on a stand-alone basis), non-transferable, worldwide, limited license to reproduce the Wiley Materials for the purpose specified in the licensing process. This license, **and any CONTENT (PDF or image file) purchased as part of your order,** is for a one-time use only and limited to any maximum distribution number specified in the license. The first instance of republication or reuse granted by this license must be completed within two years of the date of the grant of this license (although copies prepared before the end date may be distributed thereafter). The Wiley Materials shall not be used in any other manner or for any other purpose, beyond what is granted in the license. Permission is granted subject to an appropriate acknowledgement given to the author, title of the material/book/journal and the publisher. You shall also duplicate the copyright notice that appears in the Wiley publication in your use of the Wiley Material. Permission is also granted on the understanding that nowhere in the text is a previously published source acknowledged for all or part of this Wiley Material. Any third party content is expressly excluded from this permission.

- With respect to the Wiley Materials, all rights are reserved. Except as expressly granted by the terms of the license, no part of the Wiley Materials may be copied, modified, adapted (except for minor reformatting required by the new Publication), translated, reproduced, transferred or distributed, in any form or by any means, and no derivative works may be made based on the Wiley Materials without the prior permission of the respective copyright owner.**For STM Signatory Publishers clearing permission under the terms of the STM Permissions Guidelines only, the terms of the license are extended to include subsequent editions and for editions in other languages, provided such editions are for the work as a whole in situ and does not involve the separate exploitation of the permitted figures or extracts,** You may not alter, remove or suppress in any manner any copyright, trademark or other notices displayed by the Wiley Materials. You may not license, rent, sell, loan, lease, pledge, offer as security, transfer or assign the Wiley Materials on a stand-alone basis, or any of the rights granted to you hereunder to any other person.

- The Wiley Materials and all of the intellectual property rights therein shall at all times remain the exclusive property of John Wiley & Sons Inc, the Wiley Companies, or their respective licensors, and your interest therein is only that of having possession of and the right to reproduce the Wiley Materials pursuant to Section 2 herein during the continuance of this Agreement. You agree that you own no right, title or interest in or to the Wiley Materials or any of the intellectual property rights therein. You shall have no rights hereunder other than the license as provided for above in Section 2. No right, license or interest to any trademark, trade name, service mark or other branding ("Marks") of WILEY or its licensors is granted hereunder, and you agree that you shall not assert any such right, license or interest with respect thereto

- NEITHER WILEY NOR ITS LICENSORS MAKES ANY WARRANTY OR REPRESENTATION OF ANY KIND TO YOU OR ANY THIRD PARTY, EXPRESS, IMPLIED OR STATUTORY, WITH RESPECT TO THE MATERIALS OR THE ACCURACY OF ANY INFORMATION CONTAINED IN THE MATERIALS, INCLUDING, WITHOUT LIMITATION, ANY IMPLIED WARRANTY OF MERCHANTABILITY, ACCURACY, SATISFACTORY QUALITY, FITNESS FOR A PARTICULAR PURPOSE, USABILITY, INTEGRATION OR NON-INFRINGEMENT AND ALL SUCH WARRANTIES ARE HEREBY EXCLUDED BY WILEY AND ITS LICENSORS AND WAIVED

BY YOU.

- WILEY shall have the right to terminate this Agreement immediately upon breach of this Agreement by you.

- You shall indemnify, defend and hold harmless WILEY, its Licensors and their respective directors, officers, agents and employees, from and against any actual or threatened claims, demands, causes of action or proceedings arising from any breach of this Agreement by you.

- IN NO EVENT SHALL WILEY OR ITS LICENSORS BE LIABLE TO YOU OR ANY OTHER PARTY OR ANY OTHER PERSON OR ENTITY FOR ANY SPECIAL, CONSEQUENTIAL, INCIDENTAL, INDIRECT, EXEMPLARY OR PUNITIVE DAMAGES, HOWEVER CAUSED, ARISING OUT OF OR IN CONNECTION WITH THE DOWNLOADING, PROVISIONING, VIEWING OR USE OF THE MATERIALS REGARDLESS OF THE FORM OF ACTION, WHETHER FOR BREACH OF CONTRACT, BREACH OF WARRANTY, TORT, NEGLIGENCE, INFRINGEMENT OR OTHERWISE (INCLUDING, WITHOUT LIMITATION, DAMAGES BASED ON LOSS OF PROFITS, DATA, FILES, USE, BUSINESS OPPORTUNITY OR CLAIMS OF THIRD PARTIES), AND WHETHER OR NOT THE PARTY HAS BEEN ADVISED OF THE POSSIBILITY OF SUCH DAMAGES. THIS LIMITATION SHALL APPLY NOTWITHSTANDING ANY FAILURE OF ESSENTIAL PURPOSE OF ANY LIMITED REMEDY PROVIDED HEREIN.

- Should any provision of this Agreement be held by a court of competent jurisdiction to be illegal, invalid, or unenforceable, that provision shall be deemed amended to achieve as nearly as possible the same economic effect as the original provision, and the legality, validity and enforceability of the remaining provisions of this Agreement shall not be affected or impaired thereby.

- The failure of either party to enforce any term or condition of this Agreement shall not constitute a waiver of either party's right to enforce each and every term and condition of this Agreement. No breach under this agreement shall be deemed waived or excused by either party unless such waiver or consent is in writing signed by the party granting such waiver or consent. The waiver by or consent of a party to a breach of any provision of this Agreement shall not operate or be construed as a waiver of or consent to any other or subsequent breach by such other party.

- This Agreement may not be assigned (including by operation of law or otherwise) by you without WILEY's prior written consent.

- Any fee required for this permission shall be non-refundable after thirty (30) days from receipt by the CCC.

- These terms and conditions together with CCC's Billing and Payment terms and conditions (which are incorporated herein) form the entire agreement between you and WILEY concerning this licensing transaction and (in the absence of fraud) supersedes all prior agreements and representations of the parties, oral or written. This Agreement may not be amended except in writing signed by both parties. This Agreement shall be binding upon and inure to the benefit of the parties' successors, legal representatives, and authorized assigns.

- In the event of any conflict between your obligations established by these terms and conditions and those established by CCC's Billing and Payment terms and conditions, these terms and conditions shall prevail.

- WILEY expressly reserves all rights not specifically granted in the combination of (i) the license details provided by you and accepted in the course of this licensing transaction, (ii) these terms and conditions and (iii) CCC's Billing and Payment terms and conditions.

- This Agreement will be void if the Type of Use, Format, Circulation, or Requestor Type was misrepresented during the licensing process.

- This Agreement shall be governed by and construed in accordance with the laws of the State of New York, USA, without regards to such state's conflict of law rules. Any legal action, suit or proceeding arising out of or relating to these Terms and Conditions or the breach thereof shall be instituted in a court of competent jurisdiction in New York County in the State of New York in the United States of America and each party hereby consents and submits to the personal jurisdiction of such court, waives any objection to venue in such court and consents to service of process by registered or certified mail, return receipt requested, at the last known address of such party.

WILEY OPEN ACCESS TERMS AND CONDITIONS

Wiley Publishes Open Access Articles in fully Open Access Journals and in Subscription journals offering Online Open. Although most of the fully Open Access journals publish open access articles under the terms of the Creative Commons Attribution (CC BY) License only, the subscription journals and a few of the Open Access Journals offer a choice of Creative Commons Licenses. The license type is clearly identified on the article.

The Creative Commons Attribution License

The Creative Commons Attribution License (CC-BY) allows users to copy, distribute and transmit an article, adapt the article and make commercial use of the article. The CC-BY license permits commercial and non-

Creative Commons Attribution Non-Commercial License

The Creative Commons Attribution Non-Commercial (CC-BY-NC)License permits use, distribution and reproduction in any medium, provided the original work is properly cited and is not used for commercial purposes.(see below)

Creative Commons Attribution-Non-Commercial-NoDerivs License

The Creative Commons Attribution Non-Commercial-NoDerivs License (CC-BY-NC-ND) permits use, distribution and reproduction in any medium, provided the original work is properly cited, is not used for commercial purposes and no modifications or adaptations are made. (see below)

Use by commercial "for-profit" organizations

Use of Wiley Open Access articles for commercial, promotional, or marketing purposes requires further explicit permission from Wiley and will be subject to a fee.

Further details can be found on Wiley Online Library
http://olabout.wiley.com/WileyCDA/Section/id-410895.html

Other Terms and Conditions:

v1.10 Last updated September 2015

Questions? customercare@copyright.com.

From: Andre White
To: Dominic Reeve
Subject: RE: Request to use figure from book
Date: 18 December 2023 13:10:00

Thanks and noted Prof Reeve.

Regards,
AOAW

From: Dominic Reeve <d.e.reeve@swansea.ac.uk>
Sent: 15 December 2023 23:39
To: Andre White <andre.white@plymouth.ac.uk>
Subject: Re: Request to use figure from book

Dear Andre

Yes, that should be OK for a thesis. You should acknowledge the source of the figure in your figure caption.
The publishers, CRC, hold the publication rights so if you were to use the figure in a journal paper or a book then you would need their permission.

Regards

Professor Dominic Reeve

Energy & Environment Research Group

ESRI Building | College of Engineering

Swansea University | Bay Campus

Swansea | SA2 8PP

(: +44 (0)1792 606566
E: d.e.reeve@swansea.ac.uk

From: Andre White <andre.white@plymouth.ac.uk>
Sent: 15 December 2023 8:54 PM
To: Dominic Reeve <D.E.Reeve@Swansea.ac.uk>
Subject: Request to use figure from book

Dear Prof Reeve:
I am just completing my PhD in offshore wind and would like to know if it is possible to use a figure from your book entitled, "Coastal Engineering: Processes, Theory and Design Practice."

Thank you.

Regards,
AOAW

From: lixin
To: Andre White
Subject: 回复: Request to use figure from paper
Date: 25 December 2023 00:01:05

Hi,

It is Ok. You can use these figures in your PH.D dissertation.

Best regards,

Xin Li
Ph.D.
Professor
Faculty of Infrastructure Engineering
Dalian University of Technology
Tel: +86 411 84707784
Email: lixin@dlut.edu.cn

From: Andre White
Date: 2023-12-21 22:01
To: lixin@dlut.edu.cn
Subject: Request to use figure from paper

Hi Xin,
I am just completing my PhD in offshore wind and would like to know if it is possible to use some of the figures from your paper entitled, "Analysis of Dynamic Characteristics of an Ultra-Large Semi-Submersible Floating Wind Turbine." I will make sure that the figures are properly referenced.

Thank you.

Regards,
AOAW

RE: Request to use figure from MoorDyn manual in my PhD

Hall, Matthew <Matthew.Hall@nrel.gov>

Thu 08/02/2024 16:23

To:Andre White <andre.white@plymouth.ac.uk>

Hi Andre,
Sure, just cite the source and you're good.
Thanks for checking,
Matt

From: Andre White <andre.white@plymouth.ac.uk>
Sent: Thursday, February 8, 2024 6:59 AM
To: Hall, Matthew <Matthew.Hall@nrel.gov>
Subject: Request to use figure from MoorDyn manual in my PhD

Hi Matthew:
I am requesting your permission to use the lumped mass figure from the MoorDyn Manual in my PhD Thesis.

Thank you.

Regards,
Andre White

Marketplace

Order Date	07-Feb-2024	Type of Use	Republish in a thesis/dissertation
Order License ID	1448240-1		
ISBN-13	9780471956518	Publisher	J. Wiley
		Portion	Chart/graph/table/figure

LICENSED CONTENT

Publication Title	Wind Loads on Structures	Country	United Kingdom of Great Britain and Northern Ireland
Author/Editor	Dyrbye, Claës., Hansen, Svend Ole.	Rightsholder	John Wiley & Sons - Books
Date	01/23/1997	Publication Type	Book
Language	English, Danish		

REQUEST DETAILS

Portion Type	Chart/graph/table/figure	Distribution	Worldwide
Number of Charts / Graphs / Tables / Figures Requested	1	Translation	Original language of publication
		Copies for the Disabled?	No
Format (select all that apply)	Electronic	Minor Editing Privileges?	Yes
Who Will Republish the Content?	Academic institution	Incidental Promotional Use?	Yes
Duration of Use	Life of current edition	Currency	GBP
Lifetime Unit Quantity	Up to 499		
Rights Requested	Main product		

NEW WORK DETAILS

Title	Assessment of floating offshore wind turbines in extreme conditions	Institution Name	University of Plymouth
		Expected Presentation Date	2024-02-28
Instructor Name	Deborah Greaves		

ADDITIONAL DETAILS

The Requesting Person / Organization to Appear on the License	AndreWhite

REQUESTED CONTENT DETAILS

Title, Description or Numeric Reference of the Portion(s)	Figure explaining wind turbulence intensity	Title of the Article / Chapter the Portion Is From	Chapter 3
Editor of Portion(s)	n/a	Author of Portion(s)	Dyrbye, Claës.; Hansen, Svend Ole.

Volume / Edition	1	**Publication Date of Portion**	1997-01-23
Page or Page Range of Portion	5 to 48		

RIGHTSHOLDER TERMS AND CONDITIONS

No right, license or interest to any trademark, trade name, service mark or other branding ("Marks") of WILEY or its licensors is granted hereunder, and you agree that you shall not assert any such right, license or interest with respect thereto. You may not alter, remove or suppress in any manner any copyright, trademark or other notices displayed by the Wiley material. This Agreement will be void if the Type of Use, Format, Circulation, or Requestor Type was misrepresented during the licensing process. In no instance may the total amount of Wiley Materials used in any Main Product, Compilation or Collective work comprise more than 5% (if figures/tables) or 15% (if full articles/chapters) of the (entirety of the) Main Product, Compilation or Collective Work. Some titles may be available under an Open Access license. It is the Licensors' responsibility to identify the type of Open Access license on which the requested material was published, and comply fully with the terms of that license for the type of use specified Further details can be found on Wiley Online Library http://olabout.wiley.com/WileyCDA/Section/id-410895.html.

Marketplace Permissions General Terms and Conditions

The following terms and conditions ("General Terms"), together with any applicable Publisher Terms and Conditions, govern User's use of Works pursuant to the Licenses granted by Copyright Clearance Center, Inc. ("CCC") on behalf of the applicable Rightsholders of such Works through CCC's applicable Marketplace transactional licensing services (each, a "Service").

1) **Definitions.** For purposes of these General Terms, the following definitions apply:

"License" is the licensed use the User obtains via the Marketplace platform in a particular licensing transaction, as set forth in the Order Confirmation.

"Order Confirmation" is the confirmation CCC provides to the User at the conclusion of each Marketplace transaction. "Order Confirmation Terms" are additional terms set forth on specific Order Confirmations not set forth in the General Terms that can include terms applicable to a particular CCC transactional licensing service and/or any Rightsholder-specific terms.

"Rightsholder(s)" are the holders of copyright rights in the Works for which a User obtains licenses via the Marketplace platform, which are displayed on specific Order Confirmations.

"Terms" means the terms and conditions set forth in these General Terms and any additional Order Confirmation Terms collectively.

"User" or "you" is the person or entity making the use granted under the relevant License. Where the person accepting the Terms on behalf of a User is a freelancer or other third party who the User authorized to accept the General Terms on the User's behalf, such person shall be deemed jointly a User for purposes of such Terms.

"Work(s)" are the copyright protected works described in relevant Order Confirmations.

2) **Description of Service.** CCC's Marketplace enables Users to obtain Licenses to use one or more Works in accordance with all relevant Terms. CCC grants Licenses as an agent on behalf of the copyright rightsholder identified in the relevant Order Confirmation.

3) **Applicability of Terms.** The Terms govern User's use of Works in connection with the relevant License. In the event of any conflict between General Terms and Order Confirmation Terms, the latter shall govern. User acknowledges that Rightsholders have complete discretion whether to grant any permission, and whether to place any limitations on any grant, and that CCC has no right to supersede or to modify any such discretionary act by a Rightsholder.

4) **Representations; Acceptance.** By using the Service, User represents and warrants that User has been duly authorized by the User to accept, and hereby does accept, all Terms.

5) **Scope of License; Limitations and Obligations.** All Works and all rights therein, including copyright rights, remain the sole and exclusive property of the Rightsholder. The License provides only those rights expressly set forth in the terms and conveys no other rights in any Works

6) **General Payment Terms.** User may pay at time of checkout by credit card or choose to be invoiced. If the User chooses to be invoiced, the User shall: (i) remit payments in the manner identified on specific invoices, (ii) unless otherwise specifically stated in an Order Confirmation or separate written agreement, Users shall remit payments upon receipt of the relevant invoice from CCC, either by delivery or notification of availability of the invoice via the Marketplace

platform, and (iii) if the User does not pay the invoice within 30 days of receipt, the User may incur a service charge of 1.5% per month or the maximum rate allowed by applicable law, whichever is less. While User may exercise the rights in the License immediately upon receiving the Order Confirmation, the License is automatically revoked and is null and void, as if it had never been issued, if CCC does not receive complete payment on a timely basis.

7) **General Limits on Use.** Unless otherwise provided in the Order Confirmation, any grant of rights to User (i) involves only the rights set forth in the Terms and does not include subsequent or additional uses, (ii) is non-exclusive and non-transferable, and (iii) is subject to any and all limitations and restrictions (such as, but not limited to, limitations on duration of use or circulation) included in the Terms. Upon completion of the licensed use as set forth in the Order Confirmation, User shall either secure a new permission for further use of the Work(s) or immediately cease any new use of the Work(s) and shall render inaccessible (such as by deleting or by removing or severing links or other locators) any further copies of the Work. User may only make alterations to the Work if and as expressly set forth in the Order Confirmation. No Work may be used in any way that is unlawful, including without limitation if such use would violate applicable sanctions laws or regulations, would be defamatory, violate the rights of third parties (including such third parties' rights of copyright, privacy, publicity, or other tangible or intangible property), or is otherwise illegal, sexually explicit, or obscene. In addition, User may not conjoin a Work with any other material that may result in damage to the reputation of the Rightsholder. Any unlawful use will render any licenses hereunder null and void. User agrees to inform CCC if it becomes aware of any infringement of any rights in a Work and to cooperate with any reasonable request of CCC or the Rightsholder in connection therewith.

8) **Third Party Materials.** In the event that the material for which a License is sought includes third party materials (such as photographs, illustrations, graphs, inserts and similar materials) that are identified in such material as having been used by permission (or a similar indicator), User is responsible for identifying, and seeking separate licenses (under this Service, if available, or otherwise) for any of such third party materials; without a separate license, User may not use such third party materials via the License.

9) **Copyright Notice.** Use of proper copyright notice for a Work is required as a condition of any License granted under the Service. Unless otherwise provided in the Order Confirmation, a proper copyright notice will read substantially as follows: "Used with permission of [Rightsholder's name], from [Work's title, author, volume, edition number and year of copyright]; permission conveyed through Copyright Clearance Center, Inc." Such notice must be provided in a reasonably legible font size and must be placed either on a cover page or in another location that any person, upon gaining access to the material which is the subject of a permission, shall see, or in the case of republication Licenses, immediately adjacent to the Work as used (for example, as part of a by-line or footnote) or in the place where substantially all other credits or notices for the new work containing the republished Work are located. Failure to include the required notice results in loss to the Rightsholder and CCC, and the User shall be liable to pay liquidated damages for each such failure equal to twice the use fee specified in the Order Confirmation, in addition to the use fee itself and any other fees and charges specified.

10) **Indemnity.** User hereby indemnifies and agrees to defend the Rightsholder and CCC, and their respective employees and directors, against all claims, liability, damages, costs, and expenses, including legal fees and expenses, arising out of any use of a Work beyond the scope of the rights granted herein and in the Order Confirmation, or any use of a Work which has been altered in any unauthorized way by User, including claims of defamation or infringement of rights of copyright, publicity, privacy, or other tangible or intangible property.

11) **Limitation of Liability.** UNDER NO CIRCUMSTANCES WILL CCC OR THE RIGHTSHOLDER BE LIABLE FOR ANY DIRECT, INDIRECT, CONSEQUENTIAL, OR INCIDENTAL DAMAGES (INCLUDING WITHOUT LIMITATION DAMAGES FOR LOSS OF BUSINESS PROFITS OR INFORMATION, OR FOR BUSINESS INTERRUPTION) ARISING OUT OF THE USE OR INABILITY TO USE A WORK, EVEN IF ONE OR BOTH OF THEM HAS BEEN ADVISED OF THE POSSIBILITY OF SUCH DAMAGES. In any event, the total liability of the Rightsholder and CCC (including their respective employees and directors) shall not exceed the total amount actually paid by User for the relevant License. User assumes full liability for the actions and omissions of its principals, employees, agents, affiliates, successors, and assigns.

12) **Limited Warranties.** THE WORK(S) AND RIGHT(S) ARE PROVIDED "AS IS." CCC HAS THE RIGHT TO GRANT TO USER THE RIGHTS GRANTED IN THE ORDER CONFIRMATION DOCUMENT. CCC AND THE RIGHTSHOLDER DISCLAIM ALL OTHER WARRANTIES RELATING TO THE WORK(S) AND RIGHT(S), EITHER EXPRESS OR IMPLIED, INCLUDING WITHOUT LIMITATION IMPLIED WARRANTIES OF MERCHANTABILITY OR FITNESS FOR A PARTICULAR PURPOSE. ADDITIONAL RIGHTS MAY BE REQUIRED TO USE ILLUSTRATIONS, GRAPHS, PHOTOGRAPHS, ABSTRACTS, INSERTS, OR OTHER PORTIONS OF THE WORK (AS OPPOSED TO THE ENTIRE WORK) IN A MANNER CONTEMPLATED BY USER; USER UNDERSTANDS AND AGREES THAT NEITHER CCC NOR THE RIGHTSHOLDER MAY HAVE SUCH ADDITIONAL RIGHTS TO GRANT.

13) **Effect of Breach.** Any failure by User to pay any amount when due, or any use by User of a Work beyond the scope of the License set forth in the Order Confirmation and/or the Terms, shall be a material breach of such License. Any breach not cured within 10 days of written notice thereof shall result in immediate termination of such License without further notice. Any unauthorized (but licensable) use of a Work that is terminated immediately upon notice thereof may be liquidated by payment of the Rightsholder's ordinary license price therefor; any unauthorized (and unlicensable) use that is not terminated immediately for any reason (including, for example, because materials containing the Work cannot

reasonably be recalled) will be subject to all remedies available at law or in equity, but in no event to a payment of less than three times the Rightsholder's ordinary license price for the most closely analogous licensable use plus Rightsholder's and/or CCC's costs and expenses incurred in collecting such payment.

14) **Additional Terms for Specific Products and Services.** If a User is making one of the uses described in this Section 14, the additional terms and conditions apply:

a) ***Print Uses of Academic Course Content and Materials (photocopies for academic coursepacks or classroom handouts).*** For photocopies for academic coursepacks or classroom handouts the following additional terms apply:

i) The copies and anthologies created under this License may be made and assembled by faculty members individually or at their request by on-campus bookstores or copy centers, or by off-campus copy shops and other similar entities.

ii) No License granted shall in any way: (i) include any right by User to create a substantively non-identical copy of the Work or to edit or in any other way modify the Work (except by means of deleting material immediately preceding or following the entire portion of the Work copied) (ii) permit "publishing ventures" where any particular anthology would be systematically marketed at multiple institutions.

iii) Subject to any Publisher Terms (and notwithstanding any apparent contradiction in the Order Confirmation arising from data provided by User), any use authorized under the academic pay-per-use service is limited as follows:

A) any License granted shall apply to only one class (bearing a unique identifier as assigned by the institution, and thereby including all sections or other subparts of the class) at one institution;

B) use is limited to not more than 25% of the text of a book or of the items in a published collection of essays, poems or articles;

C) use is limited to no more than the greater of (a) 25% of the text of an issue of a journal or other periodical or (b) two articles from such an issue;

D) no User may sell or distribute any particular anthology, whether photocopied or electronic, at more than one institution of learning;

E) in the case of a photocopy permission, no materials may be entered into electronic memory by User except in order to produce an identical copy of a Work before or during the academic term (or analogous period) as to which any particular permission is granted. In the event that User shall choose to retain materials that are the subject of a photocopy permission in electronic memory for purposes of producing identical copies more than one day after such retention (but still within the scope of any permission granted), User must notify CCC of such fact in the applicable permission request and such retention shall constitute one copy actually sold for purposes of calculating permission fees due; and

F) any permission granted shall expire at the end of the class. No permission granted shall in any way include any right by User to create a substantively non-identical copy of the Work or to edit or in any other way modify the Work (except by means of deleting material immediately preceding or following the entire portion of the Work copied).

iv) Books and Records; Right to Audit. As to each permission granted under the academic pay-per-use Service, User shall maintain for at least four full calendar years books and records sufficient for CCC to determine the numbers of copies made by User under such permission. CCC and any representatives it may designate shall have the right to audit such books and records at any time during User's ordinary business hours, upon two days' prior notice. If any such audit shall determine that User shall have underpaid for, or underreported, any photocopies sold or by three percent (3%) or more, then User shall bear all the costs of any such audit; otherwise, CCC shall bear the costs of any such audit. Any amount determined by such audit to have been underpaid by User shall immediately be paid to CCC by User, together with interest thereon at the rate of 10% per annum from the date such amount was originally due. The provisions of this paragraph shall survive the termination of this License for any reason.

b) ***Digital Pay-Per-Uses of Academic Course Content and Materials (e-coursepacks, electronic reserves, learning management systems, academic institution intranets).*** For uses in e-coursepacks, posts in electronic reserves, posts in learning management systems, or posts on academic institution intranets, the following additional terms apply:

i) The pay-per-uses subject to this Section 14(b) include:

A) **Posting e-reserves, course management systems, e-coursepacks for text-based content,** which grants authorizations to import requested material in electronic format, and allows electronic access to this material to members of a designated college or university class, under the direction of an instructor designated by the college or university, accessible only under appropriate electronic controls (e.g., password);

B) **Posting e-reserves, course management systems, e-coursepacks for material consisting of photographs or other still images not embedded in text,** which grants not only the authorizations described in Section 14(b)(i)(A) above, but also the following authorization: to include the requested material in course materials for use consistent with Section 14(b)(i)(A) above, including any necessary resizing, reformatting or modification of the resolution of such requested material (provided that such modification does not alter the underlying editorial content or meaning of the requested material, and provided that the resulting modified content is used solely within the scope of, and in a manner consistent with, the particular authorization described in the Order Confirmation and the Terms), but not including any other form of manipulation, alteration or editing of the requested material;

C) **Posting e-reserves, course management systems, e-coursepacks or other academic distribution for audiovisual content,** which grants not only the authorizations described in Section 14(b)(i)(A) above, but also the following authorizations: (i) to include the requested material in course materials for use consistent with Section 14(b)(i)(A) above; (ii) to display and perform the requested material to such members of such class in the physical classroom or remotely by means of streaming media or other video formats; and (iii) to "clip" or reformat the requested material for purposes of time or content management or ease of delivery, provided that such "clipping" or reformatting does not alter the underlying editorial content or meaning of the requested material and that the resulting material is used solely within the scope of, and in a manner consistent with, the particular authorization described in the Order Confirmation and the Terms. Unless expressly set forth in the relevant Order Conformation, the License does not authorize any other form of manipulation, alteration or editing of the requested material.

ii) Unless expressly set forth in the relevant Order Confirmation, no License granted shall in any way: (i) include any right by User to create a substantively non-identical copy of the Work or to edit or in any other way modify the Work (except by means of deleting material immediately preceding or following the entire portion of the Work copied or, in the case of Works subject to Sections 14(b)(1)(B) or (C) above, as described in such Sections) (ii) permit "publishing ventures" where any particular course materials would be systematically marketed at multiple institutions.

iii) Subject to any further limitations determined in the Rightsholder Terms (and notwithstanding any apparent contradiction in the Order Confirmation arising from data provided by User), any use authorized under the electronic course content pay-per-use service is limited as follows:

A) any License granted shall apply to only one class (bearing a unique identifier as assigned by the institution, and thereby including all sections or other subparts of the class) at one institution;

B) use is limited to not more than 25% of the text of a book or of the items in a published collection of essays, poems or articles;

C) use is limited to not more than the greater of (a) 25% of the text of an issue of a journal or other periodical or (b) two articles from such an issue;

D) no User may sell or distribute any particular materials, whether photocopied or electronic, at more than one institution of learning;

E) electronic access to material which is the subject of an electronic-use permission must be limited by means of electronic password, student identification or other control permitting access solely to students and instructors in the class;

F) User must ensure (through use of an electronic cover page or other appropriate means) that any person, upon gaining electronic access to the material, which is the subject of a permission, shall see:

- a proper copyright notice, identifying the Rightsholder in whose name CCC has granted permission,
- a statement to the effect that such copy was made pursuant to permission,
- a statement identifying the class to which the material applies and notifying the reader that the material has been made available electronically solely for use in the class, and
- a statement to the effect that the material may not be further distributed to any person outside the class, whether by copying or by transmission and whether electronically or in paper form, and User must also ensure that such cover page or other means will print out in the event that the person accessing the material chooses to print out the material or any part thereof.

G) any permission granted shall expire at the end of the class and, absent some other form of authorization, User is thereupon required to delete the applicable material from any electronic storage or to block electronic access to the applicable material.

iv) Uses of separate portions of a Work, even if they are to be included in the same course material or the same university or college class, require separate permissions under the electronic course content pay-per-use Service. Unless otherwise provided in the Order Confirmation, any grant of rights to User is limited to use completed no later than the end of the academic term (or analogous period) as to which any particular permission is granted.

v) Books and Records; Right to Audit. As to each permission granted under the electronic course content Service, User shall maintain for at least four full calendar years books and records sufficient for CCC to determine the numbers of copies made by User under such permission. CCC and any representatives it may designate shall have the right to audit such books and records at any time during User's ordinary business hours, upon two days' prior notice. If any such audit shall determine that User shall have underpaid for, or underreported, any electronic copies used by three percent (3%) or more, then User shall bear all the costs of any such audit; otherwise, CCC shall bear the costs of any such audit. Any amount determined by such audit to have been underpaid by User shall immediately be paid to CCC by User, together with interest thereon at the rate of 10% per annum from the date such amount was originally due. The provisions of this paragraph shall survive the termination of this license for any reason.

c) ***Pay-Per-Use Permissions for Certain Reproductions (Academic photocopies for library reserves and interlibrary loan reporting) (Non-academic internal/external business uses and commercial document delivery).*** The License expressly excludes the uses listed in Section (c)(i)-(v) below (which must be subject to separate license from the applicable Rightsholder) for: academic photocopies for library reserves and interlibrary loan reporting; and non-academic internal/external business uses and commercial document delivery.

i) electronic storage of any reproduction (whether in plain-text, PDF, or any other format) other than on a transitory basis;

ii) the input of Works or reproductions thereof into any computerized database;

iii) reproduction of an entire Work (cover-to-cover copying) except where the Work is a single article;

iv) reproduction for resale to anyone other than a specific customer of User;

v) republication in any different form. Please obtain authorizations for these uses through other CCC services or directly from the rightsholder.

Any license granted is further limited as set forth in any restrictions included in the Order Confirmation and/or in these Terms.

d) ***Electronic Reproductions in Online Environments (Non-Academic-email, intranet, internet and extranet).*** For "electronic reproductions", which generally includes e-mail use (including instant messaging or other electronic transmission to a defined group of recipients) or posting on an intranet, extranet or Intranet site (including any display or performance incidental thereto), the following additional terms apply:

i) Unless otherwise set forth in the Order Confirmation, the License is limited to use completed within 30 days for any use on the Internet, 60 days for any use on an intranet or extranet and one year for any other use, all as measured from the "republication date" as identified in the Order Confirmation, if any, and otherwise from the date of the Order Confirmation.

ii) User may not make or permit any alterations to the Work, unless expressly set forth in the Order Confirmation (after request by User and approval by Rightsholder); provided, however, that a Work consisting of photographs or other still images not embedded in text may, if necessary, be resized, reformatted or have its resolution modified without additional express permission, and a Work consisting of audiovisual content may, if necessary, be "clipped" or reformatted for purposes of time or content management or ease of delivery (provided that any such resizing, reformatting, resolution modification or "clipping" does not alter the underlying editorial content or meaning of the Work used, and that the resulting material is used solely within the scope of, and in a manner consistent with, the particular License described in the Order Confirmation and the Terms.

15) **Miscellaneous.**

a) User acknowledges that CCC may, from time to time, make changes or additions to the Service or to the Terms, and that Rightsholder may make changes or additions to the Rightsholder Terms. Such updated Terms will replace the prior terms and conditions in the order workflow and shall be effective as to any subsequent Licenses but shall not apply to Licenses already granted and paid for under a prior set of terms.

b) Use of User-related information collected through the Service is governed by CCC's privacy policy, available online at www.copyright.com/about/privacy-policy/.

c) The License is personal to User. Therefore, User may not assign or transfer to any other person (whether a natural person or an organization of any kind) the License or any rights granted thereunder; provided, however, that, where

applicable, User may assign such License in its entirety on written notice to CCC in the event of a transfer of all or substantially all of User's rights in any new material which includes the Work(s) licensed under this Service.

d) No amendment or waiver of any Terms is binding unless set forth in writing and signed by the appropriate parties, including, where applicable, the Rightsholder. The Rightsholder and CCC hereby object to any terms contained in any writing prepared by or on behalf of the User or its principals, employees, agents or affiliates and purporting to govern or otherwise relate to the License described in the Order Confirmation, which terms are in any way inconsistent with any Terms set forth in the Order Confirmation, and/or in CCC's standard operating procedures, whether such writing is prepared prior to, simultaneously with or subsequent to the Order Confirmation, and whether such writing appears on a copy of the Order Confirmation or in a separate instrument.

e) The License described in the Order Confirmation shall be governed by and construed under the law of the State of New York, USA, without regard to the principles thereof of conflicts of law. Any case, controversy, suit, action, or proceeding arising out of, in connection with, or related to such License shall be brought, at CCC's sole discretion, in any federal or state court located in the County of New York, State of New York, USA, or in any federal or state court whose geographical jurisdiction covers the location of the Rightsholder set forth in the Order Confirmation. The parties expressly submit to the personal jurisdiction and venue of each such federal or state court.

Last updated October 2022

Re: Request to use figures from VolturnUS-s definition paper in my PhD Thesis

Barter, Garrett <Garrett.Barter@nrel.gov>

Thu 08/02/2024 16:29

To:Andre White <andre.white@plymouth.ac.uk>;Hall, Matthew <Matthew.Hall@nrel.gov>

Hi Andre,

Yes, you are more than welcome to use the images with an appropriate citation.

Cheers,
Garrett

From: Andre White <andre.white@plymouth.ac.uk>
Date: Thursday, February 8, 2024 at 9:22 AM
To: Garrett Barter <Garrett.Barter@nrel.gov>, "Hall, Matthew" <Matthew.Hall@nrel.gov>
Subject: Request to use figures from VolturnUS-s definition paper in my PhD Thesis

Hi Garrett/Matthew:
There is a publication by Allen et al. (2020), "Definition of the UMaine VolturnUS-S Reference Platform Developed for the IEA Wind 15-Megawatt Offshore Reference Wind Turbine," I would like to use 3 figures of the FOWT in my Thesis. I have reached out to Allen over 2 months ago but did not hear back from him.

Can I get permission to use the figures of the VolturnUS-S platform in my Thesis?

Thank you.

Regards,
AOAW

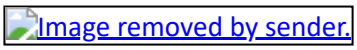

Andre White

From: Andre White
Sent: 15 December 2023 20:58
To: chba@dtu.dk
Subject: Request to use figure from your paper

Dear Christian:
I am just completing my PhD in offshore wind and would like to know if it is possible to use a figure from your book entitled, “The DTU 10-MW Reference Wind Turbine.”

Thank you.

Regards,
AOAW

Re: Request to use Image from NOAA website in my PhD Thesis

Mary Fairbanks - NOAA Federal <mary.fairbanks@noaa.gov>

Thu 08/02/2024 16:51

To:Andre White <andre.white@plymouth.ac.uk>
Cc:Mary Fairbanks - NOAA Federal <mary.fairbanks@noaa.gov>

Thank you for your message and interest in our content. Please provide attribution to NOAA's National Weather Service's Online School for Weather, JetStream, when using the image. All of our information is in the public domain and free to use.

Take care.
Mary Scarzello Fairbanks

On Thu, Feb 8, 2024 at 11:42 AM Andre White <andre.white@plymouth.ac.uk> wrote:

> Dear Sir or Madam:
> I am requesting permission to use a copy of the image below in my PhD Thesis.
>
> Thank you.
>
> 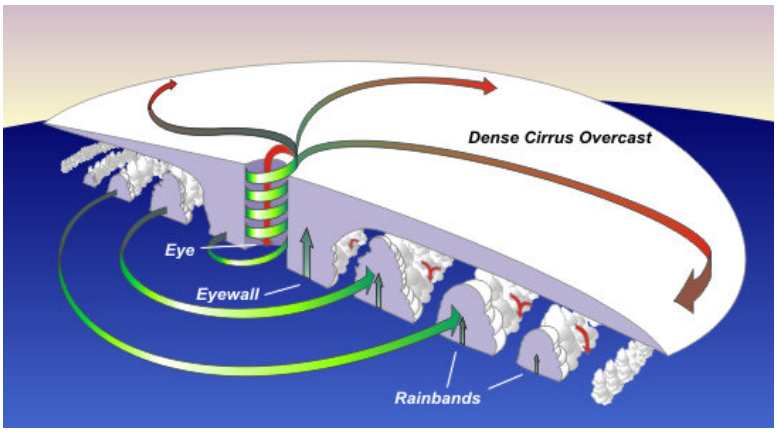
>
>
> Regards,
> Andre White
> University of Plymouth

--

Mary Scarzello Fairbanks
Meteorologist, National Weather Service Education and Outreach Lead
NOAA/National Weather Service Communications Division
443 745 6354

Andre White

From: Zhiming Yuan <zhiming.yuan@strath.ac.uk>
Sent: 19 December 2023 08:32
To: Andre White
Subject: Re: Request to use a figure from your paper

Dear Andre,

Thanks for your email. please go ahead to use the figure of the paper with a proper reference.

Kind regards,
Zhiming

From: Andre White <andre.white@plymouth.ac.uk>
Date: Friday, 15 December 2023 at 20:38
To: Zhiming Yuan <zhiming.yuan@strath.ac.uk>
Subject: Request to use a figure from your paper

Dear Zhiming:
I am just completing my PhD and would like to know if it is possible to use a figure from your paper entitled, "Dynamic and structural performances of offshore floating wind turbines in turbulent wind flow."

Thank you.

Regards,
AOAW

List of references

ABS (2011), Design standards for offshore wind turbines, Government document, American Bureau of Shipping.

Ali, A., De Risi, R. & Sextos, A. (2021), 'Seismic assessment of wind turbines: How crucial is rotor-nacelle-assembly numerical modeling?', *Soil Dynamics and Earthquake Engineering* **141**, 106483.

Allen, C., Viscelli, A., Dagher, H., Goupee, A., Gaertner, E., Abbas, N., Hall, M. & Barter, G. (2020), 'Definition of the umaine volturnus-s reference platform developed for the iea wind 15-megawatt offshore reference wind turbine', pp. NREL/TP–5000–76773.

Anderson, T. R., Hawkins, E. & Jones, P. D. (2016), 'CO2, the greenhouse effect and global warming: from the pioneering work of arrhenius and callendar to today's earth system models', *Endeavour* **40**(3), 178–187.

Archer, C. L., Colle, B. A., Monache, L. D., Dvorak, M. J., Lundquist, J., Bailey, B. H., Beaucage, P., Churchfield, M. J., Fitch, A. C., Kosovic, B., Lee, S., Moriarty, P. J., Simao, H., Stevens, R. J. A. M., Veron, D. & Zack, J. (2014), 'Meteorology for coastal/offshore wind energy in the united states: Recommendations and research needs for the next 10 years', *Bulletin of the American Meteorological Society* **95**, 515–519.

Arshad, M. & O'Kelly, B. (2013), 'Offshore wind-turbine structures: A review', *Proceedings of the Instituion of Civil Engineers – Energy* **166**, 139–152.

Bae, Y., Kim, M., Im, S. & Chang, I. (2011), Aero-Elastic-Control-Floater-Mooring Coupled Dynamic Analysis of Floating Offshore Wind Turbines, *in* 'Proceedings of the Twenty-first (2011) International Offshore and Polar Engineering Conference', pp. 429–435.

Bak, C., Zahle, F., Bitsche, R. D., Kim, T., Yde, A., Henriksen, L. C., Hansen, M. H., Blasques, J. P. A. A., Gaunaa, M. & Natarajan, A. (2013), The dtu 10-mw reference wind turbine, *in* 'DTU Department of Wind Energy'.

Banton, J. (2002), Parametric models and methods of hindcast analysis for hurricane waves, Master's thesis, IHE Delft.

Brennan (2019), 'Chernobyl death toll: How many people were killed by the nuclear disaster?', Accessed at: https://www.newsweek.com/chernobyl-disaster-death-toll-estimates-radiation-cancer-1444029. Accessed: 23/4/2020.

Bryan, G. H., Worsnop, R. P., Lundquist, J. K. & Zhang, J. A. (2017), 'A simple method for simulating wind profiles in the boundary layer of tropical cyclones', *Boundary-Layer Meteorology* **162**, 475–502.

Burton, T., Sharpe, D., Jenkins, N. & Bossanyi, E. (2001), *Wind Energy Handbook*, 1 edn, John Wiley & Sons Ltd.

Butterfield, S., Musial, W. & Jonkman, J. (2005), Engineering challenges for floating offshore wind turbines, Technical report, National Renewable Energy Laboratory.

Caires, S. (2011), Extreme value analysis:wave data (JCOMM technical report 57), Technical report, World Meteorological Organizations.

Caires, S. & van Gent, M. (2008), Extreme wave loads, *in* 'Proceedings of the ASME 2008 27th International Conference on Offshore Mechanics and Arctic Engineering. Volume 2: Structures, Safety and Reliability', Vol. 2, pp. 945–953.

CarbonTrust (2015), Floating offshore wind - market and technology review: Prepared for the scottish government, Government document, Carbon Trust.

Chadee, X. T. & Clarke, R. M. (2014), 'Large-scale wind energy potential of the Caribbean region using near-surface reanalysis data', *Renewable and Sustainable Energy Reviews* **30**, 45–58.

Chai, W. & Leira, B. J. (2018), 'Environmental contours based on inverse SORM', *Marine Structures* **60**, 34–51.

Chakrabarti, S. K. (1987), *Hydrodynamics of Offshore Structures*, 3 edn, Computational Mechanics.

Chryssostomidis, C. & Liu, Y. (2011), Lecture 14: Mooring dynamics (iii), *in* 'Design of Ocean Systems — MIT Course No. 2.019'. MIT Open Courseware.
URL: *https://ocw.mit.edu*

Cione, J., Kalina, E. A., Uhlhorn, E., Farber, A. M. & Damiano, B. (2016), 'Coyote unmanned aircraft system observations in hurricane edouard (2014)', *Earth and Space Science* **3**, 370 – 380.

Coles, S. (2001), *An Introduction to Statistical Modeling of Extreme Values*, 1 edn, Springer-Verlag, London.

Cordle, A. & Jonkman, J. (2011), State of the art in floating wind turbine design tools, *in* 'Proceedings of the Twenty-first International Offshore and Polar Engineering Conference, Maui, Hawaii, USA, June 2011'.

Costoya, X., deCastro, M., Santos, F., Sousa, M. C. & Gómez-Gesteira, M. (2019), 'Projections of wind energy resources in the Caribbean for the 21st century', *Energy* **178**, 356–367.

DNV (2010*a*), Recommended pracrtice DNV-RP-C205: Environmental conditions and environmental loads, Technical manual, Det Norske Veritas.

DNV (2010*b*), Recommended pracrtice DNV-RP-F205: Global performance analysis of deepwater floating structures, Technical manual, Det Norske Veritas.

DNV (2014), Offshore wind standard DNV-OS-J101: Design of offshore wind turbine structures, Technical manual, Det Norske Veritas.

DNV-GL (2016), Load and site conditions for wind turbines, Technical manual, DNV GL.

DNV-GL (2018), Met characterization recommended practices for U.S. offshore wind energy, Technical manual, DNV GL.

DOE (2017), 2016 offshore wind technologies market report, Government document, Department of Energy.

DOE (2019), 2018 offshore wind technologies market report, Government document, Department of Energy.

DOE (2022), 2022 offshore wind technologies market report, Government document, Department of Energy.

DOE (2023), 'Wind turbines: the bigger the better', Available at: https://www.energy.gov/eere/articles/wind-turbines-bigger-better. Accessed: 24/11/2023.

Donnou, H. E. V., Akpo, A. B., Houngue, G. H. & Kounouhewa, B. (2020), 'Assessment of IEC Normal Turbulence Model and Modelling of the Wind Turbulence Intensity for Small Wind Turbine Design in Tropical Area: Case of the Coastal Region of Benin', *International Journal of Renewable Energy Development* **9**, 263–286.

Dyrbye, C. & Hansen, S. O. (1997), *Wind Load on Structures*, John Wiley & Sons Ltd.

Eckert-Gallup, A., Sallaberry, C., Dallman, A. & Neary, V. (2016), 'Application of principal component analysis (PCA) and improved joint probability distributions to the

inverse first-order reliability method (I-FORM) for predicting extreme sea states', *Ocean Engineering* **112**, 307–319.

Eckert-Gallup, A., Sallaberry, C. & Neary, V. (2014), Modified inverse first order reliability method (I-FORM) for predicting extreme sea states, Technical report, Sandia National Laboratories.

Edenhofer, O., Madruga, R. P., Sokona, Y., Minx, J. C., Farahani, E., Kadner, S., Seyboth, K., Adler, A., Baum, I., Brunner, S., Eickemeier, P., Kriemann, B., Savolainen, J., Schlömer, S., von Stechow, C. & Zwickel, T. (2014), IPCC 2014: Climate change 2014: Mitigation of climate change. working group III contribution to the fifth assessment report of the Intergovernmental Panel on Climate Change, Technical report, IPCC.

Edenhofer, O., Madruga, R. P., Sokona, Y., Seyboth, K., Matschoss, P., Kadner, S., Zwickel, T., Eickemeier, P., Hansen, G., Schlömer, S. & Stechow, C. (2011), 'Renewable energy sources and climate change mitigation: Special report of the Intergovernmental Panel on Climate Change', *Renewable Energy Sources and Climate Change Mitigation: Special Report of the Intergovernmental Panel on Climate Change* pp. 1–1075.

Edwards, E. C., Holcombe, A., Brown, S., Ransley, E., Hann, M. & Greaves, D. (2023), 'Evolution of floating offshore wind platforms: A review of at-sea devices', *Renewable and Sustainable Energy Reviews* **183**, 113416.

Elliott, D. L., Aspliden, C. I., Gower, G. L., Holladay, C. G. & Schwartz, M. N. (1987), 'Wind energy resource assessment of the Caribbean and Central America', Technical report Available at = https://www.osti.gov/servlets/purl/971424.

Elliott, D. L. & Barchet, W. R. (1980), 'Wind energy resource atlas: Volume 1 the northwest region', Technical report Available at https://digital.library.unt.edu/ark:/67531/metadc1066633/.

Eskeland, C. (2017), Environmental Contours, Master's thesis, University of Oslo.

Esteban, M. D., Diez, J. J., López, J. S. & Negro, V. (2011), 'Why offshore wind energy?', *Renewable Energy* **36**(2), 444–450.

Esteban, M. D., Lopez-Gutierrez, J., Negro, V., Matutano, C. & M. García-Flores Francisco, Ángel Millán, M. (2014), 'Offshore wind foundation design: Some key issues', *Journal of Energy Resources Technology* **137**.

ETI (2015), Offshore wind floating, Government document, Energy Technologies Institute.

EWEA (2013), Deep water:the next step for offshore wind energy, Government document, European Wind Energy Association.

Failla, G. & Arena, F. (2015), 'New perspectives in offshore wind energy', *Philosophical Transactions of the Royal Society A: Mathematical, Physical and Engineering Sciences* **373**.

Faltinsen, O. (1990), *Sea Loads on Ships and Offshore Structures*, Cambridge University Press.

French, J. R., Drennan, W. M., Zhang, J. A. & Black, P. G. (2007), 'Turbulent Fluxes in the Hurricane Boundary Layer. Part I: Momentum Flux', *Journal of the Atmospheric Sciences* **64**, 1089–1102.

Gaertner, E., Rinker, J., Sethuraman, L., Zahle, F., Anderson, B., Barter, G., Abbas, N., Meng, F., Bortolotti, P., Skrzypinski, W., Scott, G., Feil, R., Bredmose, H., Dykes, K., Shields, M., Allen, C. & Viselli, A. (2020), Definition of the IEA 15-megawatt offshore reference wind turbine, Technical report, National Renewable Enery Laboratory (NREL).

Gao, L., Li, B. & Hong, J. (2021), 'Effect of wind veer on wind turbine power generation', *Physics of Fluids* **33**, 015101.

Gilleland, E. & Katz, R. (2016), 'extRemes 2.0: An extreme value analysis package in R', *Journal of Statistical Software* **72**, 1–39.

GL (2010), Guidelines for the certification of wind turbines, Technical manual, Germanischer Lloyd.

Goda, Y. (2000), 'Random seas and design of maritime structures', *Advanced Series on Ocean Engineering* **15**.

GOJ (2010), National renewable energy policy 2009, Government document, Ministry of Energy and Mining (Jamaica).

GWEC (2012), GWEC - global wind report: Annual market update 2011, Government document, Global Wind Energy Council.

GWEC (2018), GWEC-global wind statistics 2017, Government document, Global Wind Energy Council.

GWEC (2019), GWEC - global wind statistics 2018, Government document, Global Wind Energy Council.

GWEC (2022), Global offshore wind report 2021, Government document, Global Wind Energy Council.

GWEC (2023), Global wind report 2023, Government document, Global Wind Energy Council.

Hall, M. (2017), MoorDyn User's Guide, Government document, University of Prince Edward Island.

Hannon, M., Topham, E., Dixon, J., McMillan, D. & Collu, M. (2019), Offshore wind ready to float? global and UK trends in the floating offshore wind market, Technical report, University of Strathclyde, Glasgow.

Harper, B. A., Kepert, J. D. & Ginger, J. D. (2010), Guidelines for converting between various wind averaging periods in tropical cyclone conditions, Technical report, World Meteorologocal Organization.

Haver, S. & Winterstein, S. (2008), 'Environmental contour lines: A method for estimating long term extremes by a short term analysis', *Transactions - Society of Naval Architects and Marine Engineers* **116**.

Hiles, C. E., Robertson, B. & Buckham, B. J. (2019), 'Extreme wave statistical methods and implications for coastal analyses', *Estuarine, Coastal and Shelf Science* **223**, 50–60.

Huebler, C., Gebhardt, C. G. & Rolfes, R. (2018), 'Assessment of a standard ULS design procedure for offshore wind turbine sub-structures', *Journal of Physics: Conference Series* **1104**, 012013.

IEA (2019), Key world energy statistics, Report, International Energy Agency.

IEC-61400-1 (2019), *IEC 61400-1: 2019 Wind Energy Generation Systems - Part 1: Design requirements*, International Electrotechnical Commission.

IEC-61400-3-1 (2019), *IEC 61400-3-1: 2019 Wind Energy Generation Systems - Part 3-1: Design requirements for fixed offshore wind turbines*, International Electrotechnical Commission.

IPCC (2018), Global warming of 1.5 degrees celsius: An IPPC special report on the impacts of global warming of 1.5 degrees celcius above pre-industrial levels and related global greenhouse gasemission pathways, in the context of strengthening the global response to the threat of climate change, sustainable development, and efforts to eradicate poverty, Government document, Intergovernmental Panel on Climate Change.

IPCC (2023), Syhthesis report of the IPCC sixth asessment report, Government document, Intergovernmental Panel on Climate Change.

IRENA (2016a), Innovation outlook offshore wind, Report, IRENA.

IRENA (2016b), Floating founations: A game changer for offshore wind power, Report, IRENA.

IRENA (2016c), A path to prosperity: Renewable energy for islands third edition, Report, IRENA.

IRENA (2019*a*), Future of wind: Deployment, investment, technology, grid integration and socio-economic aspects, Report, IRENA.

IRENA (2019*b*), Renewable capacity highlights 31 march 2019, Report, IRENA.

Ishihara, T., Yamaguchi, A. & Sarwar, M. W. (2012), 'A study of the normal turbulence model in IEC 61400-1', *Wind Engineering* **36**, 759 – 765.

Jonathan, P. & Ewans, K. (2013), 'Statistical modelling of extreme ocean environments for marine design: A review', *Ocean Engineering* **62**, 91–109.

Jonkman, J. M. & Buhl, Jr, M. L. (2005), FAST user's guide - updated august 2005, Technical manual, National Renewable Energy Laboratory (NREL).

Jonkman, J. M. & Buhl, Jr, M. L. (2006), Turbsim user's guide, Technical manual, National Renewable Energy Laboratory (NREL).

Jonkman, J. M. & Matha, D. (2011), 'Dynamics of offshore floating wind turbines - analysis of three concepts', *Wind Energy* **14**(4), 557–569.

Jonkman, J., Wright, A., Hayman, G. & Robertson, A. (2018), Full-system linearization for floating offshore wind turbines in openfast (pre-print), *in* 'Proceedings of the ASME 2018 1st International Offshore Wind Technical Conference, ASME'.

Kaldellis, J. K. & Kapsali, M. (2013), 'Shifting towards offshore wind energy - recent activity and future development', *Energy Policy* **53**, 136–148.

Kaldellis, J. K. & Zafirakis, D. (2011), 'The wind energy revolution: A short review of a long history', *Renewable Energy* **36**(7), 1887–1901.

Kapoor, A., Ouakka, S., Arwade, S. R., Lundquist, J. K., Lackner, M., Myers, A. T., Worsnop, R. P. & Bryan, G. H. (2020), 'Hurricane eyewall winds and structural response of wind turbines', *Wind Energy Science* **5**, 89–104.

Karimirad, M. (2014), *Offshore Energy Structures - For Wind Power, Wave Energy and Hybrid Marine Platforms*, Springer.

Kim, E. & Manuel, L. (2014), 'Hurricane-induced loads on offshore wind turbines with considerations for nacelle yaw and blade pitch control', *Wind Engineering* **38**, 413 – 423.

Kim, H.-C. & Kim, M. H. (2016), 'Comparison of simulated platform dynamics in steady/dynamic winds and irregular waves for OC4 semi-submersible 5mw wind turbine against deepcwind model-test results', *Ocean Systems Engineering* **6**, 1–21.

Kim, J., Pham, T. D. & Shin, H. (2019), 'Validation of a 750 kw semi-submersible floating offshore wind turbine numerical model with model test data, part II: Model-II', *International Journal of Naval Architecture and Ocean Engineering* **12**, 213–225.

Kogaki, T., Matsumiya, H., Abe, H. & Ogawa, S. (2009), 'Wind characteristics and wind models for wind turbine design in Japan - 1st report: Analysis of NEDO FT data on turbulence characteristics and new turbulence model incorporating these results', *Journal of Environment and Engineering* **4**, 467–478.

Le, C., Li, Y. & Ding, H. (2019), 'Study on the coupled dynamic responses of a submerged floating wind turbine under different mooring conditions', *Energies* **12**(3).

Lefebvre, S. & Collu, M. (2012), 'Preliminary design of a floating support structure for a 5 MW offshore wind turbine', *Ocean Engineering* **40**, 15–26.

Leu, T. S., Yo, J.-M., Tsai, Y. T., Miau, J. J., Wang, T.-C. & Tseng, C.-C. (2014), Assessment of IEC 61400-1 normal turbulence model for wind conditions in taiwan west coast areas, *in* 'Proceedings of the fifth International Symposium on Physics of Fluids (ISPF5). International Journal of Modern Physics: Conference Series', Vol. 34, p. 1460382.

Li, J., Li, Z., Jiang, Y. & Tang, Y. (2022), 'Typhoon resistance analysis of offshore wind turbines: A review', *Atmosphere* **13**(3), 451.

Li, L., Liu, Y., Yuan, Z. & Gao, Y. (2019), 'Dynamic and structural performances of offshore floating wind turbines in turbulent wind flow', *Ocean Engineering* **179**, 92–103.

LIFE50+ (2015*a*), Qualification of innovative floating substructures for 10mw wind turbines and water depths greater than 50m - D1.1 oceanographic and meteorological conditions for the design, Government document, LIFE50+.

LIFE50+ (2015*b*), Qualification of innovative floating substructures for 10mw wind turbines and water depths greater than 50m - D4.4 overview of the numerical models used in the consurtium and their qualification, Government document, LIFE50+.

LIFE50+ (2015*c*), Qualification of innovative floating substructures for 10mw wind turbines and water depths greater than 50m - D7.1 review of fowt guidelines and design practice, Government document, LIFE50+.

Lindsey, R. (2023), 'Climate change: Atmospheric carbon dioxide', Available at: https://www.climate.gov/news-features/understanding-climate/climate-change-atmospheric-carbon-dioxide. Accessed: 24/11/2023.

Liu, J., Thomas, E., Manuel, L., Griffith, D. T., Ruehl, K. & Barone, M. F. (2018), 'Integrated system design for a large wind turbine supported on a moored semi-submersible platform', *Journal of Marine Science and Engineering* **6**(1), 9.

Liu, S., Chuang, Z., Qu, Y., Li, X., Li, C. & He, Z. (2022), 'Dynamic performance evaluation of an integrated 15 mw floating offshore wind turbine under typhoon and ecd conditions', *Frontiers in Energy Research* **10**, 874438.

Liu, Y., Xiao, Q., Incecik, A., Peyrard, C. & Wan, D. (2017b), 'Establishing a fully coupled CFD analysis tool for floating offshore wind turbines', *Renewable Energy* **112**, 280–301.

Liu, Z., Fan, Y., Wang, W. & Qian, G. (2019a), 'Numerical study of a proposed semi-submersible floating platform with different numbers of offset columns based on the deepcwind prototype for improving the wave-resistance ability', *Applied Sciences* **9**(6), 1255.

Liu, Z., Zhou, Q., Tu, Y., Wang, W. & Hua, X. (2019b), 'Proposal of a novel semi-submersible floating wind turbine platform composed of inclined columns and multi-segmented mooring lines', *Energies* **12**(9), 1809.

Lucas, C. & Guedes Soares, C. (2016), Bivariate distributions of significant wave height and peak period of sea states in deep and shallow waters offshore portugal, *in* 'Proceedings of the 3rd International Conference on Maritime Technology and Engineering', Vol. 03, pp. 1045–1050.

Mahfouz, M. Y., Molins, C., Trubat, P., Hernández, S., Vigara, F., Pegalajar-Jurado, A., Bredmose, H. & Salari, M. R. (2021), 'Response of the iea wind 15-mw windcrete and activefloat floating wind turbines to wind and second-order waves', *Wind Energy Science* **6**(3), 867–883.

Malhotra, S. (2007), Design and construction considerations for offshore wind turbine foundations in north america, *in* 'ASME 2007 26th International Conference on Offshore Mechanics and Arctic Engineering', Vol. 42711, pp. 635–647.

Manolas, D., Riziotis, V., Papadakis, G. & Voutsinas, S. (2020), 'Hydro-servo-aeroelastic analysis of floating offshore wind turbines', *Fluids* **5**(4), 200.

Manwell, J., Mcgowan, J. & Rogers, A. (2009), *Wind Energy Explained: Theory, Design and Application*, 2 edn, John Wiley & Sons Ltd.

Mishnaevsky, L., Branner, K., Petersen, H., Beauson, J., Mcgugan, M. & Sørensen, B. F. (2017), 'Materials for wind turbine blades: An overview', *Materials* **10**(11), 1285.

Myers, A. T., Arwadeb, S. R. & Manwellc, J. F. (2013), Consideration of hurricanes and tropical cyclones in the design of offshore wind turbines, *in* 'Proceedings of European Wind Energy Association'.

Natarajan, A., Hansen, M. H. & Wang, S. (2016), Design load basis for offshore wind turbines: DTU wind energy report No. E-0133, Technical report, Technical University of Denmark (DTU).

Neary, V. S., Ahn, S., Seng, B. E., Allahdadi, M. N., Wang, T., Yang, Z. & He, R. (2020), 'Characterization of extreme wave conditions for wave energy converter design and project risk assessment', *Journal of Marine Science and Engineering* **8**(4), 289.

Negro, V., Lopez-Gutierrez, J. S., Esteban, M. D., Alberdi, P., Imaz, M. & Serraclara, J. M. (2017), 'Monopiles in offshore wind: Preliminary estimate of main dimensions', *Ocean Engineering* **133**, 253–261.

NREL (1997), Wind resource assessment handbook - fundamentals for conducting a successful monitoring program, Government document, National Renewable Energy Laboratory.

Ochi, M. (1993), New approach for estimating the severest sea state from statistical data, *in* 'Coastal Engineering Proceedings', pp. 512–525.

Ochi, M. K. (1993b), On hurricane-generated seas, *in* 'Ocean wave measurement and analysis', ASCE, pp. 374–387.

OpenFAST (2021), 'Openfast documentation release v2.5.0', Available at: https://openfast.readthedocs.io/en/main/. Accessed: 5/5/2021.

OREAC (2020), The power of our ocean, Technical report, Offshore Renewable Energy Coalition.

ORECatapult (2018), Offshore wind industry prospectus, Government document, ORE Catapult Offshore Wind Industry Council.

Orimolade, A. P., Haver, S. & Gudmestad, O. T. (2016), 'Estimation of extreme significant wave heights and the associated uncertainties: A case study using nora10 hindcast data for the barents sea', *Marine Structures* **49**, 1–17.

Otter, A., Murphy, J., Pakrashi, V., Robertson, A. & Desmond, C. (2022), 'A review of modelling techniques for floating offshore wind turbines', *Wind Energy* **25**(5), 831–857.

Palutikof, J. P., Brabson, B. B., Lister, D. H. & Adcock, S. T. (1999), 'A review of methods to calculate extreme wind speeds', *Meteorological Applications* **6**(2), 119–132.

Panchang, V., Jeong, C. & Demirbilek, Z. (2013), 'Analyses of extreme wave heights in the Gulf of Mexico for offshore engineering applications', *Journal of Offshore Mechanics and Arctic Engineering* **135**, 031104.

Panofsky, H. A., Tennekes, H., Lenschow, D. H. & Wyngaard, J. C. (1977), 'The characteristics of turbulent velocity components in the surface layer under convective conditions', *Boundary-Layer Meteorology* **11**, 355–361.

Papadimitriou, V. (2004), 'Prospective primary teachers' understanding of climate change, greenhouse effect, and ozone layer depletion', *Journal of Science Education and Technology* **13**, 299–307.

Pasilliao, Jr, E. L. (1995), Joint distribution function of significant wave height and zero-crossing period, Master's thesis, University of Florida.

Quancard, R., Girandier, C., Robic, H. & Gueydon, S. (2019), D.4.2 – design brief: Specifications of a generic wind turbine, Report, INNOSEA.

Reeve, D., Chadwick, A. & Fleming, C. (2004), *Coastal Engineering: Processes, Theory and Design Practice*, Spon Press.

Robertson, A., Jonkman, J., Masciola, M., Song, H., Goupee, A., Coulling, A. & Luan, C. (2014), Definition of the semisubmersible floating system for phase II of OC4, Technical report, National Renewable Energy Laboratory (NREL).

Robertson, A., Jonkman, J., Vorpahl, F., Popko, W., Qvist, J., Froyd, L., Chen, X., Azcona, J., Uzungoglu, E., Guedes Soares, C., Luan, C., Yutong, H., Pengcheng, F., Yde, A., Larsen, T., Nichols, J., Builds, R., Lei, L., Anders Nygard, T. & et al. (2014b), Offshore code comparison collaboration, continuation within IEA wind task 30: Phase II results regarding a floating semisubmersible wind system: Preprint, Technical report, National Renewable Energy Laboratory (NREL).

Roddier, D., Cermelli, C., Aubault, A. & Weinstein, A. (2010), 'Windfloat: A floating foundation for offshore wind turbines', *Journal of Renewable and Sustainable Energy* **2**(3).

Roscoe, K., Caires, S., Diermanse, F. & Groeneweg, J. (2010), Extreme offshore wave statistics in the North Sea, *in* 'WIT Transactions on Ecology and the Environment', Vol. 133, pp. 47–58.

Saint-Drenan, Y.-M., Besseau, R., Jansen, M., Staffell, I., Troccoli, A., Dubus, L., Schmidt, J., Gruber, K., Simões, S. G. & Heier, S. (2020), 'A parametric model for wind turbine power curves incorporating environmental conditions', *Renewable Energy* **157**, 754–768.

Schubel, P. & Crossley, R. (2012), 'Wind turbine blade design review', *Wind Engineering* **36**(4), 365–388.

Sengupta, A. (2020), Sustainable development goals goal 13 : Climate action, *in* 'Council for Scientific and Industrial Research (CSIR)–Summer Research Training Program 2020, North East Institute of Science and Technology (NEIST)', India.

Shahan, Z. (2014), 'History of wind turbines', Available at: https://www.renewableenergyworld.com/2014/11/21/history-of-wind-turbines/. Accessed: 1/2/2019.

Sharma, S. & Sinha, S. (2019), 'Indian wind energy and its development-policies-barriers: An overview', *Environmental and Sustainability Indicators* **1-2**(1), 100003.

Shi, W., Zhang, L., Ning, D., Jiang, Z., Michailides, C. & Karimirad, M. (2019), A comparative study on the dynamic response of three semisubmersible floating offshore wind turbines, *in* 'International Conference on Offshore Mechanics and Arctic Engineering', Vol. 58899, p. V010T09A074.

Shin, H., Yu, Y., Pham, T. D., Kim, J. & Kumar, R. (2019), Numerical simulations of oc3 spar and oc4 semi-submersible type platforms under extreme conditions in the east sea, korea, *in* 'International Conference on Offshore Mechanics and Arctic Engineering', Vol. 58899, American Society of Mechanical Engineers, p. V010T09A069.

Siddiqui, M. S., Rasheed, A., Kvamsdal, T. & Tabib, M. V. (2015), 'Effect of turbulence intensity on the performance of an offshore vertical axis wind turbine', *Energy Procedia* **80**, 312–320.

Sparrevik, P. (2019), Offshore wind turbine foundations state of the art, *in* 'From Research to Applied Geotechnics', IOS Press, pp. 216–238.

Stern, D. P., Bryan, G. H. & Aberson, S. (2016), 'Extreme low-level updrafts and wind speeds measured by dropsondes in tropical cyclones', *Monthly Weather Review* **144**, 2177–2204.

Stern, D. P., Vigh, J. L., Nolan, D. S. & Zhang, F. (2012), 'Revisiting the relationship between eyewall contraction and intensification', *Journal of the Atmospheric Sciences* **72**, 1283–1306.

Teena, N., Sanil Kumar, V., Kotteppad, S. & Sajeev, R. (2012), 'Statistical analysis on extreme wave height', *Natural Hazards* **64**.

Tran, T. T. & Kim, D.-H. (2016), 'Fully coupled aero-hydrodynamic analysis of a semi-submersible fowt using a dynamic fluid body interaction approach', *Renewable Energy* **92**, 244–261.

Türk, M. & Emeis, S. (2010), 'The dependence of offshore turbulence intensity on wind speed', *Journal of Wind Engineering and Industrial Aerodynamics* **98**, 466–471.

UKSTATS (2010), 'National statistics: Household projections(2008 to 2033) in England', Available at: https://www.gov.uk/government/statistics/household-projections-2008-to-2033-in-england. Accessed: 23/4/2020.

UN (1987), Report of the world commission on environment and development: Our common future, Government document, United Nations.

UNFCC (2019), 'What is the Koyoto protocol', Available at: https://unfccc.int/kyoto__protocol. Accessed: 23/3/2020.

UpWind (2010), Project UpWind – integrated wind turbine design, WP4: Offsore foundations and support structures, Technical report. Website: https://repository.tudelft.nl/islandora/object/uuid:a176334d-6391-4821-8c5f-9c91b6b32a27/datastream/OBJ/download.

USFOS (2010), USFOS hydrodynamics. theory description of use verification, Technical manual, DNV.

Valamanesh, V., Myers, A. & Arwade, S. (2015), 'Multivariate analysis of extreme metocean conditions for offshore wind turbines', *Structural Safety* **55**, 60–69.

van Kuik, G. A. M., Peinke, J., Nijssen, R., Lekou, D., Mann, J., Sørensen, J. N., Ferreira, C., van Wingerden, J. W., Schlipf, D., Gebraad, P., Polinder, H., Abrahamsen, A., van Bussel, G. J. W., Sørensen, J. D., Tavner, P., Bottasso, C. L., Muskulus, M., Matha, D., Lindeboom, H. J., Degraer, S., Kramer, O., Lehnhoff, S., Sonnenschein,

M., Sørensen, P. E., Künneke, R. W., Morthorst, P. E. & Skytte, K. (2016), 'Long-term research challenges in wind energy - a research agenda by the European Academy of Wind Energy', *Wind Energy Science* **1**(1), 1–39.

Vanem, E. & Bitner-Gregersen, E. M. (2015), 'Alternative environmental contours for marine structural design-a comparison study', *Journal of Offshore Mechanics and Arctic Engineering* **137**(5), 051601.

Velarde, J., Vanem, E., Kramhøft, C. & Sørensen, J. D. (2019), 'Probabilistic analysis of offshore wind turbines under extreme resonant response: Application of environmental contour method', *Applied Ocean Research* **93**, 101947.

Vázquez, A., Izquierdo, U., Enevoldsen, P., Andersen, F.-H. & Blanco, J. M. (2022), 'A macroscale optimal substructure selection for Europe's offshore wind farms', *Sustainable Energy Technologies and Assessments* **53**, 102768.

Wang, C., Utsunomiya, T., Wee, S. & Choo, Y. s. (2010), 'Research on floating wind turbines: A literature survey', *The IES Journal Part A: Civil & Structural Engineering* **3**, 267–277.

Wang, H., Barthelmie, R. J., Pryor, S. C. & Kim, H. G. (2014), 'A new turbulence model for offshore wind turbine standards', *Wind Energy* **17**, 1587–1604.

Watson, C. & Schalatek, L. (2019), 'Climate finance briefing: Small island developing states', Avalibale at https://climatefundsupdate.org/publications/climate-finance-briefing-small-island-developing-states-2018/. Accessed:10/8/2019.

White, A., Hann, M., Miles, J., Rawlinson-Smith, R. & Greaves, D. (2021), An univariate extreme sea state and extreme wind speed for an offshore wind turbine off the south coast of Jamaica, *in* '31st International Ocean and Polar Engineering Conference', pp. ISOPE–I–21–1217.

Wind-Europe (2019*a*), 'History of Europe's wind energy', Avaliable at: https://windeurope.org/about-wind/history/;http://www.ewea.org/fileadmin/apps/30years/. Accessed:11/08/2020.

Wind-Europe (2019*b*), Offshore wind in Europe: Key trends and statistics 2018, Report, Wind Europe.

Winterstein, S. R., Ude, T. C., Cornell, C. A., Bjerager, P. & Haver, S. (1993), 'Environmental parameters for extreme response: Inverse FORM with omission factors', *Proc. of Intl. Conf. on Structural Safety and Reliability (ICOSSAR-93), Innsbruck, Austria* pp. 551–557.

Worsnop, R. P., Bryan, G. H., Lundquist, J. K. & Zhang, J. A. (2017b), 'Using large-eddy simulations to define spectral and coherence characteristics of the hurricane boundary layer for wind-energy applications', *Boundary-Layer Meteorology* **165**, 55–86.

Worsnop, R. P., Lundquist, J. K., Bryan, G. H., Damiani, R. & Musial, W. (2017), 'Gusts and shear within hurricane eyewalls can exceed offshore wind turbine design standards', *Geophysical Research Letters* **44**(12), 6413–6420.

Yang, H.-S., Tongphong, W., Ali, A. & Lee, Y.-H. (2023), 'Comparison of different fidelity hydrodynamic-aerodynamic coupled simulation code on the 10 mw semi-submersible type floating offshore wind turbine', *Ocean Engineering* **281**, 114736.

Zhang, J., Fowai, I. & Sun, K. (2016), 'A glance at offshore wind turbine foundation structures', *Brodogradnja* **67**, 101–113.

Zhao, Z., Li, X., Wang, W. & Shi, W. (2019), 'Analysis of dynamic characteristics of an ultra-large semi-submersible floating wind turbine', *Journal of Marine Science and Engineering* **7**(6), 169.

Zheng, C. w. & Pan, J. (2014), 'Assessment of the global ocean wind energy resource', *Renewable and Sustainable Energy Reviews* **33**, 382–391.

Zheng, C.-w., Xiao, Z.-n., Peng, Y.-h., Li, C.-y. & Du, Z.-b. (2018), 'Rezoning global offshore wind energy resources', *Renewable Energy* **129**, 1–11.

Zhou, S., Shan, B., Xiao, Y., Li, C., Song, X., Liu, Y. & Hu, Y. (2017), 'Directionality effects of aligned wind and wave loads on a y-shape semi-submersible floating wind turbine under rated operational conditions', *Energies* **10**(12), 2097.